The stress granule response in wild-type and ALS-mutant neurons

Matthew Peter Bentham

Institute of Neurology

Academic supervisors:

Pietro Fratta, Giampietro Schiavo
and Elizabeth Fisher

Thesis submitted for the degree of
Doctor of Philosophy
University College London
6th March 2020

I, Matthew Peter Bentham confirm that the work presented in this thesis is my own. Where information has been derived from other sources, I confirm that this has been indicated in the thesis.

Abstract

Stress granules (SGs) are cytoplasmic ribonucleoprotein aggregates which form in response to cellular stress and disassemble following stress cessation. Mutations in human SG proteins cause the neurodegenerative disease amyotrophic lateral sclerosis (ALS) and have been demonstrated to alter granule dynamics. Further, SGs have a compositional protein overlap with the post-mortem cytoplasmic inclusions that characterise ALS, suggesting that SGs may act as a precursor to, or seed, these inclusions.

For this thesis, I first optimised the use of different SG inducers in mouse primary fibroblast and neuronal cultures. Following this, I cultured primary neurons in compartmentalised devices, applying the oxidative stressor sodium arsenite to either the somal or axonal compartment, to investigate the kinetics of SG formation. I observed a delayed SG assembly response in neuronal somas when arsenite was applied axonally, for both cortical and sensory neurons. This response is decreased by inhibition of dynein or protein translation in the axonal compartment.

Further, I investigated the effect of ALS-causing mutations on the SG response, using a novel FUS-mutant mouse model. This model expresses a humanised C-terminal disease-causing mutation that results in a frameshifted amino acid sequence downstream of the mutation, eradicating the nuclear localisation signal of the FUS protein. This frameshift sequence allowed for the generation of antibodies able to distinguish between wild-type and mutant FUS. Using these antibodies, I observed that the normally predominately nuclear FUS protein mislocalised to the cytoplasm in neurons heterozygous and homozygous for the mutation. Additionally, I demonstrated that the mutant protein is present in SGs at a higher level than the wild-type protein.

Finally, I optimised a method for sorting neuronal somas following labelling with fluorescently-tagged retrograde toxin subunits.

These results demonstrate the ability of neuronal axons to respond to exogeneous oxidative stressors and highlight the importance of the SG response in ALS-mutant cells.

Impact Statement

Stress granules (SGs) are cytoplasmic ribonucleoprotein aggregates that form in response to a wide range of extracellular stimuli including oxidative stress, heat stress and viral infection. In healthy cells, their formation is thought to be pro-survival, compartmentalising specific RNAs and proteins and hence modulating the stress-specific proteome and transcriptome in order to prioritise stress signalling pathways. However, it has been demonstrated numerous times that the composition and dynamics of SGs can be altered in the pathogenesis of a large number of diseases; particularly those associated with viral infection or neurodegeneration.

The neurodegenerative diseases amyotrophic lateral sclerosis (ALS; a disease exhibiting progressive degeneration of motor neurons) and Alzheimer's disease both present with pathological intraneuronal inclusions, which have an overlapping protein composition with SGs. This has led to the hypothesis that SGs, or the processes underlying their formation, could result in the formation of disease inclusions and hence neuronal death. Investigation of SG dynamics and interactions may therefore identify novel therapeutic targets for development of treatments for ALS and similar diseases relating to SG alterations.

The work presented in this thesis further characterises the ability of neurons to respond to stress. I present the first reports of SGs in primary sensory neurons, and identify two novel SG-inducing compounds, which impact upon calcium homeostasis and mitochondrial function. I further observe a novel pathway by which neuronal axons can detect axonal oxidative stress and subsequently form SG aggregates in the cell body. This process requires polysome disassembly and may rely on local axonal translation and retrograde (axon-to-soma) transport via the microtubule-motor dynein. This finding provides the first reports that exogenous stressors in the periphery could result in aggregation in a completely separate region of the body, which has major implications for the spread of aggregate pathology.

In addition, I investigated the role of ALS-causing *FUS* mutations on SG function. I demonstrated that ALS-mutant FUS protein mislocalises in motor neurons to both the cytoplasm in basal conditions, but also to cytoplasmic SGs following oxidative stress. While this has previously been demonstrated, these experiments were performed in a novel FUS-mutant mouse model, which expresses disease-relevant levels of FUS protein, yet displays progressive degeneration of motor neurons. The

findings in motor neurons are replicated in sensory neurons, which are less susceptible to ALS pathogenesis. This data indicates that neither the mislocalisation of FUS to the cytoplasm, nor to SGs are the reason for this difference in susceptibility.

Finally, I developed a new technique for the isolation of the somas of neurons whose axons have been exposed to exogenous soluble stimuli, using a fluorescent-toxin-based retrograde sorting system. While I applied this to axonal stress, it will be useful for the study of axon development and regeneration.

Acknowledgements

There are a lot of people that need to be thanked here, so I'll start with my many supervisors.

Thank you to Pietro for hundreds of hours of scientific discussion, and for teaching me that it is good to throw my personality into my work. Thank you to Gipi for questioning and criticising every minute aspect of my project, and making me a better scientist for it. And a massive thank you to Lizzy for looking out for me and making sure that everything actually got done.

Thanks to everybody in the Schiavo, Greensmith, Fratta, Fisher and Isaacs labs, and everybody else I met at the ION. You have provided me with your extensive knowledge, thousands of fun memories and so much cake. A massive thank you in particular to Charli, Ellie, Charlotte, Oscar, Anna-Leigh and Martha for proof-reading this thesis.

Further special thanks to Alex and Ione for making me feel welcome in London, to Ellie for brightening my days through even the most frustrating parts of my project and to Nicol, for teaching me literally everything I know about working in a cell biology lab.

A final thank you to my wonderful and patient boyfriend Scott, as well as Charli, Ant, Jack and my real family, for a wonderful 4 years, and for saving me from going mad during the write-up experience.

Table of Contents

List of Figures

List of Tables

Abbreviations

AGO2 – argonaute-2

ALS – amyotrophic lateral sclerosis

ANG – angiogenin

ANOVA – analysis of variance

APC - adenomatous polyposis coli

APEX - ascorbate peroxidase

AraC - arabinosylcytosine C

ARS – sodium arsenite

ATP5B - ATP synthase F1 subunit beta

ATXN2 – ataxin-2

BAPTA-AM - 1,2-bis(o-aminophenoxy)ethane-N,N,N′,N′-tetraacetic acid acetoxymethyl ester

BDNF - brain-derived neurotrophic factor

Cas9 – caspase 9

CCCP - carbonyl cyanide m-chlorophenyl hydrazine

ChAT – choline acetyltransferase

ChIP-seq - chromatin immunoprecipitation sequencing

CHX – cycloheximide

CIRP – cold-inducible RNA-binding protein

CN – cortical neuron

CNTF - ciliary neurotrophic factor

COX – cyclooxygenase

CREB - cAMP-responsive element

CRISPR - clustered regularly interspaced short palindromic repeats

Cry2 – cryptochrome-2 domain (from *Arabidopsis thaliana*)

CTxB-488 - cholera toxin subunit B conjugated to a 488 fluorophore

C9orf72 - chromosome 9 open reading frame 72

DAPI - 4′,6-diamidino-2-phenylindole

DCTN1 - dynactin subunit 1

DIV – days in vitro

DMSO - dimethyl sulfoxide

DPR – dipeptide repeats

DR – dose response

DRG – dorsal root ganglion

DRGN – DRG neuron

DSB - double-stranded break

D14 – delta14 FUS

dsRNA – double-stranded RNA

DYNC1H1 - cytoplasmic dynein 1 heavy chain 1

EBOV - Ebola virus

EDTA - ethylenediaminetetraacetic acid

eEF2 - eukaryotic translation elongation factor 2

EHNA - erythro-9-(2-hydroxy-3-nonyl)adenine

EIF2α - Eukaryotic translation initiation factor 2α

EIF4(E) - Eukaryotic translation initiation factor 4(E)

ELAVL4 - ELAV-like protein 4

EMCV - encephalomyocarditis virus

ER – endoplasmic reticulum

EWS – Ewing's sarcoma

FACS – fluorescence-activated cell sorting

FBS – foetal bovine serum

FCCP - carbonyl cyanide-4-(trifluoromethoxy)phenylhydrazone

FdU - 5-Fluoro-2'-deoxyuridine

FET – FUS, EWS & TAF15 family

FMRP - fragile X mental retardation protein

FRAP – fluorescence recovery after photobleaching

FTD - frontotemporal dementia

FUS – fused-in-sarcoma

FUS-D14 – FUSDelta14-mutant FUS

FUS-KO – FUS-knock-out

FUS-WT – wild-type FUS

GADD34 - growth arrest and DNA damage-inducible protein

G3BP - GTPase-activating protein-binding protein

GDNF - glial cell line-derived neurotrophic factor

GCN2 - general control non-derepressible-2

GluA1 – glutamate A1 receptor subunit

GR – glycine-arginine dipeptide repeat

GRN – granulin/progranulin

GTP - guanosine-5'-triphosphate

γH2AX - H2A histone family member X phosphorylated on serine 139

HBSS – Hanks' balanced salt solution

HDAC1/6 - histone deacetylase 1/6

HET – heterozygous for FUSDelta14 mutation

HEK293 - Human embryonic kidney 293 cells

HeLa – immortal cervical cancer cell line

HIV-1 – human immunodeficiency virus, type 1

HuR - human antigen R

H_2O_2 – hydrogen peroxide

HNRNPA1 - Heterogeneous nuclear ribonucleoprotein A1

HOM – homozygous for FUSDelta14 mutation

HRI - heme-regulated inhibitor kinase

HS – horse serum

HSP – heat shock protein

IBM - inclusion body myositis

iCLIP - individual-nucleotide resolution cross-linking and immunoprecipitation

IDR – intrinsically disordered region

IL-6 – interleukin 6

INF-β – interferon-β

iPSC – induced-pluripotent stem cell

ISH – *in situ* hybridisation

KIF5 - kinesin Family Member 5

KRAS – k-Ras protein

LCD – low-complexity domain

LLPS – liquid-liquid phase separation

lncRNA - long non-coding RNA

Loa - legs at odd angles mouse model with a mutation in *Dync1h1* gene

MAPT - microtubule-associated protein tau

MATR3 – matrin-3

MECP2 - methyl CpG binding protein 2

MEF – mouse embryonic fibroblast

MFC – microfluidic chamber

mGluR5 - metabotropic glutamate receptor subtype 5

miRISC - microRNA-induced silencing complex

miRNA – microRNA

MK2 - MAPKAP kinase-2

MN – motor neuron

MSP - multisystem proteinopathy

mTOR - mammalian target of rapamycin

mTORC1 - mTOR complex 1

NDD – neurodegenerative disorder

NEAT1 - nuclear enriched abundant transcript 1

NGF – nerve growth factor

NIH/3T3 – fibroblast cell line

NLS – nuclear localisation signal

NMD – nonsense-mediated decay

NMJ – neuromuscular junction

NNC – non-neuronal cell

NO – nitric oxide

NONO - non-POU domain-containing octamer-binding protein

NPC - neural progenitor cell

NSC-34 cells - mouse motor neuron-like hybrid cell line

PBS – phosphate-buffered saline

PCR – polymerase chain reaction

PDMS – polydimethylsiloxane

PERK - protein kinase RNA-like endoplasmic reticulum kinase

PFN1 – profilin 1

POLR2A - RNA Polymerase II Subunit A

PrLD – prion-like domains

PFA – paraformaldehyde

PKR - protein kinase R

PR – proline-arginine dipeptide repeat

PSF - protein-associated splicing factor

PSP1 - paraspeckle protein-1

PTM – post-translational modification

PY-NLS - proline-tyrosine nuclear localization signal

RACK1 - receptor for activated C kinase 1

RBP – RNA-binding protein

RGG domain - arginine/glycine-rich domain

RINe (RNA integrity number equivalent

RNAi – RNA interference

RNAP2 - RNA polymerase II

RNP – ribonucleoprotein

rRNA - ribosomal RNA

RRM - RNA-recognition motif

RSK2 - p90 ribosomal S6 kinase

RT-PCR – real-time polymerase chain reaction

ROI – region of interest

ROS - reactive oxygen species

RT – room temperature

SAPK – stress-activated protein kinase

SFPQ - splicing factor proline and glutamine rich

SG – stress granule

SG_{50} - the time point at which 50% of the max stress granule response has been elicited

SG_{MAX} – the highest percentage of somas with stress granules during the time course

siRNA – small interfering RNA

SIN-1 - 3-morpholinosydnonimine

SCA - spinocerebellar ataxia

SMA - spinal muscular atrophy

SMN - survival of motor neuron protein

snRNP - small nuclear ribonucleoprotein

SOD1 – superoxide dismutase 1

SCA - spinocerebellar ataxia ()

SQSTM1 - sequestosome 1

ssRNA – single-stranded RNA

SYGQ domain - serine-tyrosine-glycine-glutamine domain

TAF15 - TATA-binding protein-associated factor 15

TARDBP - TAR DNA-binding protein 43

TBE - tris-borate-ethylenediaminetetraacetic acid

TBP - *tert*-Butyl peroxide

TC – time course

TDP-43 - transactive response DNA binding protein 43 kDa

TIA1 - T cell intracytoplasmic antigen

TIAR - TIA1 cytotoxic granule-associated RNA binding protein-like 1

TNF – tumor necrosis factor

TNFR1 - tumour necrosis factor receptor 1

TNPO1 – transportin-1

TRAF2 - TNFα receptor-associated factor 2

tRNA – transfer RNA

$tRNA_i^{Met}$ - initiator methionine tRNA

TSS - transcription start site

TTP – tristetraprolin

TUBA4 - tubulin alpha-4A

UBQLN2 – ubiquilin-2

UPF3 - regulator of nonsense transcripts

UVA – ultraviolet A

U2OS - human osteosarcoma U2OS cell line

VCP – valosin-containing protein

ZIKV - Zika virus

ZnF – zinc finger domain

4E-BP - 4E (eIF4E)-binding protein 1

1 Introduction

1.1 Amyotrophic lateral sclerosis and frontotemporal dementia

Amyotrophic lateral sclerosis (ALS) is a progressive and fatal neurodegenerative disorder characterized by the loss of both upper and lower motor neurons (MNs) (Couratier et al., 2017). Upper MN cell bodies are located within the motor cortex and descend into the spinal cord, while lower MN cell bodies originate in the spinal cord and project into the periphery to innervate skeletal muscle. Loss of upper and lower MNs results in paralysis of skeletal muscle, with a typical disease-onset between 40-70 years old, and subsequent death within 5 years, from respiratory failure (Ajroud-Driss and Siddique, 2015). There is currently no cure for the disease, with the most effective treatment, riluzole, extending lifespan by only 2-3 months (Ajroud-Driss and Siddique, 2015).

Frontotemporal dementia (FTD) is also a progressive, fatal neurodegenerative disorder (Takada, 2015). It results in the loss of neurons from the frontal and temporal lobes of the brain and can lead to personality, language and behavioural changes, followed by cognitive decline and death around 7 years after symptom onset; the mean onset is 53 years old (Ratnavalli et al., 2002). As with ALS, there is no cure for FTD.

ALS and FTD are thought to be part of the same disease spectrum for multiple reasons. Firstly, they exhibit an overlapping clinical presentation, with 50% of ALS patients displaying frontal lobe dysfunction and 15% FTD patients developing MN dysfunction (Murphy et al., 2007). Secondly, both diseases present with intraneuronal protein inclusions. 97% of ALS cases present with inclusions positive for both transactive response DNA binding protein 43 kDa (TDP-43) and ubiquitin; the remaining percentage being positive for either fused-in sarcoma (FUS) or superoxide dismutase 1 (SOD1) (Scotter et al., 2015). TDP-43-positive inclusions are characteristic of around 50% of FTD cases, the remainder presenting with either tau (40%) or FUS-positive (5-10%) inclusions (Mackenzie and Neumann, 2016). In addition to clinical and pathological overlap, genetic studies have highlighted further similarities between the two diseases (discussed in the next section).

1.1.1 Genetics of ALS-FTD

While the majority of ALS cases occur sporadically, 10% are inherited (familial), with genetic causes identified for 11% and 68% of sporadic and familial cases respectively (Renton et al., 2014). In 1993, mutations were first identified in the *SOD1* (superoxide dismutase 1) gene, which encodes the SOD1 protein (Rosen et al., 1993). This discovery resulted in a large amount of research into SOD1, including development of the now widely-used $SOD1^{G93A}$ mouse model (Gurney et al., 1994). Since the discovery of *SOD1* mutations, >20 more genes have been identified as harbouring ALS-causing mutations. Of these, hexanucleotide (GGGGCC) expansions in a non-coding region of the *C9orf72* (chromosome 9 open reading frame 72) gene explain the highest percentage of ALS cases (7% and 39% of sporadic and familial cases respectively) (Majounie et al., 2012)).

Of the genes identified, at least 8 encode RNA-binding proteins (RBPs) (***Table 1.1***), highlighting the likely importance of a role for RNA metabolism in ALS pathogenesis (Ito et al., 2017, Nguyen et al., 2018). This is supported by the observation that the RBPs TDP-43 and FUS are present within the cytoplasmic inclusions characteristic of the disease. TDP-43 is present in inclusions in all sporadic ALS cases and those where *TARDBP* (the gene encoding the TDP-43 protein) is mutated; *FUS* and *SOD1* mutations result in FUS (fused-in-sarcoma) and SOD1-positive inclusions respectively (Scotter et al., 2015).

Gene	Protein	Reference
TARDBP	TDP-43 (transactive response DNA binding protein 43 kDa)	(Sreedharan et al., 2008)
FUS	FUS (fused-in-sarcoma)	(Shang and Huang, 2016)
MATR3	Matrin-3	(Johnson et al., 2014)
HNRNPA1	hnRNPA1 (heterogeneous nuclear ribonucleoprotein A1)	(Kim et al., 2013)
TIA1	T cell intracytoplasmic Antigen	(Mackenzie et al., 2017)
ATXN2	Ataxin2	(Elden et al., 2010)
ANG	Angiogenin	(Wu et al., 2007)
SFPQ	SFPQ (splicing factor, proline- and glutamine-rich)	(Thomas-Jinu et al., 2017)

Table 1.1 Genes encoding RNA-binding proteins which are mutated in amyotrophic lateral sclerosis.

FTD is a largely heritable disorder, with around 40% of cases demonstrating some family history (Rohrer et al., 2009). Mutations in some genes, such as *GRN* (progranulin) and *MAPT* (microtubule-associated protein tau), result in FTD but not ALS (Takada, 2015). Mutations in other genes however can lead to FTD with or without ALS co-morbidity, including *TARDBP*, *FUS*, *VCP* and *UBQLN2*, as well as hexanucleotide expansions in the *C9orf72* gene (Takada, 2015). As with ALS, some of the proteins mutated in FTD are RBPs (***Table 1.2***). Unlike with ALS, FUS mutations are very rare, and FUS mutations have not been demonstrated to result in FUS-positive FTD inclusions (Bampton et al., 2020).

Gene	Protein	Reference
TARDBP	TDP-43 (transactive response DNA binding protein 43 kDa)	(Borroni et al., 2009)
FUS	FUS (fused-in-sarcoma)	(Broustal et al., 2010)
TIA1	T cell intracytoplasmic Antigen	(Mackenzie et al., 2017)

Table 1.2 Genes encoding RNA-binding proteins which are mutated in frontotemporal dementia.

1.1.2 Fused-in-sarcoma

FUS, a protein commonly mutated in ALS, is a multi-functional RBP that was initially identified as part of an onco-fusion protein which results in a malignant liposarcoma (Rabbitts et al., 1993). It is part of the FET family of proteins, along with TAF15 (TATA binding associated factor 15) and EWS (Ewing Sarcoma), which are ubiquitously and highly expressed (Svetoni et al., 2016). These proteins are largely homologous, with a number of shared domains: a zinc finger domain (ZnF) for nucleic acid binding; one RNA-recognition motif (RRM); an N-terminal serine-tyrosine-glycine-glutamine (SYGQ) domain; three glycine-arginine (RGG) rich regions, which are also important for RNA-binding (Svetoni et al., 2016).

In addition, all three proteins contain a non-classical C-terminal proline-tyrosine-nuclear localisation signal (PY-NLS). This region is bound by TNPO1 (transportin-1), which promotes the entry of the FET family members into the nucleus (Zhang and Chook, 2012). This domain is important, as all three proteins display a high nuclear localisation compared to the cytoplasm, which is key for a number of their intracellular roles.

1.1.2.1 Physiological roles of FUS

FUS has been demonstrated to have numerous physiological functions related to its capacity to bind RNA, protein and both single- and double-stranded DNA (Ling et al., 2013) (***Table 1.3***). While a strong nuclear localisation is required for many of its functions, FUS also plays many key roles in the cytoplasm (reviewed in Birsa et al., 2019).

Physiological Role	**References**
DNA repair	(Baechtold et al., 1999)
Transcription	(Luo et al., 2015)
RNA splicing	(Rogelj et al., 2012)
Paraspeckle formation	(Nishimoto et al., 2013)
miRNA processing	(Morlando et al., 2012)
RNA stability	(Kapeli et al., 2016)
RNA transport	(Kanai et al., 2004)
Translation	(Yasuda et al., 2013)
The stress granule response	(Sama et al., 2013)

Table 1.3 Physiological roles of the FUS protein.

DNA repair

The binding of FUS to DNA regulates the DNA damage response. FUS knockout mouse fibroblasts exhibit increased chromosome abnormalities and breakage (Hicks et al., 2000). Upon DNA damage, FUS facilitates oligonucleotide 'D-loop' formation, which promotes homologous recombination and repair of double-stranded breaks (DSBs) (Baechtold et al., 1999). In addition, FUS binds other key factors at DSB sites. In cortical neurons, FUS interacts with HDAC1 (histone deacetylase 1) at baseline, though this is markedly increased after induction of DNA damage with etoposide or following laser micro-irradiation (Wang et al., 2013). Further siRNA-mediated knockdown of FUS decreases HDAC1 recruitment to DSBs, suggesting a role for recruitment of proteins to sites of DNA damage.

Transcription

FUS also associates with DNA to regulate transcription. Chromatin immunoprecipitation sequencing (ChIP-seq) has demonstrated that FUS enriches at the transcription start site (TSS) of almost 10,000 genes in a similar pattern to RNA polymerase II (RNAP2) (Schwartz et al., 2012). FUS regulates RNAP2 availability at

the TSS by directly binding its C-terminal domain and preventing hyperphosphorylation of the Ser2 residue.

Splicing regulation

FUS has been demonstrated to alter the splicing of multiple pre-mRNAs. Of note, the FUS protein can autoregulate its own expression by binding *FUS* pre-mRNA (Zhou et al., 2013). Specifically, FUS binds a highly conserved region of exon 7 where it acts as a splicing repressor; the skipping of exon 7 results in nonsense-mediated decay of the transcript. FUS alters the splicing of other transcripts by directly binding their mRNA, as well as binding spliceosomal snRNPs (small nuclear ribonucleoproteins) (Gerbino et al., 2013) and SMN (survival of motor neuron protein), which regulates snRNP maturation (Yamazaki et al., 2012). Individual-nucleotide resolution cross-linking and immunoprecipitation (iCLIP) has demonstrated that FUS binds along the length of RNA, with a saw-tooth pattern in long genes and limited sequence-specificity (Rogelj et al., 2012). Knockout of FUS in embryonic mouse brain altered alternative splicing, with increased FUS iCLIP crosslinking sites detected near repressed exons (Rogelj et al., 2012).

Paraspeckle formation

FUS can bind long non-coding RNAs (lncRNAs) such as *NEAT1*, a key component of paraspeckles, which are a type of nuclear ribonucleoprotein (RNP) granule (Nishimoto et al., 2013). Transfected FUS, as well as TDP-43, colocalises with *NEAT1* in paraspeckles (as labelled by both PSF and PSP1). Further siRNA-mediated knockdown of FUS results in a decreased number of cells with paraspeckles, highlighting a role for FUS in paraspeckle formation (Naganuma et al., 2012). The prion-like domain (PrLD) of FUS is required for its localisation to paraspeckles and promotes paraspeckle formation (Hennig et al., 2015).

miRNA processing

In both the nucleus and the cytoplasm, FUS regulates microRNA (miRNA)-related pathways. miRNA are short non-coding (21-23 nucleotides) RNAs which form part of the RNP microRNA-induced silencing complex (miRISC), which facilitates post-transcriptional silencing of mRNA targets (Zhang et al., 2018). siRNA-mediated FUS knockdown results in deregulation of around 15% of miRNAs, with 90% downregulated (Morlando et al., 2012). In the nucleus, FUS regulates the initial step of pre-miRNA transcription by promoting the recruitment of Drosha to the chromatin of FUS-dependent miRNA loci (Morlando et al., 2012). In the cytoplasm,

downstream of miRNA biogenesis, FUS interacts directly with the core miRISC protein AGO2 (argonaute-2). Further, FUS knockout MEFs demonstrate a decreased capacity to silence a cytoplasmic miRNA-dependent luciferase reporter system (Zhang et al., 2018).

RNA stability

Another cytoplasmic role of FUS is in the regulation of RNA stability, with 330 transcripts stabilised and 44 destabilised in FUS knockdown human neural progenitor cells (Kapeli et al., 2016). For example, in primary hippocampal neurons, FUS promotes the stability of the *GluA1* transcript as part of a protein complex with 3'-end processing factors (Udagawa et al., 2015). Lentivirus-mediated FUS knockdown results in deadenylation, decreased transcript stability and decreased protein levels.

RNA localisation & transport

In the cytoplasm, FUS is also involved in determining the intracellular localisation of RNA. RNA localisation is particularly important in neurons, because they have complex, highly polarised structures, with multiple sub-compartments to maintain. mRNAs are transported as part of RNP complexes via molecular motors, such as kinesin, dynein and myosin (reviewed in Sahoo et al., 2018). Cytoplasmic FUS is present within both dendrites and axons and co-precipitates with both the KIF5 kinesin heavy chain (Kanai et al., 2004) and the myosin-Va motor (Yoshimura et al., 2006). Following mGluR5 (metabotropic glutamate receptor 5) activation in hippocampal neuron cultures, FUS knockout significantly reduces transport of *Nd1-L* transcripts to dendritic spines and leads to abnormal spine morphology; overexpression of *Nd1-L* rescues these abnormalities (Fujii et al., 2005).

Translation

FUS also regulates the translation of cytoplasmic mRNAs. FUS is part of an RNP complex with APC (adenomatous polyposis coli) at mouse fibroblast protrusions, where it regulates translation of constituent RNAs, as determined by both RT-PCR and fluorescence *in situ* hybridisation (ISH) of isolated protrusions (Yasuda et al., 2013).

The stress granule response

FUS is a component of cytoplasmic stress granules (SGs), which will be discussed in detail in ***section 1.3.3***.

1.1.2.2 FUS mutations in ALS

Following the discovery of TDP-43 in ALS inclusions (Arai et al., 2006, Neumann et al., 2006) and missense mutations in the *TARDBP* gene (Gitcho et al., 2008, Sreedharan et al., 2008), the identification of mutations in the *FUS* gene in familial ALS solidified the case for investigation of RNA metabolism in ALS pathogenesis (Kwiatkowski et al., 2009, Vance et al., 2009). Mutations in the *FUS* gene account for 5% of familial ALS cases, as well as a smaller fraction of sporadic cases (Shang and Huang, 2016).

A high proportion of ALS-causing FUS mutations affect amino acids at the C-terminus of the protein, particularly within the NLS (Vance et al., 2013). ALS-causing mutations within the NLS have been demonstrated to weaken the binding of FUS to TNPO1, resulting in increased cytoplasmic FUS protein (Dormann et al., 2010, Swetha et al., 2017). While some of these are point mutations, others are deletions of the whole/parts of the NLS (Belzil et al., 2012, Nakaya and Maragkakis, 2018), or frameshift mutations resulting in a different C-terminal amino acid sequence (DeJesus-Hernandez et al., 2010, Bertolin et al., 2014). NLS mutations are correlated with an increased cytoplasmic mis-localisation of FUS protein and a decreased age of disease-onset (Higelin et al., 2016). Further, over 60% of FUS-ALS cases present with a disease-onset of younger than 45 years old (Shang and Huang, 2016), including some juvenile cases presenting under 20 years (Baumer et al., 2010, Huang et al., 2010).

Recently, NLS-dependent FUS-Transportin 1 interactions have been demonstrated to compete with FUS-FUS interactions. There is increasing evidence that disruption to the NLS increases the propensity of FUS to undergo phase separation (discussed further in ***section 1.2.1.1***) (Yoshizawa et al., 2018). Hence, C-terminal FUS mutations result in a high abundance of aggregation-prone FUS in the cytoplasm, which has major implications for FUS function, as FUS levels are usually tightly autoregulated (Ling et al., 2019). Additionally, many ALS-causing FUS mutations are within low-complexity regions of the protein, highlighting a role for phase separation and the SG response in FUS-ALS pathogenesis (discussed further in ***section 1.3.3***) (Shang and Huang, 2016).

1.1.2.3 Mouse models of FUS-ALS

When studying mutations in genes encoding RBPs, it is critical to have the correct model. A large proportion of the current RBP-related disease research relies on the transfection and/or overexpression of wild-type (WT) and mutant proteins into cells (Bosco et al., 2010). Overexpression models are problematic, as the expression levels of RBPs are usually tightly regulated (Muller-McNicoll et al., 2019). Further, in the study of RNP structures, overexpression can lead to artificial situations. In SG research for example, transfection of key SG RBPs such as TIA1 initiate SG formation in the absence of stressors (Gilks et al., 2004). Likewise, overexpression of WT FUS, a typically nuclear protein, can result in cytoplasmic FUS aggregates (Ju et al., 2011). Taken together, these points highlight the necessity to maintain physiological expression levels when developing models to study RBP-related diseases.

No animal model perfectly models human ALS, so instead the most appropriate model must be matched to the research question (De Giorgio et al., 2019). Researchers have simplified the validation of animal models into three categories: construct, face and predictive validity (van der Staay et al., 2009). Construct validity relates to the mechanism used to induce the animal disease phenotype. For ALS, models with mutations most similar to the human disease, with the same number of mutant alleles will have a higher construct validity. Face validity relates to the ability of the model to replicate the human disease phenotype. In ALS, for example, models which display a progressive degeneration of motor neurons over the lifetime of the animal and a decreased lifespan will have higher face validity. Predictive validity relates to how well a model can be used to predict unknown features of the disease, including the prediction of therapeutic outcomes. This is harder to define in ALS as the most effective treatment, riluzole, only extends lifespan by two to three months, so comparisons to other treatments may not be suitable (van der Staay et al., 2009).

For many years, ALS research has relied on the use of the $SOD1^{G93A}$ mouse model (Gurney et al., 1994). As more genes have been discovered, more mouse models have been developed whereby a disease-like phenotype is driven by the non-physiological overexpression of human transgenes (Alrafiah, 2018). While some of these models exhibit progressive motor-neurodegenerative phenotypes (higher face validity), these may not truly represent the pathomechanisms occurring in human patients with single autosomal dominant point mutations (lower construct validity).

To date, the majority of FUS-ALS mouse models developed (reviewed in detail in De Giorgio et al., 2019) have been transgenic, whereby a human *FUS* transgene was inserted randomly into the mouse genome. Random integration often produces multicopy transgenic lines, thereby encoding FUS at far greater than endogenous levels. In one model, overexpression of WT FUS, driven by the mouse prion protein (PrP) promoter, resulted in progressive hindlimb paralysis, significant loss of large motor neurons and FUS-positive, ubiquitin-negative inclusions in both the spinal cord and brain (Mitchell et al., 2013).

To overcome overexpression artefacts, 'knock-in' FUS mouse models have now been developed whereby the desired gene or mutation is targeted to a specific locus. One study inserted WT or mutant FUS (FUS^{R521C} and FUS^{P525L}) into *MAPT* locus, to produce different mouse models with equal expression levels (Sharma et al., 2016). They demonstrated cytoplasmic mislocalisation of the mutant proteins (not WT protein) but no aggregation. Only mutant FUS was deemed to be toxic in this system, with progressive MN loss and muscle denervation in both mutant models, but not for the WT. This study additionally determined these phenotypes to be cell autonomous, replicating both MN loss and muscle denervation trends in mice expressing the transgenic proteins exclusively in ChAT-positive MNs, by using a CRE-recombinase system.

Gene-targeting has also enabled more complex model generation at endogenous mouse genes, which is preferable as there will only be one copy of FUS in its endogenous locus. One such example is the FUSDelta14 model (Devoy et al., 2017), which will be discussed in detail in ***section 1.1.2.4***. Another example is the FUSΔNLS model, in which mice express a truncated FUS protein where the C-terminal NLS has been removed (Scekic-Zahirovic et al., 2016). This model was also combined with a ChAT-specific CRE-mediated expression system to enable the rescue of this truncation (i.e. the expression of the WT FUS protein) specifically in MNs. As with the Sharma et al. model, mutant FUS was mislocalised to the cytoplasm, and a cell autonomous MN loss phenotype was observed (Sharma et al., 2016).

To test whether a disease mutation causes a of loss-of-function or a gain-of-toxic-function, it is possible to compare both physiological and knockout (FUS-KO) mouse models and cells. While the FUSΔNLS and FUS-KO models are both perinatally lethal and exhibit some overlapping RNA expression changes compared to WT, MN loss is not observed in the FUS-KO model (Scekic-Zahirovic et al., 2016). Sharma

et al. also demonstrated that FUS-KO does not result in MN loss (Sharma et al., 2016). Taken together, the MN death phenotypes observed in overexpression and knock-in models, but not in FUS-KO models, seem to point towards a gain-of-toxic-function for FUS in ALS pathogenesis, rather than a loss-of-function.

1.1.2.4 The FUS-Delta14 model of ALS

The mouse model chosen for use in this thesis is the FUSDelta14 (D14) knock-in mouse model (Devoy et al., 2017), based on an early-onset, rapidly-progressing ALS case (DeJesus-Hernandez et al., 2010). This mouse model expresses a point mutation (A → G) in the splice acceptor site of intron 13, meaning this site is no longer recognised by the spliceosome complex. In turn, the next available splice acceptor site (intron 14) is used, resulting in the deletion of exon 14 from the processed mRNA transcript. The exon 14 deletion induces a single nucleotide frameshift in the downstream sequence, resulting in a different sequence of amino acids being encoded for by exon 15, which removes the entirety of the NLS (***Figure 1.1***). This alternative C-terminal amino acid sequence has enabled the generation of an antibody specific to the mutant protein (FUS-D14), providing a useful tool for the comparison of WT and mutant FUS localisation in heterozygous mutant mice.

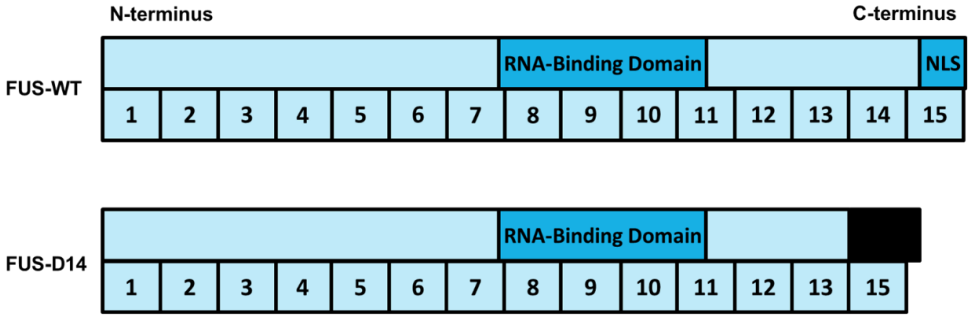

Figure 1.1 The wild-type FUS and FUSDelta14 proteins

The wild-type FUS protein (FUS-WT) is encoded by 15 exons; exon 15 encodes for the nuclear localisation signal (NLS). The FUSDelta14 mouse has a point mutation in the splice acceptor site of intron 13-14, resulting in exon 14 being spliced out of the processed mRNA transcript. This induces a single nucleotide frameshift and a different C-terminal amino acid sequence being encoded by exon 15 for the mutant protein (FUS-D14), removing the NLS (shown in black). The alternative C-termini can be recognised by antibodies specific to either FUS-WT or FUS-D14.

The loss of the NLS from FUS results in the cytoplasmic mislocalisation of the protein, which increases with ageing (from 3- to 18-months). FUS is not completely depleted from the nucleus and does not form cytoplasmic aggregates like those observed in human disease. FUS-D14 does however localise to cytoplasmic SGs, RNP aggregates formed under stress conditions, to a higher extent than WT FUS in D14 mutant fibroblasts treated with sodium arsenite (ARS) (Devoy et al., 2017).

Despite the absence of aggregates, this model displays a progressive motor-neurodegenerative phenotype, with 14% spinal MN loss at 12-months and 20% at 18-months. There is also a decrease in the number of motor units (15%) and neuromuscular junction (NMJ) innervation at 18-months (compared to 3-months). Correspondingly, 3-month old FUSDelta14 heterozygotes do not display motor impairment, but gait is altered at 18-months and hindlimb deficits are observed in the horizontal ladder test at both 15- and 18-months (Devoy et al., 2017).

Unlike the majority of existing ALS models, the FUSDelta14 and FUSΔNLS knock-in models display progressive motor deficits, MN degeneration and cytoplasmic mislocalisation in heterozygosity, despite expressing physiological levels of FUS.

1.1.3 Pathomechanisms in ALS-FTD

Since the discovery of the first ALS mutations in *SOD1*, a combination of cellular, pathological and clinical methods, as well as animal models, have been used to understand the basic mechanisms underlying ALS pathogenesis. This extensive body of research has been reviewed many times in recent years, so for the purpose of this chapter, only *FUS* mutations will be discussed, to illustrate the key pathways identified. Various mutations in *FUS* can result in loss-of-function of the protein, a gain-of toxic-function, or both. Alterations in SG homeostasis and phase separation will be discussed in detail in ***section 1.3.1***.

DNA repair

ALS-mutant FUS has a decreased capacity to promote DNA repair. Transgenic FUS^{R521C} mutant mice have increased γH2AX (H2A histone family member X phosphorylated on serine 139) DNA localisation, indicating increased DNA damage. Further, FUS^{R521C} protein displays a decreased interaction via immunoprecipitation with HDAC1, a key chromatin remodelling factor during DNA damage (Wang et al., 2013, Qiu et al., 2014). Further, transfected GFP-FUS^{R521G} has a reduced capacity

to localise to sites of ultraviolet A (UVA) laser-induced DNA damage (Rulten et al., 2014). Fibroblasts from human ALS patients (FUS^{R521G} and FUS^{P525L} mutations) have increased cytoplasmic FUS localisation and increased DNA strand breaks (Wang et al., 2018); iPSC-derived MNs (from the same patients) show a delay to repair DNA strand breaks compared to control.

Transcription

FUS mutations (FUS^{R521G} and FUS^{R495X}) decrease the amount of FUS bound to active chromatin domains, indicating loss-of-function in transcription (Yang et al., 2014). Further, RNAP2 C-terminal phosphorylation is increased in FUS^{H517Q} and ΔNLS patient fibroblasts, a similar pattern to FUS loss-of-function, and overexpression of the same mutants alters the cellular localisation of RNAP2 (Schwartz et al., 2012).

RNA splicing

FUS mutations result in splicing alterations in its own and other transcripts. Transfection of *FUS* constructs with mutations resulting in increased cytoplasmic localisation (FUS^{R521G}, FUS^{R522G} or $FUS^{\Delta Exon15}$) exhibit defective exon 7 repression and hence altered protein autoregulation (Zhou et al., 2013). Splicing of other transcripts can also be altered by *FUS* mutations. For example expression of mutant FUS (FUS^{R521C} and FUS^{R521H}) in the U87 cell line leads to altered splicing of *MECP2* transcripts (Coady and Manley, 2015). Transfection of both mutants resulted in a >15-fold increase in levels of *MECP2e1*, the shorter splice isoform, but a slight decrease in the longer *MECP2e2* transcript. This resulted in an overall increase in *MECP2* mRNA, which colocalised with FUS protein in cytoplasmic aggregates.

One mechanism by which FUS may alter splicing is via its binding to key nuclear spliceosomal snRNPs. Mutations in FUS do not affect this binding, and hence when mutant FUS (FUS^{R514G}, FUS^{R521G}) is mislocalised to the cytoplasm, so too are these snRNPs (Gerbino et al., 2013).

Paraspeckle formation

FUS promotes the formation of nuclear paraspeckles, and mutations have been demonstrated to alter paraspeckle structure (An et al., 2019, Shelkovnikova et al., 2014). Expression of $FUS^{\Delta NLS}$/FUS^{R522G} in the SH-SY5Y cell line results in cytoplasmic FUS aggregates which sequester the key paraspeckle component NONO (Shelkovnikova et al., 2014). Further, a transgenic mouse model expressing

a truncated FUS protein exhibited both nuclear and cytoplasmic neuronal inclusions, which were positive for WT-FUS and NONO; PSF accumulated in nuclear inclusions only. This was replicated in spinal motor neurons of human FUS-ALS cases, but not other ALS cases or healthy controls (Shelkovnikova et al., 2014).

A more recent study compared CRISPR/Cas9-modified SH-SY5Y cells expressing $FUS^{\Delta NLS}$ to controls, demonstrating that physiological levels of mutant FUS can result in excessive paraspeckle formation and *NEAT1* upregulation (An et al., 2019). However, mutant FUS displays a decreased interaction (by proximity ligation assay; PLA) with key paraspeckle proteins (NONO/SFPQ), indicating that these paraspeckles are defective.

miRNA processing

While knockdown studies have shown FUS to be important for miRNA-mediated silencing, the evidence linking FUS-ALS mutations to miRNA-related pathways is limited. One study however demonstrates that FUS^{R495X} expression, but not FUS^{R521C}, significantly reduces miRNA-mediated silencing in two miRNA-target reporter systems (Zhang et al., 2018). This is likely due to a decreased interaction of FUS with AGO2, as determined by immunoprecipitation in HEK293 cells.

RNA stability

FUS has been determined to regulate the stability of multiple mRNAs. One key pathway altered by FUS-ALS mutations is the nonsense-mediated decay (NMD) pathway, a mechanism by which cells can degrade defective mRNAs. In FUS-ALS fibroblasts (FUS^{R521G}, FUS^{P525R}), NMD complex assembly is promoted, with two activators of NMD (UPF1/UPF3b) upregulated and a negative regulator (UPF3a) downregulated (Kamelgarn et al., 2018). Other studies have suggested that FUS mutations may promote RNA stability; for example, the binding of FUS^{P525L} to the 3' UTR of *ELAVL4* (De Santis et al., 2019).

Intracellular transport

ALS-mutant proteins, including SOD1, TDP-43 and FUS, have been linked to impairments in axonal transport (Bilsland et al., 2010, Alami et al., 2014, Guo et al., 2017). MNs derived from FUS^{R521H} and FUS^{P525L} patient iPSCs, but not those derived from control patient iPSCs, exhibit progressive axonal transport defects; mitochondrial and ER vesicle transport were investigated. These defects can be rescued via CRISPR/Cas9-mediated correction of the *FUS* mutation (Guo et al., 2017).

Translation

Recent work has demonstrated that FUS-ALS mutations can impair axonal protein translation, associated with increased eIF2α phosphorylation, in a transgenic mouse model expressing human FUS^{R521H} (Lopez-Erauskin et al., 2018). Likewise, FUS mutants (FUS^{R522G}, FUS^{R524S}, FUS^{R495X}) transfected into *Xenopus* retinal ganglion cells result in impaired protein synthesis at growth cones (Murakami et al., 2015).

Autophagy regulation

Autophagy is the process by which components within a cell are targeted for degradation and subsequent recycling. It is regulated by a large protein network, which includes the autophagy-related (ATG) proteins, as well as a number of proteins mutated in ALS, such as SQSTM1/p62, optineurin and ubiquilin-2 and VCP (Ramesh and Pandey, 2017). Overexpression of FUS-ALS mutants (FUS^{P525L}, FUS^{R522G}), but not WT-FUS, leads to inhibition of autophagy by preventing the formation of omegasomes (autophagosome precursors) and autophagosomes (Soo et al., 2015). A different study demonstrated that overexpression of WT-FUS or FUS^{R521C} does not impair autophagic flux, but did show that autophagy is key for the removal of FUS-positive SGs (Ryu et al., 2014).

Mitochondrial Function

The localisation of the predominately nuclear FUS protein to the cytoplasm in FUS-ALS has implications for interactions with cytoplasmic organelles, in particular mitochondria. Expression of both WT FUS and FUS^{P525L} in HEK293 cells results in mitochondrial localisation, reduced mitochondrial size, loss of cristae and increased cell death (Deng et al., 2018). This study further demonstrated that FUS binds ATP5B, the catalytic subunit of the mitochondrial ATP synthesis complex, disrupting formation of the complex and activating the mitochondrial unfolded protein response. Mitochondrial damage is also observed in FUS-FTD patient brain samples, when compared with controls (Deng et al., 2015). Further, transcriptomic analysis of FUSDelta14 spinal cords showed a decrease in the expression of transcripts encoding proteins related to mitochondrial function (Devoy et al., 2017).

1.2 The stress granule response

1.2.1 The physiological stress granule response

The world is a hostile place for a cell. Toxic chemicals, temperature perturbations and invasion by pathogens are just a few obstacles to correct cell function. In order to survive both exogenous and endogenous stressors, cells have evolved a variety of programmed coping strategies. One highly conserved mechanism is the assembly of stress-induced membraneless organelles, such as cytoplasmic stress granules (SGs). Initially described in chicken embryo fibroblasts, homologous mechanisms have subsequently been observed in mammalian and plant cells, as well as yeast and other unicellular organisms (Collier and Schlesinger, 1986, Collier et al., 1988).

1.2.1.1 Liquid-liquid phase separation and membraneless organelles

Membraneless organelles are hypothesised to form via liquid demixing and subsequent liquid-liquid phase separation (LLPS); this involves the separation of components within a solution and the formation of smaller, concentrated regions of biomolecules within a larger, more dilute mixture (Guzikowski et al., 2019). This process is thermodynamically favourable, enabling the two distinct phases to co-exist; in this case RNP granules within the bulk cytoplasm.

LLPS is likely driven intracellularly by low-affinity protein-RNA and protein-protein interactions; the latter mediated by protein low complexity domains (LCDs; also known as intrinsically disordered regions (IDR) or prion-like domains) (Molliex et al., 2015). These peptide sequences have a low amino acid diversity, with a small number of charged and polar amino acids overrepresented. These unstructured regions likely form weak interactions with other LCD regions via cation–pi, pi–pi and electrostatic interactions (Vernon et al., 2018). LCDs are a common feature within RBPs (Molliex et al., 2015) and LCD-mediated LLPS has been proposed to be critical for the formation of a number of membraneless cell compartments, including SGs, P bodies, paraspeckles and Cajal bodies.

1.2.1.2 Stress granule structure and dynamics

SGs are 0.1–2 μm RNP granules which are highly dynamic and exhibit liquid-like properties such as fusion, fission and exchange of components with the bulk cytosol, as demonstrated by FRAP (fluorescence recovery after photobleaching) experiments (Wheeler et al., 2016). While SGs are capable of exchanging components with the cytoplasm during the stress response, FRAP experiments have identified a more stable, less-dynamic core at their centre (Jain et al., 2016). In the last two decades, a large body of research has investigated the pathways modulating the assembly, dynamics and disassembly of SGs (***Figure 1.2***).

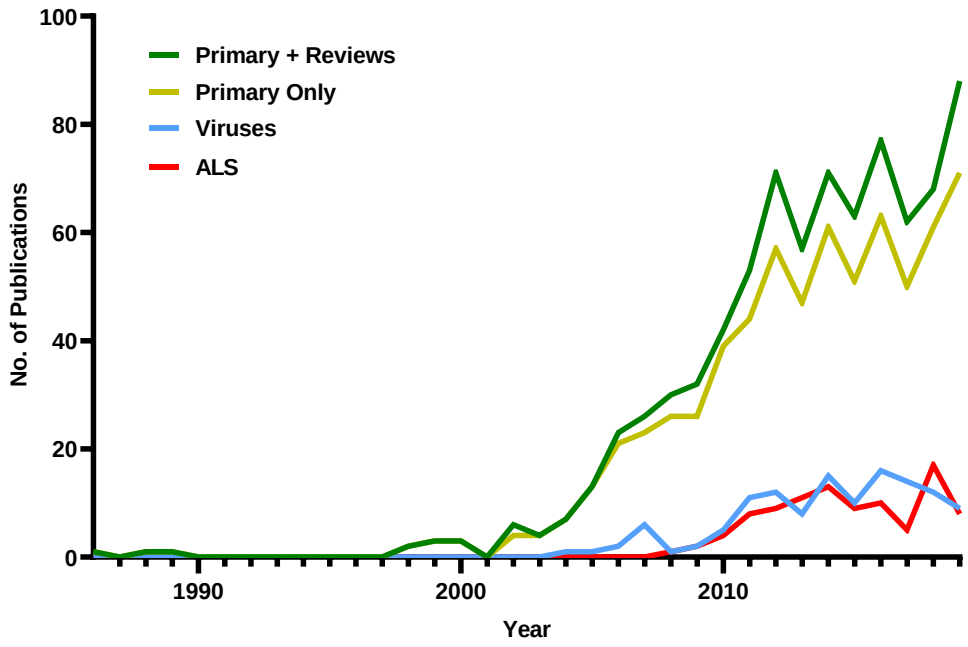

Figure 1.2 The total number of stress granule research articles per year

Primary research articles only (light green); combined primary and review articles (dark green); primary articles linking stress granules to viruses (blue) or amyotrophic lateral sclerosis (ALS; red). PubMed (https://www.ncbi.nlm.nih.gov/pubmed/) was searched for "stress granules" on 27/11/19.

Stress granules: Proteins

While hundreds of proteins have been demonstrated to localise to SGs (Jain et al., 2016, Markmiller et al., 2018), in mammalian cells, only a handful have been determined to be essential for their assembly, including G3BP (GTPase-activating protein-binding protein) (Tourrière et al., 2003) and TIA1 (T cell intracytoplasmic

antigen) (Kedersha et al., 1999). A double knockout of both the G3BP1 (GTPase-activating protein-binding protein 1) and G3BP2 proteins completely blocks SG formation in U2OS cells (Kedersha et al., 2016). Knockout of TIA-1, but not TIAR (TIA1 cytotoxic granule associated RNA binding protein like 1) inhibits SG formation following ARS stress in mouse embryonic fibroblasts (MEFs) (Gilks et al., 2004). Further, overexpression of both proteins induces SGs in the absence of a stress stimulus.

These essential SG proteins likely act as 'drivers' or scaffolds for the assembly of SGs, in turn attracting the 'client' RNAs and proteins with which they would usually interact. While not required for SG formation, a number of client proteins have been demonstrated to be important for normal SG function. Client proteins elicit wide-ranging effects on SG dynamics, assembly, disassembly and function.

It is important to note that SG research has been carried out using vastly different cell-types, types of stressor and duration of stress, and hence conflicting conclusions have often been drawn. While G3BP is deemed essential for ARS-induced SG formation, it is dispensable for osmotic stress and heat shock-induced SGs (Kedersha et al., 2016). Further, proximity labelling via conjugation of the biotinylating enzyme ascorbate peroxidase (APEX) to G3BP and subsequent mass spectrometry, has demonstrated that the SG proteome differs between both cell-type and stress-type (Markmiller et al., 2018). These studies highlight the importance of identifying differences in experimental setup when comparing SG studies.

Stress granules: RNAs

Early SG research determined that granule markers colocalise with poly(A)-positive mRNA (Kedersha et al., 2000), but in recent years, it has been possible to isolate SG cores and subsequently perform RNA sequencing to identify the species contained within SGs (Khong et al., 2017). These studies confirm the presence of mRNA (78% of transcripts), as well as non-coding RNAs. In addition, single molecule fluorescence ISH has demonstrated that SGs induced by different stressors can result in different local transcriptomes; for example *POLR2A* mRNA is enriched in SGs following sorbitol stress and heat shock when compared to thapsigargin and ARS.

RNA also plays an important role in SG formation and dynamics. The presence of RNA promotes LLPS for HNRNPA1 and FUS (Molliex et al., 2015, Lin et al., 2015). While the LCD of HNRNPA1 undergoes LLPS alone *in vitro*, RNA increases its

propensity to do so (Molliex et al., 2015). This is further increased by the presence of its RNA-recognition motif (RRM), and further by the full-length protein. RNA is able to self-assemble *in vitro*, and these interactions also likely promote the formation of membraneless structures *in vivo* (reviewed in Van Treeck and Parker, 2018).

Stress granules: Post-translational modifications

Post-translational modifications (PTMs) of SG components have also been demonstrated to alter the structure and dynamics of SGs, including phosphorylation (Tourrière et al., 2003, Stoecklin et al., 2004), methylation (Dolzhanskaya et al., 2006, De Leeuw et al., 2007, Goulet et al., 2008), ubiquitination (Kwon et al., 2007) and O-GlcNAcylation (Ohn et al., 2008).

For example, phosphorylation of the key SG driver protein G3BP at Ser149 regulates SG formation, with ARS-induced stress promoting dephosphorylation of this site (Tourrière et al., 2003). Accordingly, a phosphomimetic G3BP mutant (S149E) prevents self-association of the protein and does not induce SGs when transiently expressed in the Cos cell line (Tourrière et al., 2003). Likewise phosphorylation of tristetraprolin (TTP), a protein localised to SGs following FCCP-induced mitochondrial stress, at Ser52 and Ser178 by MAPKAP kinase-2 (MK2) excludes it from SGs and leads to the formation of cytoplasmic RNP complexes with AU-rich mRNA (Gilks et al., 2004).

Other PTMs can promote protein localisation to SGs. Methylation of the cold-inducible RNA-binding protein (CIRP) at arginine residues in its RGG domain is necessary for the protein to exit the nucleus and subsequently enter SGs (De Leeuw et al., 2007). SGs are also highly positive for ubiquitin, and histone deacetylase 6 (HDAC6) requires its ubiquitin-binding domain to form SGs (Kwon et al., 2007).

Dynamic regulation of SG protein PTMs likely promotes rapid SG formation under stress conditions, and rapid disassembly upon stress cessation.

1.2.1.3 Stress granule assembly and translation inhibition

The assembly of SGs appears to be tightly linked to translation inhibition, with multiple translation-related pathways initiating the SG response. This link is highlighted by the observation that SG markers colocalise with 40S ribosomal

subunits and various translation factors, but not 80S subunits, suggesting that SGs contain stalled translation pre-initiation complexes (Kedersha et al., 2002, Kimball et al., 2003). SGs are hypothesised to be in dynamic equilibrium with actively translating polysomes (Kedersha et al., 2000), with pathways that initiate translation inhibition resulting in the disassembly of polysomes, in turn releasing mRNAs which, along with RBPs and other proteins, form into membraneless organelles (Aulas et al., 2017). This hypothesis appears to be true experimentally, with compounds that trap mRNA within polysomes (e.g. cycloheximide) preventing SG formation (Kedersha et al., 2000). Conversely, compounds which promote polysome disassembly, such as puromycin, increase SG formation (Kedersha et al., 2000).

The two best characterised pathways which induce both translation inhibition and SG formation are the eIF2 and eIF4F pathways. eIF2 forms a ternary complex with the initiator methionine tRNA ($tRNA_i^{Met}$) and GTP, which acts to deliver $tRNA_i^{Met}$ to the 40S subunit and mRNA start codon (Wolozin and Ivanov, 2019). Different stressors activate a number of protein kinases (PERK, HRI, GCN2, PKR), which converge on the phosphorylation of the eIF2α (eukaryotic translation initiation factor 2α) subunit at its Ser51 residue. This phosphorylation inhibits reloading of the ternary complex with GTP, preventing translation inhibition. Of the four kinases, ARS-induced eIF2α phosphorylation and SG formation are only inhibited in HRI (heme-regulated inhibitor kinase) knockout MEFs (McEwen et al., 2005), while thapsigargin-induced endoplasmic reticulum stress requires PERK (protein kinase RNA-like endoplasmic reticulum kinase) (Aulas et al., 2017).

eIF4F is an mRNA cap-binding complex of three translation intiation factors: eIF4A, eIF4E and eIF4G. eIF4F binds the 5’-cap of mRNA and interacts with PABP (poly(A)-binding protein) bound at the 3’-end, which promotes translation intiation (Wolozin and Ivanov, 2019). At baseline, mTOR (mammalian target of rapamycin) constitutively phosphorylates eIF4E-binding protein (4E-BP), which prevents 4E-BP binding to eIF4E. Under stress conditions however, mTOR becomes inactivated, resulting in avid binding of 4E-BP to eIF4E, leading to diassembly of eIF4F from the mRNA 5’-cap. Some chemical stimuli target this pathway to induce SGs, independent of eIF2α phosphorylation, including selenite (Fujimura et al., 2012) and hydrogen peroxide (Emara et al., 2012).

1.2.1.4 Stress granule functions

The formation of SGs during cellular stress has long been determined to be pro-survival, with an inability to form SGs often correlated with increased cell death during stress. Knockdown of SG driver proteins (e.g. G3BP) (Wang et al., 2019b) or treatment with compounds that negatively regulate SG formation (Christen et al., 2019), decrease cell viability during ARS and other chemical stresses. Further, knockdown of other SG proteins, such as RSK2 (p90 ribosomal S6 kinase) and TDP-43, decrease cell survival during stress (Eisinger-Mathason et al., 2008, Aulas et al., 2012).

It has been suggested that SGs may sequester RNAs and proteins to remove them from the cytoplasm, thereby altering the non-SG cytosolic transcriptome and proteome. There is a specificity to the proteins and RNAs sequestered by SGs, resulting in a modulation of the stress-specific proteome and transcriptome, which can differ by both cell-type and stressor-type (Khong et al., 2017, Markmiller et al., 2018). This specificity in SG composition likely reflects a need for certain species to remain in, or be sequestered from, the cytosol during specific stress responses.

One well-characterised pathway that SGs have been determined to modulate is apoptosis. Type I stressors (e.g. ARS or heat shock) induce SG formation, while type II stressors (e.g. X-rays) induce apoptosis. RACK1 (receptor for activated C kinase 1) localises to SGs during type I stress, preventing its binding to the key apoptosis mediator MTK1 and subsequent induction of the stress-activated p38 and JNK MAPK (SAPK) pathway and apoptosis (Arimoto et al., 2008). Expression of a non-ribosome-binding RACK1 mutant, which does not localise to SGs, prevents inhibition of apoptosis during Type I stress. Further, when both stressors are applied, RACK1 sequestration into SGs prevents Type II-induction of SAPK and apoptosis. SGs also alter mTORC1 (mTOR complex 1)-induced apoptotic signalling by recruiting raptor (Thedieck et al., 2013).

SGs can also modulate other signalling pathways. Under heat stress conditions, SGs modulate the tumour necrosis factor (TNF) signalling pathway by sequestering TNF-α receptor-associated factor 2 (TRAF2) (Kim et al., 2005). This sequestration prevents its cytoplasmic interaction with TNFR1 (tumour necrosis factor receptor 1), reducing activation of NF-κB.

It is important to note that not all SGs have been deemed to be pro-survival. SGs induced by selenite are non-canonical and do not immunostain for eIF3B or the pro-

surival proteins RACK1, Rsk2 and HDAC6 (Fujimura et al., 2012). A separate study further demonstrated that during 3-morpholinosydnonimine (SIN-1)-induced nitric oxide (NO) stress, the initial SGs that form are similar to those induced by ARS (i.e. pro-survival SGs), though these convert to eIF3B-negative, pro-death SGs over time (Aulas et al., 2018). The formation of eIF3B-negative SGs appears to promote cell death; SIN-1-induced cell death is significantly reduced by G3BP1/2 double knockout, pharmacological inhibition of SG formation and mutations preventing eIF2α Ser51 phosphorylation (S51A).

1.2.1.5 Stress granule disassembly

Sub-lethal stressors induce the formation of transient SGs, which should disassemble within hours from the point when the stressor is removed, while lethal stressors result in permanent SG assembly and subsequent cell death (Kedersha et al., 1999). SG disassembly facilitates the release of component RNAs and proteins into the cytoplasm, allowing them to reprise their basal functions and ensure cell recovery. This recycling process comes at a lower energy cost compared to degradation and *de novo* synthesis of these components.

Disassembly is facilitated by a number of known pathways. Following proteasome inhibition, HSP72 (heat shock protein 72) is required for the disassembly of SGs; HSP72 is upregulated during stress, overexpression prevents SG formation and siRNA-mediated knockdown reduces SG disassembly and translation recovery (Mazroui et al., 2007). Recruitment of Hsp70 and other chaperones has been suggested to prevent the formation of more solid-like phase separations (termed ‘aberrant’ SGs) and promote SG disassembly. HSP27/HSP70 chaperones are recruited to aberrant SGs preferentially and pharmacological HSP70 inhibition promotes SG persistence (Mateju et al., 2017).

Persisting aberrant SGs can be targeted to the aggresome for degradation by autophagy. Six hours following stress cessation, remaining SGs colocalise with the autophagy receptor p62 and vimentin (Mateju et al., 2017). In the presence of the autophagy inhibitor wortmannin, most SGs disassemble rapidly and persisting SGs decrease in size, though SG markers colocalise with the aggresome. Taken together this data highlights that SGs can be disassembled rapidly, or targeted for degradation by autophagy. Another study supported this conclusion, demonstrating that only a small fraction of SGs require autophagy for removal, with the majority

requiring Hsp70 chaperones (Ganassi et al., 2016). Knockdown of the ALS-associated protein VCP has also been shown to impair SG removal via autophagy (Buchan et al., 2013).

The balance between SG assembly and disassembly is tightly regulated, and failure to manage these processes has profound implications for cell health. On one hand, a failure to assemble SGs may harm the chances of a cell surviving a stressful event, such as invasion by a pathogen. On the other hand, defective SG disassembly has been hypothesised to promote the formation of the aggregates associated with ALS and other neurological diseases. Both of these concepts will be discussed in the next chapter.

1.3 Stress granules and disease

Almost two decades after the discovery of stress-induced membraneless organelles, research groups in widely different fields began to link them to disease. Unsurprisingly, as infection manipulates multiple stress-related pathways, SGs have been demonstrated to modulate the pathogenesis of both viral and bacterial diseases. In addition, a rich literature has proposed a role for SGs in the progression of neurological diseases, in particular amyotrophic lateral sclerosis (ALS). Further human diseases associated with SG homeostasis are displayed in ***Table 1.4***.

Disease/Condition	**No. of Primary Articles**	**Example reference**
Alzheimer's Disease	4	(Ash et al., 2014)
ALS-FTD	95	See ***Section 1.3.3***
Atherosclerosis	1	(Herman et al., 2019)
Atrial fibrillation	1	(Dong et al., 2019)
Bacterial Infection	2	(Vonaesch et al., 2017)
Cancer	25	(Valentin-Vega et al., 2016)
Fragile X Syndrome	2	(Didiot et al., 2009)
Hearing Loss	2	(Towers et al., 2011)
High Fat Diet	1	(Bai et al., 2016)
Inclusion body myositis (IBM)	1	(Rodriguez-Ortiz et al., 2016)
IBM-like Diseases	1	(Wang et al., 2019a)
Inflammation	2	(Ansari and Haqqi, 2016)
Ischemia	4	(Ayuso et al., 2016)
Kidney Disease	2	(Wang et al., 2019b)
Multisystem proteinopathy (MSP)	1	(Kim et al., 2013)
Multiple Sclerosis	2	(Salapa et al., 2018)
Myopathy	1	(Mensch et al., 2018)
Myotonic Dystrophy	2	(Ravel-Chapuis et al., 2016)
Neurodegeneration (in general)	4	(Mateju et al., 2017)
Parkinson's Disease	1	(Repici et al., 2019)
Prion Disease	1	(Goggin et al., 2008)
Retinitis pigmentosa	1	(Fathinajafabadi et al., 2014)
Spinocerebellar ataxia (SCA)	2	(Nonhoff et al., 2007)
Spinal Muscular Atrophy (SMA)	3	(Zou et al., 2011)
Systemic Sclerosis	1	(Johnson et al., 2016)
Tauopathies	7	(Vanderweyde et al., 2012)
Trypanosome Infection	1	(Kramer et al., 2008)
VCP-related Diseases	1	(Wang et al., 2016b)
Viral Infection	125	(Visser et al., 2019)
Welander Distal Myopathy	1	(Hackman et al., 2013)

Table 1.4 Diseases associated with stress granules, the number of primary research articles published concerning this link and a referenced example article.

1.3.1 Stress granules and viral infection

A large body of research has investigated the link between SGs and viruses. Viral infection induces SG formation via both eIF2a-dependent and independent mechanisms and SGs are thought to be antiviral (Zhang et al., 2019b). Both RNA and DNA viruses have been demonstrated to activate PKR (protein kinase R), a kinase which phosphorylates eIF2a resulting in SG formation. PKR interacts with double stranded-RNA (dsRNA), which induces dimerization and subsequent phosphorylation, resulting in activation (Willis et al., 2011).

Purified dsRNA from dsRNA viruses (e.g. rotaviruses) can directly activate PKR (Rojas et al., 2010), while single stranded RNA (ssRNA) from ssRNA-viruses (e.g. HIV1) can dimerise to form dsRNA, promoting dimerization of PKR monomers (Heinicke et al., 2009). DNA viruses can also activate PKR. Early gene transcription of the dsDNA genome of the vaccinia virus generates dsRNA and activates PKR, a mechanism suppressed by the viral K1 protein (Willis et al., 2011). Viruses can also induce eIF2a phosphorylation independent of PKR activation. The ssRNA genome of the Sindbis virus enhances GCN2 autophosphorylation, increases eIF2a phosphorylation and inhibits early viral translation (Berlanga et al., 2006). Other viruses, such as the Rift Valley fever virus, inhibit global translation by inhibiting 4E-BP phosphorylation (Hopkins et al., 2015).

SGs appear to be cytoprotective during viral stress, as viruses have evolved strategies aimed at inhibiting SG formation. Unlike some viruses, infection of cells with poliovirus (PV) or encephalomyocarditis virus (EMCV) induces acute SGs which are resolved by later timepoints (SGs present at 2 hours post-infection but not at 4-6 hours) (White et al., 2007, Ng et al., 2013). SG resolution correlates with increased viral replication, and the SG driver protein G3BP1 is cleaved by viral cysteine proteases ($3C^{pro}$ protein for PV infection). Expression of cleavage-resistant G3BP1 rescues SG presence at later timepoints. The foot-and-mouth disease virus leader protease (L^{pro}) cleaves both G3BP1 and G3BP2, and this is conserved in related viruses (Visser et al., 2019). For EMCV, expression of the cleavage-resistant mutant also enhances cytokine induction (IL-6, INF-β mRNA) at later timepoints, highlighting the importance of SG presence during viral infection (Ng et al., 2013).

Other viruses, such as the Zika Virus (ZIKV), hinder SG formation by binding and sequestering SG component proteins (Hou et al., 2017). Immunoprecipitation assays demonstrate ZIKV capsid proteins bind to key SG proteins G3BP1 and

Caprin1, while G3BP1 also interacts with ZIKV genomic RNA. Further, siRNA-mediated knockdown of G3BP1 and Caprin1 decrease ZIKV replication, suggesting that these components may be hijacked by the virus. Similarly, Ebola virus (EBOV) infection does not induce SGs, and the EBOV protein VP35 blocks ARS-induced SGs when transfected into mammalian cells (Le Sage et al., 2017). Transfected VP35 has no effect on eIF2a phosphorylation and binds SG components (G3BP1, eEF2 and eIF3), suggesting EBOV may inhibit SG formation by sequestering key driver proteins.

In summary, a wide variety of viruses have developed mechanisms to overcome the host cell SG response. Promoting the SG response during acute infection may prove useful in developing novel antiviral therapies.

1.3.2 Stress granules and cancer

SGs have also been identified as a potential target in cancer research, with both tumours and chemotherapeutic agents demonstrated to alter SG formation (reviewed in Gao et al., 2019). Tumours with mutations in the *KRAS* gene, which encodes the GTPase K-Ras, have high chemotherapeutic resistance (Wang et al., 2010). *KRAS*-mutant cells have increased SG coverage per cell area compared to non-*KRAS* cancer cells following treatment with ARS or chemotherapeutic drugs such as oxaliplatin and bortezomib. An increase in SGs is also observed *in vivo*, in pancreatic lesions of a *KRAS*-mutant mouse model and in human pancreatic adenocarcinoma, compared to adjacent normal pancreatic tissue. Blocking the formation of SGs in *KRAS*-mutant cells with emetine (which stalls mRNA on polysomes) enhances apoptosis following ARS stress. Treatment with diclofenac sodium, a cyclooxygenase (COX) inhibitor, inhibits SG formation and decreases *KRAS*-mutant cell viability in response to oxaliplatin.

A range of chemotherapeutic drugs have been demonstrated to induce SG formation including sorafenib (Adjibade et al., 2015), bortezomib (Fournier et al., 2010), 5-fluorouracil (Kaehler et al., 2014) and vinca alkaloid drugs (Szaflarski et al., 2016). The natural product psammaplysin F, which is isolated from a marine sponge, has recently been demonstrated to inhibit SG formation and prevent eIF2α phosphorylation in mammalian cells (Christen et al., 2019). Co-administration of psammaplysin F with chemotherapeutic agents (bortezomib and sorafenib), increased the efficacy of these drugs, decreasing the viability of three cancer cell lines.

SGs appear to be beneficial to tumour cells during chemotherapy, so using compounds which inhibit SG formation in conjunction with standard chemotherapy drugs may increase therapeutic efficacy.

1.3.3 Stress granules and ALS-FTD mutations

Besides viral infection, the largest body of SG disease research pertains to neurological diseases, in particular those associated with ageing, such as ALS. The link between SGs and neurodegenerative diseases (NDDs) is logical, as both are associated with protein aggregation. This association has led many groups to hypothesise that altered phase separation or SG homeostasis could result in the build-up of disease inclusions over time.

A large number of the proteins which are mutated in ALS-FTD have been demonstrated to localise to SGs, including both RBPs and non-RBPs, such as VCP, DCTN1, PFN1 and TUBA4A (shown in ***Table 1.5***). A handful of the RBPs mutated in ALS have been demonstrated to undergo LCD-driven phase separation *in vitro* (hnRNPA1, FUS, TIA1), with further evidence that ALS-causing mutations increase their propensity to do so (Molliex et al., 2015, Murakami et al., 2015, Mackenzie et al., 2017). Further, ALS-causing mutations have been shown to elicit varying effects on SG dynamics, abundance and morphology, as shown in ***Table 1.6***.

Gene	Reference
FUS	(Markmiller et al., 2018, Jain et al., 2016)
TDP-43	(Jain et al., 2016)
VCP	(Jain et al., 2016)
TIA1	(Markmiller et al., 2018, Jain et al., 2016)
C9ORF72	(Maharjan et al., 2017)
ANG	(Pizzo et al., 2013)
ATXN2	(Markmiller et al., 2018, Jain et al., 2016)
DCTN1	(Jain et al., 2016)
PFN1	(Jain et al., 2016)
hnRNPA1	(Jain et al., 2016)
SFPQ	(Jain et al., 2016)
TUBA4A	(Jain et al., 2016)

Table 1.5 ALS mutant proteins which localise to stress granules.

Gene	Reference	Effect
TIA1	(Mackenzie et al., 2017)	Delayed SG Disassembly
TDP-43	(Dewey et al., 2011)	Larger SGs
TDP-43	(Orru et al., 2016)	Fewer SGs
TDP-43	(Gopal et al., 2017)	Less dynamic SGs
FUS	(Baron et al., 2013)	Delayed SG Assembly Larger SGs More abundant SGs More dynamic SGs Faster SG Disassembly
C9ORF72	(Boeynaems et al., 2017)	Less Dynamic
PFN1	(Figley et al., 2014)	Impaired SG assembly Delayed SG disassembly
SOD1	(Gal et al., 2016)	Delayed SG assembly

Table 1.6 The effects of ALS-causing mutations on stress granule dynamics and morphology

Stress granules: FUS

Despite research demonstrating that WT FUS is not included within SGs following oxidative stress (Andersson et al., 2008, Sama et al., 2013), studies using more sensitive techniques, such as mass spectrometry and proximity labelling have confirmed its presence (Jain et al., 2016, Markmiller et al., 2018). This finding is unsurprising, as WT FUS can undergo LLPS *in vitro*, with ALS-causing mutations increasing its propensity to do so (Murakami et al., 2015, Patel et al., 2015). Despite its localisation, WT FUS has not been demonstrated to have an impact on SG dynamics following oxidative stress (Aulas et al., 2012). However WT FUS has been shown to play a more important role during osmotic stress. Sorbitol-induced osmotic stress results in the redistribution of FUS from the nucleus to the cytoplasm and its inclusion within SGs in HeLa cells (Sama et al., 2013), neurons and microglia, but

not astrocytes (Hock et al., 2018). Further, an shRNA-mediated reduction in FUS levels decreases the survival of NSC-34 cells following sorbitol stress, but not ARS-induced stress, indicating a pro-survival role for FUS during hyperosmolar stress (Sama et al., 2013).

While WT FUS appears to be present in SGs at low levels, mutations in *FUS* result in a much higher inclusion of the mutant protein (Bosco et al., 2010). This is also the case in model systems where the FUS protein is expressed at physiological levels, such as patient-derived fibroblasts (Lo Bello et al., 2017) and iPSC-derived MNs (Lenzi et al., 2015), as well as knock-in mouse models (Devoy et al., 2017). This increase correlates with the amount of cytoplasmic FUS mislocalisation induced by the mutation (Dormann et al., 2010). Mutations impairing TNPO1 binding to the FUS PY-NLS promote cytoplasmic mislocalisation, but also promote cytoplasmic aggregation in a second manner: as well as mediating nuclear import, TNPO1 can also act as cytosolic chaperone. By binding WT FUS, but not NLS mutants, TNPO1 regulates the LLPS dynamics of FUS and its inclusion into SGs (Hofweber et al., 2018, Guo et al., 2018).

ALS-causing mutations in *FUS* have been demonstrated to alter SG dynamics and properties. In FUS^{P525L} fibroblasts, FUS was severely mislocalised to the cytoplasm and SGs, SGs were more numerous and they persisted for longer after stress cessation (Lo Bello et al., 2017). One recent study used background-deflection Brillouin microscopy to demonstrate that expression of mutant FUS (FUS^{P525L}) in HeLa cells increases both the stiffness and viscosity of SGs (Antonacci et al., 2018); these properties may explain the slowed disassembly of the granules. Likewise, transgenic zebrafish (*Danio rerio*) expressing FUS^{R521C} displayed increased SG assembly and slower disassembly in cultured neurons when compared with neurons from transgenic FUS^{WT} animals (Acosta et al., 2014). However, a conflicting study showed that expression of mutant FUS (FUS^{R495X}, FUS^{H517Q}) in HEK293 cells slowed SG assembly and resulted in more dynamic SGs, which disassembled faster (Baron et al., 2013).

Stress granules: TDP-43

The WT TDP-43 protein has also been demonstrated to localise to SGs following osmotic stress by immunostaining (Dewey et al., 2011), as well as by ARS treatment by both immunostaining (Colombrita et al., 2009) and mass spectrometry (Jain et al., 2016). Other studies however have demonstrated that it does not localise to SGs: by immunostaining (Orru et al., 2016) and by proximity labelling using G3BP-linked APEX in HEK293T cells (Markmiller et al., 2018). Unlike FUS, TDP-43 knockdown has been demonstrated to impact on SG dynamics, causing both delayed assembly/coalescence and accelerated disassembly of SGs, through alteration of the expression of key SG proteins, such as G3BP1 and TIA1 (McDonald et al., 2011, Aulas et al., 2012, Khalfallah et al., 2018).

ALS-mutant TDP-43 has also been demonstrated to impact upon various aspects of SG biology, increasing SG size (Dewey et al., 2011) and decreasing SG abundance (Orru et al., 2016). In human fibroblasts, the $TARDBP^{A382T}$ mutation has been demonstrated to reduce SG formation independently of SG localisation, by downregulating the expression of the SG driver protein G3BP1 (Orru et al., 2016).

TDP-43 has been demonstrated to undergo LLPS *in vitro* (Molliex et al., 2015) and form aggregates *in vitro* and in yeast, with ALS-causing mutations increasing its propensity to aggregate (Johnson et al., 2008). Further, similar mutations have been demonstrated to alter the biophysical properties of RNP granules within neurons. Axonal TDP-43 granules display liquid-like properties (including fusion and rapid FRAP), with mutations disrupting transport and increasing granule viscosity (by FRAP experiments) (Gopal et al., 2017). These alterations have implications for SG properties.

Stress granules: VCP

VCP (valosin-containing protein) is an ATPase that regulates a range of intracellular pathways by binding to ubiquitylated proteins including autophagy, a process which in-part influences SG disassembly (Meyer and Weihl, 2014). Both immunostaining and mass spectrometry have demonstrated the localisation of VCP to SGs (Buchan et al., 2013, Jain et al., 2016). VCP is thought to be required for normal SG dynamics: both siRNA-mediated knockdown and chemical inhibition of VCP activity (Eeyarestatin I; DBeQ; ML240) result in defective SG clearance following stress cessation (Buchan et al., 2013).

Mutations in VCP result in both ALS and FTD (Koppers et al., 2012), and the overexpression of FTD-causing VCP mutants (VCP^{A232E} and VCP^{R155H}) in HeLa cells induces SG-like granule formation which co-localises with eIF3 and TDP-43 (Buchan et al., 2013). siRNA-mediated knockdown of VCP, and its autophagy cofactors (PLAA and UFD1L), has also been demonstrated to impair SG induction by both proteasome inhibition and ARS (Seguin et al., 2014). Pathological mutations at the N-terminus of VCP inhibit its SUMOylation, which in WT cells serves to promote stress-induced co-factor binding, targeting of VCP to SGs and decrease cell vulnerability to stress (Wang et al., 2016b).

Stress granules: SOD1

Mutations in the *SOD1* gene, which encodes superoxide dismutase 1, were the first to be identified as causative for ALS (Rosen et al., 1993) and account for 20% of familial ALS cases. It is believed that these mutations induce a gain-of-function, though the mechanism of toxicity is still not fully understood. Though the inclusions formed in SOD1-ALS pathogenesis are not positive for TDP-43 like the majority of ALS cases (Mackenzie et al., 2007), both SOD1- and TDP-43-immunoreactive ALS have been linked to SGs.

Unlike the WT SOD1 protein, mutant SOD1 ($SOD1^{A4V}$, $SOD1^{G85R}$ and $SOD1^{G93A}$) has been demonstrated to bind to the SG driver protein G3BP1 by immunoprecipitation in an RNA-independent manner (Gal et al., 2016). Further, G3BP1 has been detected in SOD1 pathological inclusions in spinal cord tissue from transgenic $SOD1^{G93A}$ mice, as well as in human patient fibroblasts ($SOD1^{L144F}$). A separate study showed that stably-expressed $SOD1^{A4V}$ mutant protein, but not $SOD1^{WT}$, in HeLa cells colocalises with stably-expressed FUS in SGs (Mateju et al., 2017). In terms of dynamics, expression of mutant $SOD1^{A4V}$ by transfection in N2A cells interferes with SG assembly, decreasing the number of SGs following 30 minutes of ARS or hyperosmolar stress compared to WT; this catches up by 60 minutes (Gal et al., 2016).

Stress granules: C9ORF72

Hexanucleotide repeat expansions in a non-coding region of *C9ORF72* (G_4C_2) are linked to the highest percentage of ALS cases (7% and 39% of sporadic and familial cases respectively) (Majounie et al., 2012). It remains to be determined whether

these expansions result in a loss-of-gene function or a gain-of-toxic RNA or protein function. These hexanucleotide repeats are both transcribed, and translated by RAN translation into dipeptide repeat (DPR) proteins (Balendra and Isaacs, 2018).

Repeat expansions result in decreased expression of the endogenous C9ORF72 protein (Waite et al., 2014). This may impact SG dynamics, as C9ORF72 has been demonstrated to play a role in the regulation of autophagy, which itself plays a role in SG disassembly. Endogenous C9ORF72 protein immunoprecipitates with SG proteins and localises to SGs following a range of stressors in both cell lines and neurons (Maharjan et al., 2017, Chitiprolu et al., 2018). siRNA-mediated knockdown of C9ORF72 dysregulates autophagosome formation, a key step in autophagy, (Farg et al., 2014) and decreases SG disassembly (Chitiprolu et al., 2018). A separate study showed a drastic inhibition of SG assembly following CRISPR/Cas9-mediated knockdown of C9ORF72, potentially via a large reduction in TIA-1 and HuR (human antigen R) protein levels (Maharjan et al., 2017).

In terms of gain-of-function, both C9ORF72 RNA and DPR proteins have been demonstrated to perturb the SG response. Transfection of $(G_4C_2)_n$ RNA, but not $(C_4G_2)_n$ RNA, induces the formation of G3BP1-positive granules (also positive for eIFs and poly(A)-mRNA) in a repeat-length-dependent manner; in addition, it promotes *in vitro* phase separation (Fay et al., 2017). Arginine-rich DPRs (PR and GR; proline-arginine and glycine-arginine) can also undergo *in vitro* phase separation, and overexpression of $(PR)_{100}$ (100 proline-arginine dipeptide repeats) in human cell lines induces DPR/G3BP-positive puncta, which are dependent upon G3BP expression and eIF2α phosphorylation for formation (Boeynaems et al., 2017). PR_{100}-containing SGs are less dynamic than ARS-induced SGs, displaying a slower FRAP recovery time. Granules induced by overexpression of $(GR)_{50}$/$(PR)_{50}$ are also poorly dynamic (Lee et al., 2016).

Stress granules: TIA1

TIA-1 is one of the key SG driver proteins that, if knocked out inhibits SG formation and if overexpressed, induces SG formation (Gilks et al., 2004). One of the most compelling pieces of evidence for the link between SGs and ALS pathogenesis is the observation of ALS-causing mutations in the *TIA1* gene (Mackenzie et al., 2017); other groups have however suggested that there is insufficient evidence to support this causality (van der Spek et al., 2018). *In vitro*, these mutations ($TIA1^{P362L}$, $TIA1^{A381T}$, and $TIA1^{E384K}$) result in an increased propensity of TIA-1 to undergo LLPS, and when transfected into HeLa cells, these mutant proteins drastically impair SG disassembly compared to $TIA1^{WT}$ expression; 3-7 fold increase in the number of cells displaying SGs after 2 hours for all mutations.

Stress granules: ATXN2

Ataxin-2 is an RBP which contains a poly-glutamine (polyQ; CAG_n) region, expansions in which have been demonstrated to cause the neurodegenerative disease spinocerebellar ataxia type 2 (SCA2; >34 repeat expansions) (Imbert et al., 1996). Intermediate length expansions (23-34 repeats) have also been identified as a risk factor for ALS (Elden et al., 2010).

Ataxin-2 has been demonstrated to bind directly to PABP, an often used SG marker, and localises to SGs under stress conditions (Ralser et al., 2005, Nihei et al., 2012). In addition, it co-localises with FUS in both granules induced by mutant FUS (FUS^{R521C}, FUS^{R521H}) transfection and in patient spinal cord inclusions (both sporadic and familial cases) (Farg et al., 2013). Ataxin-2 levels also appear to regulate SG formation, as siRNA-mediated knockdown drastically reduces the number of SGs per cell (Nonhoff et al., 2007).

Stress granules: PFN1

Mutations in *PFN1*, which encodes the profilin 1 protein, have been demonstrated as a cause of familial ALS (Wu et al., 2012). Profilin 1 interacts with the ataxin-2 protein and localises to SGs, but siRNA-mediated knockdown does not alter SG assembly or disassembly kinetics in U2OS cells (Figley et al., 2014). In the same cell-type however, transfection of ALS-mutant PFN1 protein does alter SG dynamics compared to WT, indicating a potential gain-of-function mechanism. It is worth

noting that transfection of WT PFN1 induces SG formation in 19% of cells in the absence of stress and transfection of all mutant and WT proteins delayed SG disassembly (in particular PFN^{E117G}). Further, $PFN1^{C71G}$, $PFN1^{M114T}$, and $PFN1^{T109M}$ impaired assembly of PFN1 transfection granules and were less enriched in arsenite-induced SGs.

Stress granules: hnRNPA1

Mutations in the gene encoding the RBP hnRNPA1 (Heterogeneous nuclear ribonucleoprotein A1) have been observed in rare cases of ALS (Kim et al., 2013, Naruse et al., 2018). hnRNPA1 undergoes both *in vitro* LCD-mediated LLPS (Molliex et al., 2015) and RNA-dependent localisation to SGs (Guil et al., 2006), with disease-causing mutations increasing the propensity of hnRNPA1 to localise to SGs (Kim et al., 2013). Further, hnRNPA1 plays a cytoprotective role during stress, as its RNAi-mediated knockdown decreases cell viability during osmotic stress (Guil et al., 2006).

Stress granules: ANG

Mutations in *ANG* can also result in ALS (Wu et al., 2007); *ANG* encodes the ANG (angiogenin) protein, which is also related to RNA metabolism. Angiogenin localises to SGs (Pizzo et al., 2013) and contributes to an eIF2a-independent mechanism of SG assembly. In this mechanism, ANG serves to cleave tRNAs into tiRNAs (tRNA-derived stress-induced RNAs), a subset of which can displace eIF4F from capped mRNA, inhibiting the initiation of translation, and resulting in SG formation (Emara et al., 2010, Ivanov et al., 2011, Ivanov et al., 2014).

1.3.4 Stress granules and ALS-FTD inclusions

While the assembly of SGs is transient, with RBP accumulations only present during the period of stress, the aggregates associated with NDDs, such as ALS, are more permanent. The processes which may convert SG dysregulation into inclusions likely occur over a chronic time frame. Evidence exists that stresses, including oxidative and ER stresses, increase with human ageing (Martinez et al., 2017, Romano et al., 2010). Importantly, both of these stresses can activate the SG response, leading to an increased interaction of LCD-containing proteins. *In vitro* experiments have demonstrated that repeated cycles of LLPS can result in the

formation of insoluble fibrils within LLPS structures; a process which is exacerbated by, but not necessarily caused by, ALS mutations (Molliex et al., 2015, Murakami et al., 2015). An increase in cellular stress and hence LLPS-driven interactions with ageing provides a potential mechanism by which both sporadic and familial ALS may occur.

The link between SGs and ALS inclusions was initially highlighted by the observation that they have an overlapping protein composition, enriched for RBPs. ALS-FTD aggregates in both patient spinal cord and brain tissue have been shown to co-localise with SG markers, for both TDP-43 (TIA-1, eIF3, PABP-1) (Liu-Yesucevitz et al., 2010, Bentmann et al., 2012, McGurk et al., 2014) and FUS (PABP-1 and eIF4G) (Dormann et al., 2010) inclusions; though other studies have not replicated this (Colombrita et al., 2009). This is not just the case for ALS however, as SG proteins have also been demonstrated to localise to inclusions in the brain tissue of Alzheimer's disease patients and in the brain tissue of a P301L-tau transgenic mouse model (TIA-1) (Vanderweyde et al., 2012).

The observed co-localisation of SG components with ALS inclusions has resulted in the hypothesis that SGs may either seed inclusions, or act as precursors to them. The latter suggests a failure of SG disassembly or clearance as cells age, with a progressive build-up of insoluble SGs. This is a possibility as autophagy, which has been demonstrated to remove a subset of SGs (discussed in ***section 1.2.1.5***), is regulated by a number of ALS-related proteins, including VCP and C9ORF72 (as discussed in ***section 1.3.3***); the knockdown of VCP, in particular, phenocopies the inhibition of autophagy (Buchan et al., 2013).

The alternative, that SGs could serve as pro-aggregative platforms for the generation of inclusions, is also supported. *In vitro* studies have demonstrated that insoluble fibrils can form within RBP (hnRNPA1, FUS, TIA1) phase separations, and ALS-causing mutations can increase their propensity to do so (Molliex et al., 2015, Murakami et al., 2015, Mackenzie et al., 2017). In addition, ALS mutations can promote the irreversibility of phase separations, along with a decreased detergent-solubility, indicating the formation of more-condensed fibrils; this was also observed by electron microscopy (Murakami et al., 2015). Critically, these phase separations can trap other RBPs, such as SMN and STAU-1. Mutations which impair the mobility of TIA1 *in vitro* result in a similar prolongation of SG disassembly in HeLa cells. These granules recruit TDP-43, decreasing its mobility (by FRAP) and reducing its detergent solubility (Mackenzie et al., 2017).

In the past decade, the concept that SGs could mature to promote the formation of insoluble aggregates has been demonstrated in a number of cell models. One study, using paraquat as a chronic (24 hour) oxidative stressor in HeLa cells, showed that insoluble, ubiquitin-positive TDP-43 aggregates persisted 6 hours after the cessation of stress; while SGs were disassembled by CHX, these TDP-43-granules were not (Parker et al., 2012).

Another study demonstrated that mutant SOD1 protein ($SOD1^{A4V}$) accumulates over time; it is not visible after 10-30 minutes of heat stress but increases over time, plateauing after 2 hours (Mateju et al., 2017). Simultaneously, SG levels of G3BP and FUS decrease over time. FRAP experiments demonstrate that the mobility of SOD1 (but not FUS or G3BP) is decreased after 2 hours of heat stress. Structured illumination microscopy also highlights that SOD1 accumulations within SGs form distinct domains, towards the periphery of the SG.

One method has been recently developed to overcome the off-target effects of cell stressors, instead inducing the formation of chronic SG-like granules using optogenetic techniques (Zhang et al., 2019a). To do this, the G3BP1 SG driver protein was fused to a blue light-dependent dimerization domain (Cry2-like domain), transfected into U2OS cells or iPSC-derived MNs, and exposed to (continuous or intermittent) blue light over a period of 5 hours. The use of this technique demonstrated a time-dependent conversion of SG-like granules, which co-localise with ubiquitin and TDP-43, into ALS-like inclusions, which become progressively more immunoreactive for phosphorylated-TDP-43, as well as p62. It is worth noting however that chronic blue light exposure also induced cytotoxicity. This data strongly supports the idea that mobile RNP granules could evolve into the immobile inclusions observed in disease.

Some recent evidence has however emerged suggesting that TDP-43 inclusions may form independently of SGs. The first study developed a light-inducible model of TDP-43 aggregation, by fusing a Cry2-like domain to the N-terminus of the TDP-43 protein (Mann et al., 2019). These light-inducible aggregates showed minimal recovery after photobleaching, detergent-insolubility and the recruitment of non Cry2-TDP-43, ubiquitin and p62. In this set-up, RNA-binding was shown to antagonise phase separation, as presence of the TDP-43 RNA-recognition motifs (RRMs) prevented the light inducible-LLPS of the LCD of TDP-43; the RRM of FUS also prevented this. In addition, expression of a cytoplasmic TDP-43 variant, followed by either ARS or heat stress resulted in two types of granule: those that co-

localise or do not with SG markers (G3BP1/eIF4G). The SG-negative TDP-43 granules were larger and lacked RNA, while SG-positive granules co-localised with RNA. Further, removal of the TDP-43 RRMs abolished all SG co-localisation. While SG-positive TDP-43 granules were dynamic, SG-negative inclusions were static, hyperphosphorylated and p62-positive. This paper suggests that acute SGs and inclusions may form in parallel, rather than inclusions evolving from SGs.

A second study demonstrated that ARS treatment in U2OS cells expressing cytoplasmic (∆NLS) TDP-43 induced SGs after 20 minutes with some TDP-43 immunoreactivity, which increased until 40 minutes (Gasset-Rosa et al., 2019). By 50 minutes however, TDP-43 also starts to develop into rounded SG-component-negative accumulations and by 90 minutes, the majority of cytoplasmic TDP-43 localises to these; though SGs are still present at this time-point, TDP-43 within SGs re-localises to these accumulations. Importantly, application of CHX prior to ARS treatment prevents SG formation but not formation of the TDP-43 accumulations, which still form over the same timescale. Further, these accumulations can form at concentrations of ARS which do not induce SGs (this is replicated in McGurk et al., 2018). This demonstrates that TDP-43 accumulations can form without SG formation and that they do not require polysome disassembly to assemble.

Neither of the above papers demonstrate the formation of accumulations independent of exogenous stress, albeit independent of SGs. Regardless, there remains the possibility that the processes which influence the formation of both types of accumulation overlap and SGs may regardless influence aggregate formation. Both papers suggest that RNA inhibits, or is dispensable for, aggregate formation. This is in agreement with a study showing that RNA plays a key role in the regulation of phase separation: for example, in the nucleus, a reduction in RNA levels promotes excessive phase separation and the formation of more solid-like structures (Maharana et al., 2018).

Regardless of whether altered SG homeostasis results in the formation of ALS inclusions, the study of SGs and other phase separated organelles may be key to understanding ALS pathogenesis. Further, there is no concrete evidence that the inclusions formed during disease are the cause of neurodegeneration. Alternatively, both neuron death and inclusion formation may result in parallel from the same disease-induced perturbations to LLPS pathways. One piece of evidence that inclusions are not necessary for neurodegeneration is from knock-in mouse models, For example, the FUSDelta14 mouse model displays motor-neurodegeneration in

the absence of FUS/p62/ubiquitin-positive pathological inclusions (Devoy et al., 2017).

1.4 Project aims

The above literature review highlights a physiological role for phase separation within cells, and demonstrates methods by which alterations to it can contribute to disease pathogenesis. Despite a rich literature investigating SGs in relation to ALS-FTD, comparatively little has been done to investigate this in disease-relevant cell types, including neurons. Another caveat of SG-ALS research is that mutant proteins are often overexpressed, even though this can result in confounding effects when studying phase separation.

Neurons differ from the majority of cell-types in that a part of their volume, the axon, can project over very long distances, up to >1 metre for some sensory and motor neurons. The axon therefore represents a large surface area of each neuron, but little has been done to examine the responses of axons to external stressors (with the exception of mechanical injury): particularly in relation to how the axon communicates stress to the soma.

Hence, in this thesis I aimed to:

Chapter 3: Investigate the SG response in multiple primary neurons types, to multiple different stressors.

Chapter 4: Use primary neurons to determine whether axonally-applied stressors could induce SGs in the soma.

Chapter 5: Investigate the effect of a C-terminal FUS-ALS mutation on the localisation of FUS to SGs in both motor and sensory neurons using a ‘knock-in’ mouse model: FUSDelta14.

Chapter 6: Develop a method of isolating neuronal somas whose axons had been exposed to stimuli using retrograde labelling and fluorescence-activated cell sorting.

This research aimed to increase our understanding of how neuronal cells respond to exogeneous stressors, and further, how ALS-mutations can alter these responses to cause disease. More generally, I aimed to increase our understanding of the basic pathomechanisms affecting the SG response, which may in future prove useful in discovering novel therapies for ALS and similar diseases.

2 Materials and methods

2.1 Animal Procedures

Wild-type (WT) and genetically-modified mice were housed in humidity- and temperature-controlled conditions, with 12-hour light-dark cycles. Experiments and procedures were performed according to the Animals (Scientific Procedures) Act 1986, following ethical approval from UCL Institute of Neurology and under License from the UK Home Office.

Wild-type (WT) C57BL6/J mice were cross-bred with SJL-Elite mice to increase the number of embryos per litter. FUSDelta14 mice were maintained on a C57BL6/J background and management of mouse colonies and genotyping was performed by Christian Bodo, Nicol Birsa, Cheryl Maduro and myself.

2.1.1 FUSDelta14 genotyping

To determine whether mice or embryos were negative (WT), heterozygous (HET) or homozygous (HOM) for the FUSDelta14 mutation, DNA was first extracted from mouse ear biopsies or embryo tail clippings. Tissue was lysed by adding 25 mM NaOH with 0.2 mM EDTA (ethylenediaminetetraacetic acid) and was then incubated at 95°C for 30 minutes using a dry heating block. This was neutralised by the addition of 40 mM Tris-HCl (pH5.5) and subsequently centrifuged at 13,000 x g for 5 minutes.

PCR (polymerase chain reaction) was performed using 7.5 µl GoTaq Green Master Mix (Promega; M7121), 4.5 µl water, 1 µl of sample DNA and 1 µl of each primer (forward and reverse; 10 pM) for each sample. The following PCR settings were used: 95°C for 3 minutes; 95°C for 30 seconds, 62°C for 30 seconds and 72°C for 15 seconds, with 35 cycles; 4°C hold. Using Fus-specific primers (forward: GGTTGGGAGAATGGAGCTGA and reverse: GATTAGGAGGTGGGCTAGGG; obtained from Thermo Fisher Scientific), a 126 bp (base pair) or 160 bp PCR product was detected for the WT or FUSDelta14 mutant gene respectively. For each PCR performed, positive, negative and water controls were run in parallel.

PCR samples were then electrophoresed on a 2% agarose gel (with 1X Gel Red; Biotium; 41003) for 75 minutes at 120 V in 1X TBE buffer (Tris-Borate-

ethylenediaminetetraacetic acid; composed of 90 mM Tris-HCl, 90 mM boric acid and 2 mM EDTA, pH 8.0). Gels were then imaged using the ChemiDoc Touch Imaging System (Bio-Rad; 732BR1025). Tissue was determined to be WT or HOM by the presence of a single 126 bp or 160 bp band respectively, or HET if both bands were detected.

2.2 Materials

2.2.1 Chemicals

All chemicals were purchased from Sigma-Aldrich unless otherwise stated. Phosphate buffered saline (PBS) tablets (100X) were purchased from Oxiod, UK and diluted in milliQ water. Other chemicals are shown in ***Table 2.1***. Drugs were either dissolved in water or DMSO depending on solubility; for drugs dissolved in DMSO, the equivalent volume of DMSO was present in the control treatment.

Compound	**Provider**	**Use**
Cholera toxin subunit B (Recombinant), Alexa Fluor™ 488, 555 or 647 Conjugate	Invitrogen (C34775) Invitrogen (C34776) Invitrogen (C34778)	Retrograde tracer
Sodium (meta)arsenite ≥90%	Sigma-Aldrich (S7400)	Stress granule inducer
Thapsigargin	Calbiochem (67526-95-8)	Endoplasmic stress inducer
DAPI	Sigma-Aldrich (D8417)	Nucleus stain
Phalloidin-488	Invitrogen (A12379)	F-actin stain (1:200)
Cycloheximide	Sigma Aldrich (C34859)	Protein synthesis inhibitor
EHNA, hydrochloride	Calbiochem (51350-19-7)	Dynein ATPase inhibitor
Puromycin	Sigma Aldrich (P9620)	Protein synthesis inhibitor
Guanabenz	Sigma Aldrich (G110)	GADD34 phosphatase inhibitor
BAPTA-AM	Calbiochem (126150-97-8)	Cell-permeant Ca^{2+} chelator
KB-R7943 mesylate	Tocris (1244)	Mitochondrial Na+/Ca2+ exchanger inhibitor
Diclofenac sodium	Sigma-Aldrich (D6899)	COX inhibitor
tert-Butyl peroxide	Sigma-Aldrich (168521)	Inducer of oxidative stress

Table 2.1 Chemicals used in this thesis, their provider and the intended use

2.2.2 Antibodies

The antibodies used for immunostaining experiments in this thesis are shown in ***Table 2.2***.

Antigen	Host	Provider	Dilution
FUS-565 (N-terminal)	Rabbit	Novus Biologicals; NB100-565	1:300
FUS-562 (C-terminal)	Rabbit	Novus Biologicals; NB100-562	1:300
FUS-D14	Goat	(Devoy et al., 2017)	1:300
βIII tubulin	Rabbit	Sigma-Aldrich; T2200	1:1000
βIII tubulin	Mouse	BioLegend; 801202	1:1000
βIII tubulin	Chicken	Synaptic Systems; 302-306s	1:500
G3BP	Mouse	BD Biosciences; 611127	1:200
TIAR	Goat	Santa Cruz; sc-1749	1:200
FMRP	Rabbit	Abcam; ab17722	1:200
Secondary antibodies (various)	Donkey	Invitrogen	1:1000

Table 2.2 All antibodies used in this thesis, their source and dilution for immunofluorescence.

2.2.3 Primary dorsal root ganglia/motor neuron medium

Medium for the culture of mouse primary embryonic dorsal root ganglion (DRG) neurons was made weekly, using the components shown in ***Table 2.3***; for primary embryonic motor neurons, this was made without nerve growth factor (NGF).

Component	Concentration	Provider
Neurobasal Medium	1x	Gibco; 21103049
B27 Supplement	2%	Gibco; 17504044
Heat-inactivated horse serum	2%	Gibco; 26050088
Glutamax	1x	Gibco; 35050061
B-mercaptoethanol	24.8 µM	Gibco; 31350-010
Penicillin/Streptomycin	1%	Gibco; 15140122
CNTF (ciliary neurotrophic factor)	10 ng/ml	Peprotech; 450-50
BDNF (brain-derived neurotrophic factor)	1 ng/ml	Peprotech; 450-02
GDNF (glial cell line-derived neurotrophic factor)	0.1 ng/ml	Peprotech; 450-44
NGF (nerve growth factor) [only for DRG neurons]	50 ng/ml	Peprotech; 450-34

Table 2.3 All components of primary dorsal root ganglion neuron (DRGN) medium and primary motor neuron (MN) medium, their source and final concentration. Note: NGF is not included in the MN medium.

2.2.4 Primary cortical neuron medium

Medium for the culture of mouse primary embryonic cortical neurons was made weekly, using the components shown in ***Table 2.4***.

Component	Concentration	Provider
Neurobasal Medium	1x	Gibco; 21103049
B27 Supplement	2%	Gibco; 17504044
Glutamax	1x	Gibco; 35050061
Glucose	0.6%	VWR; 27480
Sodium Chloride	37 mM	Sigma-Aldrich; 13423
Penicillin/Streptomycin	1%	Gibco; 15140122

Table 2.4 All components of primary cortical neuron (CN) medium, their source and final concentration.

2.2.5 Primary mouse embryonic fibroblast medium

Medium for the culture of primary mouse embryonic fibroblasts was made weekly, using the components shown in ***Table 2.5***.

Component	Concentration	Provider
Dulbecco's modified eagle medium (DMEM)	1x	Gibco; 41966
Foetal bovine serum (FBS)	10%	Hyclone; SV30160.03
Penicillin/Streptomycin	1%	Gibco; 15140122

Table 2.5 All components of primary mouse embryonic fibroblast (MEF) medium, their source and final concentration.

2.3 Fabrication of Microfluidic Chambers

Microfluidic chambers (MFCs) were assembled in-house (based on designs from Park et al., 2006). A 10:1 ratio of polydimethylsiloxane (PDMS): curing agent (Dow Corning; VWR: 634165S) was mixed vigorously, de-bubbled under vacuum for 45 minutes, poured into epoxy resin masters and baked at 67°C for 1 hour. PDMS inserts were then removed from the masters using tweezers, cut-to-shape with a 28mm punch and 4 wells were cut with a 5mm punch. Inserts were then cleaned with tape, sterilised and fixed to 50mm glass-bottomed dishes (Willco Wells; HBST-5040) using a plasma cleaner (Diener plasma-surface-technology). MFCs were filled with 0.8% BSA (in phosphate-buffered saline; PBS) overnight at 37°C prior to coating.

Bipartite MFC design consists of two parallel compartments, designated as somal and axonal (length 20 mm, width 1 mm, height 150 µm), connected by an array of microgrooves (length 800 or 500 µm, width 10 µm, height 3-4 µm) (***Figure 2.1A***).

Tripartite MFC design consists of three parallel compartments, connected by an array of microgrooves (length 500 µm, width 10 µm, height 3-4 µm). The central compartment is designated as the somal compartment (length 20 mm, width 1 mm, height 150 µm), with the flanking compartments designated as axonal compartments (length 20 mm, width 1 mm, height 150 µm) (***Figure 2.1B***).

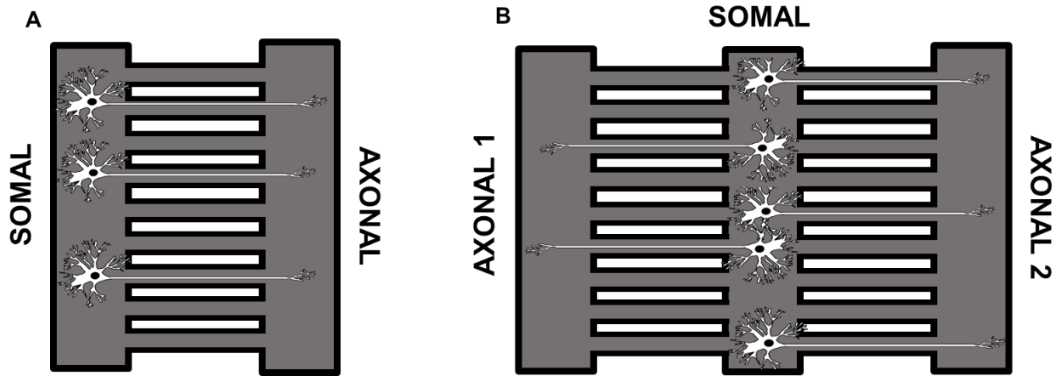

Figure 2.1 Bipartite and tripartite microfluidic chambers

A: Bipartite MFC design consists of two parallel compartments, designated as somal and axonal (length 20mm, width 1mm, height 150µm), connected by an array of microgrooves (length 500/800µm, width 10µm, height 3-4µm). **B**: Tripartite MFC design consists of three parallel compartments, connected by an array of microgrooves (length 500µm, width 10µm, height 3-4µm). The central compartment is designated as the somal compartment (length 20mm, width 1mm, height 150µm), with the flanking compartments designated as axonal compartments (length 20mm, width 1mm, height 150µm). For both designs, neurons are plated into the somal compartment, and project their axons into the/both axonal compartment(s), prior to use on DIV5-7 for experiments.

2.4 Primary embryonic neuron dissection, culture & plating

All cell culture experiments were performed in a Class II hood, with cells maintained in a 37˚C incubator (5% CO_2).

Primary neurons were either plated on 13 mm glass coverslips or into MFCs. Both were coated before use with 3 µg/ml poly-L-ornithine (Sigma; P4538) in water for 4 hours, followed by 0.33µg/ml laminin (Sigma-Aldrich; L2020) in Neurobasal medium (ThermoFisher Scientific; 21103049) overnight.

For MFCs, cells were resuspended in 5 µl neuron culture medium per chamber and pipetted directly into the channel of the somal compartment. 10 µl neuron culture medium was added to the axonal compartment. Cells were left to settle for 2 hours, following which 150 µl and 100 µl medium were added to the somal and axonal compartments respectively. This volume difference creates a small hydrostatic pressure difference which maintains fluidic isolation throughout culture.

2.4.1 Primary dorsal root ganglion dissection & culture

Primary embryonic dorsal root ganglion neurons (DRGNs) were isolated between embryonic day 12.5 (E12.5) and E14.5. Pregnant females were killed in accordance with Animals (Scientific Procedures) Act 1986 by intraperitoneal injection of a lethal overdose of Euthatal (Merial Animal Health Ltd), followed by confirmation by cervical dislocation.

A pair of straight-end forceps were used to remove the head and tail of the embryo. The embryo was then pinned down and the skin of the back was removed to expose the spinal column. Upon removal of the spinal column, DRGs were exposed and harvested. 20-30 ganglia per embryo were collected in an Eppendorf tube containing 1ml of HBSS (Hanks' balanced salt solution; Gibco; 24020117). DRGs from embryos of the same genotype were pooled prior to dissociation.

Ganglia were pelleted by centrifugation, HBSS removed and subsequently digested in 20 units/ml papain (Sigma; P4762) for 10 minutes at 37˚C, followed by digestion with a solution of 1% collagenase IV (Gibco; 17101015) with 1.5 units/ml dispase II (Invitrogen; 17105041) for 40 minutes at 37˚C. After digestion, cells were pelleted, the supernatant was discarded and the pellet was resuspended in 300 µl of DRG medium. Cells were then triturated with a series of fire-polished glass Pasteur pipettes with decreasing bore size. This was followed by a final centrifugation, removal of the supernatant and resuspension in a small volume of DRG medium.

2.4.2 Primary motor neuron culture

Primary ventral horn cultures were generously donated by Ione Meyer and Nicol Birsa for SG experiments. In brief, the spinal cord was dissected from E12.5-E14.5 embryos, the meninges removed, and the ventral cord roughly chopped and digested for 10 minutes with 0.025% Trypsin at 37°C. Following this, ventral cords were triturated in DNase (0.1mg/ml, then 0.02mg/ml) and then centrifuged with a 4% BSA cushion at 1,500 rpm for 5 minutes. Cells were then resuspended in MN medium and plated onto 13 mm glass coverslips.

2.4.3 Primary cortical neuron culture

Cortices from E12.5-E14.5 mouse embryos were dissected and collected in Hibernate E medium (Gibco; A1247601). Cortices were subsequently washed three times with warm HBSS and then incubated in a warm 1:1 mix of HBSS and accutase (Gibco; A1110501) at 37°C for 10 minutes. Cortices were then washed three times with cortical neuron (CN) medium and subsequently triturated in a small volume of CN medium using a series of fire-polished glass Pasteur pipettes with decreasing bore size. Suspended neurons were then diluted and plated at the desired concentration.

2.5 Primary mouse embryonic fibroblast culture

The head, spinal cord and red organs were removed from E12.5-E14.5 mouse embryos. The remaining parts were suspended in 1 ml of HBSS with 0.25% trypsin-EDTA (Gibco; 25200056) and finely minced with a scalpel. This was subsequently triturated with a 28 g needle, transferred to an Eppendorf tube and incubated at 37°C for 15 minutes with intermittent shaking. Trypsin was inactivated by resuspension by the addition of 9 ml of MEF medium, followed by centrifugation at 200 x g for 5 minutes. The supernatant was removed and the pellet was resuspended in 1ml of MEF medium. This was transferred to one well of a 6-well plate, containing a further 1ml medium, and allowed to grow overnight. These cells were split the next day by a ratio of 1:3. MEFs were plated for experiments from passage 2-5. Cells were routinely passaged by washing once with PBS, addition of trypsin for 2-5 minutes at 37°C and inactivation with 2 ml MEF medium followed by centrifugation. These cells were then split at a ratio of 1:2-5 depending on growth and plated onto 13 mm coverslips or into MFCs for experiments.

2.6 Immunocytochemistry & Microscopy

Cells were fixed in 4% paraformaldehyde (PFA) with 4% sucrose in PBS for 15 minutes at room temperature (RT). Coverslips were washed three times with PBS, permeabilised for 10 min using a solution of 0.5% BSA, 10% heat-inactivated horse serum (HS), 0.2% Triton-X in PBS and then blocked for 30 min (same solution as permeabilization without Triton-X) at RT. Both primary and secondary antibodies were diluted in the blocking solution. Cells were incubated with primary antibody for

1 hour at RT, washed three times and then incubated with fluorophore-conjugated secondary antibodies for 1 hour at RT. Cells were washed three times and then incubated for 10 minutes with 1:1000 DAPI, followed by three more washes and mounting onto slides using Mowiol (Sigma; 81381). Coverslips were imaged using an inverted Zeiss LSM 510 confocal microscope (all images acquired with 63x, 1.4 NA DIC Plan-Apochromat oil immersion objectives). Images were analysed using ImageJ as stated in ***Chapter 5.2***.

2.7 Stress granule induction in primary neuron cultures on coverslips

To induce SGs in DIV (days *in vitro*) 5-6 neuronal cultures on coverslips, 100 µl of 5X sodium arsenite (ARS) (Sigma-Aldrich; S7400) in neuronal culture medium was added to 400 µl of medium in the well, resulting in a final 1X ARS concentration. ARS was applied for the desired time (indicated in ***Chapters 3.2*** & ***5.2***) in a 37°C incubator, removed and subsequently cells were fixed. To determine the presence or absence of SGs, antibodies against key SG proteins were used, such as G3BP, TIAR and FMRP; either alone or in combination depending on the other antibodies required for the experiment.

2.8 Stress granule induction in primary neuron cultures in microfluidic chambers

To induce SGs in DIV5-7 neuronal cultures in an MFC, all medium was aspirated from the compartment being stressed, followed by addition of a 1X ARS solution in neuronal culture medium. This was applied for the desired time (indicated in ***Chapter 4.2*** & ***6.2***) in a 37°C incubator, aspirated and then cells were fixed.

To stain selectively for cells which projected into the axonal compartment of MFCs, the axonal compartment was incubated with 0.15 mg/ml of cholera toxin subunit B conjugated to a 488 fluorophore (CTxB-488; ThermoFisher Scientific; C34775) in medium for 3 hours prior to addition of ARS. CTxB is taken up by neuronal axons and retrogradely transported to the cell soma (Lanciego and Wouterlood, 2011).

Fluidic isolation was maintained by having 100 µl more medium in the somatic compartment than the axonal compartment during ARS or CTxB-488 incubation.

2.9 Fluorescence-activated cell sorting

Fluorescence-activated cell sorting (FACS) was performed by The Flow Cytometry Translational Technology Platform at the UCL Cancer Institute, specifically by Barry Wilbourn and George Morrow, using a BD FACSAria Fusion (BD Biosciences; San Jose, CA). Specific FACS procedures will be discussed in detail in ***Chapter 6.2***.

2.10 RNA extraction and quantification

For the experiment in ***Chapter 6.2.3***, RNA was extracted from FACS-sorted neuronal cell bodies. Somas were sorted directly using the BD FACSAria Fusion cell sorter into 200 µl of lysis Buffer RLT (Qiagen; 79216) in Eppendorf tubes and placed on ice for transportation. RNA was then extracted from these cells using the Qiagen RNeasy micro kit (Qiagen; 74004), eluting in 14 µl RNase-free water.

The RNA collected was then analysed using the Agilent 4200 TapeStation System (Agilent, Santa Clara, CA; G2991A) with High Sensitivity RNA ScreenTape (Agilent; 5067). This system performs automated electrophoresis of the RNA input and is able to determine RNA concentrations as low as 100 pg/µl. In addition it determines the level of RNA degradation by calculating a RIN^e (RNA integrity number equivalent) score for each sample; obtained by comparing the 18S rRNA (ribosomal RNA) peak in relation to the background signal.

2.11 Statistical Testing

Significance was defined as $p<0.05$ for statistical tests. Statistical differences between groups are indicated on graphs as so: * $p \leq 0.05$, ** $p \leq 0.01$; *** $P \leq 0.001$.

Figure	Independent Variable	Dependent Variable	Test	Post-Hoc
Axonal Stress Dose Response (Figure 4.1 & 4.4B)	1 categorical variable, with 5 groups	1 continuous variable	One-way ANOVA	Tukey
Axonal Stress & CTxB (Figure 4.1D & 4.4D)	1 categorical variable, with 2 groups	1 nominal variable, with 3 groups	Pearson X^2	N/A
MEFs in MFCs & ARS (Figure 4.2B)	1 categorical variable, with 3 groups	1 continuous variable	One-way ANOVA	Tukey
Axonal Stress & Whole-cell/Axonal CHX (Figure 4.3 & 4.7)	1 categorical variable, with 2 groups	1 continuous variable	Independent samples t-test	N/A
Axonal Stress Time Course SG_{MAX} and SG_{50} (Figure 4.5)	1 categorical variable, with 2 groups	1 continuous variable	Independent samples t-test	N/A
Axonal Stress & Axonal EHNA (Figure 4.6)	1 categorical variable, with 3 groups	1 continuous variable	One-way ANOVA	Tukey
FUS Stress Granule Localisation (Figure 5.1, 5.3, 5.4 & 5.5)	1 categorical variable, with 3 groups	1 continuous variable	One-way ANOVA	Tukey
FUS Nuclear/Cytoplasmic Localisation (Figure 5.2)	1 categorical variable, with 3 groups	2 continuous variables	One-way MANOVA	One-way ANOVA & Tukey

Table 2.6 Variables and statistical tests investigated in this report

3 The stress response of primary cells to chemical stressors

3.1 Specific Aims

The methods used to create the existing body of stress granule (SG) research have been heterogeneous, with a wide-variety of stressors demonstrated to induce SGs in a range of different cell-types. Certain paradigms are overrepresented, with sodium arsenite (ARS) the most commonly used stressor, along with other soluble compounds such as endoplasmic reticulum (ER) stressors (e.g. thapsigargin) (Kimball et al., 2003), proteasome inhibitors (e.g. MG132) (Mazroui et al., 2007) and mitochondrial stressors (CCCP) (Kwon et al., 2007). Physical cell stressors have also been demonstrated to induce SGs, including heat shock (Kedersha et al., 1999), cold shock (Hofmann et al., 2012), UV radiation (Kwon et al., 2007) and osmotic stress (e.g. by NaCl and sorbitol) (Kedersha et al., 2016). In addition, starving cells of key components (e.g. glucose, glutamine, pyruvate and serum) induces SG formation (Reineke et al., 2018).

Growing evidence has demonstrated that it is wrong to assume SGs induced by different stimuli have the same composition and function. It has been shown, for example, that wild-type (WT) FUS localises to SGs at far higher levels following osmotic stress, compared to SGs induced by ARS (Sama et al., 2013). Further, proximity labelling has demonstrated that SGs induced by ARS and thapsigargin have overlapping, but non-identical proteomes (Markmiller et al., 2018). In terms of function, while most SGs have been deemed to be pro-survival, those formed following starvation stress have been demonstrated to be pro-death (Reineke et al., 2018).

In addition to stressor-type, a wide variety of cell-types have been used to study SGs. The majority of experiments, particularly early studies, were performed using cancer cell lines. It has been demonstrated however that cell lines (HEK293T; human embryonic kidney cells) and neural progenitor cells (NPCs) have non-identical SG proteomes; although again these are overlapping (Markmiller et al., 2018). These observed differences not only caution the comparison of data from different cell-types, but also highlight the necessity of selecting an appropriate cell model to study certain diseases in relation to SGs. While cancer cell lines may be useful for studying the pathomechanisms underlying cancer, they may not, for example, be appropriate for the study of neurodegeneration (NDD). In addition,

while the majority of SG research has been performed using cancer cell lines, specific tumorigenic mutations have been demonstrated to perturb the SG response. For example, *KRAS* mutations markedly increase the number of SGs per cell (Grabocka and Bar-Sagi, 2016).

While cell lines and non-neuronal cells (NNCs) remain useful for the study of basic SG biology, for the study of neurological disorders it is likely more useful to use neurons or neuron-like cell lines, such as NSC-34 cells (Baron et al., 2013). The use of induced-pluripotent stem cells (iPSCs) and neurons derived from these cells, is becoming increasingly more common, but the study of SGs in primary neurons derived from animal tissue remains less common (Khalfallah et al., 2018). The development in recent years of 'knock-in' mouse models, such as the FUSDelta14 model (Devoy et al., 2017), which express disease-relevant levels of mutant proteins but still display progressive neurodegenerative phenotypes, make the use of these cell-types for disease research more attractive. Unlike human iPSC-derived neurons, with primary neurons it is possible to compare many different cell- and neuron-types from the same animal across various developmental and disease timepoints, and subsequently test potential therapeutic modifiers of NDD in a background-matched disease model.

Besides stressor- and cell-type, another varying experimental factor is the duration of treatment. SGs are commonly induced acutely, for example, by 1 hour of ARS treatment. However, in disease pathogenesis, stressors can also be present chronically. A number of stressors have been shown to induce SGs after prolonged treatments, including 1 mM paraquat overnight in HeLa cells (Meyerowitz et al., 2011) and 36 µM puromycin for 24 hours (Martinez et al., 2016). Some stressors only induce SGs after a longer treatment, for example, SGs induced by starvation stress only appear after 16 hours (Reineke et al., 2018). However, another paper has shown that primary hippocampal neurons fail to maintain the assembly of SGs chronically (Shelkovnikova et al., 2017).

The aim of this chapter was to investigate different SG inducers in a range of primary cell-types derived from WT embryonic mouse tissue. For all experiments, dose responses (DRs) were performed, as different cell-types can display drastically different susceptibilities to even well-characterised stressors; published drug concentrations demonstrated to induce stress were chosen. Firstly, I demonstrated the acute induction of SGs with the commonly-used stressor ARS in three different primary neuron types: motor neurons (MNs), dorsal root ganglion neurons (DRGNs)

and cortical neurons (CNs). I then attempted to determine a concentration of ARS by which DRGNs would display SGs following chronic ARS treatment, concluding that ARS was too intense a stimulus in this paradigm. Following this, I demonstrated the formation of SGs in CNs using two other known SG inducers: thapsigargin and guanabenz (Shelkovnikova et al., 2017). Finally, using primary mouse embryonic fibroblasts (MEFs), I screened three compounds to see if they were novel inducers of SGs, at three different timepoints. I demonstrated that the cell-permeable Ca^{2+}-chelator BAPTA-AM is a novel inducer of SGs and this finding is replicated in primary CNs.

3.1.1 Materials and methods

The results in this chapter were obtained by culturing primary motor, sensory and cortical neurons, as well as MEFs, on glass coverslips; dissection and cell culture are detailed in ***Chapter 2.4***. Following various DIV, these cells were exposed to a range of stress-inducing compounds, for both time course and dose response experiments, as detailed in ***Chapter 2.7***. This was followed by fixation and subsequent immunostaining, using stress granule marker antibodies (G3BP, TIAR, FMRP), for the observation of stress granules using confocal microscopy, as detailed in ***Chapter 2.6***.

3.2 Results

3.2.1 Sodium arsenite induces stress granules in a range of primary neuron types

An interesting point in the pathogenesis of many neurological diseases is the specificity of the disease pathogenesis for specific neuron types, over other cells. For example, in ALS-FTD, both MNs and CNs are affected, with sensory neurons (such as DRGNs) comparatively unaffected (though this is debated (Tao et al., 2018) and discussed further in ***Chapter 4.3***). This highlights the importance of comparing multiple neuron types in disease research; of note, no published research papers have demonstrated SGs in DRGNs.

With this in mind, I performed an ARS DR (0, 0.125, 0.25, 0.5 and 1 mM ARS) in MNs, CNs and DRGNs. Primary neurons were cultured on coverslips until DIV5-6 and then exposed to increasing concentrations of the oxidative stressor ARS; typically used at 0.5 mM (Kedersha et al., 1999). Cells were subsequently fixed, permeabilised and stained using antibodies against SG proteins (G3BP/TIAR for

MN/DRGNs; FMRP for CNs), as well as βIII-tubulin. Representative images are displayed in ***Figure 3.1***.

SGs were observed in all three neuron types, as well as in NNCs within cultures, for ARS concentrations of 0.25 mM and higher; for CNs also at 0.125 mM. All cells treated with 0.25 mM ARS or higher had some alterations to βIII tubulin staining, particularly with 1 mM. SGs in NNCs were distributed throughout the cytoplasm and SGs in MNs and CNs appeared to be closer to the nucleus (***Figure 3.1A*** and ***Figure 3.1C*** respectively). G3BP/TIAR-positive SGs in DRGNs however localise closer to the plasma membrane (***Figure 3.1B***).

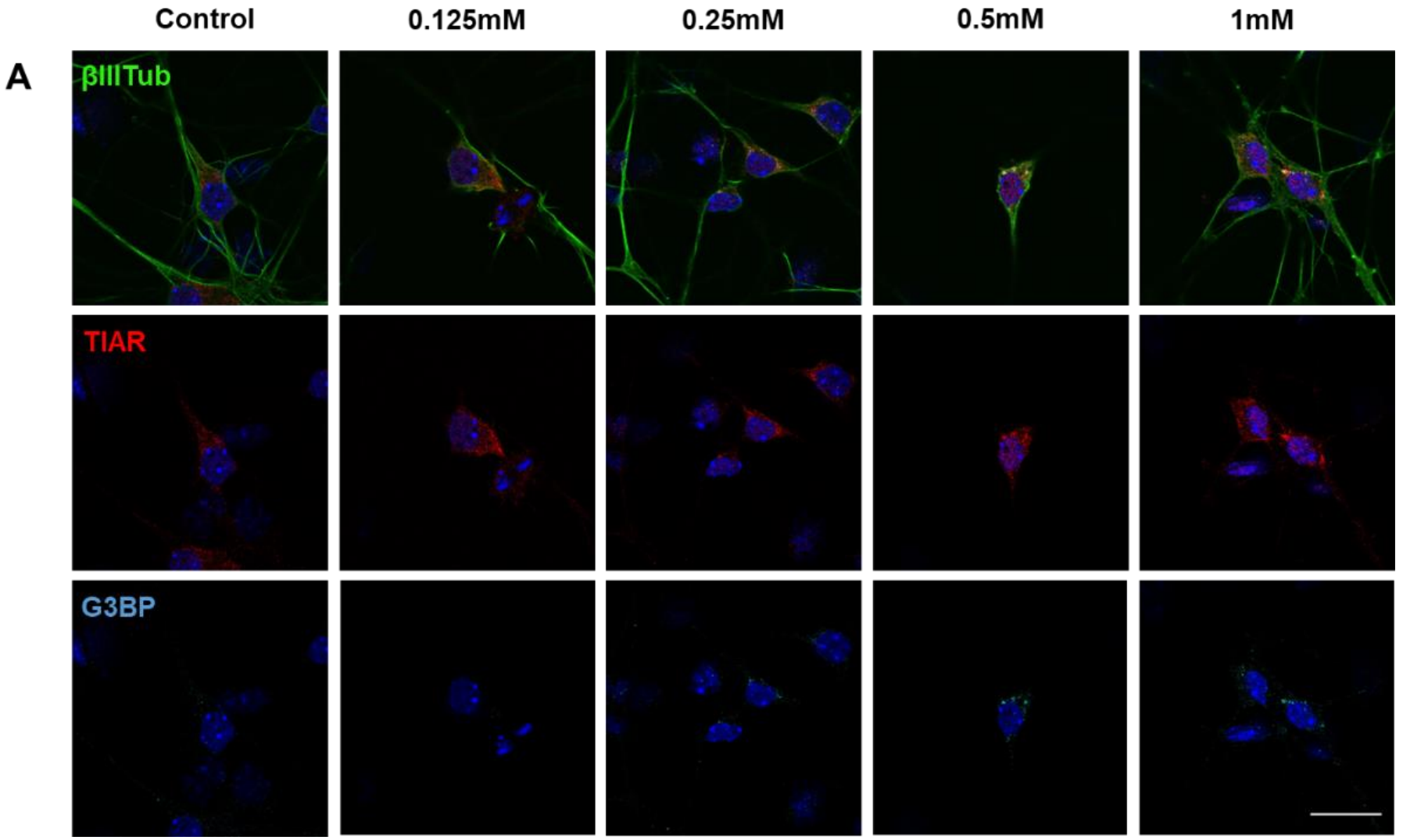
A
Control
0.125mM
0.25mM
0.5mM
1mM
βIIITub
TIAR
G3BP

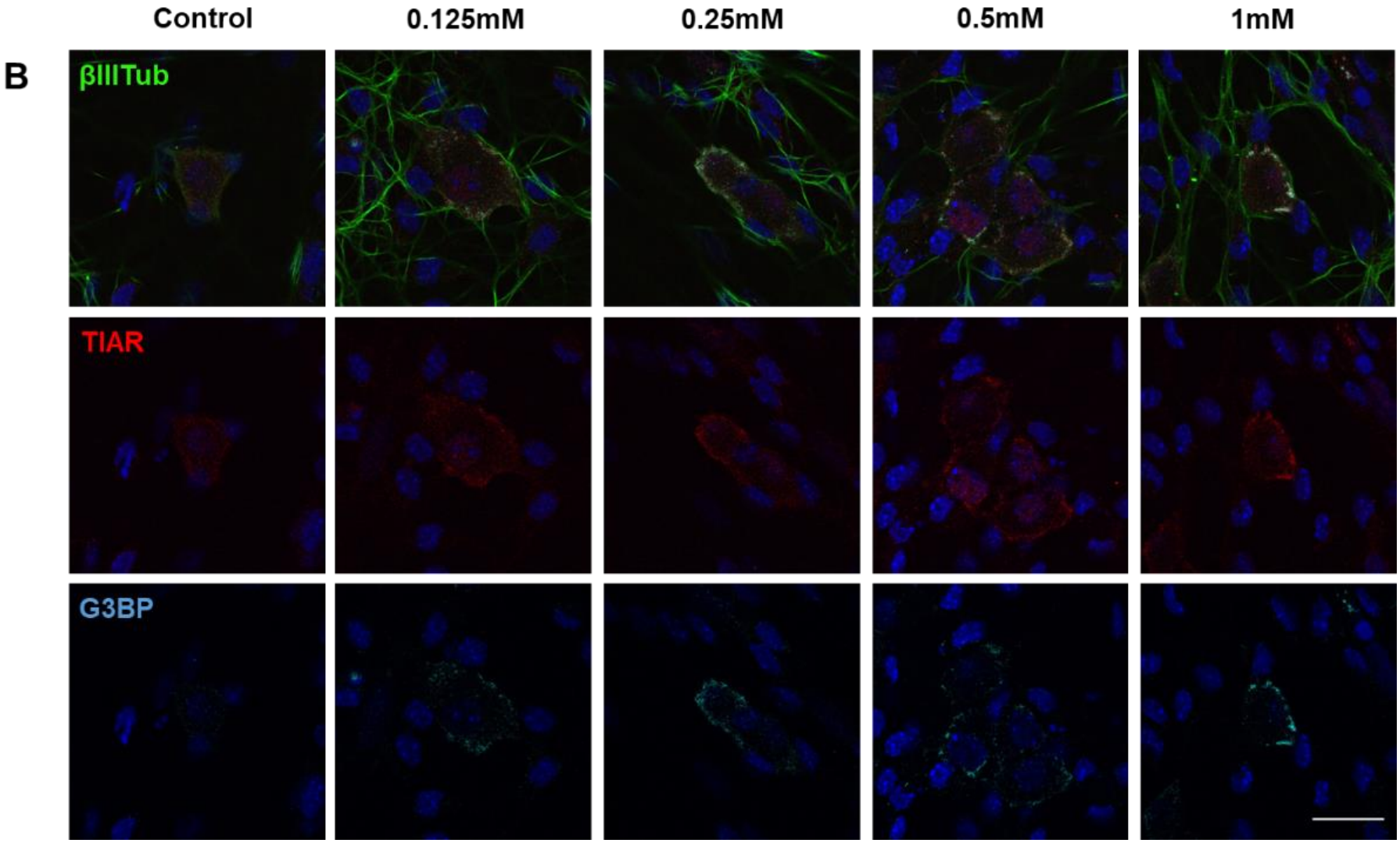
B
Control
0.125mM
0.25mM
0.5mM
1mM
βIIITub
TIAR
G3BP

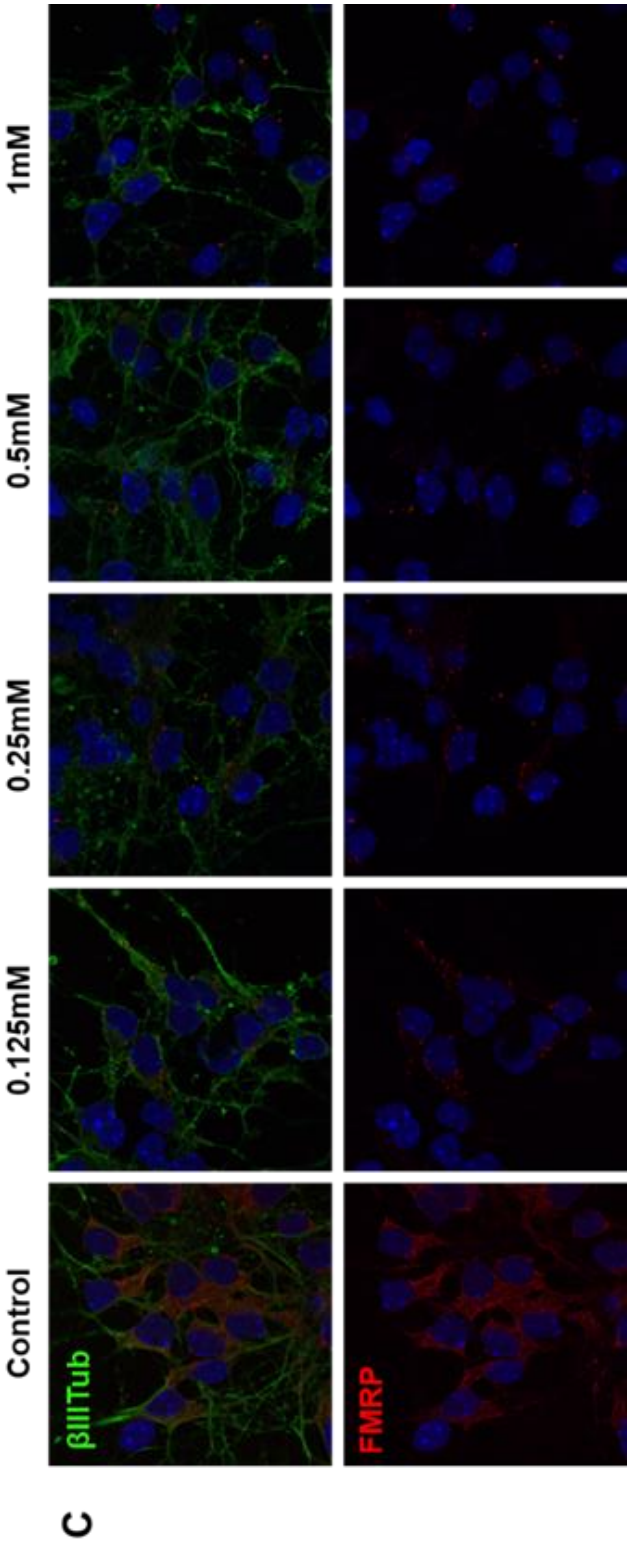

Figure 3.1 Sodium arsenite induces stress granules in a range of primary neuron types

Primary motor neurons (**A**), dorsal root ganglion neurons (**B**) and cortical neurons (**C**) cultured from wild-type E13.5 mouse embryos by sodium arsenite (0, 0.125, 0.25, 0.5mM and 1mM). G3BP/TIAR- (A-B) and FMRP- (C) positive stress granules are induced in all neurons treated with >0.25mM arsenite, and also with 0.125mM in cortical neurons. Cells are also stained with β3-tubulin/DAPI. Scale bar is 20μm. 2 replicates.

3.2.2 Attempting to determine a chronic arsenite concentration which induces stress granules

The previous DRs, as with the majority of the current SG literature, investigated acute (1 hour) cellular stress. As the stress associated with NDD is likely to be longer in duration, I aimed to investigate chronic cell stress. In order to determine a concentration of ARS which elicited chronic SGs, rather than an acute incubation, I performed a series of DR/time course (TC) experiments. For all experiments, primary embryonic DRGNs from E13.5 WT embryos were cultured on coverslips until DIV5-6 and exposed to increasing concentrations/durations of ARS (as indicated in ***Table 3.1***; all dose/time conditions have two replicates). Cells were subsequently fixed, permeabilised and stained using antibodies against G3BP, TIAR and βIII-tubulin.

The longest time period that SGs were present for was 6 hours with 0.25 mM ARS. The βIII-tubulin stain however indicated that cell health was poor. Indeed, most cells were dead at the same concentration 2 hours later. At longer time points (8/24 hours) cells were either alive with no SGs or dead. I concluded that ARS is not a suitable chronic stressor in primary DRGNs.

[ARS] (mM)	0.004	0.008	0.016	0.031	0.63	0.125	0.25	0.5	1	2
1 Hour	N/A	N/A	N/A	N/A	Few DRGNs with SGs	Some DRGNs with SGs	SGs	SGs	SGs	SGs
2 Hours	N/A	N/A	N/A	N/A	N/A	SGs	SGs	N/A	N/A	N/A
4 Hours	N/A	N/A	N/A	N/A	N/A	SGs, Rough membranes	SGs, Rough membranes	N/A	N/A	N/A
6 Hours	N/A	N/A	N/A	N/A	N/A	N/A	SGs, Rough membrane	N/A	N/A	N/A
8 Hours	N/A	Alive, No SGs	Alive, No SGs	Alive, No SGs	Alive, No SGs	Dead	Dead	N/A	N/A	N/A
24 Hours	Alive, No SGs	Alive, No SGs	Dead	Dead	Dead	Dead	Dead	Dead	N/A	N/A

Table 3.1 Sodium arsenite is not suitable for use as a chronic stressor in primary dorsal root ganglion neurons

Table indicating results of sodium arsenite dose response /time course experiments in DIV5-6 primary dorsal root ganglion neuron cultures. No chronic (≥4 hours) concentration of arsenite was determined where cells looked healthy and G3BP/TIAR-positive stress granules were present. N/A indicates that a particular DR/TC combination was not investigated; two replicates.

3.2.3 Acute thapsigargin induces stress granules in primary cortical neurons

Another well-characterised SG inducer is the ER stressor thapsigargin (Kimball et al., 2003). In the literature, thapsigargin has been applied at a range of concentrations and durations: 30 minutes & 50 µM in HeLa cells (Sama et al., 2013); 50 minutes at 1 µM in NIH/3T3 cells (Kimball et al., 2003). For testing in primary neurons, CNs were obtained from E13.5 embryos and cultured on coverslips until DIV6, when they were exposed to increasing concentrations of thapsigargin (0, 12.5, 25, 50 µM). After 1 hour, cultures were fixed, permeabilised and stained using antibodies against the SG marker FMRP, as well as βIII-tubulin. Representative images are displayed in ***Figure 3.2***. FMRP-positive SGs were observed at all concentrations tested.

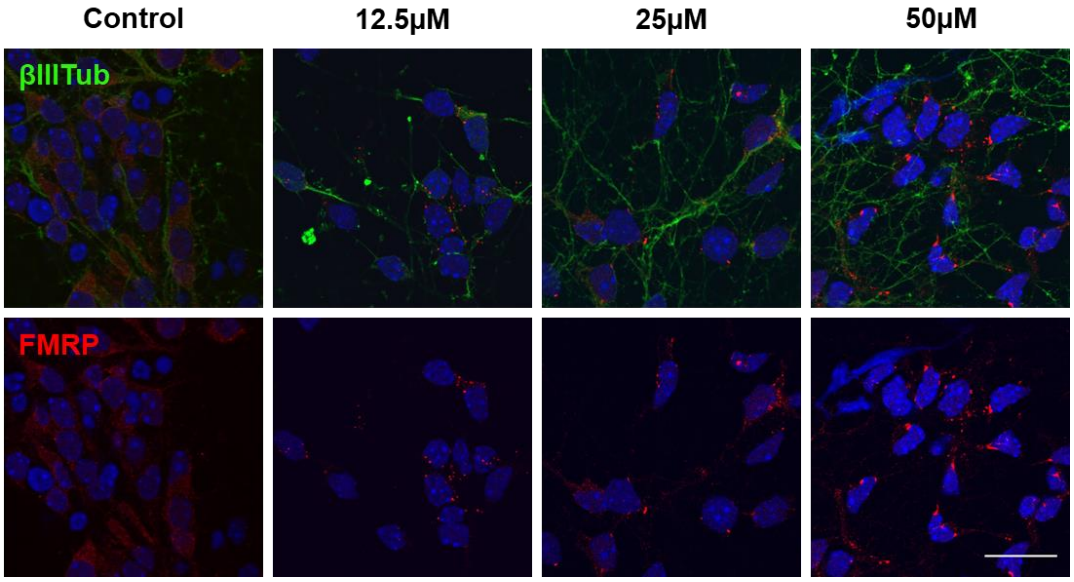

Figure 3.2 Acute thapsigargin induces stress granules in primary cortical neurons

Primary cortical neurons cultured from wild-type E13.5 mouse embryos were treated with thapsigargin (0, 12.5, 25, 50µM). FMRP-positive stress granules (red) were induced in all thapsigargin treated cells. Cells were also stained with β3-tubulin (green)/DAPI (blue). Scale bar is 20µm. 2 replicates.

3.2.4 Acute guanabenz induces stress granules in primary cortical neurons

One less-characterised SG inducer is guanabenz. While initially used as an α2-adrenergic receptor agonist (Takeuchi et al., 1987), it has subsequently been demonstrated to inhibit GADD34 (Tsaytler et al., 2011). GADD34 is a phosphatase regulatory subunit that is upregulated following increased eIF2α phosphorylation, which creates a negative feedback mechanism by promoting eIF2α

dephosphorylation. It follows, that GADD34 inhibition with guanabenz prevents this negative feedback, shifting the equilibrium towards the phosphorylated state and maintaining or facilitating SG assembly (see ***Chapter 1.2.1.3***). Acute guanabenz treatment has been used alone to induce SG assembly (Ruggieri et al., 2012) and in conjunction with other stressors (Shelkovnikova et al., 2017).

To determine whether acute guanabenz could induce SGs in primary neurons, CNs were first obtained from E13.5 embryos and cultured on coverslips. On DIV6, cells were exposed to increasing concentrations of guanabenz (0, 200, 400, 600 µM) for 1 hour. Cultures were then fixed, permeabilised and stained using antibodies against the SG marker FMRP, as well as βIII-tubulin. Representative images are displayed in ***Figure 3.3***. FMRP-positive SGs were observed at all concentrations tested, but within a higher fraction of cells for 400/600 µM than for 200 µM.

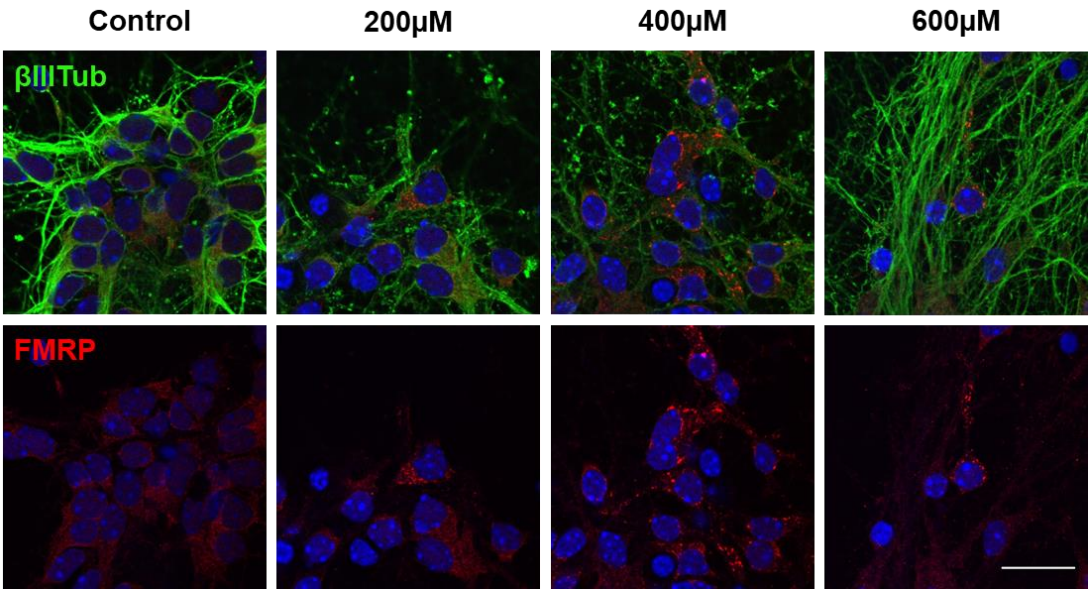

Figure 3.3 Acute guanabenz induces stress granules in primary cortical neurons

Primary cortical neurons cultured from wild-type E13.5 mouse embryos were treated with guanabenz (0, 200, 400, 600µM). FMRP-positive stress granules (red) were induced in all guanabenz-treated cells. Cells were also stained with β3-tubulin (green)/DAPI (blue). Scale bar is 20µm. 2 replicates.

3.2.5 BAPTA-AM is a novel stress granule inducer in primary mouse embryonic fibroblasts

Though neurons are a better model for the study of neurological diseases than other cell-types, it can be quicker and less labour-intensive to perform initial experiments

in proliferating cell lines. MEFs have a further advantage over cell lines, as you can match the genetic background of these cells to those of your other primary cell-types. I aimed to use primary WT MEFs derived from E13.5 mouse embryos to search for novel SG-inducing compounds: performing a DR at 3 different timepoints (1, 6, 24 hours; time-points performed on different days; one replicate).

BAPTA-AM is a cell-permeable Ca^{2+}-chelator that only binds to calcium once its AM (acetoxymethyl ester)-moiety has been cleaved by cytoplasmic esterases (Tymianski et al., 1994). Compounds which alter cellular Ca^{2+} homeostasis have previously been demonstrated to induce SGs: thapsigargin depletes ER Ca^{2+}, increasing cytoplasmic Ca^{2+} levels (Jackson et al., 1988). I performed a BAPTA-AM DR using the set-up described above, fixing and permeabilising cells after 1 hour, and then staining using an antibody against FMRP, as well as DAPI and phalloidin-647. Representative images of the FMRP stain at all time-points/concentrations are shown in ***Figure 3.4***.

At higher concentrations, BAPTA-AM was determined to be an acute inducer of SGs with SGs present following 65/130 µM treatment for 1 hour. At 6 hours, SGs were present in all cells at 32.5/65 µM, with a lower number of cells displaying them at 16.25 µM. Distinct SGs were not present at 24 hours, with high levels of cell death observed for 32.5 µM an above. Marked levels of cell death were observed at higher concentrations for the 6 and 24 hour timepoints, with almost all cells dead at 130 µM (6 and 24 hours) and 65 µM (24 hours).

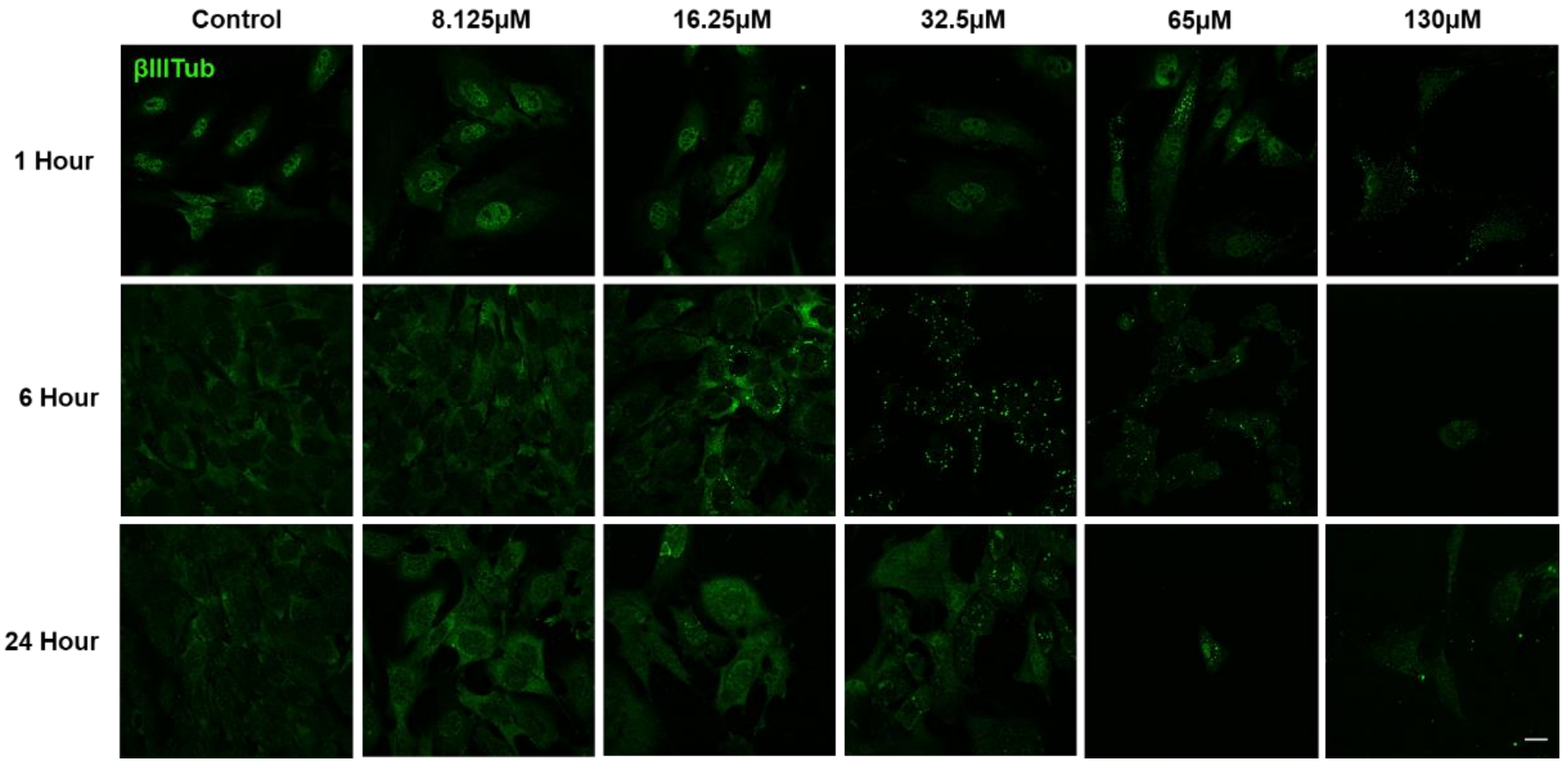
Control
8.125μM
16.25μM
32.5μM
65μM
130μM
βIIITub
1 Hour
6 Hour
24 Hour

Figure 3.4 BAPTA-AM is a novel stress granule inducer in primary mouse embryonic fibroblasts

Primary mouse embryonic fibroblasts (MEFs) cultured from wild-type E13.5 embryos were treated with BAPTA-AM (0, 8.125, 16.25, 32.5, 65, 130μM) for either 1, 6 or 24 hours. FMRP-positive stress granules (green) were induced in after 1 hour (≥65μM) and 6 hours (≥16.25μM) treated cells. Scale bar is 20μm. 1 replicate.

3.2.6 KB-R7943 is a novel stress granule inducer in primary mouse embryonic fibroblasts

Compounds acting on metabolic pathways have been demonstrated to induce SGs. Acute treatment with the glycolysis inhibitor 2-DG (2-deoxygluclose), and to a lesser extent 3PO ((2E)-3-(3-Pyridinyl)-1-(4-pyridinyl)-2-propen-1-one), induces SG formation (Wang et al., 2019b). In addition, inhibitors of mitochondrial function, such as CCCP (carbonyl cyanide *m*-chlorophenyl hydrazine; which disrupts mitochondrial membrane potential) and azide (complex IV inhibitor), induce SG formation (Wang et al., 2019b, Kwon et al., 2007).

I aimed to test whether KB-R7943, an inhibitor of mitochondrial complex I (Brustovetsky et al., 2011), also induces SG formation. Using the same experimental set-up, time points and immunostaining as ***section 3.2.5***, a dose response was performed for KB-R743 (0, 2.5, 5, 10, 20, 40 μM); representative images are shown in ***Figure 3.5***. FMRP-positive SGs were only observed in conditions that induced high amounts of cell death: 20/40 μM for 1 hour; 40 μM for 6 hours; other conditions did not induce SGs.

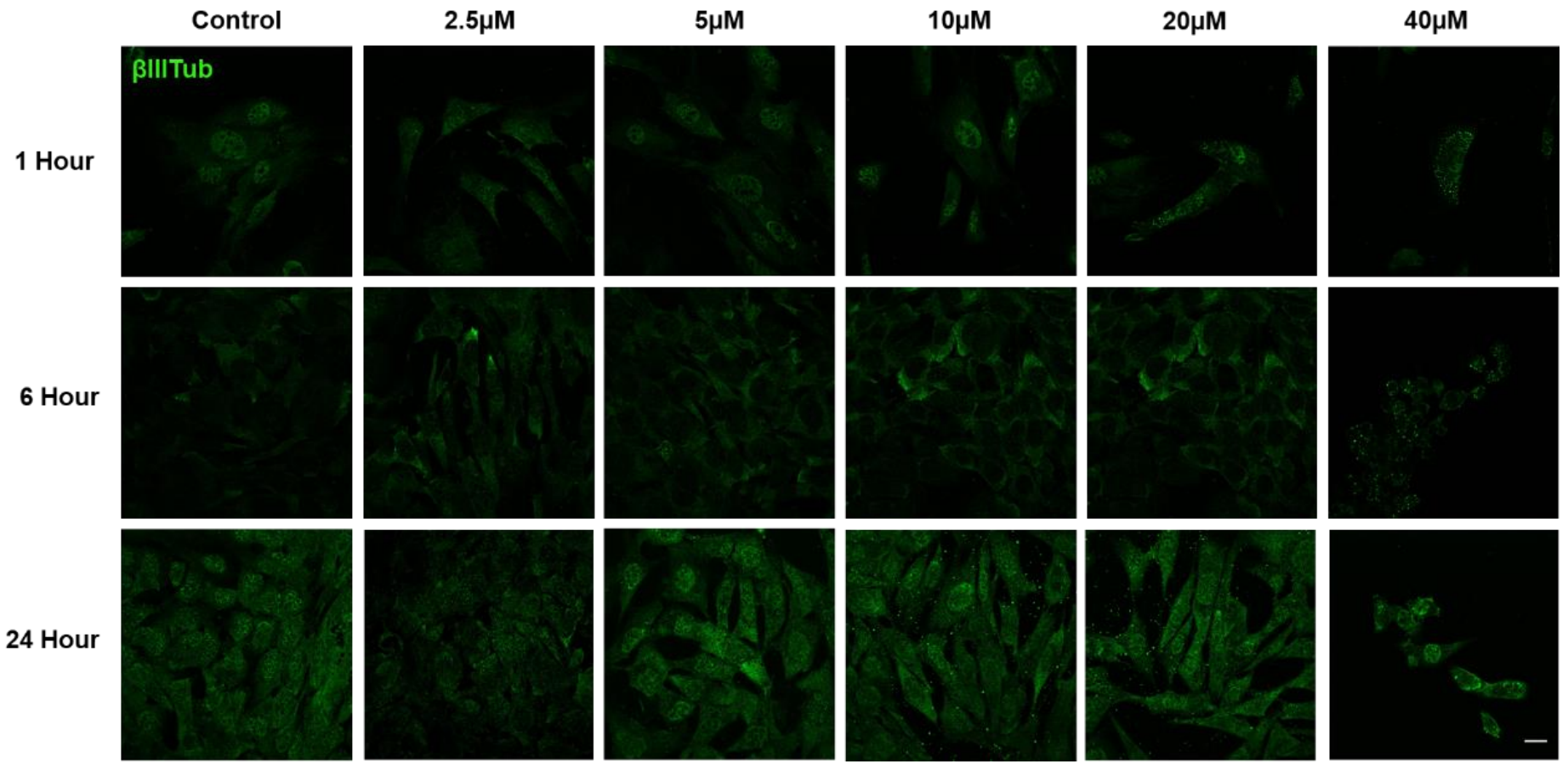
Control
2.5μM
5μM
10μM
20μM
40μM
βIIITub
1 Hour
6 Hour
24 Hour

Figure 3.5 KB-R7943 is a novel stress granule inducer in primary mouse embryonic fibroblasts

Primary mouse embryonic fibroblasts (MEFs) cultured from wild-type E13.5 embryos were treated with KB-R7943 (0, 2.5, 5, 10, 20, 40µM) for either 1, 6 or 24 hours. FMRP-positive stress granules (green) were induced in after 1 hour (≥20µM) and 6 hours (40µM only) treated cells. Scale bar is 20µm. 1 replicate.

3.2.7 tert-Butyl-peroxide does not induce stress granules in primary mouse embryonic fibroblasts

H_2O_2 has previously been reported to induce SGs in HeLa (1.5 mM for 2 hours) (Sama et al., 2013) and U2OS (0.5-2 mM for 1-2 hours) (Emara et al., 2012) cells. *tert*-Butyl peroxide (TBP) is more stable oxidant than H_2O_2, so I aimed to investigate whether this would induce SGs in primary MEFs. Using the same experimental set-up, time points and immunostaining as ***section 3.2.5***, a dose response was performed for TBP (0, 62.5, 125, 250, 500, 1000 µM). Neither FMRP-positive SGs, nor obvious cell death were observed at any concentration or time point investigated, indicating that TBP is likely not a SG inducer; representative images are shown in ***Figure 3.6***.

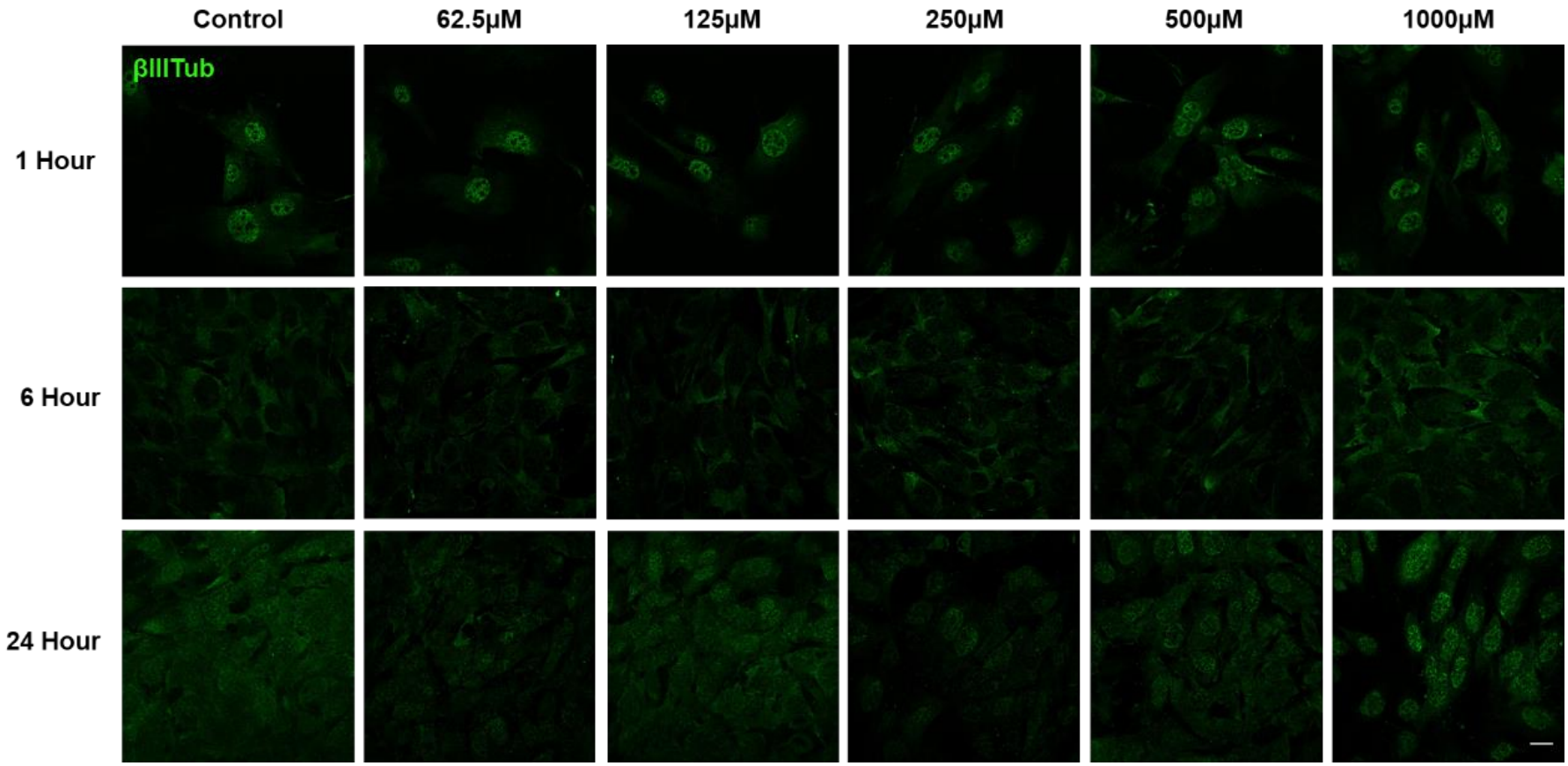
Control
62.5μM
125μM
250μM
500μM
1000μM
βIIITub
1 Hour
6 Hour
24 Hour

Figure 3.6 tert-Butyl-peroxide does not induce stress granules in primary mouse embryonic fibroblasts

Primary mouse embryonic fibroblasts (MEFs) cultured from wild-type E13.5 embryos were treated with tert-Butyl-peroxide (0, 62.5, 125, 250, 500, 1000µM) for either 1, 6 or 24 hours. FMRP-positive stress granules (green) were not observed for any treatment group. Scale bar is 20µm. 1 replicate.

3.2.8 Calcium chelation induces stress granules in primary cortical neurons

As discussed above, different cell-types respond to stressors in different ways and form different SGs. Following the discovery of BAPTA-AM as a SG inducer in MEFs (***section 3.2.5***) , I aimed to see if this would translate to neurons. To do so, I replicated the BAPTA-AM DR experiment in primary CNs. CNs were cultured on coverslips until DIV5-6 and then exposed to increasing concentrations of BAPTA-AM (8.125, 16.25, 32.5, 65 µM) for 1 hour. Cells were subsequently fixed, permeabilised and stained using antibodies against the SG protein FMRP, as well as βIII-tubulin; representative images are displayed in ***Figure 3.7***.

As with MEFs, FMRP-positive SGs were detected in CNs following BAPTA-AM stress. Unlike MEFs however, SGs were even observed at the lowest concentration used (8.125 µM), suggesting an increased susceptibility of CNs to intracellular calcium depletion.

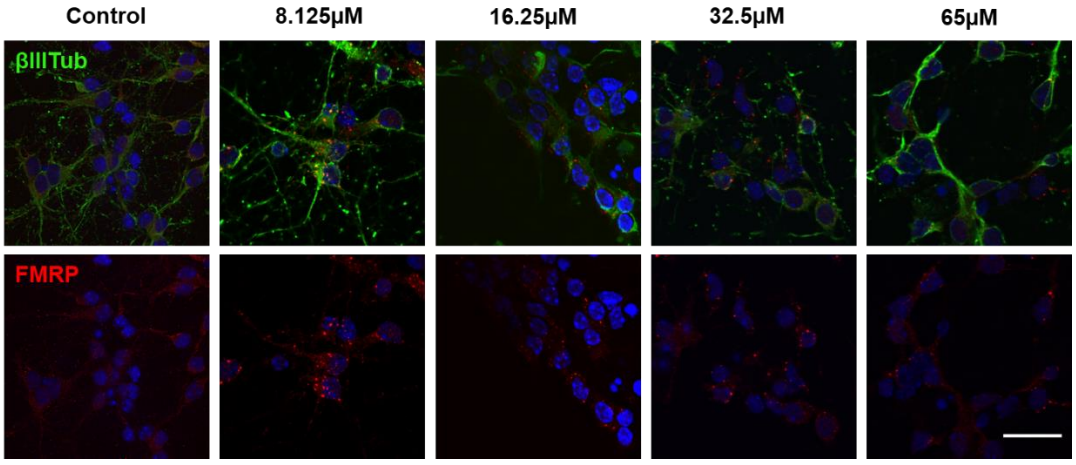

Figure 3.7 BAPTA-AM induces stress granules in primary cortical neurons

Primary cortical neurons cultured from wild-type E13.5 mouse embryos were treated with BAPTA-AM (0, 8.125, 16.25, 32.5, 65µM) for 1 hour. FMRP-positive stress granules (red) were induced in all BAPTA-AM-treated cells. Cells were also stained with β3-tubulin (green)/DAPI (blue). Scale bar is 20µm. 2 replicates.

3.3 Discussion

The results of this chapter further characterise the SG response in primary embryonic neurons and fibroblasts. The most commonly used SG inducer, ARS, induced granules in primary MNs, CNs (both demonstrated in Khalfallah et al., 2018) and DRGNs at a range of concentrations. Of note, this chapter demonstrates one of the first reports of SGs in sensory neurons (DRGNs). In this cell-type, SGs form towards the periphery of the cell (near the plasma membrane), rather than distributing randomly throughout the cytoplasm as in other cell-types. As the formation of SGs is random (Ohshima et al., 2015), highly dynamic (Wheeler et al., 2016) and dynein-transport mediated (Tsai et al., 2009), this peripheral SG localisation may be indicative of a mechanism by which these neurons concentrate SG components near to the membrane in order to facilitate their rapid aggregation by proximity. This may be important as DRGNs vary in size and can have a much larger cytoplasm than the other neuronal types investigated. This concept is supported by the observation of a “halo”-like stain following 1 hour of 0.125 mM ARS stress (***Figure 3.1B***) which is different to the distinct G3BP/TIAR-positive puncta observed for ≥0.25 mM ARS, but also from control treatment. This could be interpreted as an intermediate stage between SG-positive and SG-negative cells.

Another interesting point is that CNs appear to be more susceptible to ARS than both MNs and DRGNs, with distinct FMRP-positive SGs forming at 0.125 mM; while 0.25 mM is required for the other two cell-types. However, CNs and MNs/DRGNs are cultured in a different medium, which may have an effect. For example, only MN/DRGN medium contains β-mercaptoethanol, which is a known antioxidant (Kitagawa et al., 2004) and could reduce the efficacy of ARS at inducing SGs. This chapter also demonstrated the formation of SGs in primary CNs by thapsigargin and guanabenz treatment, at all concentrations investigated.

In order to develop a more disease-relevant stress model, I attempted to determine a protocol by which SGs could be induced chronically. Despite testing a wide-variety of concentrations and durations of ARS treatment, no combination was observed which resulted in chronic SGs. While the observed cell death and altered βIII tubulin staining may suggest that oxidative SGs cannot persist chronically, ARS has many SG-independent mechanisms of action which may be hindering the study (Singh et al., 2011). These include alterations to focal adhesion (Yancy et al., 2005), microtubule dynamics (Zhao et al., 2012) and autophagy (Bolt et al., 2010). It is

possible that using an alternative oxidative stressor, such as hydrogen peroxide, would enable these issues to be overcome (Emara et al., 2012).

While a few studies in cell lines have described chronic (18-24 hours) SGs following oxidative stress (Meyerowitz et al., 2011, Parker et al., 2012, Moujalled et al., 2013, Boyd et al., 2014), one recent paper concluded that SGs cannot persist chronically in neurons due to a negative feedback mechanism (Shelkovnikova et al., 2017). This paper does however propose a drug, guanabenz, which blocks this negative feedback loop. Either alone, or in conjunction with conventional SG-inducers, it is possible that guanabenz may allow SGs to persist chronically. In contrast to this, a few studies have demonstrated using induced-pluripotent stem cell-derived MNs that chronic incubation (24 hours) with the protein synthesis inhibitor puromycin induces SGs (Markmiller et al., 2018, Martinez et al., 2016). In this chapter, SGs were demonstrated to persist in MEFs at 6 hours (BAPTA-AM and KB-R7943) but not at 24 hours.

This chapter also demonstrated the use of MEFs to determine novel inducers of SGs, with findings replicated in CNs. The drawing of comparisons between the data produced in these experiments should be approached cautiously, as each experiment had one replicate and each timepoint (1, 6 and 24 hours) was performed separately; hence this does not account for week-to-week variations in cell health, cell proliferation and experimental procedure. It is however appropriate to draw information from the wider trends observed in these experiments: for example, increasing SG formation or death as drug concentration or time increases.

Despite previous reports that H_2O_2 induces the formation of SGs (Emara et al., 2012, Sama et al., 2013), TBP (a similar oxidant) did not induce SGs in MEFs. This is in agreement with other studies that have demonstrated that H_2O_2 treatment does not induce SGs in MEFs (Takahashi et al., 2013) or human iPSCs (Palangi et al., 2017). A separate study went further, not only demonstrating a lack of SG-induction, but also that oxidation of the SG-nucleating TIA1 protein by H_2O_2 in U2OS cells inhibits thapsigargin-induced SG formation (Arimoto-Matsuzaki et al., 2016). Hence our observations contribute to the body of evidence suggesting that oxidative stress does not induce SGs.

In agreement with studies demonstrating that metabolic inhibition induces SG formation, I demonstrated that KB-R7943, a mitochondrial complex I inhibitor, induces SGs at higher concentrations, though a large amount of cell death was observed. These experiments should be performed with a narrower range of DR/TC

conditions, in order to determine conditions whereby SGs are induced without significant cell death.

I also demonstrated that acute (1-6 hours) BAPTA-AM is a novel inducer of SGs in primary MEFs. This finding is interesting, as acute thapsigargin treatment induces the depletion of ER Ca^{2+} stores and a corresponding increase in cytosolic Ca^{2+}, but also induces SGs. BAPTA-AM, a cell permeable Ca^{2+}-chelator should elicit the reverse, decreasing available cytosolic Ca^{2+} levels. The mechanisms underlying BAPTA-AM-induced SG formation remain to be determined, although starvation of cellular nutrients can induce SGs, so there may be similar mechanisms converting detected decreases in cytosolic Ca^{2+} into SG formation (Reineke et al., 2018), potentially in conjunction with cellular calcium surveillance mechanisms (Grabarek, 2011).

The induction of SGs by BAPTA-AM in MEFs is replicated in primary CNs, supporting the use of MEFs for the primary screening of potential novel SG-inducing candidates. Of note, the BAPTA-AM concentration required to induce SG formation in CNs (8.125 µM) was far lower than that for MEFs (32.5 µM), indicating a much higher susceptibility of CNs to calcium-depletion stress. The induction of stress by BAPTA-AM is unsurprising, as similar concentrations (26, 39 µM) for 3-6 hours have been demonstrated to induce ER stress and decreased cell viability in primary CNs (Paschen et al., 2003). The concentrations which induced SGs in both MEFs and CNs are comfortably within the boundaries of concentrations which have commonly been used to chelate Ca^{2+} in the literature (Niesen et al., 1991, Tymianski et al., 1994).

3.3.1 Future Work

Quantification

The work described in this chapter, along with a large portion of the current SG literature, is descriptive rather than quantitative; this was for time reasons to prioritise other experiments. I used DRs and TCs to observe overall changes in SG formation, categorising either the presence or absence of SGs using one or two SG markers. To better determine the ideal concentrations to use for SG induction in different cell-types, it would be useful to quantify factors such as the percentage of cells within a culture displaying SGs, as well as SG size and number.

Live imaging of stress granule dynamics

Another flaw in the methodology of this chapter is that in order to immunostain and examine cells, they must be permeabilised and fixed, meaning that you cannot perform a true time course experiment. A number of SG studies have performed live time course experiments by transfecting fluorescently-tagged SG proteins, such as G3BP, into cells prior to imaging. This however has the confounding issue that uncontrolled transfection (i.e. overexpression) of SG proteins can induce SG or aggregates in the absence of stress (Kedersha et al., 2008). Hence, the best method to perform this experiment would be to generate a stable-cell line expressing a fluorescently-tagged SG protein (Wheeler et al., 2016), preferably at its endogenous locus.

Comparison of cell susceptibility to specific stressors

In this chapter, CNs appeared to be more susceptible to ARS than MNs and DRGNs, with SGs visible at lower ARS concentrations. However, these experiments were performed on different days, in different cell culture media (as different neuron types require different growth factors and media supplements for optimal growth conditions), using different SG markers (due to changes in the availability of antibodies from suppliers). In order to determine accurate differences in susceptibility to stress inducers, it will be necessary to control for each of these factors in future experiments.

Determine a chronic cell stress paradigm

I determined in this chapter that ARS is not an appropriate stressor to use for the induction of chronic SGs, likely in part due to its wide-ranging cytotoxic effects. In order to circumvent similar issues, a method of SG induction with fewer off-

target/non-SG-inducing effects should be used. As discussed above, a number of stressors have been reported to induce chronic SGs, but all will induce damaging cytotoxic effects. Even guanabenz, which directly targets the dephosphorylation of eIF2α, has well characterised adrenergic off-target effects (Takeuchi et al., 1987). One method described which aimed to remove these off-target effects is the optogenetic induction of SGs, although chronic blue light exposure has been shown to induce cytotoxicity (Zhang et al., 2019a).

Characterisation of BAPTA-AM- and KB-R7943 induced stress granules

Both BAPTA-AM and KB-R7943 were demonstrated to be novel SG inducers in MEFs, as well as neurons for BAPTA-AM. Both were demonstrated with only 1 replicate, so further trials remain to be performed. In addition, the only SG marker investigated was FMRP, so further characterisation is required to confirm the identity of these puncta: for example, immunostaining for additional SG driver proteins (G3BP/TIA-1) and eIFs, as well as *in situ* hybridisation to detect the presence of absence of RNA within these granules. Following the confirmation that these granules are SGs, it will be interesting to determine the mechanism facilitating the induction of these granules. For KB-R7943, this will likely be homologous to mechanisms previously described for inhibitors of glycolysis and mitochondrial respiration (Wang et al., 2019b). Interestingly, low levels of cytosolic Ca^{2+} have not yet been linked to SG formation, meaning further exploration of the BAPTA-AM-induced mechanism of SG formation is required.

3.4 Conclusions

This chapter has further characterised the ability of primary neurons to form SGs in response to a wide-variety of chemical stimuli, including one of the first descriptions of SGs in primary DRGNs and the identification of two novel SG inducers: BAPTA-AM and KB-R7943. Thorough dose response and time course experiments are a useful method of determining the relative susceptibilities of different cell-types to stressors, but the application of this field to neurodegenerative research remains hindered by the use of acute stressors over chronic inducers of phase separation.

4 The stress response of primary neurons to axonal stressors

4.1 Specific aims

Although ALS mutant proteins are expressed ubiquitously, the disease preferentially targets MNs over other cell-types. Compared to other cells, neurons differ in that they can cover vast distances to propagate signals via their axons, up to 1 meter in motor/sensory neurons (Stifani, 2014). Additionally, while the cell bodies of these neurons remain inside the spinal cord or ganglia, axons of lower motor neurons exit the central nervous system, meaning they are comparatively exposed to extracellular trauma (Chen et al., 2012). Further, ageing leads to increased peripheral nerve inflammation (Yuan et al., 2018), which has been demonstrated to weaken the blood-nerve barrier, further increasing susceptibility of peripheral neurons to exogeneous stressors (Skaper, 2017). These factors may play a role in ALS pathogenesis, as evidence from an ALS mouse model suggests a “dying-back” disease progression, from the axons to the soma (Fischer et al., 2004, Dadon-Nachum et al., 2011). Work on the widely-used $SOD1^{G93A}$ ALS mouse model demonstrates neuromuscular junction loss (Fischer et al., 2004, Frey et al., 2000), axon transport deficits (Bilsland et al., 2010) and motor unit loss (Kennel et al., 1996) as preceding the onset of disease symptoms, particularly in larger axons (Fischer et al., 2004).

Disease-related inclusions form within the neuronal soma, but it is unknown whether axonal insult could result in these inclusions; axonal stress has not yet been studied in relation to stress granules (SGs) or phase separation in the soma. So far, axon-to-soma responses to stress have predominately been characterized following physical injury (reviewed in Richardson et al., 2009). These studies have highlighted mechanisms of increased axonal local translation (Hanz et al., 2003, Terenzio et al., 2018), dynein-mediated retrograde (from the axon towards the cell body along microtubes via molecular motors, e.g. dynein) feedback to the soma (Hanz et al., 2003, Chen et al., 2012) and somal transcriptional/translational responses (Cho et al., 2015).

In vivo, axotomy and crush injury have been demonstrated to increase local oxidative stress (Sayir et al., 2013), however, little has been done to characterize the axon-to-soma responses of neurons to oxidative stress or other non-mechanical

stressors. The aim of this part of my thesis was to investigate whether axonal stress could induce somal SGs in primary neurons.

In order to study this, I used microfluidic chambers (MFCs). MFCs are cell culture platforms that use small channels to direct the growth of axons from one compartment into another, and use volume differences to maintain a hydrostatic pressure difference between the compartments (Park et al., 2006). This enables the fluidic isolation of the two compartments: a somal compartment (containing somas, non-neuronal cells (NNCs), axons and dendrites) and an axonal compartment (containing only axons). This fluidic isolation enables the exposure of one compartment only to soluble compounds, including stressors such as the oxidative stressor sodium arsenite (ARS) (Li and Chou, 1992).

For this chapter, both primary embryonic cortical neurons (CNs) and DRG neurons (DRGNs) were plated into MFCs: CNs were used because they are related to multiple neurodegenerative diseases and their preparations results in a high cell-yield; DRG neurons were used because they project efficiently and extensively into the axonal compartment. Neurons which project into the axonal compartment can be specifically labelled with retrograde toxins, enabling the direct comparison of neurons whose axons have been exposed to a stressor, versus those that have not. For these experiments, I labelled these somas with cholera toxin subunit B conjugated to a 488 fluorophore (CTxB-488) (Lanciego and Wouterlood, 2011).

Using CTxB-488, I confirmed that both CNs and DRGNs with ARS-exposed axons formed somal SGs in a dose-dependent manner, while CTxB-488-negative cells were free from SGs. NNCs in the somal compartment, which do not come into contact with the ARS in the axonal compartment, were negative for SGs. In addition, I identified a delayed time course for cells stressed axonally compared to somally for both cell types, suggesting a mechanism for the detection of ARS stress by axons and subsequent propagation to the cell body. This mechanism may be dynein-dependent, and may also require local protein translation in the axon. Further, neither physical axotomy, nor thapsigargin-induced endoplasmic reticulum (ER) stress appear to induce the same response.

4.1.1 Materials and methods

The results in this chapter were obtained by culturing primary cortical and sensory neurons, as well as MEFs, in MFCs. The fabrication of MFCs is detailed in ***Chapter 2.3***, and dissection and cell culture are detailed in ***Chapter 2.4***. Following various DIV, the axonal or somal compartment of MFCs was exposed to CTxB-488, and

range of stress-inducing compounds (predominately arsenite), for both time course and dose response experiments, as detailed in ***Chapter 2.8***; some experiments were performed in the presence of inhibitor drugs (EHNA; CHX) as indicated in specific results sections. This was followed by fixation and subsequent immunostaining, using stress granule marker antibodies (FMRP), for the observation of stress granules using confocal microscopy, as detailed in ***Chapter 2.6***.

4.2 RESULTS

4.2.1 Axonal arsenite stress induces stress granules in the cell soma of primary cortical neurons

In order to investigate whether axonal ARS could induce somal SGs, I performed an axonal ARS dose response on neurons in MFCs. Primary CNs from E13.5 WT embryos were plated into the somal compartment of MFCs until DIV7 to allow for axonal projections to grow. The axonal compartment was incubated with 0.15mg/ml CTxB-488 for 3 hours, in order to retrogradely label the somas of neurons projecting into the axonal compartment. Axons were then stressed with 0.25, 0.5, 1 or 2.5 mM ARS for 1 hour. Both compartments were subsequently fixed, permeabilised and stained using antibodies against the SG protein FMRP and βIII-tubulin, as well as DAPI.

To quantify this, 100 CTxB-488-positive somas were counted and classified as either SG-positive (distinct FMRP-positive puncta), SG-negative (homogenous cytoplasmic FMRP stain) or an intermediate phenotype (altered distribution of FMRP compared to the typical negative stain) (***Figure 4.1A***). At 0.25, 0.5, 1 and 2.5 mM ARS, SGs were observed in 11.7%, 37.3%, 55% and 70.7% of somas respectively, with 0.5 mM, 1 mM and 2.5 mM significantly higher than control ($F(4,10)=28.36$, $p<0.0005$; post-hoc $p<0.0005$) by one-way-ANOVA and post-hoc Tukey tests (***Figure 4.1B-C***).

Due to the hydrostatic pressure difference established by the 100 µl volume difference between the somal and axonal compartments, fluidic isolation should be maintained (Park et al., 2006), meaning it is unlikely the ARS is leaking into the somal compartment and exerting whole-cell stress. To confirm this, I compared the proportion of CTxB-488-positive cells containing SGs following 2.5 mM axonal ARS to CTxB-488-negative somas in the same compartment, predicting that SGs would be present in CTxB-488-postive cells, but not CTxB-488-negative cells, counting 100 cells for each condition. CTxB-488-status was significant by chi-squared test,

with 70.7% of CTxB-positive cells displaying SGs, compared to 3.3% in CTxB-negative cells ($X^2(2, n=3) = 104.5$, $p<0.0005$) (***Figure 4.1C-D***).

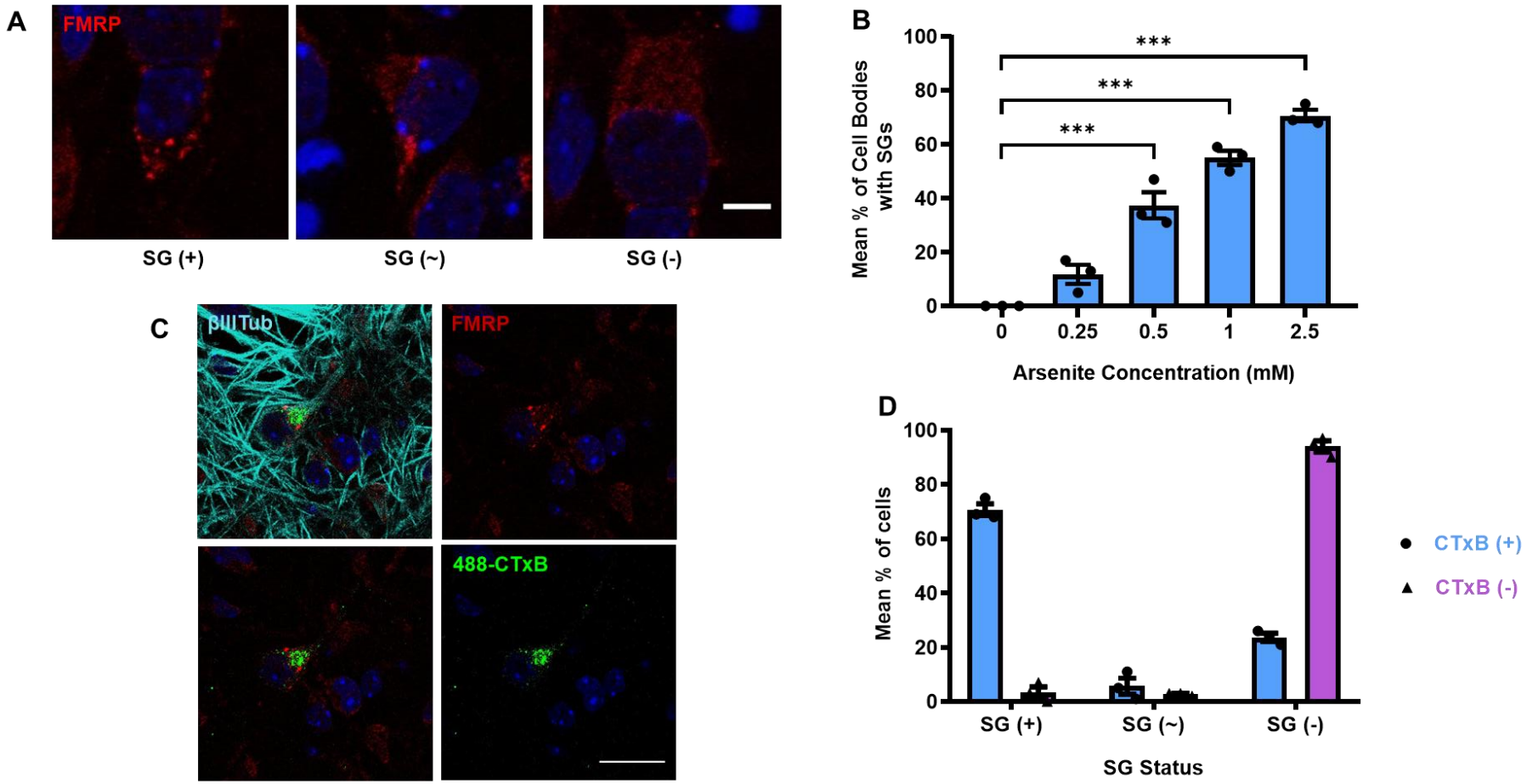
A
FMRP
SG (+)
SG (~)
SG (-)
B
Mean % of Cell Bodies with SGs
100
80
60
40
20
0
***
***
***
0
0.25
0.5
1
2.5
Arsenite Concentration (mM)
C
βIIITub
FMRP
488-CTxB
D
Mean % of cells
100
80
60
40
20
0
SG (+)
SG (~)
SG (-)
SG Status
CTxB (+)
CTxB (-)

Figure 4.1 Axonal arsenite stress induces somal stress granules

A: FMRP stain (red) in the cell body of cortical neurons following acute axonal arsenite stress was used to define cells as either as stress granule (SG)-positive (SG (+)), stress granule-negative (SG(-)) or an intermediate phenotype (SG (~)). Scale bar is 5μm. **B:** Primary cortical neurons (DIV7) from WT E13.5 embryos were cultured in microfluidic chambers. The axonal compartment was incubated with CTxB-488 for 3hrs, followed by 0, 0.25, 0.5, 1 or 2.5mM sodium arsenite for 1 hour. A dose-dependent increase in the % of cell bodies containing SGs was observed. 0.5, 1mM and 2.5mM were significantly higher than control ($F(4,10)=28.36$; $p<0.0005$; post-hoc $p<0.0005$) by one-way-ANOVA and post-hoc Tukey tests **C-D:** FMRP-positive SGs (red puncta) are induced in CTxB-488-positive (green) neuron somas but not in CTxB-488-negative somas. Neurons were stained with β3-tubulin (cyan)/DAPI (blue). Scale bar is 20μm. CTxB-488-status was significant by chi-squared test ($X2(2, n=3) = 104.5$, $p<0.0005$). N=3 biological replicates

To further confirm that ARS was isolated to the axonal compartment, I plated primary MEFs into the somal chamber of a MFC. On DIV1, 0, 2.5 or 5 mM ARS was applied to the axonal compartment for 1 hour in the same manner as the previous experiments; cells then were fixed, permeabilised and stained using an antibody against the SG protein FMRP, DAPI and the f-actin-binding dye phalloidin-488 (100 MEFs were counted per condition). As MEFs do not have axonal projections, I predicted that these cells would not contact the ARS, and hence would not display SGs. As predicted, the number of MEFs exhibiting SGs following treatment of the axonal compartment with ARS did not significantly differ from negative controls, as determined by one way ANOVA and post-hoc Tukey tests ($F(2,6)=5.333$, $p=0.047$; post-hoc $p=0.067$/$p=1$). In fact, the percentage of SGs was borderline significantly higher in the ARS-negative condition (post-hoc $p=0.067$; 1.67% and 0.33% for negative control and both axonal arsenite treatments respectively; ***Figure 4.2***). In addition, while the phalloidin-488 stain is more rounded in the positive control, the stain for the axonal ARS treatment resembles that of the negative control. Together, this suggests that fluidic isolation is maintained during the 1 hour timeframe of our neuronal experiments.

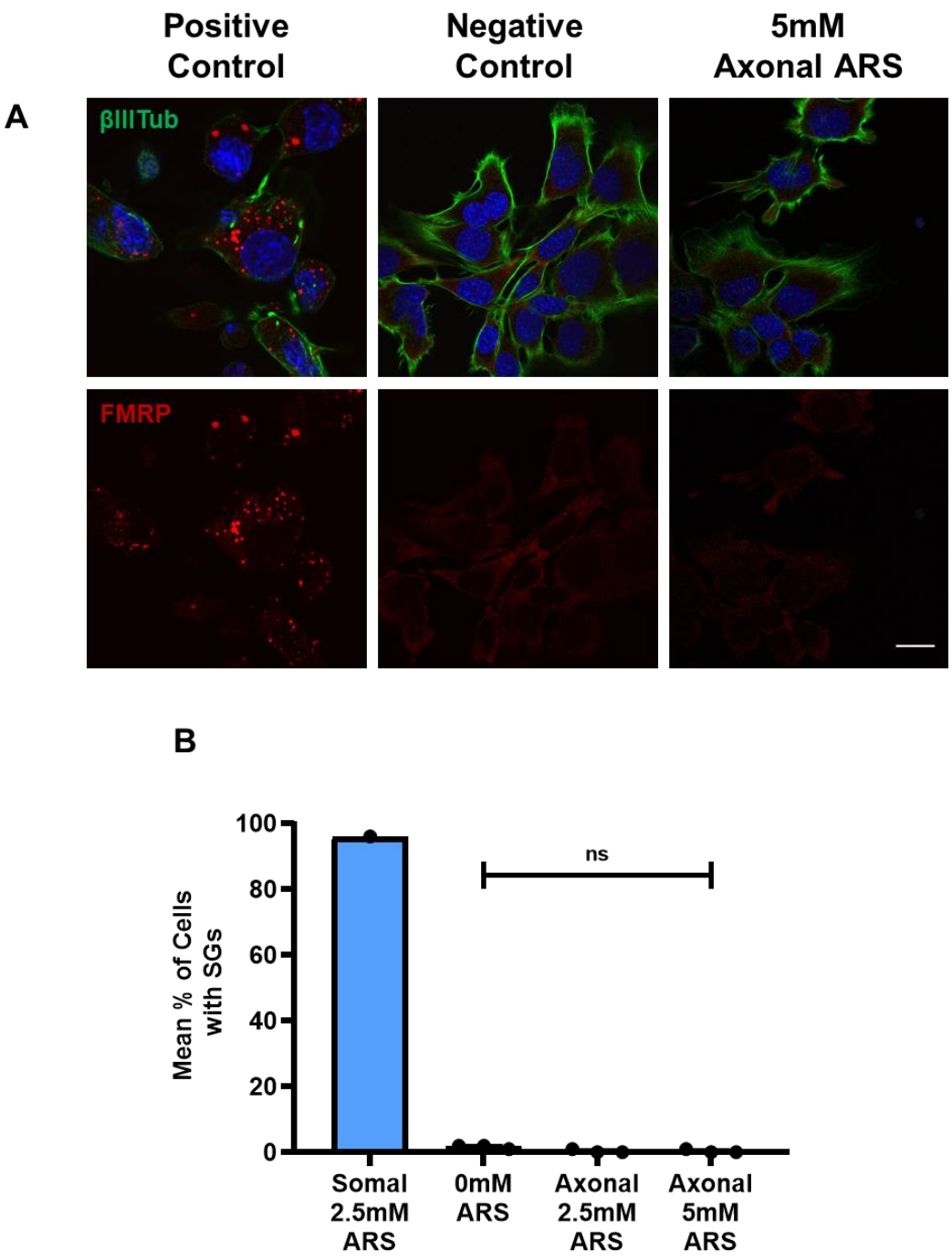

Figure 4.2 Arsenite applied to the axonal compartment of a microfluidic chamber does not induce stress granules in mouse embryonic fibroblasts plated in the somal compartment

Primary mouse embryonic fibroblasts (MEFs) obtained from WT E13.5 embryos were plated into the somal compartment of microfluidic chambers. On DIV1, 0, 2.5 or 5mM sodium arsenite (ARS) was applied to the axonal compartment for 1 hour. A positive control (n=1) was performed by applying 2.5mM ARS to the somal compartment. MEFs were stained with the F-actin stain Phalloidin-488 (green) and the stress granules (SG) marker FMRP (red). No significant increase in the % of MEFs displaying SGs was observed between the axonal treatments, as determined by one way ANOVA and post-hoc Tukey tests ($F(2,6)=5.333$; $p=0.047$; post-hoc $p=0.067/p=1$). N=3 replicates.

4.2.2 The induction of somal stress granules by axonal arsenite is replicated in primary sensory neurons.

I next aimed to determine whether the observed response was exclusive to CNs, or whether it occurred in other neuron types. To do so, I performed an axonal ARS dose response on sensory neurons. Primary embryonic DRGNs from E13.5 WT embryos were plated into the somal compartment of MFCs until DIV6 to allow for axonal projections to grow. The axonal compartment was incubated with 0.15 mg/ml CTxB-488 for 3 hours and axons were then stressed with 0.25, 0.5, 1 or 2.5 mM ARS for 1 hour. Both compartments were subsequently fixed, permeabilised and stained using antibodies against the SG protein FMRP and βIII-tubulin, as well as DAPI.

100 CTxB-488 somas were counted and classified as either SG-positive (distinct FMRP-positive puncta), SG-negative (homogenous cytoplasmic FMRP stain) or an intermediate phenotype (an altered distribution of FMRP with a halo-like enrichment near the plasma membrane) (***Figure 4.3A***). At 0.5, 1 and 2.5 mM ARS, SGs were observed in 10%, 38% and 66% of somas respectively, with 1 mM (post-hoc $p=0.004$) and 2.5 mM (post-hoc $p<0.0005$) significantly higher than control ($F(4,10)=28.36$, $p<0.0005$) by one-way-ANOVA and post-hoc Tukey tests (***Figure 4.3B-C***). While the response was replicated in DRG neurons, the 10% and 38% SG-positive somas observed at 0.5 mM and 1 mM ARS respectively were considerably lower than that observed for CNs (37.3% and 55% respectively).

As before, the proportion of CTxB-488-positive cells containing SGs following 2.5 mM axonal ARS and CTxB-488-negative somas in the same compartment were counted to assess fluidic isolation; 100 positive and 100 negative somas were counted. CTxB-488-status was significant by chi-squared test, with 67% of CTxB-positive cells displaying SGs, compared to <1% in CTxB-negative cells ($X^2(2, n=3) = 149.2$, $p<0.0005$)) (***Figure 4.3C-D***). This result was even more convincing than that for the CNs, as only one CTxB-488-negative soma was SG-positive across 3 replicates.

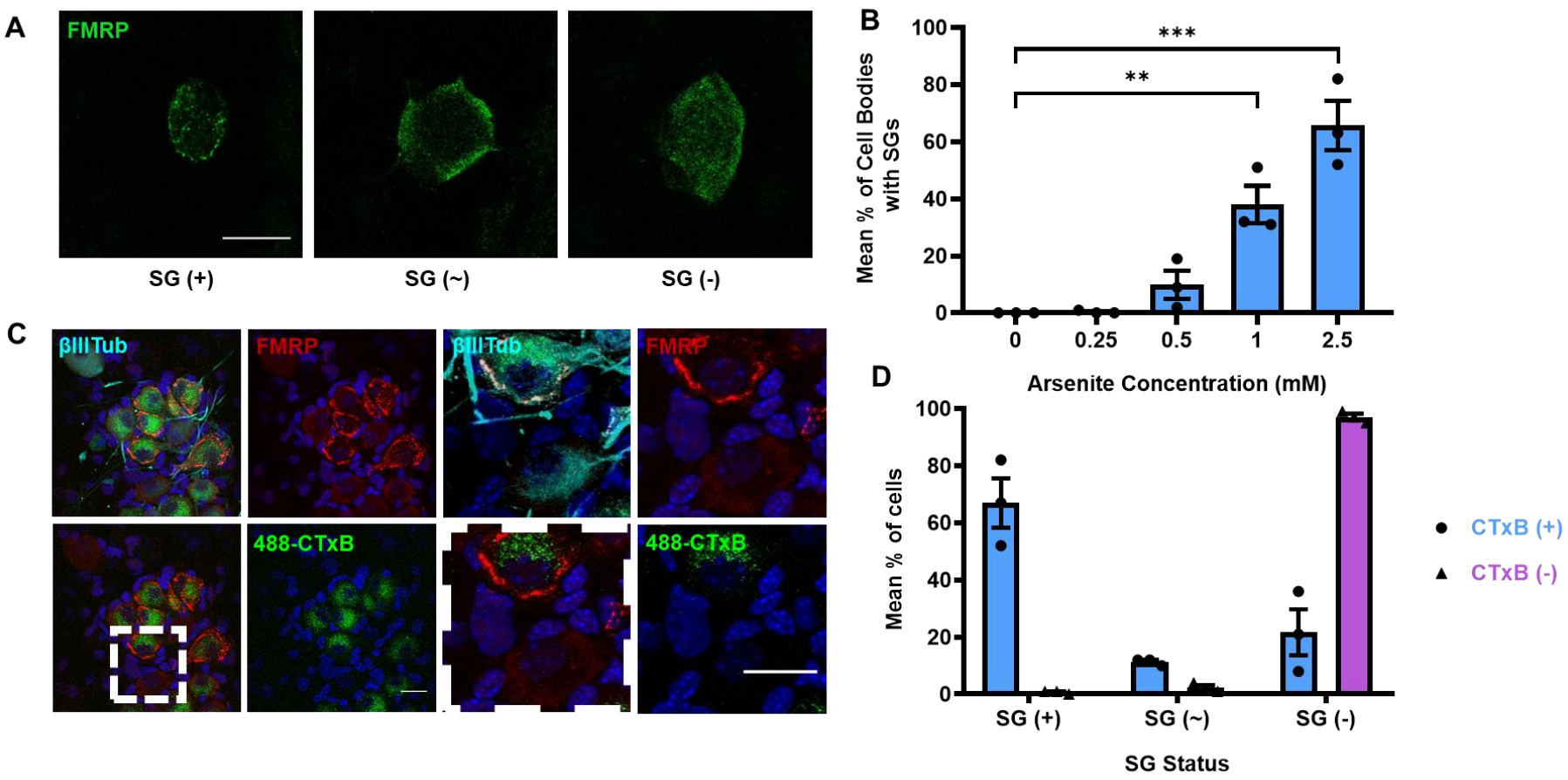
A
FMRP
SG (+)
SG (~)
SG (-)
B
Mean % of Cell Bodies with SGs
100
80
60
40
20
0
***
**
0
0.25
0.5
1
2.5
Arsenite Concentration (mM)
C
βIIITub
FMRP
βIIITub
FMRP
488-CTxB
488-CTxB
D
Mean % of cells
100
80
60
40
20
0
SG (+)
SG (~)
SG (-)
SG Status
CTxB (+)
CTxB (-)

Figure 4.3 The induction of somal stress granules by axonal arsenite is replicated in primary sensory neurons

A: FMRP (green) stain in the cell body of dorsal root ganglion (DRG) neurons following acute axonal arsenite stress was used to define cells as either as stress granule (SG)-positive (SG (+)), stress granule-negative (SG(-)) or an intermediate phenotype (SG (~)). Scale bar is 20μm. **B:** Primary DRG neurons (DIV6) from WT E13.5 embryos were cultured in microfluidic chambers. The axonal compartment was incubated with CTxB-488 for 3hrs, followed by 0, 0.25, 0.5, 1 or 2.5mM sodium arsenite for 1 hour. A dose-dependent increase in the % of cell bodies containing SGs was observed. 1mM (post-hoc $p=0.004$) and 2.5mM (post-hoc $p<0.0005$) are significantly higher than control ($F(4,10)=28.36$; $p<0.0005$) by one-way-ANOVA and post-hoc Tukey tests **C-D:** FMRP-positive SGs (red) are induced in CTxB-488-positive (green) neuron somas but not CTxB-488-negative somas. Neurons were stained with β3-tubulin/DAPI. Scale bar is 20μm. CTxB-488-status was significant by chi-squared test ($X2(2, n=3) = 149.2$, $p<0.0005$). N=3 biological replicates.

4.2.3 Whole-cell cycloheximide prevents the formation of somal stress granules following axonal arsenite stress.

The large body of SG research has determined a number of properties intrinsic to canonical SGs. One such property is the ability to block SG induction using cycloheximide (CHX); it is thought that CHX prevents the release of mRNA from polysomes, in turn hindering phase separation. In order to determine if these axon stress-induced, somal FMRP granules exhibited this property, I cultured primary CNs in MFCs and on DIV7 the axonal compartment was incubated with 0.15 mg/ml CTxB-488 for 3 hours, followed by pre-incubation of both compartments with 10 μg/ml CHX for 1 hour (as in Kedersha et al., 2000). 1 mM ARS was then applied to the axonal compartment for 1 hour (co-applied with 10 μg/ml CHX). Both compartments were subsequently fixed, permeabilised and stained using antibodies against FMRP and βIII-tubulin, as well as DAPI.

Whole-cell CHX completely prevented the formation of somal SGs following axonal ARS stress, suggesting that, as for whole-cell stress, polysome disassembly is required for the formation of the somal SGs induced by axon stress (***Figure 4.4***). This was significant by independent samples t-test ($t(4)=16.531$, $p=0.003$).

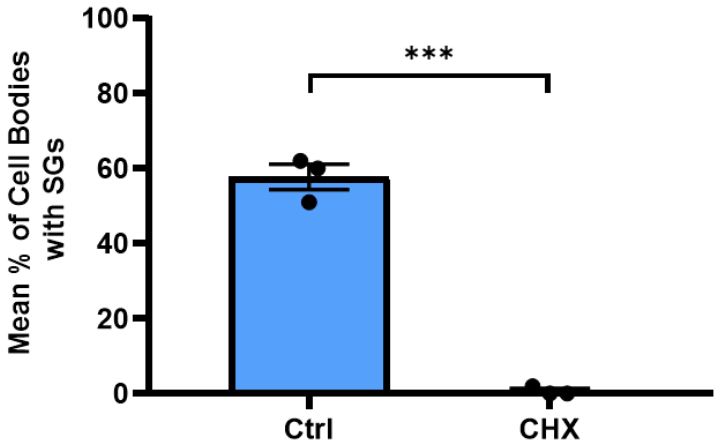

Figure 4.4 Whole-cell cycloheximide prevents the formation of somal stress granules following axonal arsenite stress

A-B: Primary cortical neurons (DIV7) from WT E13.5 embryos were cultured in microfluidic chambers. The axonal compartment was incubated with CTxB-488 for 3hrs, followed by incubation of both compartments with 10µg/ml cycloheximide (CHX) for 1 hour, followed by addition of 1mM sodium arsenite (ARS) to the axonal compartment for 1 hour (co-applied with CHX). A significant decrease in the % of cell bodies containing SGs was determined by independent samples t-test ($t(4)=16.531$, $p=0.003$). N=3 biological replicates.

4.2.4 The formation of stress granules post-axonal arsenite stress has a delayed time course compared to somal arsenite stress

In order to understand the dynamics of the response, I performed an ARS time course comparing the somal and axonal compartments of MFCs. Primary embryonic CNs or DRGNs from E13.5 WT embryos were plated into the somal compartment of MFCs and on DIV6 or 7 (cortical and DRG neurons respectively), incubated with CTxB-488 for 3 hours. Either the somal or axonal compartment was stressed with ARS for 0, 10, 20, 30, 40, 50 or 60 minutes (1 or 2.5 mM for cortical or DRG neurons respectively). Both compartments were subsequently fixed, permeabilised and stained using antibodies against FMRP and βIII-tubulin, as well as DAPI.

For somal stress in both cell-types, the first sign of SGs appears between 10-20 minutes after treatment, but this is delayed to 20-30 minutes for axonal stress (***Figure 4.5***). We determined values for the maximal SG response (SG_{MAX}; the highest percentage of stress granules observed) and the time point at which 50% of the max response had been elicited (SG_{50}), comparing both via independent-

samples t-test. SG_{50} was estimated using the ECanything tool on GraphPad Prism (GraphPad, San Diego).

For CNs, the SG_{50} value for somal stress (27.0 minutes) was lower than for axonal stress (33.4 minutes), indicating a delayed SG formation, though this did not achieve significance by independent samples t-test ($t(4)=1.786$, $p=0.167$). While SG_{MAX} for the somal SG response was 92%, the axonal SG_{MAX} was significantly lower at 59.3% ($t(4)=6.795$, $p=0.002$), which plateaued at the 50 minute time-point.

Similar results were obtained for DRG neurons. The SG_{50} value for somal stress (22.8 minutes) was significantly lower than for axonal stress (33.1 minutes), indicating a delayed SG formation by independent samples t-test ($t(4)=3.971$, $p=0.021$). While the SG_{MAX} for the somal SG response was 87%, the axonal SG_{MAX} was again significantly lower at 62% ($t(4)=5.385$, $p=0.008$), again plateauing at the 50 minute time-point.

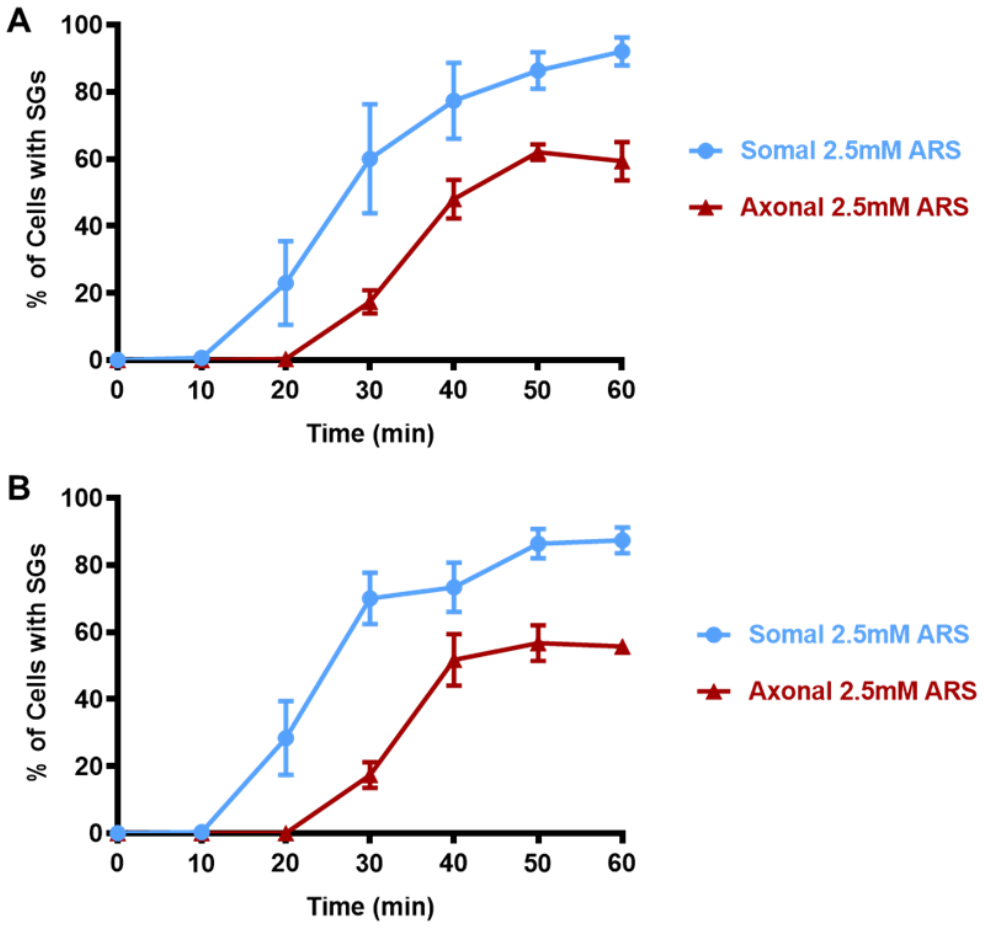

Figure 4.5 The formation of stress granules post-axonal arsenite stress has a delayed time course compared to somal arsenite stress

Primary cortical neurons (**A**; DIV7) or primary dorsal root ganglion (DRG) neurons (**B**; DIV6) from WT E13.5 embryos were cultured in microfluidic chambers. The axonal compartment was incubated with CTxB-488 for 3hrs. 2.5mM sodium arsenite was then applied to either the somal or axonal compartment for 10, 20, 30, 40, 50 or 60 minutes. A time-dependent increase in % of cell bodies containing SGs was observed for both cell types, with a delayed time course for axonal compared to somal. Somal SG50=33min; axonal SG50=23min; somal SGMAX=87%; axonal SGMAX=57%. N=3 biological replicates

4.2.5 Pharmacological inhibition of axonal dynein reduces the induction of somal stress granules by axonal arsenite stress.

Compared to whole-cell stress, axonal ARS stress has an increased SG_{50} of 6-11 minutes, indicating a delayed time course for SG formation. This delay-interval is likely too fast for simple intracellular diffusion of ARS from the axon to the soma. However, 10 minutes is consistent with the speeds described for dynein-mediated retrograde fast axonal transport (Brown, 2003).

To test whether this retrograde response was dynein-dependent, I performed the same experimental set-up, but incubated the axons with erythro-9-(2-hydroxy-3-nonyl)adenine (EHNA), an inhibitor of the dynein ATPase (Bouchard et al., 1981). As before, I cultured primary CNs in MFCs and on DIV7 the axonal compartment was incubated with 0.15 mg/ml CTxB-488 for 3 hours followed by pre-incubation of the axonal compartment with 0, 1 or 2 mM EHNA for 1 hour. 1 mM ARS was then applied to the axonal compartment for 1 hour (co-applied with 0, 1 or 2 mM EHNA). Both compartments were subsequently fixed, permeabilised and stained using antibodies against FMRP and βIII-tubulin, as well as DAPI (***Figure 4.6A***).

Axonal EHNA induced, albeit not fully, a significant decrease in the proportion of cell bodies containing SGs by one-way ANOVA ($F(2,9)=5.864$; $p=0.0234$), with post-hoc Tukey testing showing a significant decrease from control to 2mM EHNA ($p=0.0218$) This decrease indicates that there may be a role for axonal dynein in propagating the axonal ARS response to the soma. (***Figure 4.6B***).

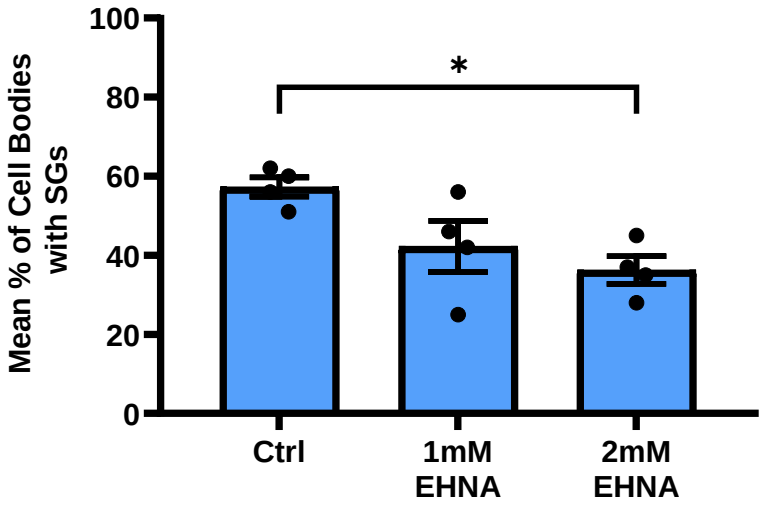

Figure 4.6 Pharmacological inhibition of axonal dynein reduces the induction of somal stress granules by axonal arsenite stress

A-B: Primary cortical neurons (DIV7) from WT E13.5 embryos were cultured in microfluidic chambers. The axonal compartment was incubated with CTxB-488 for 3hrs, followed by incubation of the axonal compartment with 0, 1 or 2mM EHNA for 1 hour and subsequent addition of 1mM sodium arsenite (ARS) to the axonal compartment for 1 hour (co-applied with EHNA). A significant decrease in the % of cell bodies containing SGs was observed by one-way ANOVA ($F(2,9)=5.864$; $p=0.0234$), in particular between the control and 2mM EHNA ($p=0.0218$). N=4 biological replicates.

4.2.6 Pharmacological inhibition of axonal protein synthesis reduces the induction of somal stress granules by axonal arsenite stress.

During the response to mechanical axon damage, the axon conveys a message to the soma by translating a protein signal from mRNA localised to the axon, which is then retrogradely transported via dynein towards the cell body (Perry et al., 2012). To test whether this was also the case for the ARS-induced response, I applied the translation inhibitor CHX to the axonal compartment.

CNs were plated into MFCs and on DIV7 the axonal compartment was incubated with 0.15 mg/ml CTxB-488 for 3 hours, followed by pre-incubation of the axon compartment with either control or 10 µg/ml CHX for 1 hour. 1mM ARS was then applied to the axonal compartment for 1 hour (co-applied with 10 µg/ml CHX). Both compartments were subsequently fixed, permeabilised and stained using antibodies against FMRP and βIII-tubulin, as well as DAPI (***Figure 4.7***).

Axonal CHX significantly decreased the formation of somal SGs following axonal ARS stress, by independent samples t-test (t(6)=3.478, p=0.0132). It remains unclear whether the reduction in the number of SGs formed is due to ability of CHX to inhibit protein translation or it's ability to prevent polysome disassembly.

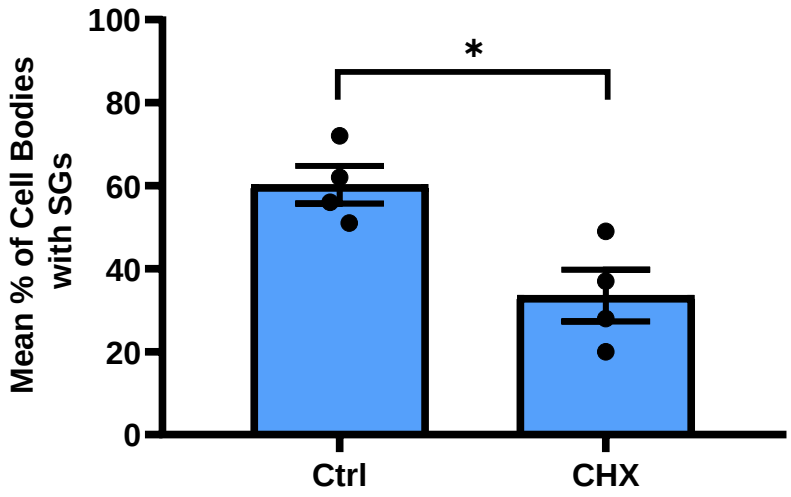

Figure 4.7 Pharmacological inhibition of axonal protein synthesis reduces the induction of somal stress granules by axonal arsenite stress

A-B: Primary cortical neurons (DIV7) from WT E13.5 embryos were cultured in microfluidic chambers. The axonal compartment was incubated with CTxB-488 for 3hrs, followed by incubation of the axonal compartment with 10µg/ml cycloheximide (CHX) for 1 hour, and subsequent addition of 1mM sodium arsenite (ARS) to the axonal compartment for 1 hour (co-applied with CHX). A significant decrease in the % of cell bodies containing SGs was determined by independent samples t-test (t(6)=3.478, p=0.0132). N=4 biological replicates.

4.2.7 Neither axonal thapsigargin stress, nor mechanical axotomy induce somal stress granules.

For axonal ARS treatment, as the concentration increases, both the formation of somal SGs and the amount of axon damage increases, as indicated by increased blebbing, increased axon fragmentation and decreased fluorescence intensity of the βIII-tubulin stain (***Figure 4.8***). To determine whether axonal damage could be partly responsible for the formation of somal SGs, I investigated whether mechanical axotomy could induce SGs in the cell body. Using both primary cortical and DRG neurons from E13.5 WT embryos at DIV6 in MFCs, I performed axotomy as previously described (Park et al., 2006), using a glass Pasteur pipette to aspirate medium directly from the axonal compartment, creating a bubble which ruptures the axons. Following this, medium was replaced and the cells were left at 37°C for 1

hour. Both compartments were subsequently fixed, permeabilised and stained using antibodies for FMRP and βIII-tubulin. No FMRP-positive SGs were observed in the somal compartment following axotomy (two replicates). Rather, the FMRP stain remained homogenous through the cytoplasm, as in control cells.

In order to determine whether the formation of somal SGs following axonal stress is only induced by ARS, I repeated the axonal stress experiment using the endoplasmic reticulum stressor thapsigargin, a commonly used SG inducer (Thomas et al., 2009). CNs were plated into MFCs and on DIV7 the axonal compartment was incubated with 0.15 mg/ml CTxB-488 for 3 hours, followed by treatment of the axon compartment with 0, 6.25, 12.5, 25 or 50 μM thapsigargin (***Figure 4.8***). No somal SGs were observed following axonal thapsigargin; two replicates. This was despite a large amount of axon damage for the higher concentrations (12.5 – 50 μM), which was comparable to, or more extensive than, the damage induced by concentrations of axonal ARS that induce SGs (***Figure 4.9***).

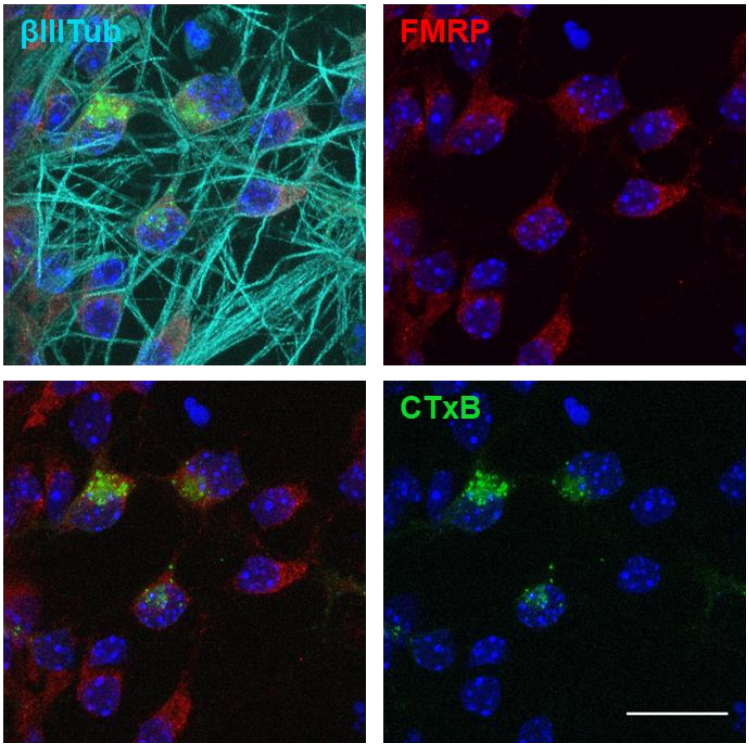

Figure 4.8 Axonal thapsigargin stress does not induce somal stress granules

Primary cortical neurons were cultured from E13.5 mouse embryos and plated into MFCs. On DIV7, the axonal compartment was incubated with 0.15mg/ml CTxB-488 for 3 hours, followed by treatment of the axonal compartment with 0, 6.25, 12.5, 25 or 50μM thapsigargin. No FMRP-positive SGs (red) were observed following axonal thapsigargin; neurons were also stained with β3-tubulin (cyan)/DAPI (blue); two replicates.

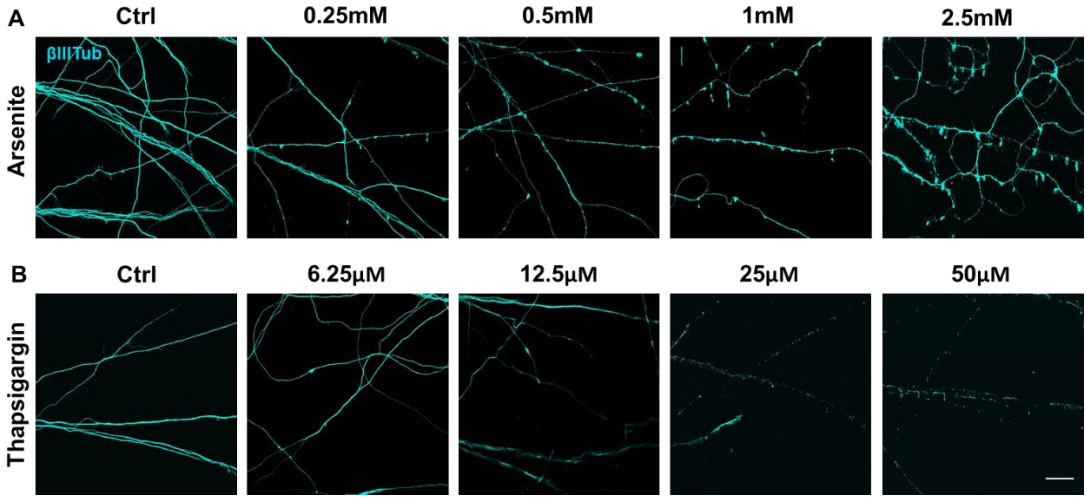

Figure 4.9 Both arsenite and thapsigargin induce axon damage

Primary cortical neurons (DIV7) from WT E13.5 embryos were cultured in microfluidic chambers and the axonal compartment was incubated with CTxB-488 for 3hrs, with subsequent addition of either **A:** sodium arsenite or **B:** thapsigargin for 1 hour (concentrations indicated in figure). Axons were stained for βIII-tubulin (cyan) in order to observe axon damage.

4.3 Discussion

The results of this chapter have further characterized the ability of neuronal cells to respond to stress. These findings demonstrate the first evidence that axons can respond to arsenite stress and subsequently propagate a signal to the soma. Based on experiments adding radioactive [^{35}S]methionine to compartmentalised chambers followed by scintillation counting, it is unlikely that the ARS is simply leaking from the axonal compartment to the somal compartment within the 1 hour timescale of our experiment (Taylor et al., 2005). Unpublished data using our own MFC designs has demonstrated that upon addition of [^{32}P]-γ-ATP to the axonal compartment, it takes over 20 hours for it to become detectable in the somal compartment (with a 40 µl volume difference; 60 µl less than used in my experimental set-up).

Further, no SGs are detected when MEFs (NNCs) are plated into MFCs and ARS is applied at high concentrations (2.5 mM or 5 mM) to the axonal compartment for 1 hour; 2.5 mM was the highest concentration used for the neuronal axonal ARS dose response. This also suggests that the fluidic isolation is intact, as these cells do not project axons and therefore shouldn't come into contact with the ARS. The MEFs in this experiment were not allowed to reach 100% confluence for ease of cell counting. It is possible that proliferation of NNCs in the CN and DRGN cultures, or the growth of axons through MFC grooves, could alter the integrity of the device and hence affect the fluidic isolation.

ARS leaking between compartments is also unlikely given the comparison of the 488-CTxB-positive vs CTxB-488-negative cells; CTxB-488-negative cells were 0% and 3% SG-positive for DRG neurons and CNs respectively. It is worth noting the difference that 3% of 488-CTxB-negative CN somas displayed SGs, while this was 0% in DRG neurons; compared to 0% in the absence of ARS for both cell-types. This may be an artefact of the technique: CNs and DRGNs were cultured in MFCs with 500 µm and 800 µm long microgrooves respectively, so ARS may be able to leak across the shorter grooves over the hour, but not the longer ones. Alternatively there may be a biological reason; for example, CN somas may have an increased capacity to transmit stress signals intercellularly. One further explanation is that CNs may die earlier than DRGNs in response to axonal ARS, with neighbouring cells becoming stressed by the surrounding cell death.

It is also worth noting that CN somas formed SGs at all ARS concentrations investigated, while DRGNs required higher concentrations (1 mM, 2.5 mM) for a

robust response. Biologically, this may be indicative of an increased susceptibility to axonal stress for CNs compared to DRGNs. This may however be an artefact of the experimental set-up (i.e. MFC groove length; see above paragraph for discussion). As discussed in ***Chapter 3.3***, CNs and DRGNs are cultured in different media (as different media conditions have been optimised in our laboratory to promote the health of different neuron subtypes), which may have induced the observed effect; for example, DRGN medium contains the antioxidant β-mercaptoethanol, but not CN medium. It will be interesting to observe whether MNs, the other main cell-type which degenerates in ALS-FTD, exhibit responses at lower concentrations.

The comparison of the dynamics of somal SG formation between axonal and somal stress demonstrated the requirement of an additional 10 minutes for the axonal stress. This short delay is likely too fast for intracellular diffusion, but does not rule out a retrograde-transport mechanism mediated by the microtubule motor dynein. Using published retrograde axon transport speeds of 1–3 μm/s (Brown, 2003) and the longer 800 μm MFC microgroove length (as used in the DRGN experiment), the time to propagate a retrograde signal to the soma lies between 4 and 13 minutes; this range for 500 μm grooves is lower. Dynein-mediated fast retrograde axonal transport has previously been demonstrated to be critical for the DRGN response to axotomy in compartmentalised chambers (Hanz et al., 2003).

The lack of significance for the CN SG_{50} appears to be due to an increased time for CNs to form SGs following whole-cell arsenite stress compared to DRGNs, as axonal SG_{50}s are similar in both cell-types. This similarity may indicate a common mechanism for axonal stress induction, and suggests a similar capacity to form SGs intracellularly post-stress induction. The 4 minute SG_{50} difference between neuron types may however represent a different biological capacity to respond to ARS, for example DRG neurons have a higher surface area to internalise ARS, but may simply be an artefact of the high variance in the CN data.

The hypothesis that the axon-to-soma response requires dynein is supported by an observed decrease in SG-positive cell bodies following axonal EHNA application. The largest decrease is observed using 2 mM EHNA, a concentration used to block the dynein ATPase in multiple studies (Cande, 1982, Fargier et al., 2013, Lin et al., 2014). Although the response is only partially blocked, incomplete transport inhibition has been described for similar experimental designs to the current study, where neuronal axons in MFCs are treated with EHNA or ciliobrevin A (Baleriola et al., 2014). As my response decreases somal SG formation by 37%, it is possible

that EHNA was only blocking dynein processing to this extent in my set-up, though this remains to be checked. An additional reason for the effect size observed may be due to a ceiling effect. The SG response begins to plateau near the SG_{MAX} between 40-60 minutes for both cell-types, so may be easier to observe an inhibition effect at an earlier time point, before the system becomes saturated (e.g. at a 30 or 40 minute timepoint).

It is also worth noting that, while commonly used to inhibit dynein, EHNA has a number of off target effects, in particular its inhibition of phoshodiesterase II (Podzuweit et al., 1995) and adenosine deaminase (Porter and Abushanab, 1992). This means that I cannot guarantee that the observed decrease in the axon-to-soma response is due to dynein inhibition. In recent years, a number of more specific dynein inhibitors have been used, including ciliobrevins (Roossien et al., 2015) and dynarrestin (Hoing et al., 2018). EHNA was selected for the experiments in this chapter because it had been previously been optimised for dynein-inhibition experiments in our laboratory, and because fewer studies have fully characterised the effects of these newer inhibitors.

While dynein provides the most likely method of signal transduction towards the soma, there are other possible mechanisms. For example, DRGNs are able detect signals via receptors on their axon terminals and subsequently propagate action potentials towards the cell body (Nascimento et al., 2018). One potential mechanism is via TRP (transient receptor potential) ligand-gated cationic channels, which are expressed on a subset of DRG neuron axons (Brenneis et al., 2013). Reactive oxygen species (ROS), which are generated by oxidative stress have been shown to cause a conformational changes in these channels, directly activating them (Yoshida et al., 2006, Westlund et al., 2010). This permits the entry of cations into the axon, increasing the probability of action potential generation and eliciting other local downstream pathways (Sousa-Valente et al., 2014). This is, however, unlikely, as action potentials are very fast so would likely not result in the 10 minute delay, and because the response is conserved in CNs.

There is another point worth noting from the dynamics experiment. When the DRGNs were stressed somally, the SG_{MAX} was 87%, compared to a lower 57% for axonally stressed cells. While it is possible that the delayed time course means we did not observed the maximum response during the timeframe of our experiment, this is unlikely as the response appears to plateau between 40-50 minutes; this plateau is conserved in CNs. One possible explanation for this is that CN/DRGN

cultures are heterogenous populations, and as such different neurons within the same culture may have different capacities to transport retrograde cargoes, or express different axonal proteins, which may alter their responses to exogenous stressors.

Like dynein-mediated transport, local axonal protein synthesis has been highlighted as a mechanism by which axons respond to mechanical injury (Hanz et al., 2003). It is possible that the induction of somal SGs by axonal stress may also be dependent upon local axonal protein synthesis, as local CHX results in a significant decrease in the number of cell bodies containing SGs. This is feasible given that significant axonal protein synthesis can occur on a very short timescale (<5 minutes) (Wong et al., 2017). As CHX also prevents polysome disassembly, it is difficult to interpret this experiment without further data: it is currently unclear whether the observed effect of CHX is due to inhibition of protein translation or changes in phase separation (due to inhibition of polysome disassembly) within the axon. Further experiments using alternative translation inhibitors which to not prevent polysome disassembly, such as puromycin, are required.

As the axon-to-soma SG response was only observed at higher ARS concentrations, it is possible that ARS was directly killing the axons; effectively an "oxidative axotomy". However, observing CNs and DRGNs 1 hour following mechanical axotomy, the FMRP stain remained the same as that for control neurons, suggesting no effect on the SG response. Unpublished data from our lab has repeated this observation in primary MNs. There is currently very little evidence directly linking mechanical axon damage to somal SGs. One study performed axotomies on the sciatic nerve of adult C57BL/6 mice and investigated the cell body 7 days post-injury, which resulted in an upregulation of TDP-43 in the cytoplasm of retrograde tracer-positive MNs and a co-localisation with the SG markers TIA-1 and staufen in a non-punctate pattern (Moisse et al., 2009). Physical damage has however been shown to induce TDP-43/FMRP-positive granules in neurons, although interestingly these do not colocalise with SG markers TIAR1 and FUS (Wiesner et al., 2018); this highlights the necessity for a further characterisation of the protein composition of the FMRP-granules observed in the current chapter.

This chapter demonstrates the ability of axonal ARS incubation, but not thapsigargin, to induce somal SGs. This does not necessarily rule out the ability of thapsigargin, nor ER stress, to induce this response. While the studied concentrations induce somal SGs, differences in axonal biology may prevent a

response during 1 hour stressor duration investigated. Furthermore, compared to thapsigargin, ARS induces stress via a wide-range of mechanisms including induction of oxidative stress via production of reactive oxygen species (ROS) (Ruiz-Ramos et al., 2009) and destruction of the cytoskeleton (Li and Chou, 1992) and focal adhesions (Yancy et al., 2005). It is possible that the effect described in this chapter using ARS was observed because the multiple converging stress pathways in combination were sufficient to pass an induction threshold.

4.3.1 Future directions

Are the FMRP-positive granules stress granules?

Throughout this chapter, FMRP has been used as a marker for SGs; however, a thorough characterisation of these granules remains to be performed. While FMRP is a major constituent of SGs (Markmiller et al., 2018), the only other evidence I have that these are canonical SGs is that these granules are morphologically similar, and that whole-cell CHX blocks their formation. Additionally, FMRP forms part of multiple different RNP granules including dendritic mRNP granules (Antar et al., 2005) and those observed following brain injury (Wiesner et al., 2018). To characterise these granules further, a panel of common SG markers will in future be used to confirm the identity of these granules: for example G3BP, TIAR and translation factors. Further, co-immuno-*in situ* hybridisation should be performed to determine whether they are positive for RNA. In addition to constituent markers, it should be determined whether these granules exhibit the dynamic properties of canonical SGs, such as rapid fluorescence recovery after photobleaching (FRAP), fusion with other granules and granule disassembly after stress cessation (Wheeler et al., 2016). The expanding SG literature has a loose definition of what a SG actually is; at its most basic form, the structures induced in this chapter are granules that are induced by stress and therefore, in the context of this wide-ranging literature, it is fair to term them SGs.

Are the FRMP granule-positive cells alive?

Arsenite is an intense stressor, targeting multiple cellular pathways (Li and Chou, 1992). For this reason, it will be important to look at the effect of axonal stress on cell-death, for example using markers for activated-caspase 3 (Porter and Janicke, 1999). If the somas exhibiting FMRP-positive granules are undergoing cell death, it will suggest that these are non-canonical SGs. It may further be interesting to see if

these granules contain or exclude eIF3, as non-canonical pro-death SGs display a loss of eIF3 proteins over time (Aulas et al., 2018). If these cells are undergoing a death pathway, this model may still prove useful in investigating axon-mediated neuronal-death pathways.

Is the response arsenite-specific?

All of the current axonal stress work has been performed with ARS. As ARS has a lot of SG-independent effects, it will be important to attempt to replicate this response using other oxidative stressors, such as hydrogen peroxide. Further it will be interesting to see if other cell stressors elicit the same response when applied axonally: ER stressors (for example, thapsigargin); protein synthesis inhibitors (e.g. puromycin); osmotic stressors (e.g. sorbitol) (Dewey et al., 2011, Arimoto-Matsuzaki et al., 2016).

Is the response conserved across neuronal cell types?

All of the current axonal stress work has been performed in primary embryonic CNs and DRGNs. Given that these two distinct neuron types both display this response, it is likely pan-neuronal. However, in terms of ALS, it will be critical to investigate whether this response is conserved in MNs. In terms of varying susceptibility to axon stress, it would be interesting to prepare these three neuron types in parallel from the same embryo, culturing them in the same medium and MFCs to fully determine whether any cell-types are more susceptible to axonal stress. Additionally, these experiments have all been performed in embryonic mouse neurons. It will be interesting to see if the response is conserved in human neurons, adult neurons, and whether it can occur in a whole organism *in vivo*.

Do other mechanisms of dynein inhibition decrease the response?

EHNA has a number of off-target effects, so it will be interesting to see if newer pharmacological dynein inhibitors, such as ciliobrevin D (Roossien et al., 2015) and dynarrestin (Hoing et al., 2018), will induce the same response. It will also be interesting to compare pharmacological inhibition with genetic methods such as siRNA-mediated knockdown of motor subunits (Tsai et al., 2009) or by obtaining primary neuron cultures from mouse models with axon transport deficits, such as the *Loa* (Legs at odd angles) mouse model. This model has a mutation in *Dync1h1*, the gene encoding the dynein heavy chain subunit, which results in the decreased velocity of signalling endosomes (Garrett et al., 2014). As EHNA did not fully inhibit the response, it may be valuable to compare the amount that 2mM EHNA inhibits

the transport of other retrograde cargoes (such as CTxB) to the inhibition of the axon-to-soma SG response.

Is the response dependent on axonal protein synthesis?

In order to separate the protein translation and polysome trapping effects of CHX, it will be important to reattempt the axon stress experiments with different protein translation inhibitors, such as puromycin; it is worth noting that puromycin promotes polysome disassembly (Kedersha et al., 2000).

What is happening in the axon during axonal stress?

Some papers have reported the presence of SGs within axons following whole-cell stress (Markmiller et al., 2018). While axonal FMRP-positive SGs have been reported post-oxidative stress, we found FMRP-staining to be punctate in axons in control neurons, making it difficult to draw conclusions. It will important to investigate the SG response in axons using markers which are not already punctate in unstressed cells.

4.4 Conclusion

This study provides the first evidence that neuronal axons can respond to oxidative stress and subsequently propagate a response to the cell body. As MN axons are longer than most cell types, it is possible that these are more susceptible to stressors, particularly during ageing as the human body provides increasing levels of oxidative- and proteostatic-stress to the extracellular environment. The observed response indicates a mechanism by which this increasingly stressful axonal environment may be translated into cytoplasmic, RNA-binding protein-positive inclusions in both sporadic and familial ALS.

5 The stress granule response in the FUS-D14 mouse model

5.1 Specific aims

Besides viral infection, the majority of research linking SGs to disease pertains to ALS. While it is debated whether SGs are a precursor to neuronal inclusions, as discussed in ***Chapter 1.3***, investigation of the dynamics and composition of acute SG aggregates in the presence of disease-causing mutations will likely have major implications for multiple cellular aggregation pathways, including those leading to inclusion formation.

A large body of the existing SG disease research has been performed using techniques that overexpress mutant proteins, such as transfection and the use of tissue from transgenic animals (Bosco et al., 2010, Dewey et al., 2011, Figley et al., 2014). However, RNA-binding proteins (RBPs), which are commonly mutated in ALS and enriched in SGs, have tightly regulated levels within cells, so overexpression systems may not be appropriate models. Models with disease-relevant mutant protein expression include patient iPSCs (induced pluripotent stem cells) (Lenzi et al., 2015) and 'knock-in' models and cell lines (Devoy et al., 2017).

Another issue with neurodegenerative disease (NDD) research is that we are aiming to study pathomechanisms which likely progress over the course of decades, with symptom onset much later in life. This is an issue for the use of cell and mouse models, which are studied on a much smaller time scale (months – a few years). In order to observe the initial pathomechanisms of NDDs, it could be beneficial to study variants of the disease which have an early-onset and rapid progression in order to maximise the chances of observing a disease phenotype. In the study of ALS, mutations in *FUS* fit this brief, as these cases present with an earlier onset and a more aggressive progression than other ALS cases; (>60% ALS-FUS have onset <45 years) (Shang and Huang, 2016). In particular, mutations in the nuclear localisation signal (NLS) of *FUS* have been reported to cause early-onset ALS; <20 years onset (Baumer et al., 2010).

NLS-mutations have been demonstrated to have major implications for intracellular cytoplasmic aggregation, and hence for the formation of SGs and inclusions, via two mechanisms. Firstly, mutations in the NLS can disrupt its binding to TNPO1, hence increasing the amount of FUS in the cytoplasm that is available to aggregate

(Dormann et al., 2010). In addition to this, FUS-TNPO1 binding has been demonstrated to compete with FUS-FUS binding, with the same NLS-mutations that decrease TNPO1-binding increasing the propensity of FUS to undergo phase separation (Yoshizawa et al., 2018).

For the current chapter, I selected the FUSDelta14 'knock-in' mouse, a model of a FUS NLS mutation based on a human case with an early disease-onset (20 years) and a rapid disease progression (2 years) (DeJesus-Hernandez et al., 2010, Devoy et al., 2017). This model exhibits a progressive motor neurodegenerative phenotype when the mutation is expressed in heterozygosity and expresses FUS at physiological levels (discussed further in ***Chapter 1.1.2.4***). The added benefit of this system is that the FUSDelta14 mutation induces a deletion and a subsequent frameshift that results in an entirely different peptide sequence downstream of the mutation. This allowed for the generation of an antibody against the novel mutant C-terminus (FUS-D14 antibody), which can be used in conjugation with an antibody against the C-terminus of the wild-type FUS protein (FUS-WT), to compare the localisation of both the FUS-WT and FUS-D14 proteins in the same heterozygous cell. The N-terminus of FUS-D14 remains unchanged, so antibodies against this region can recognise both proteins.

Though a large number of studies have shown that cytoplasmic FUS mutants localise to SGs (Baron et al., 2013, Bosco et al., 2010, Lenzi et al., 2015), the current literature is in disagreement as to whether this is also true of the FUS-WT protein, particularly following sodium arsenite (ARS) stress. While multiple immunofluorescence studies have suggested FUS-WT does not localise to ARS-induced SGs (Bosco et al., 2010, Sama et al., 2013), more sensitive techniques, such as proximity labelling (Markmiller et al., 2018) and mass spectrometry (Jain et al., 2016) have confirmed its presence.

In wild-type (WT) and heterozygous (HET) mouse embryonic fibroblasts (MEFs) derived from the FUSDelta14 model, it has been previously shown that almost no FUS-WT entered SGs following ARS stress, while the FUS-D14 protein significantly co-localised with the SG marker G3BP (Devoy et al., 2017). Further, unpublished work from our lab has demonstrated that the FUS-D14 protein mislocalises to the cytoplasm in both HET and homozygous (HOM) primary motor neurons (MNs). As MNs are the predominate cell-type which degenerates in ALS, I aimed to determine whether FUS localised to SGs in primary MNs derived from HET and HOM embryos, with comparisons to neurons from the WT. Primary embryonic cells are a

good model for the comparison of WT, HET and HOM FUSDelta14 cells, as HOM mice die perinatally (Devoy et al., 2017).

While MNs degenerate in ALS, sensory neurons (including dorsal root ganglion neurons (DRGNs)) are comparatively spared. Therefore, investigated the localisation of FUS-WT and FUS-D14 in WT, HET and HOM primary DRGNs and the localisation of FUS to ARS-induced SGs in DRGNs.

5.1.1 Materials and methods

The results in this chapter were obtained by culturing primary motor and sensory neurons on glass coverslips; dissection and cell culture are detailed in ***Chapter 2.4***. For ***section 5.2.1*** and **5.2.3**, neurons were exposed to sodium arsenite (1 hour, 0.5mM), as detailed in ***Chapter 2.7***. This was followed by fixation and subsequent immunostaining, using antibodies for SG marker proteins (G3BP, TIAR, FMRP) and FUS, for the observation of SGs, and FUS localisation using confocal microscopy; as detailed in ***Chapter 2.6***. For ***section 5.2.2***. DRGNs were unstressed, and stained for FUS antibodies at DIV5.

5.2 Results

5.2.1 FUSDelta14-mutant FUS is present in stress granules at higher levels than wild-type FUS in primary motor neurons

Primary MN cultures were first obtained from E13.5 embryos (WT, HET and HOM for the FUSDelta14 mutation) and grown on coverslips. Cells were treated with 0.5 mM ARS for 1 hour (or MN medium control), fixed, permeabilised and stained with an antibody against FMRP (a SG marker) and an antibody against the N-terminus of both the WT and mutant FUS protein (n=3) (***Figure 5.1A-B***). Cells were also stained for βIII tubulin and DAPI in order to distinguish the area covered by each neuron and its nucleus.

For each replicate, 5 MN images were acquired by confocal microscopy. A threshold for each replicate was determined for the FMRP stain to define regions of interest (ROIs) for “inside SG” and “outside SG”. “Outside SG” was defined as the area of the neuron soma, determined by the βIII tubulin stain, excluding the FMRP-positive SGs and DAPI-positive nucleus. The mean grey intensity for FUS was obtained for both ROIs; i.e. FUS intensity inside (***Figure 5.1E***) and outside (***Figure***

5.1F) SGs. Values were then determined for the fold-change upon entering a SG from the cytoplasm (SG intensity/non- SG intensity) (***Figure 5.1C***) and another for the absolute change upon entering a SG (SG intensity – non-SG intensity) (***Figure 5.1D***). Data was analysed by one-way ANOVA and post-hoc Tukey tests.

The FUS-565 antibody showed localisation to SGs for all genotypes, though this was much lower for the WT (1.29-fold increase/4 absolute increase). Both the HET and HOM demonstrated a significantly higher relative increase of >2-fold ($F(2,6)=21.28$, $p=0.002$; with post-hoc $p=0.002$ and 0.011 respectively) compared to the WT. Likewise, HET and HOM showed a significantly higher absolute increase ($F(2,6)=10.05$, $p=0.012$; with post-hoc $p=0.015$ and 0.027 respectively) compared to the WT. This indicates that while both the FUS-WT and FUS-D14 protein localise to SGs, FUS-D14 has a much higher SG localisation. Despite an extra copy of the FUSDelta14 allele, HOM MNs showed no significant differences to HET MNs (***Figure 5.1C-F***).

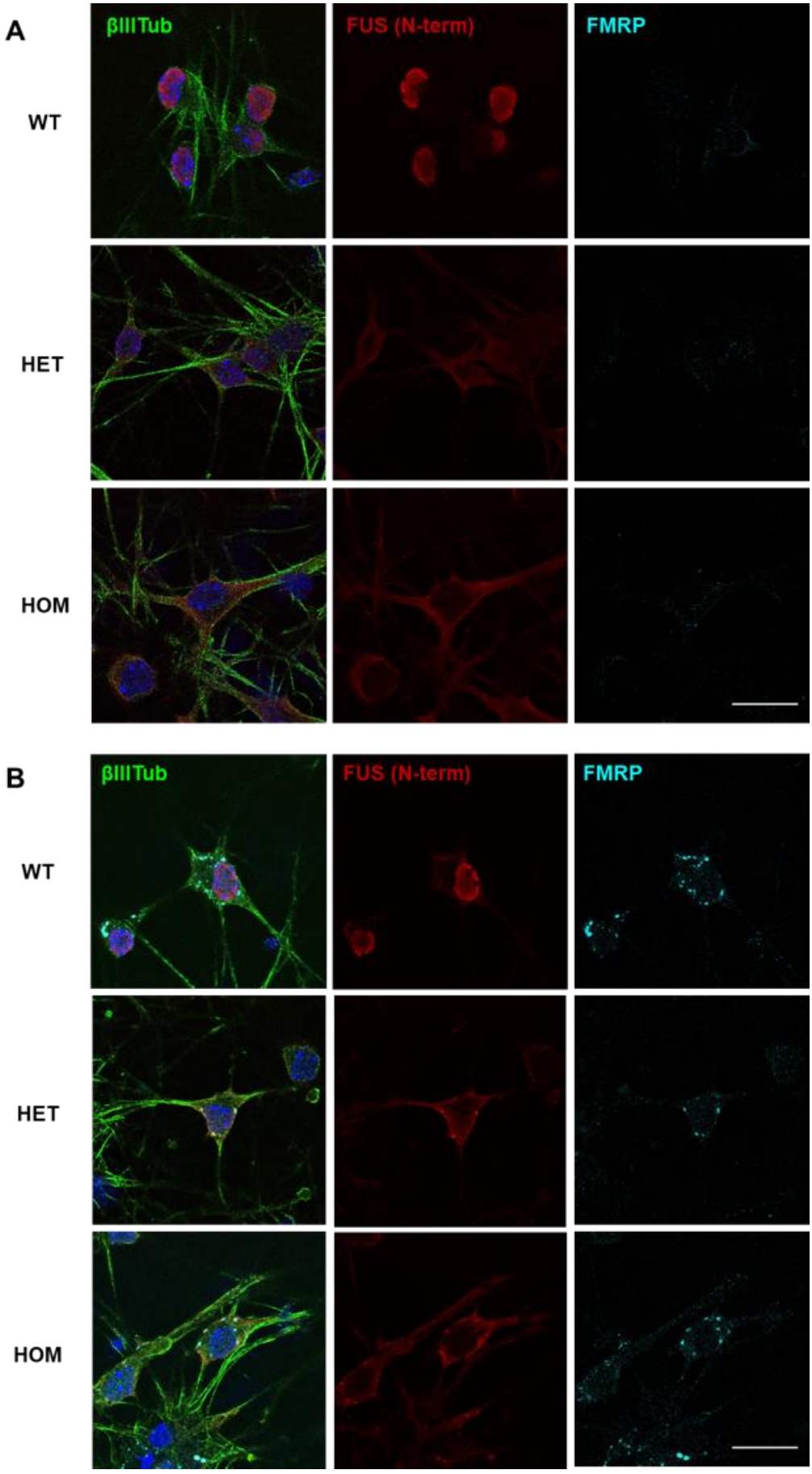
A
βIIITub
FUS (N-term)
FMRP
WT
HET
HOM
B
βIIITub
FUS (N-term)
FMRP
WT
HET
HOM

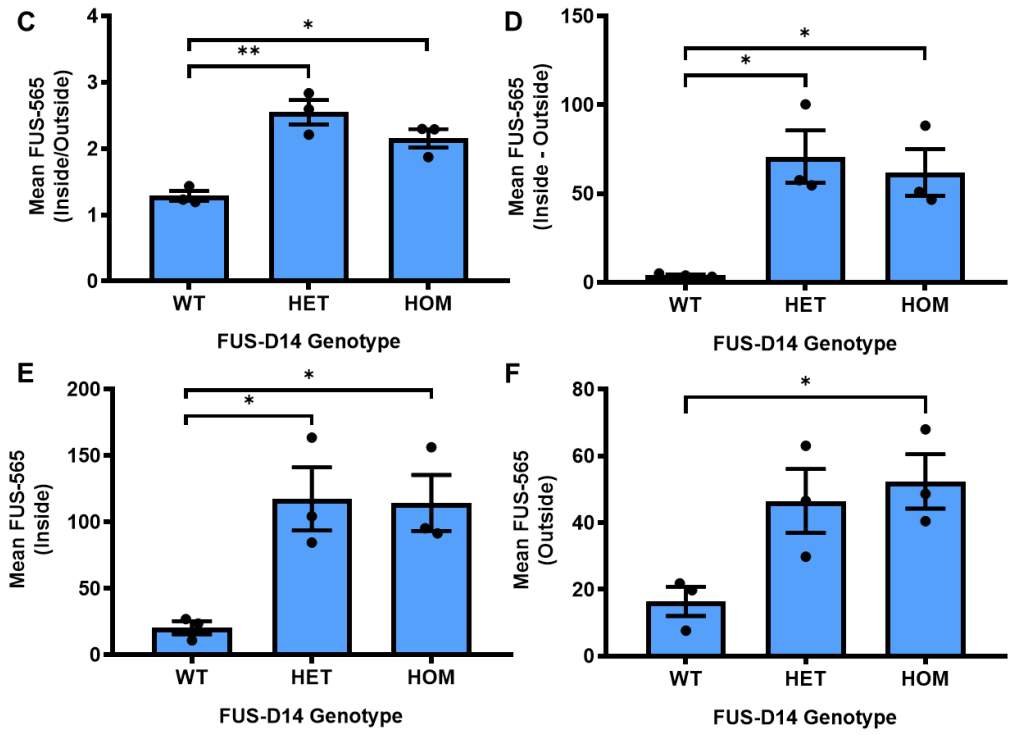

Figure 5.1 FUSDelta14-mutant FUS is present in stress granules at higher levels than wild-type FUS in primary neurons

A-B: 1 hour of 0.5mM sodium arsenite induces FMRP-positive stress granules (SGs) in DIV5 primary motor neurons cultured from wild-type (WT) E13.5 embryos or those heterozygous (HET)/homozygous (HOM) for the FUSDelta14 mutation. Neurons were also stained using antibodies against N-terminal FUS (FUS-565; red), βIII-tubulin (green) and DAPI (blue). Scale bar is 20μm. **B-F**: ROIs were determined using ImageJ for areas positive for FMRP ("inside" SG) or not ("outside" SG). FUS intensity was determined for "inside" (**E**), intensity "outside" (**F**), fold-change (**C**) and absolute change (**D**) calculated. All statistical tests by one-way ANOVA and post-hoc Tukey; n=3. C: HET (p=0.002) and HOM (p=0.011) are significantly higher than WT. D: HET (p=0.015) and HOM (p=0.027) are significantly higher than WT. E: HET (p=0.023) and HOM (p=0.027) are significantly higher than WT. F: HOM is significantly higher than WT (p=0.038). N=3 biological replicates.

5.2.2 FUSDelta14-mutant FUS mislocalises to the cytoplasm in primary sensory neurons

Previously the D14 FUS protein has been reported to mis-localise to the cytoplasm in both primary mouse embryonic fibroblasts and MNs, using antibodies specific to the C-termini of WT FUS and the D14 mutant protein (Devoy et al., 2017). It is unknown whether this phenotype is replicated in neurons which are comparatively unaffected in ALS pathogenesis, such as DRGNs. To investigate this, primary DRGN cultures were first obtained from E13.5 embryos (WT, HET and HOM for the FUSDelta14 mutation) and grown on coverslips. Cells were fixed, permeabilised and stained with specific antibodies against the C-terminus of FUS-WT (FUS-562

antibody) and the FUS-D14 (FUS-D14 antibody) mutant, as well as βIII-tubulin (***Figure 5.2A***). For each replicate, 5 DRGN images were acquired by confocal imaging, with one neuron per image adjusted for the plane with the highest DAPI intensity. Using ImageJ, background was subtracted using a rolling ball algorithm (50-pixel radius), regions of interest (ROIs) were determined for both the nucleus (using DAPI stain) and cytoplasm (using βIII-tubulin and DAPI stain) and the mean grey intensity was determined for each ROI. Mean grey intensity values were normalised to the max grey intensity value for each replicate.

Statistical analyses were performed using one-way MANOVA, with post-hoc one-way ANOVA and Tukey tests. FUSDelta14 mutation dosage was shown to have a significant effect on the localisation of the FUS-WT protein ($F(4,12)=3.632$, $p=0.037$), though post-hoc testing demonstrated no significant differences for cytoplasmic localisation ($F(2,6)=1.837$, $p=0.249$) (***Figure 5.2B***). FUSDelta14 dosage did exert an effect on nuclear FUS-WT localisation ($F(2,6)=128.807$, $p<0.0005$), with WT ($p<0.0005$) and HET ($p<0.0005$) significantly higher than HOM; there was no difference between WT and HET despite the HET containing one less copy of the FUS-WT allele ($p=0.407$).

FUSDelta14 mutation dosage also had a significant effect on the localisation of the FUS-D14 protein ($F(4,12)=7.953$, $p=0.002$), for both nuclear ($F(2,6)=7.483$, $p=0.023$) and cytoplasmic ($F(2,6)=35.975$, $p<0.0005$) localisation (***Figure 5.2C***). In the nucleus, HOM neurons showed a significant increase compared to WT ($p=0.026$), with HET showing borderline significance from WT ($p=0.053$); here there was no difference between HET and HOM, despite the additional copy of the FUSDelta14 allele for the HOM ($p=0.829$). In the cytoplasm however, FUS-D14 intensity demonstrated a FUSDelta14 allele dose-dependent increase with HET and HOM significantly higher than the WT ($p=0.022$ and $p<0.0005$ respectively), and HOM significantly higher than the HET (2-fold; $p=0.008$).

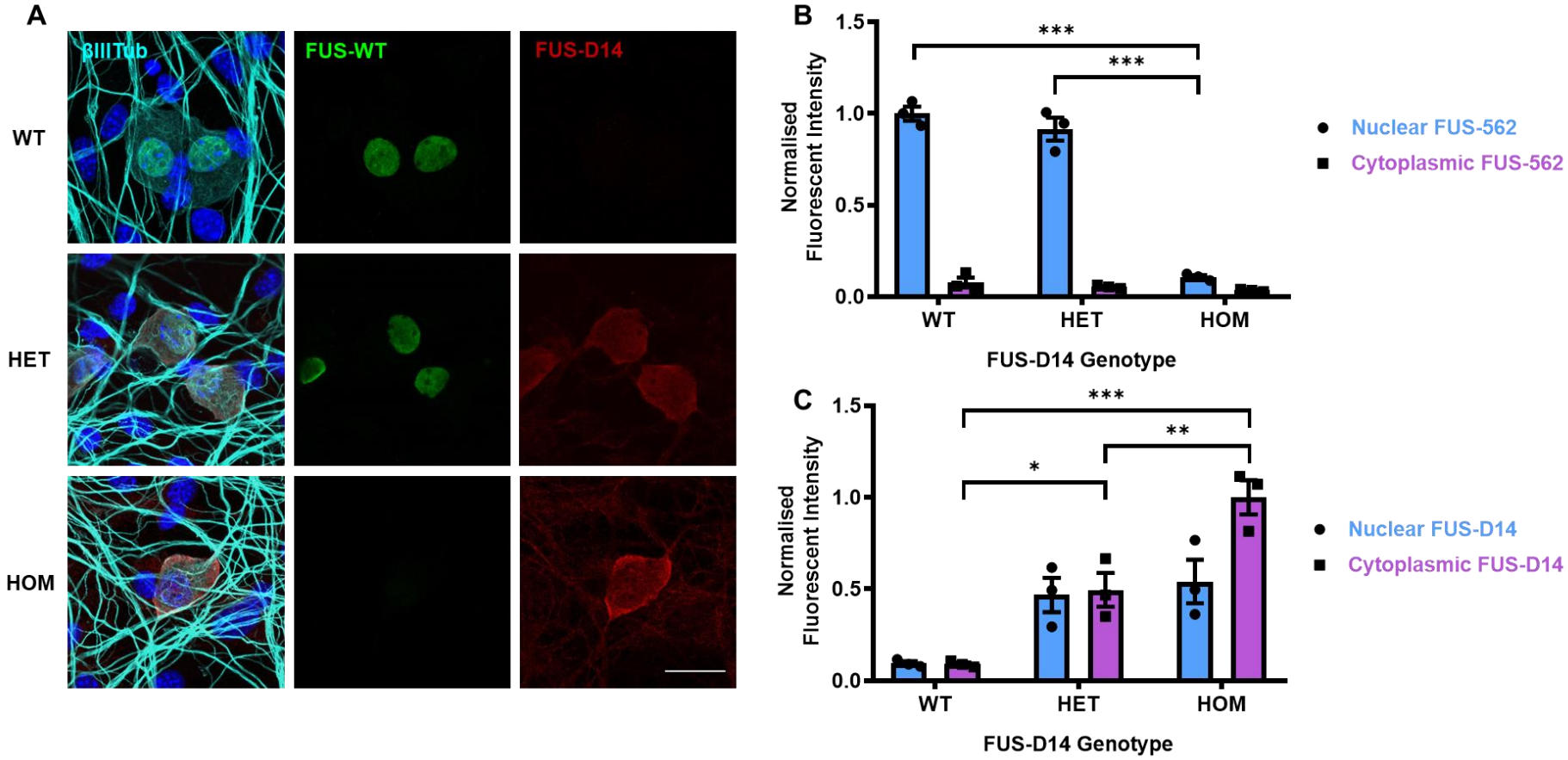
A
βIIITub
FUS-WT
FUS-D14
WT
HET
HOM
B
Normalised Fluorescent Intensity
1.5
1.0
0.5
0.0
***
***
WT
HET
HOM
FUS-D14 Genotype
Nuclear FUS-562
Cytoplasmic FUS-562
C
Normalised Fluorescent Intensity
1.5
1.0
0.5
0.0
***
**
*
WT
HET
HOM
FUS-D14 Genotype
Nuclear FUS-D14
Cytoplasmic FUS-D14

Figure 5.2 FUSDelta14-mutant FUS mislocalises to the cytoplasm in primary sensory neurons

A: Primary dorsal root ganglion neurons (DIV5) cultured from wild-type E13.5 embryos. Wild-type FUS (FUS-WT; green) is almost entirely nuclear in both WT/HET neurons. FUS-D14 (red) is both nuclear and cytoplasmic, with higher expression in the HOM cytoplasm. Cells are also stained with β3-tubulin (cyan)/DAPI (blue). Scale bar is 20μm. n=3. **B-C:** Regions of interest (ROIs) were determined for nucleus and cytoplasm, and mean grey intensity values were determined for each ROI using ImageJ. 5 neurons were investigated per n and an average determined; intensity values were normalised to the max grey intensity value for each n. FUSDelta14 mutation dosage was shown to have a significant effect on the localisation of both the FUS-WT (**B**) protein ($F(4,12)=7.953$, $p=0.002$) and the FUS-D14 (**C**) protein ($F(4,12)=3.632$, $p=0.037$) by one-way MANOVA. Post-hoc analyses one-way ANOVA and Tukey tests demonstrated an increase of cytoplasmic D14 intensity from HET to HOM neurons ($p=0.008$). N=3 biological replicates.

5.2.3 FUSDelta14-mutant FUS is present in stress granules at higher levels than wild-type FUS in primary sensory neurons

Since FUS-D14 localises to the cytoplasm in an allele dose-dependent manner in DRGNs, we decided to investigate to what extent FUS localised to SGs in DRGNs; taking advantage of three different FUS antibodies. In order to do this, primary DRGN cultures were first obtained from E13.5 embryos (WT, HET and HOM for the FUSDelta14 mutation) and grown on coverslips. Cells were then treated with 0.5 mM ARS for 1 hour (or DRGN medium control), fixed, permeabilised and stained with DAPI, antibodies against two SG markers (G3BP, TIAR or FMRP; depending on FUS antibody species) and an antibody against either the WT (C-terminal), D14 (C-terminal) or both (N-terminal) FUS proteins (n=3) (***Figure 5.3A-B; Figure 5.4A-B; Figure 5.5A-B***). It was possible to determine the shape of DRGNs in culture without βIII tubulin staining, instead using the cytoplasmic FRMP/TIAR stain.

For each replicate, 5 DRG neuron images were acquired by confocal imaging, with one neuron per image adjusted for the plane with the highest G3BP intensity. Next, for each replicate, a threshold was determined for each SG marker and two ROIs defined for “inside SG” (a region where both markers are present) and “outside SG” (cytoplasmic, but with neither marker present). The mean grey intensity for FUS was obtained for both ROIs. One value was determined for the fold-change upon entering an SG from the cytoplasm (SG intensity/non- SG intensity) and another for the absolute change upon entering an SG (SG intensity – non-SG intensity). Data was analysed by one-way ANOVA and post-hoc Tukey tests.

The non-specific N-terminal FUS antibody (FUS-565) showed a 2-3-fold increase for all genotypes, with no significant differences ($F(2,6)=0.498$, $p=0.631$), indicating that both the WT and D14 proteins are enriched in SGs in DRGNs (***Figure 5.3C***). The absolute-change however demonstrated an allele-dosage-dependent response ($F(2,6)=38.53$, $p<0.0005$), with HET ($p=0.004$) and HOM ($p<0.0005$) significantly higher than WT, and HOM significantly higher than HET ($p=0.037$) (***Figure 5.3D***).

The antibody specific to the mutant FUS-D14 protein showed a 2-3-fold increase for HET/HOM neurons (no significant differences; $F(2,6)=21.28$, $p=0.002$; with post-hoc $p=0.194$), but also a 1.3-fold increase for WT neurons (***Figure 5.4C***). This 2-3 fold increase is in-line with the values observed for the N-terminal FUS antibody, and is significantly higher than the WT fold change ($p=0.002$/$p=0.011$). This 1.3-fold change is lower than the other fold-changes observed and the absolute-change for this antibody in WT cells is also low (4 fluorescent units, compared to 70/61 units for HET/HOM respectively). This value is expected to be lower as D14-FUS is not present in WT cells, meaning the staining observed is likely due to non-specific interactions. The same pattern was observed for absolute change ($F(2,6)=10.05$, $p=0.012$), with HET ($p=0.015$) and HOM ($p=0.027$) significantly higher than WT (***Figure 5.4D***). Contradicting the N-terminal FUS antibody data, there was no trend towards absolute increase in FUS from HET to HOM ($p=0.851$).

The antibody specific to FUS-WT showed around a 2-fold increase in intensity for all genotypes (no significant differences; $F(2,6)=0.348$, $p=0.72$), despite FUS-WT not being present in HOM cells (***Figure 5.5C***). One explanation is that the C-terminal region this antibody is specific to has high homology with another SG protein (fellow FET family protein EWS). The absolute changes were all very low (8, 6 and 3 units for WT, HET and HOM respectively) with no significant differences ($F(2,6)=0.844$, $p=0.475$) (***Figure 5.5D***).

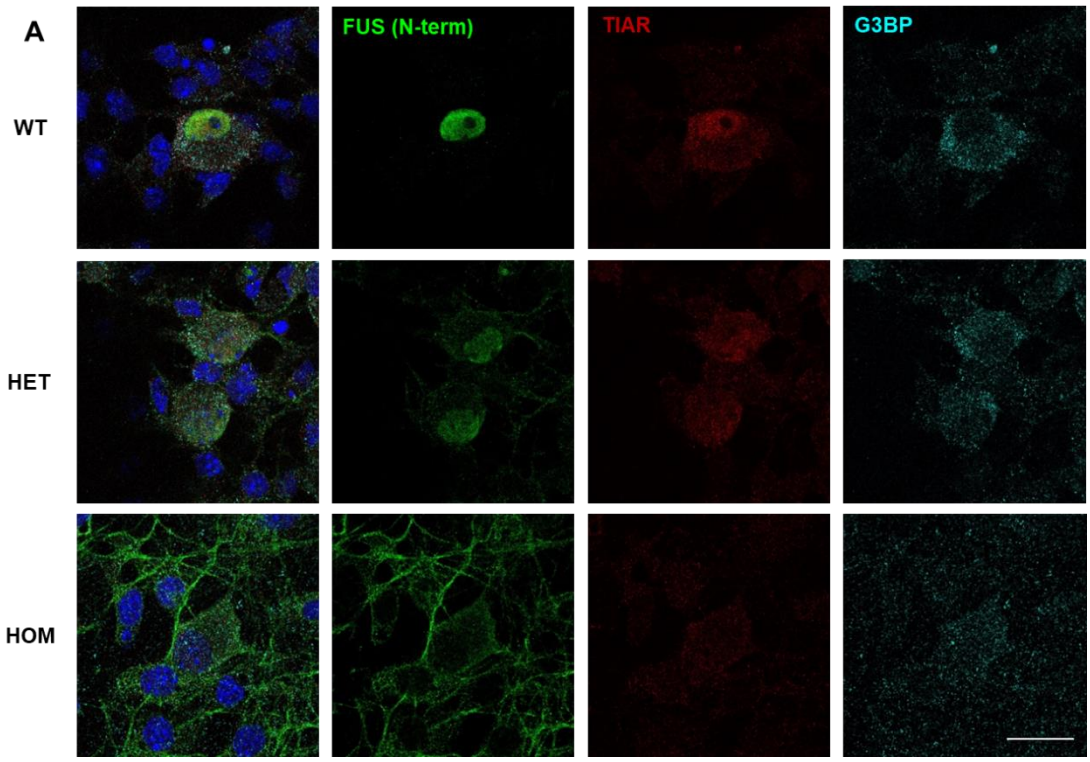
A
FUS (N-term)
TIAR
G3BP
WT
HET
HOM

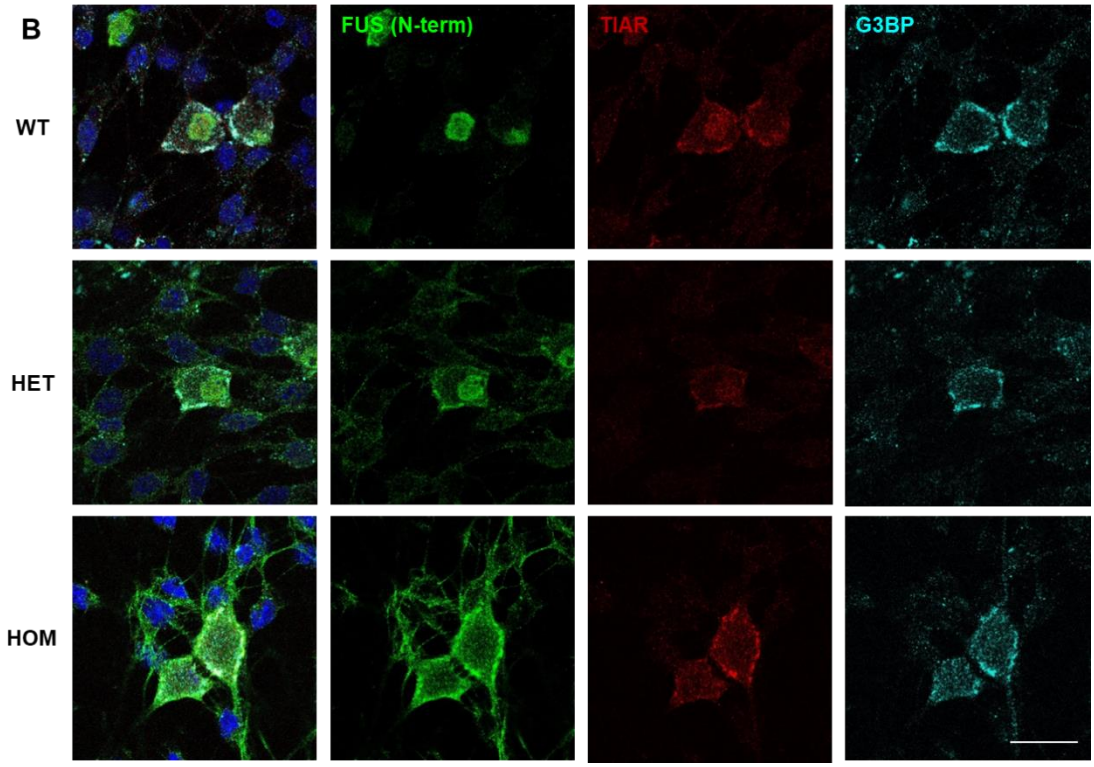
B
FUS (N-term)
TIAR
G3BP
WT
HET
HOM

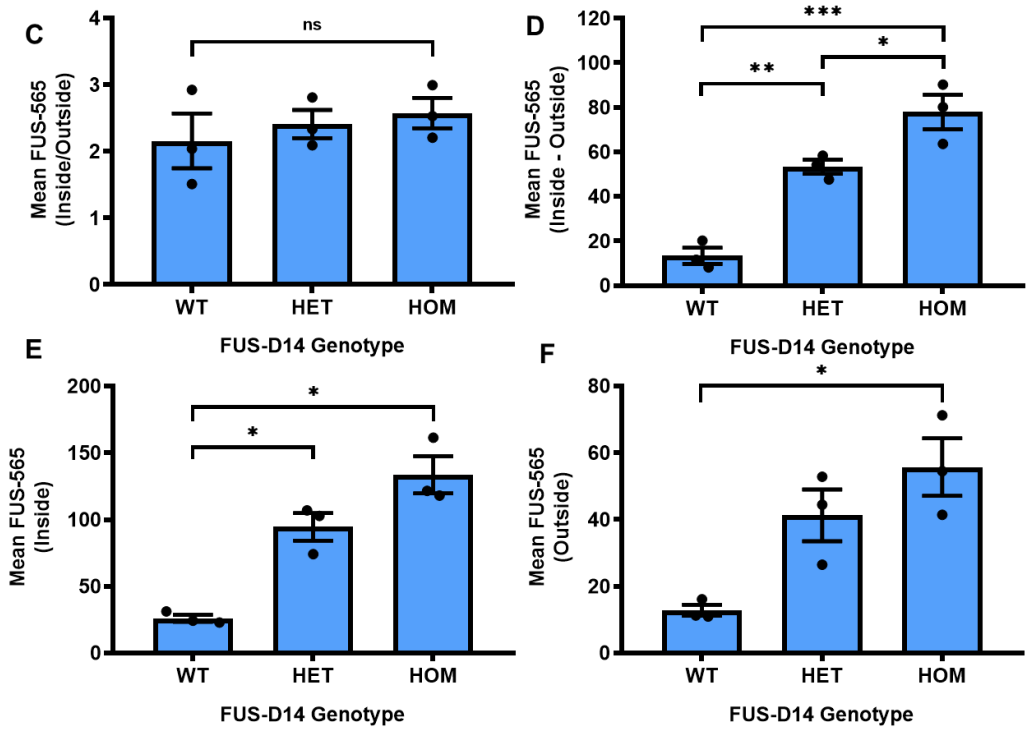

Figure 5.3 FUS is present in stress granules at higher levels in primary dorsal root ganglion neurons that are heterozygous and homozygous for the FUSDelta14 mutation, compared to wild-type neurons

A-B: 1 hour of 0.5mM sodium arsenite induces TIAR (green)/G3BP (cyan)-positive stress granules (SGs) in DIV5 primary dorsal root ganglion neurons cultured from wild-type (WT) E13.5 embryos or those heterozygous (HET)/homozygous (HOM) for the FUSDelta14 mutation. Neurons were also stained using an antibody against N-terminal FUS (FUS-565; green) and DAPI (blue). Scale bar is 20µm. **B-F**: ROIs were determined using ImageJ for areas positive for both SG markers ("inside" SG) and neither marker ("outside" SG). FUS intensity was determined for "inside" (**E**), intensity "outside" (**F**), fold-change (**C**) and absolute change (**D**) calculated. All statistical tests by one-way ANOVA and post-hoc Tukey; N=3 biological replicates. **C:** no significant differences (p=0.631). **D:** HET (p=0.004) and HOM (p<0.0005) are significantly higher than WT, and HOM is significantly higher than HET (p=0.037). **E:** HET (p=0.007) and HOM (p=0.001) are significantly higher than WT. **F:** HOM is significantly higher than WT (p=0.01).

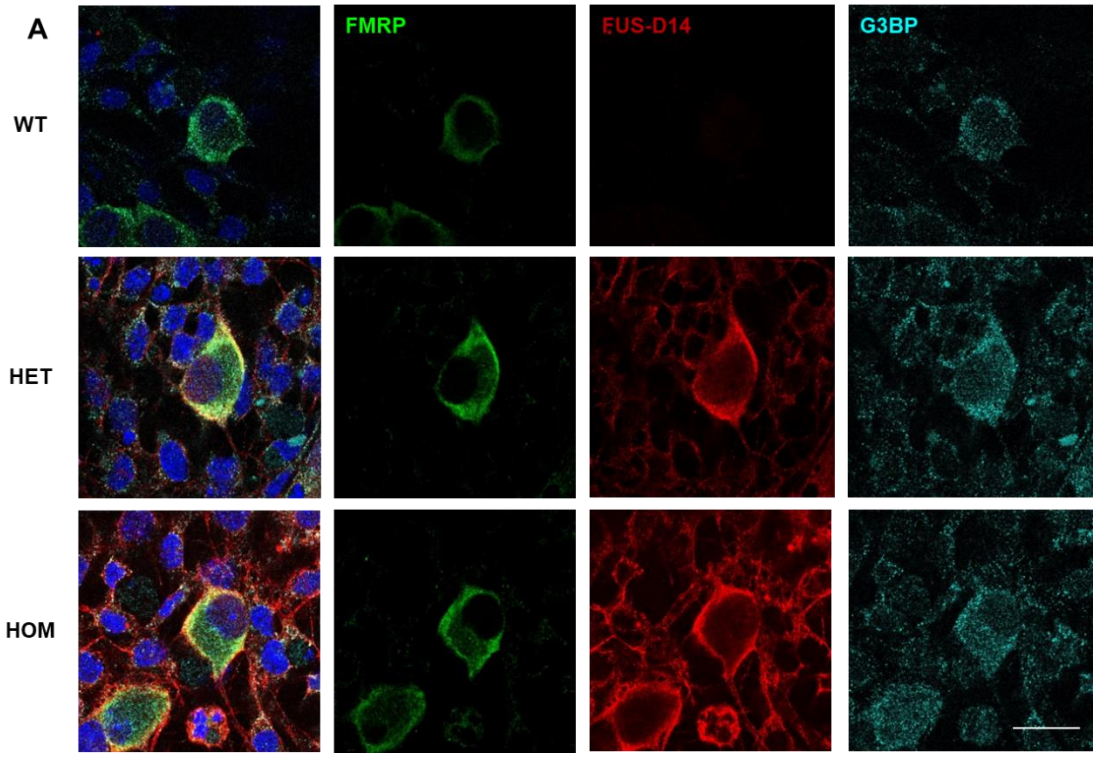
A
WT
HET
HOM
FMRP
FUS-D14
G3BP

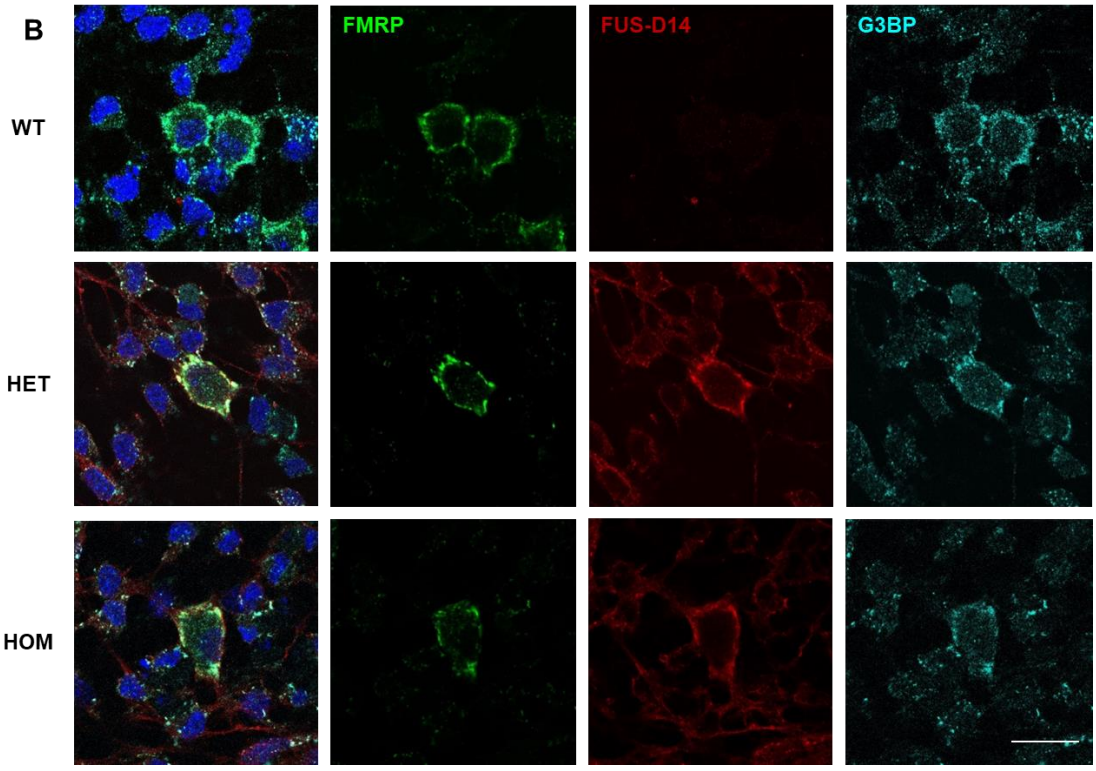
B
WT
HET
HOM
FMRP
FUS-D14
G3BP

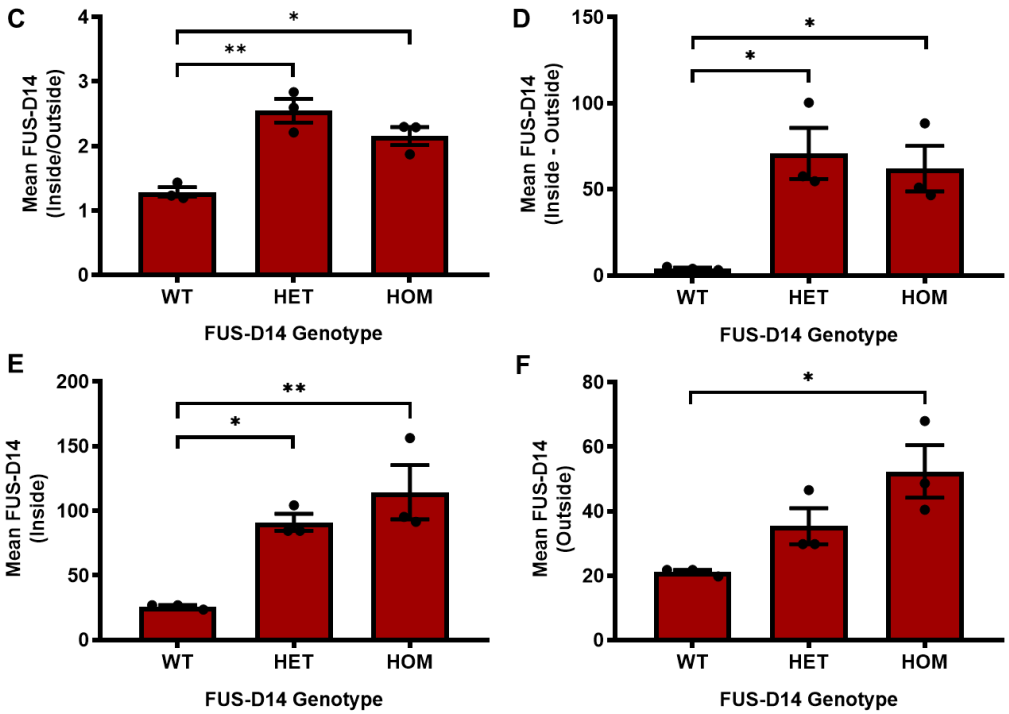

Figure 5.4 FUSDelta14-mutant FUS is present in stress granules in primary dorsal root ganglion neurons

A-B: 1 hour of 0.5mM sodium arsenite induces FMRP (green)/G3BP (cyan)-positive stress granules (SGs) in DIV5 primary dorsal root ganglion neurons cultured from wild-type (WT) E13.5 embryos or those heterozygous (HET)/homozygous (HOM) for the FUSDelta14 mutation. Neurons were also stained using an antibody against the C-terminus of the FUS-D14 mutant protein (FUS-D14; red) and DAPI. Scale bar is 20μm. **B-F**: ROIs were determined using ImageJ for areas positive for both SG markers ("inside" SG) and neither marker ("outside" SG). FUS intensity was determined for "inside" (**E**), intensity "outside" (**F**), fold-change (**C**) and absolute change (**D**) calculated. All statistical tests by one-way ANOVA and post-hoc Tukey; N=3 biological replicates. **C:** HET (p=0.002) and HOM (p=0.011) are significantly higher than WT. **D:** HET (p=0.015) and HOM (p=0.027) are significantly higher than WT. **E:** HET (p=0.026) and HOM (p=0.006) are significantly higher than WT. **F:** HOM is significantly higher than WT (p=0.02).

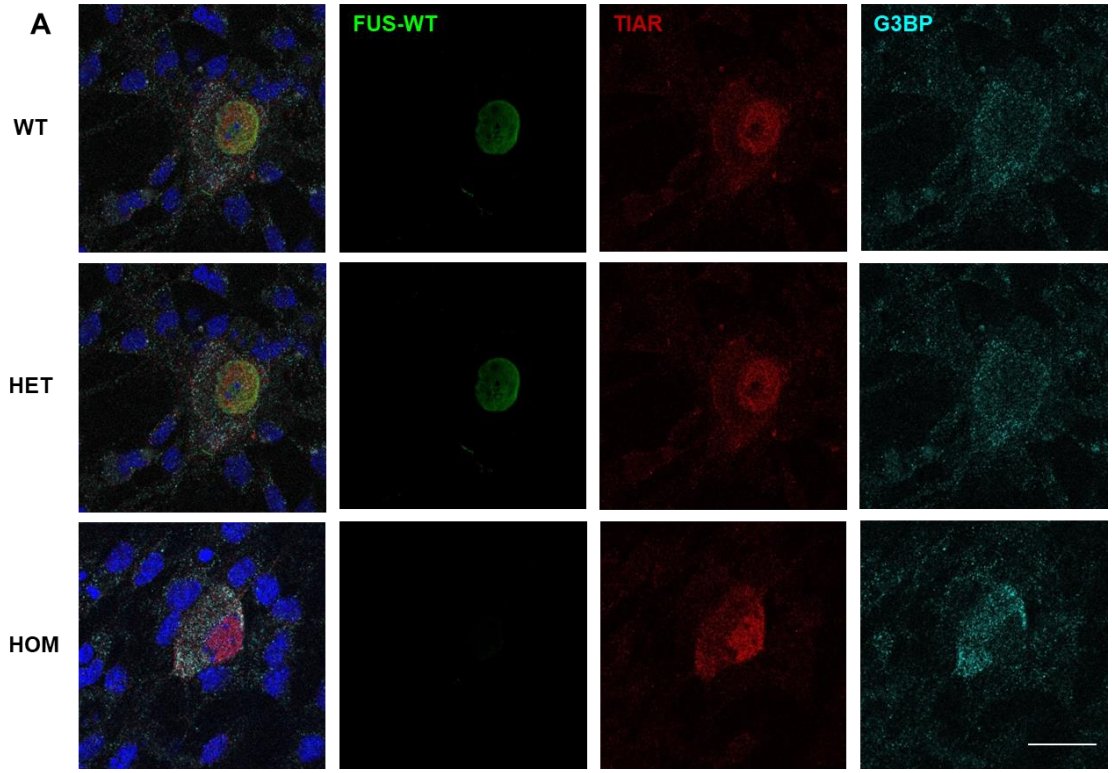
A
WT
HET
HOM
FUS-WT
TIAR
G3BP

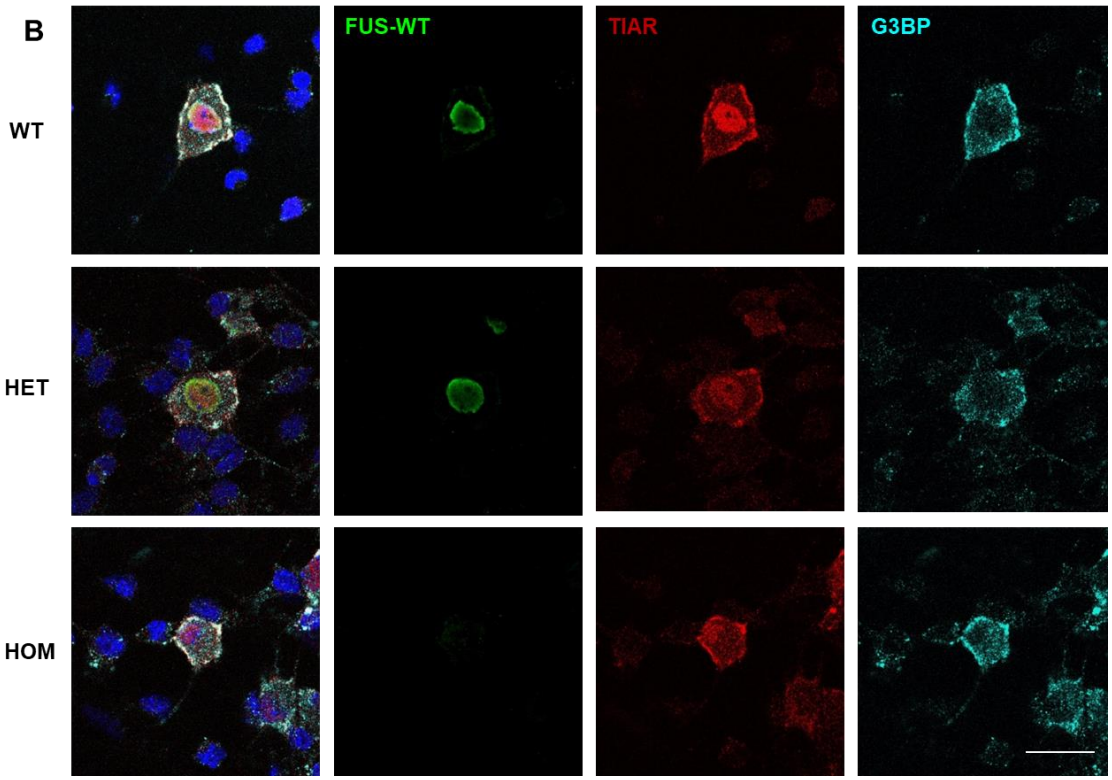
B
WT
HET
HOM
FUS-WT
TIAR
G3BP

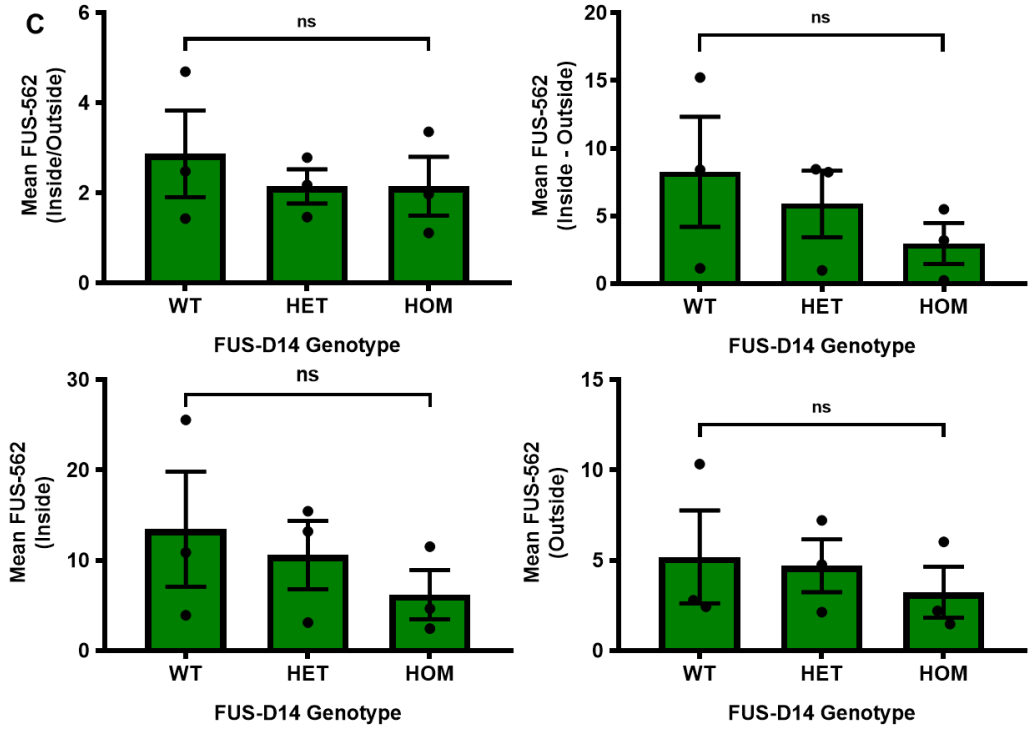

Figure 5.5 Wild-type FUS protein is present in stress granules in primary dorsal root ganglion neurons

A-B: 1 hour of 0.5mM sodium arsenite induces TIAR (red)/G3BP (cyan)-positive stress granules (SGs) in DIV5 primary dorsal root ganglion neurons cultured from wild-type (WT) E13.5 embryos or those heterozygous (HET)/homozygous (HOM) for the FUSDelta14 mutation. Neurons were also stained using an antibody against the C-terminus of the non-mutant FUS protein (FUS-562; green) and DAPI (blue). Scale bar is 20µm. **B-F**: ROIs were determined using ImageJ for areas positive for both SG markers ("inside" SG) and neither marker ("outside" SG). FUS intensity was determined for "inside" (**E**), intensity "outside" (**F**), fold-change (**C**) and absolute change (**D**) calculated. All statistical tests by one-way ANOVA and post-hoc Tukey; N=3 biological replicates. No significant differences were observed: **C:** (p=0.72) ;**D:** (p=0.475); **E:** (p=0.561); **F:** (p=0.759).

5.3 Discussion

The results of this chapter clearly replicate previous reports that the FUS protein localises to SGs at far higher levels in ALS-mutant cells when compared to WT cells. Though some studies have demonstrated this using systems where FUS is overexpressed (Bosco et al., 2010, Dewey et al., 2011, Figley et al., 2014), this study has replicated this finding in a model with disease-relevant levels of FUS and a disease-relevant cell type: the MNs of a model organism which displays progressive MN degeneration, followed by death (Devoy et al., 2017). Despite endogenous expression levels, a very high average absolute increase in fluorescence intensity from the cytoplasm into SGs was observed: 66 (HET)/57 (HOM) fluorescence units. In addition, the fold-increase for intensity was 1.3-fold for WT, but over 2-fold for HET and HOM, further indicating an increased propensity for mutant FUS to localise to SGs.

Though not as high as HET and HOM, WT neurons demonstrated a positive fold-increase for FUS into SGs. This low localisation was poorly visible by-eye, which could explain why studies which did not quantify their immunofluorescence data (Bosco et al., 2010, Sama et al., 2013) concluded an exclusion of FUS-WT from SGs following ARS treatment; this highlights the utility of applying quantification and statistical testing to immunofluorescence images for detection of protein localisation (though not for accurate quantification of protein levels). In future however, it will be important to repeat this experiment using FUS knockout cells, to ensure that the small increase observed is not due to non-specific interactions within SGs or recognition of an alternative epitope by the antibody.

The results of this chapter also demonstrate that, as for primary fibroblasts (Devoy et al., 2017) and MNs (unpublished data from our lab), FUS-D14 mislocalises to the cytoplasm in primary sensory neurons. As previously reported in FUSDelta14 HET lumbar spinal MNs, some mutant FUS remains within the nucleus despite the removal of the entire NLS, suggesting an NLS-independent mechanism of nuclear import. While nuclear : cytoplasmic FUS-D14 ratio was previously reported as 1:3 in MNs heterozygous for the mutation (Devoy et al., 2017), here I report a 1:1 ratio in DRGNs. This difference may be due to the experimental set-up: only one confocal plane of each DRG neuron was analysed. As these cells have a large cytoplasmic volume, accurate quantification of nuclear : cytoplasmic FUS ratio would require analysis of z-stack images. An extra copy of the D14 mutation further shifts the ratio of nuclear : cytoplasmic FUS-D14 towards cytoplasmic (1:2). Unlike the original

paper, no significant decrease in nuclear FUS-WT was observed in heterozygous neurons; though the analysis in this study was conducted on aged spinal, rather than embryonic, MNs (Devoy et al., 2017).

It is also worth noting that, as with the DRGN SGs described in ***Chapter 3***, the FUS-D14 protein appears to accumulate near to the periphery of the cell, with increasing fluorescent intensity towards to cell membrane. DRGNs have a larger cytoplasmic volume, so it is possible that this localisation is replicated in other cell types (MEFs/MNs), but in a less obvious manner. For example, it could be indicative of a propensity for FUS, once it is in the cytoplasm, to be actively transported away from the nucleus towards the periphery. This is possible, as in WT cells, FUS associates with APC (adenomatous polyposis coli) in fibroblast protrusions (Yasuda et al., 2013) and localises to axons in hippocampal neurons (Lopez-Erauskin et al., 2018), as well as the synapses of motor and hippocampal neurons (Fujii et al., 2005, Deshpande et al., 2019). While the results of this transport may not be usually visible for the typically low levels of cytoplasmic FUS in WT cells, it may be visualised more strikingly in a large cell-type. This may also be true for other cytoplasmic proteins in DRGNs: for example, one study demonstrated a similar staining pattern for neurofilament-heavy-chain in primary DRGNs (Jun et al., 2015).

As with MNs, FUS-WT was initially not determined to localise to SGs in primary DRGNs following treatment with ARS. However, analysis of fluorescent intensity values using both the N-terminal and C-terminal antibodies indicated that FUS-WT is enriched in SGs, but at a very low fluorescence intensity which might not be detectable by eye. For both antibodies, the fold-increase in intensity was >2-fold, which was much higher than that observed for MNs. It is difficult to draw conclusions from the experiments using the FUS-WT C-terminal-specific antibody, as this also demonstrated an >2-fold increase in HOM DRGNs, which do not express FUS-WT protein. The simplest explanation for this is the high homology of the C-terminal region of FUS with that of the fellow FET family protein EWS, which also localises to SGs (Andersson et al., 2008, Neumann et al., 2011). In order to test this, HOM DRGN cultures should be lysed and processed for western blotting to see if a specific band for the EWS protein is detected (approximately 75 kDa and 68.5 kDa molecular weight for FUS and EWS respectively).

Comparatively, mutant FUS localises at high levels to SGs in DRGNs as demonstrated by both fold-increase and absolute-increase in HET and HOM neurons; for both N-terminal and FUS-D14-specific antibody. Both antibodies

demonstrated a >2-fold increase, with the N-terminal antibody further demonstrating a FUSDelta14 allele dose-dependent absolute-increase from HET to HOM; not replicated with the FUS-D14-specific antibody despite a dose-dependent increase in the FUS-D14 raw fluorescent intensity inside SGs for both.

Comparing the N-terminal FUS antibody data for the MNs and DRGNs, the most striking difference is that of the fold-difference for the WT; 1.3-fold and >2-fold for MNs and DRGNs respectively. This may be indicative of a higher concentration of FUS present within the cytoplasm and therefore available to aggregate in DRGNs, or an increased ability to export FUS from the nucleus to the cytoplasm for aggregation. In addition, the absolute-increase for the N-terminal stain demonstrated a significant FUSDelta14 allele dose-dependent response from HET to HOM, while for the MNs HET and HOM were not significantly different. This may be because DRGNs have a much larger cytoplasm than MNs, and hence a higher amount of cytoplasmic FUS available to aggregate.

The predominate neurodegeneration associated with ALS is that of MNs, but in this study we demonstrate the mislocalisation of ALS mutant FUS to the cytoplasm in DRGNs, along with an increased localisation of the mutant protein to SGs. While sensory neuron dysfunction is not the key pathological feature of ALS, there is evidence for sensory pathology in ALS (reviewed in Tao et al., 2018). It has been demonstrated that human ALS patients present with sensory deficits (Pugdahl et al., 2007) and can display sensory neurodegeneration (Heads et al., 1991, Pradat and El Mendili, 2014). Further, it has been demonstrated that primary DRGN cultures from both $SOD1^{G93A}$ and $TDP43^{A315T}$ mouse models exhibit increased sensitivity to vincristine-induced microtubule stress (Vaughan et al., 2018).

As mutant FUS mislocalisation to the cytoplasm and SGs is observed in MNs, which are heavily affected in ALS, but also DRGNs and MEFs, it follows that these alterations may not drive ALS pathogenesis. However, the clustering of ALS-causing mutations at the NLS of FUS (Vance et al., 2013) and the observation that increasing cytoplasmic mislocalisation is correlated with decrease age of disease onset (Higelin et al., 2016) make this unlikely. It is however possible that the effect of FUS NLS-mutations on phase separation (Yoshizawa et al., 2018), independent of cytoplasmic mislocalisation, could drive the effect of the disease; for example within the nucleus.

An alternative explanation is that MNs, but not DRGNs or MEFs, may have additional properties that convert this mislocalisation into ALS pathogenesis. The

proteome, and even SG proteome (Markmiller et al., 2018), can differ drastically from cell-type to cell-type, making it possible that the cytoplasmic interaction of FUS-D14 with a MN-specific component or pathway could drive a cell-type targeted, or comparatively accelerated, neurodegeneration.

5.3.1 Future directions

Does the FUSDelta14 mutation have an effect on stress granule morphology, number and dynamics?

As HET and HOM SGs contain a significantly higher amount of (potentially more aggregation-prone) FUS compared to WT SGs, it will be interesting to observe the effect of the mutation on SG assembly, morphology, number, dynamics and in particular, disassembly; a slowed disassembly may be indicative of inefficient protein disaggregation, which has major implications for the formation of inclusions. ALS-causing mutations have already been demonstrated to have a number of effects on SGs *in vitro* (discussed in ***Chapter 1.3.3***), so the chances of observing a phenotype are high. Despite the rich literature investigating these properties, it will be important to investigate these in our model, which features a disease-relevant level of FUS expression.

Does the FUSDelta14 mutation have an effect on the stress granule proteome?

As FUS is capable of binding a range of proteins (Yamaguchi and Takanashi, 2016), it will be important to assess the effect that a large increase in FUS within the SG has on its proteome; it may result in an increase in FUS-binding partners within SGs during oxidative stress, or may result in the exclusion of other SG proteins from the SG as the more abundant FUS is included instead. While immunofluorescence is a quick, easy way to assess proteomic differences, a less biased method would be to perform mass spectrometry on isolated SG cores (Jain et al., 2016) or by proximity labelling (Markmiller et al., 2018).

Does the FUSDelta14 mutation have an effect on the stress granule transcriptome?

FUS is also capable of binding a range of RNAs (Rogelj et al., 2012), so it may be possible that FUS-binding RNAs are localised to SGs at higher levels than are permitted. To investigate SG transcriptomics, it would be possible to isolate SG

cores and subsequently perform RNA sequencing (Khong et al., 2017). Alternatively, FUS-bound transcripts could be determined bioinformatically and then assessed using co-immunofluorescence-*in situ* hybridisation experiments to observe RNA transcripts within immunostained SGs. The sequestration of a handful of mRNAs (*Mecp2*/*Kif5b*) into FUS positive cytoplasmic accumulations has already been demonstrated (Yasuda et al., 2017, Coady and Manley, 2015).

Is D14-FUS incorporated into other membraneless organelles?

Besides SGs, FUS is known to localise to, and influence the formation of, other membraneless organelles, such as nuclear paraspeckles (Naganuma et al., 2012). Phase separation is a relatively new field and roles for phase separation and new membraneless organelles likely remain to be discovered; pro-aggregative FUS-D14 may interact with any number of these organelles to elicit neurotoxic effects.

5.4 Conclusions

The current study demonstrates that, as for MNs, FUS-WT is predominately nuclear in DRGNs, but enters cytoplasmic SGs at very low levels following oxidative stress. Comparatively FUS-D14 mislocalises to the cytoplasm and enters SGs at far higher levels following oxidative stress. As this mislocalisation is present in both sensory and motor neurons, the mechanism of MN-specific death in ALS remains to be determined. Importantly, the effect of this massive inclusion of FUS protein to the SG remains to be determined.

6 Optimising a method to obtain RNA from neuronal somas using fluorescence-activated cell sorting.

6.1 Specific Aims

From development onwards, axons are exposed to a number of extracellular stimuli and stressors. These stimuli have been demonstrated to induce a number of changes within the axon, some of which serve to propagate a retrograde signal to the cell body (Ji and Jaffrey, 2014). Responses of axons to stressors, including mechanical damage are reviewed in **Chapter 1.4**.

Retrograde axon-to-somal signalling has been demonstrated to induce changes in both the somal proteome and transcriptome. For example, the application of NGF to the axons of primary embryonic dorsal root ganglion neurons has been demonstrated to induce local axonal synthesis of the transcription factor CREB (cAMP-responsive element (CRE)-binding protein), followed by its microtubule-dependent retrograde transport and a subsequent increase in somal CREB (Cox et al., 2008). This results in an increase in nuclear pCREB and an induction of CRE-dependent transcription, as demonstrated by a CRE-luciferase reporter assay. This demonstrates clearly that an axonal stimulus can alter the somal transcriptome.

This chapter aimed to develop a method of isolating cell bodies whose axons had been exposed to axonal stimuli using microfluidic chambers (MFCs; described in ***Chapter 2.3***). Normally, when using compartmentalised devices, assessing the transcriptomics or proteomics of the somal compartment presents with a key issue: the majority of cells within the culture will not have their axons exposed to the stimulus. This issue stems from two factors. Firstly, only a fraction of neurons within a culture will project their axons into the axonal compartment, with the axons of the other cells remaining in the somal compartment. Secondly, particularly for primary cultures but also for other types, cultures are heterogeneous with multiple additional cell-types such as glia and fibroblasts. These cells do not have axons and hence will not be affected by stimuli applied to the axonal compartment. The combination of these factors means that depending on your culture system, there may be a large majority of cells which will not display the changes you wish to investigate, diluting any effects which you hope to observe. It is therefore desirable to investigate the small population of cell bodies whose axons are exposed to the stimulus only, or in comparison with somas whose axons have been exposed to a negative control.

To overcome this, we aimed to use the retrogradely transported cholera toxin subunit B (CTxB), conjugated to a fluorophore. This non-toxic subunit binds to monosialoganglioside on the neuron surface and is internalised by receptor-mediated endocytosis (Trojanowski, 1983), followed by retrograde trafficking via signalling endosomes to the soma where it accumulates (Wang et al., 2016a). In order to apply this tracer to the axons only, it must be used in conjugation with a compartmentalised cell culture platform with which is possible to establish fluidic isolation, such as microfluidic chambers (MFCs) (Taylor et al., 2005) or Campenot chambers (Campenot, 1977). This fluidic isolation is further required for compartmentalisation of any stimuli that you wish to apply to the axonal compartment.

Using this set-up, we aimed to use the accumulation of CTxB fluorescence within the neuronal cell bodies to separate the CTxB-positive fluorescent somas from CTxB-negative somas via fluorescence-activated cell sorting (FACS). This initially proved difficult using primary dorsal root ganglion neurons (DRGNs), but was possible using the same procedures in primary cortical neurons (CNs). Firstly, I demonstrated the isolation of CN somas using CTxB-488, CTxB-555 and CTxB-647 in cortical neurons from bipartite MFCs (MFC design shown in ***Figure 2.1A;*** FACS procedure illustrated in ***Figure 6.1A***). This was then performed in an MFC with two axonal compartments (tripartite MFC), each incubated with different colours of CTxB (tripartite MFC design shown in **Figure 2.1B;** FACS procedure illustrated in ***Figure 6.1B***). Finally, I demonstrated the ability to obtain RNA from cell bodies isolated by this method.

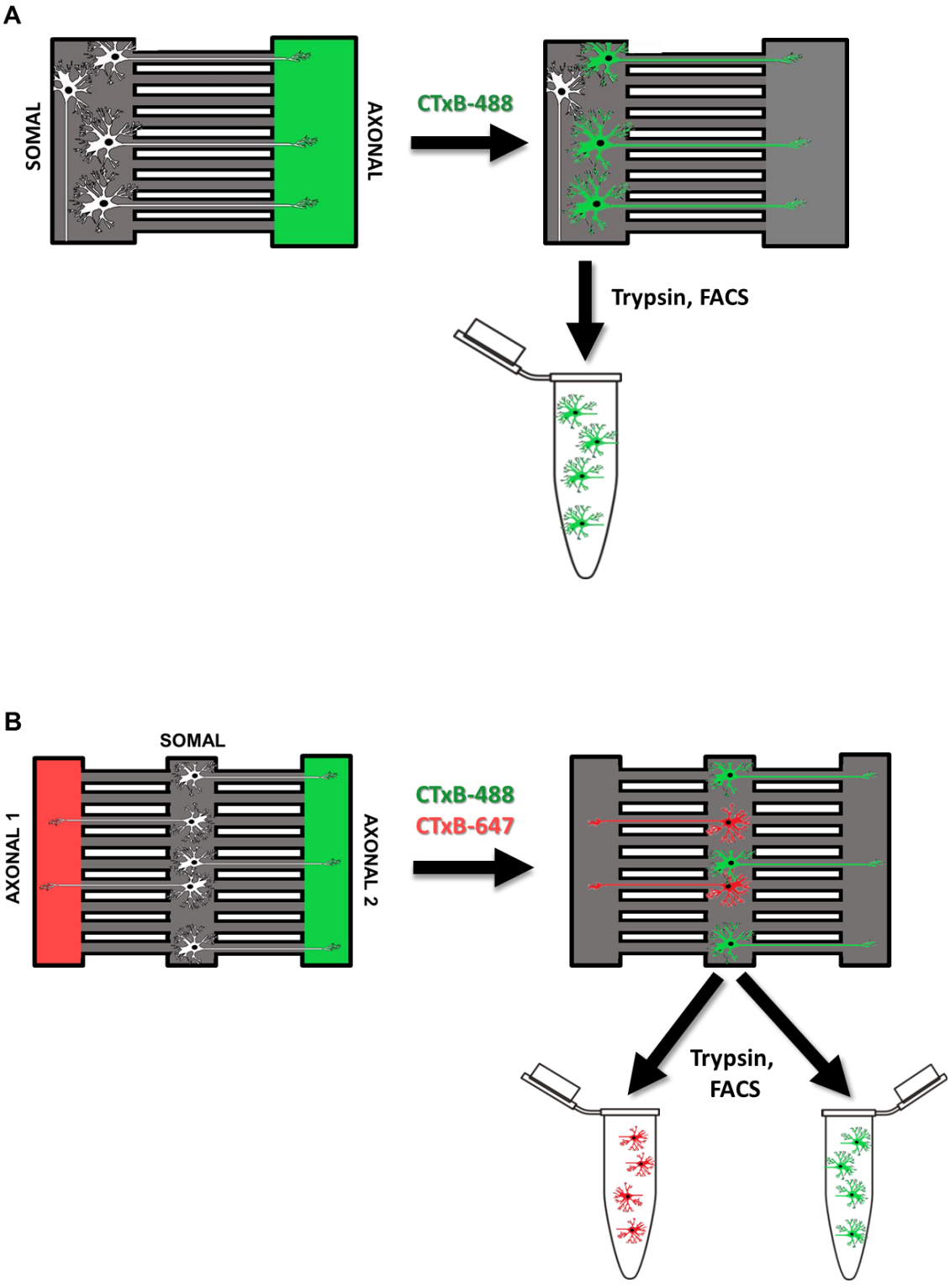

Figure 6.1 Isolation of neuronal somas using a one-colour (A) or two-colour (B) retrograde tracer-based sorting method

A: Primary neurons from E13.5 WT embryos were plated into the somal compartment of a bipartite microfluidic chamber (MFC). On DIV7, the axonal compartment was incubated with 0.15mg/ml cholera toxin subunit B conjugated to a 488-fluorophore (CTxB-FACS) for 3 hours, in order to retrogradely label the somas of neurons whose axons project into axonal compartment. At t=3 hours both compartments were washed with neuronal culture medium,

followed by aspiration of medium from both compartments. Medium in the somal compartment was replaced with 100 µl 0.25% trypsin-EDTA for 6 minutes and incubated at 37°C, in order to remove cells from the somal compartment of the MFC. Isolated CTxB-488-positive cell bodies were then sorted by fluorescence-activated cell sorting (FACS) into lysis Buffer RLT (Qiagen). **B:** Primary neurons from E13.5 WT embryos were plated into the somal compartment of a tripartite MFC. On DIV7, axonal compartment 1 was incubated with CTxB-488, and axonal compartment 2 with CTxB-647 for 3 hours. At t=3 hours, all compartments were washed, and medium in the somal compartment was replaced with 100 µl 0.25% trypsin-EDTA for 6 minutes and incubated at 37°C. Cells were removed from the somal compartment and isolated CTxB-488 or CTxB—647-positive cell bodies were then separated by FACS into Buffer RLT in two different tubes.

6.1.1 Materials and methods

The results in this chapter were obtained by first culturing primary cortical neurons in MFCs. The fabrication of MFCs is detailed in ***Chapter 2.3***, and dissection and cell culture are detailed in ***Chapter 2.4***. Following DIV6, the axonal compartment was exposed to CTxB (followed by 1 hour arsenite in specific conditions, as detailed in specific results sections). FACS experiments were performed as indicated in ***sections 6.2.1*** and ***6.2.2*** and RNA extraction performed as indicated in **section 6.2.3**.

6.2 Results

6.2.1 Isolation of neuronal somas using a one-colour retrograde tracer-based sorting method

Primary neurons from E13.5 WT embryos were plated into the somal compartment of bipartite MFCs (DRGNs/CNs with microgroove length 800/500 µm) until DIV7 to allow axons to project extensively into the axonal compartment. On DIV7, the axonal compartment was incubated with 0.15mg/ml CTxB conjugated to a fluorophore for 3 hours, in order to retrogradely label the somas of neurons whose axons project into axonal compartment. At t=3 hours both compartments were washed twice with neuronal culture medium, followed by aspiration of medium from both compartments. Media in the somal compartment was replaced with 100 µl 0.25% trypsin-EDTA for 6 minutes and incubated at 37°C. This 100 µl was used to remove cells in the somal compartment from the MFC and was then transferred to an Eppendorf tube. A further 100 µl was added to collect any remaining cells from the somal compartment and added to the Eppendorf. 800 µl neuron culture medium was added to inactivate the trypsin. After gentle trituration (pipetting up and down 10 times) to break up any cell clumps, the cell suspension was passed through a 40

µm cell strainer (Falcon; 352340) and collected in a new Eppendorf tube. Cells were then centrifuged for 5 minutes at 200 x g, followed by removal of the supernatant. The pellet was resuspended in 200 µl suspension medium (Hibernate-E Medium (Gibco; A1247601) with 2% B27 supplement (Gibco; 17504044)) and placed on ice for transportation. Cells from four MFCs were compiled for each condition (CTxB-488, CTxB-555, CTxB-647), as well as a non-CTxB control.

FACS was performed by The Flow Cytometry Translational Technology Platform at the UCL Cancer Institute using a BD FACSAria™ Fusion (BD Biosciences; San Jose, CA) cell sorter. The 200 µl cell suspension was used as the cell input, and sorted cells were collected in 200 µl Buffer RLT (Qiagen; 79216). Prior to the sorting of fluorescent cells, gating was optimised using the non-CTxB sample. This was used to determine arbitrary fluorescent gating, by which I could ensure that cells were positive for CTxB, rather than typical cellular autofluorescence. This was also used to define gating for forward-scatter and side-scatter, removing extremes of both conditions.

Initial trials were performed using DRGNs, but no CTxB-positive cells were observed following determination of gating using the negative control. Using the same methods in CNs however, it was possible to detect cells which were deemed to be CTxB fluorescence-positive (***Figure 6.2***). ***Figure 6.2A-C*** demonstrates defined gates determined based on forward scatter and side scatter (arbitrarily determined, using the negative control prior to the experiment; ***Figure 6.2A***), as well as gates where we predicted to observe cells positive for Alexa Fluor 488 (“488 gate”; filter: B 530/30; x-axis of ***Figure 6.2B***), Alex Fluor 555 (“555 gate”; filter: YG 582/15; x-axis of ***Figure 6.2C***) and Alexa Fluor 647 (“647 gate”; filter: R 670/30; y-axis of ***Figure 6.2C***).

For cells treated with CTxB-488, 488-positive cells are detected within the 488 gate (147/236,432 events; ***Figure 6.2E***), with only 11 and 1 events detected for the 555 and 647 gates respectively (***Figure 6.2F***). For those treated with CTxB-555, 555-positive cells are detected within the 555 gate (267/361,868 events; ***Figure 6.2I***), with 0 and 1 events detected for the 488 and 647 gates respectively (***Figure 6.2H-I***). For CTxB-647, 647-positive cells were detected within the 647 gate (118/238,266 events; ***Figure 6.2L***), with 0 and 1 events detected for the 488 and 555 gates respectively (***Figure 6.2K-L***). The number of positive events was always within the low hundreds out of hundreds of thousands of total events; 0-0.1% of total events. Regardless of the low yield, the fluorescence values observed are far higher than

that of the negative control, suggesting that it is possible to isolate low numbers of neuronal cell bodies via this technique.

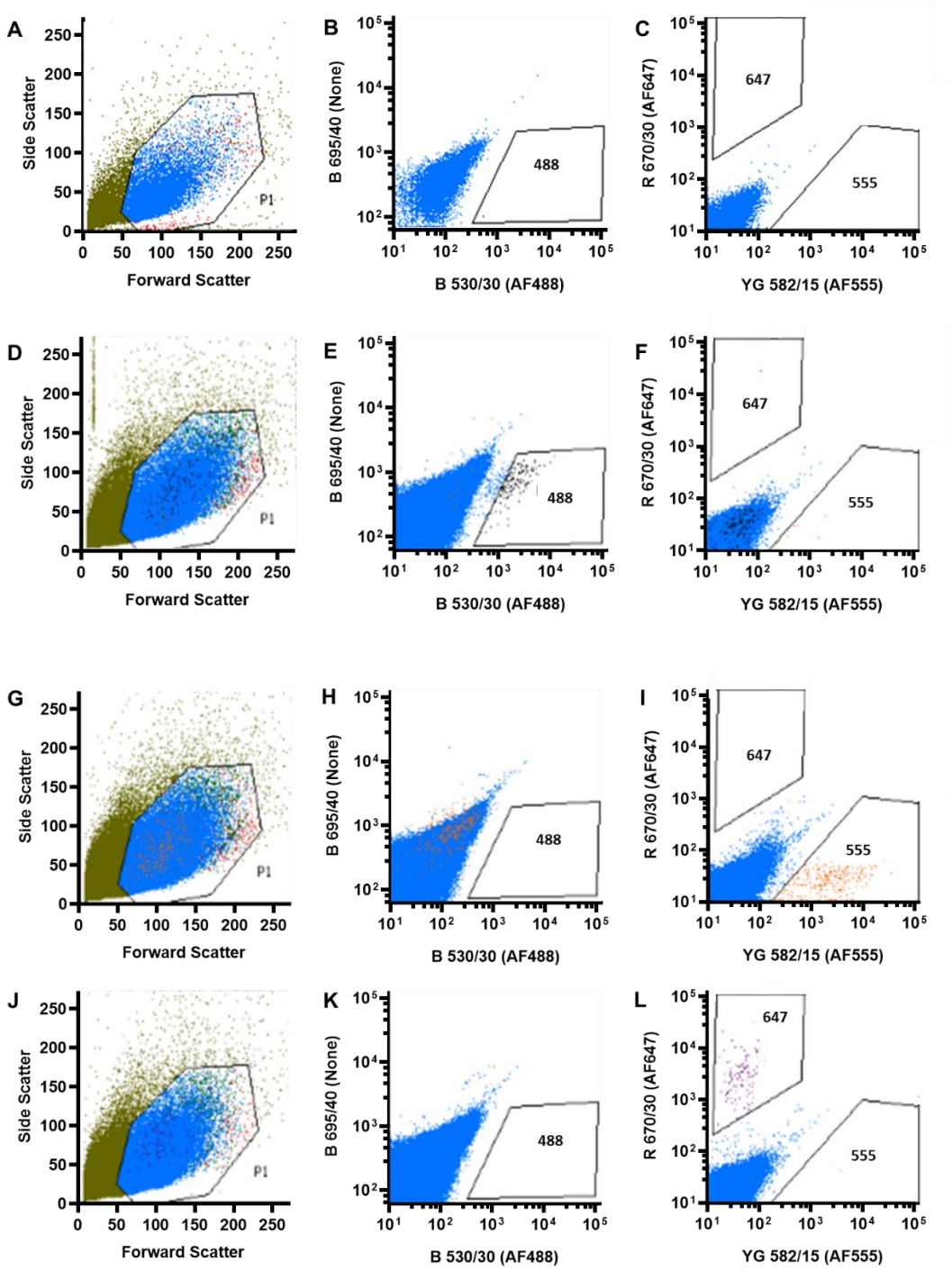

Figure 6.2 FACS plots showing the results of a one-colour retrograde tracer-based sorting method

Primary cortical neurons from E13.5 WT embryos were cultured in bipartite MFCs. On DIV7, the axonal compartment was incubated with either control (**A-C**), or 0.15mg/ml CTxB conjugated to a fluorophore for 3 hours (**D-F**: CTxB-488; **G-I**: CTxB-555; **J-L**: CTxB-647), in

order to retrogradely label the somas of neurons whose axons project into axonal compartment. These cells were then extracted from the somal compartment using 0.25% trypsin-EDTA to form a single cell suspension, which was sorted by fluorescence-activated cell sorting using a BD FACSAria™ Fusion cell sorter. Gating was optimised using the non-CTxB sample for forward and side scatter (**A**) as well as gates where we predicted to observe cells positive for Alexa Fluor 488 ("488 gate"; filter: B 530/30; x-axis of (**B**), Alex Fluor 555 ("555 gate"; filter: YG 582/15; x-axis of (**C**) and Alexa Fluor 647 ("647 gate"; filter: R 670/30; y-axis of (**C**). For cells treated with CTxB-488, 488-positive cells are detected within the 488 gate (**E**), with fewer events detected for the 555 and 647 gates respectively (**F**). For those treated with CTxB-555, 555-positive cells are detected within the 555 gate (**I**), with fewer events detected for the 488 and 647 gates respectively (**H-I**). For CTxB-647, 647-positive cells were detected within the 647 gate (**L**), with fewer events detected for the 488 and 555 gates respectively (**K-L**).

6.2.2 Isolation of neuronal somas using a two-colour retrograde tracer-based sorting method

The above section demonstrates the possibility of isolating cell somas from a bulk cell population via FACS after labelling with fluorescently tagged retrograde CTxB tracer. While it would be possible to compare CTxB-positive cells to CTxB-negative cells, this would assume no intracellular effects of the CTxB trafficking and would not select for neurons in the control population. A better scenario is to use a tripartite MFC, with a central somal compartment, connected by microgrooves on either side to two separate axonal compartments (as shown in ***Figure 6.1B***). Using this device, it is possible to treat each axonal compartment with a CTxB with a different fluorescent tag and further, to incubate one side with a treatment and the other with the negative control.

In order to test the possibility of using this set-up, primary CNs from E13.5 WT embryos were plated into the somal compartment of tripartite MFCs, allowing until DIV7 for axons to project into both axonal compartments. On DIV7, one axonal compartment was incubated with 0.15 mg/ml CTxB-488, and the other with CTxB-647, for 3 hours. At t=3 hours, CTxB was removed from both compartments and different treatments added to each compartment: control media to the CTxB-488 side and media with 1 mM sodium arsenite (ARS; in ***Chapter 4***, axonal ARS was demonstrated to induce changes in the soma). After a further hour (t=4), all three compartments were washed twice with neuronal culture medium, followed by aspiration of medium from all compartments. Media in the somal compartment only was replaced with 100 µl 0.25% trypsin-EDTA and the same method of harvesting cells for FACS was used as in ***section 6.2.1***. Cells from four tripartite MFCs were compiled for the treatment experiment, as well as for a non-CTxB control.

Again, sorting was performed using a BD FACSAria™ Fusion cell sorter, collecting cells in 200 µl Buffer RLT in an Eppendorf. Before sorting, the negative control was used to determine gating, based on values for forward and side scatter (***Figure 6.3A***) as well as two fluorescence filters: B 530/30 ("488 gate"; x-axis of ***Figure 6.2B***) and R 660/20 ("647 gate"; y-axis of ***Figure 6.3B***). Using this method, I was able to separate two populations of cells from the same sample. CTxB-488-positive cells are detected within the 488 gate and CTxB-647 detected in the 647 gate (121

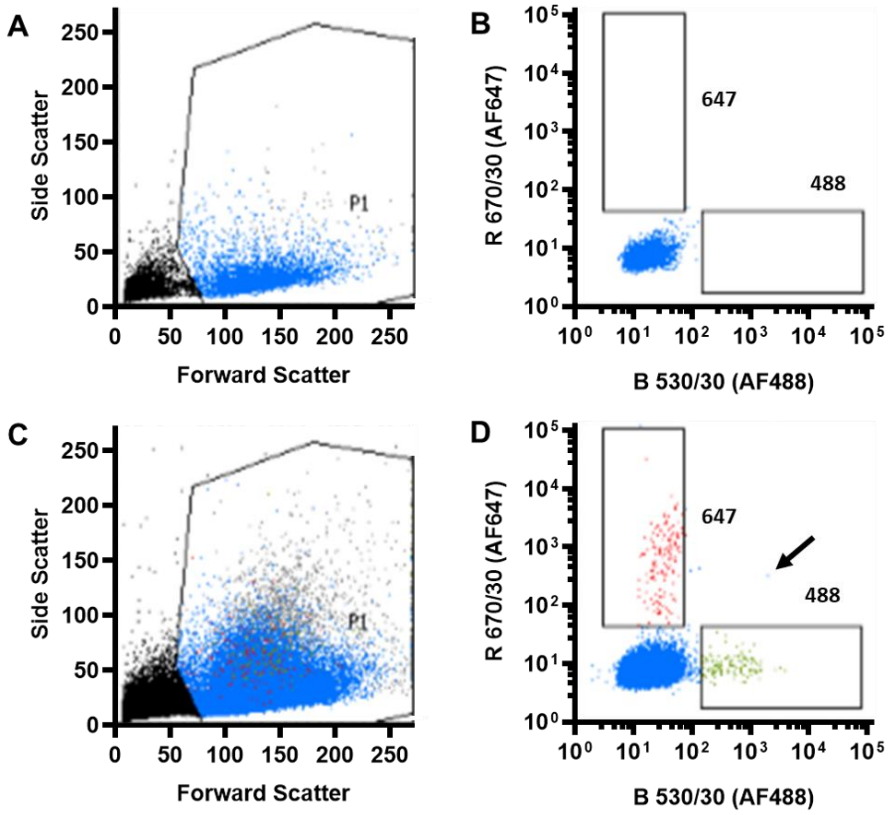

and 146 respectively out of 121,224 total events; ***Figure 6.3D***). Only 1 cell appeared to be both 488- and 647-positive (indicated by a black arrow in ***Figure 6.3D***).

Figure 6.3 FACS plots showing the results of a two-colour retrograde tracer-based sorting method

Primary cortical neurons from E13.5 WT embryos were cultured in tripartite MFCs. On DIV7, axonal compartment was incubated with either non-CTxB control in both axonal compartments (**A-B**), or 0.15mg/ml CTxB conjugated to a fluorophore for 3 hours (**C-D**): CTxB-488 in one axonal compartment, CTxB-647 in the other, in order to retrogradely label the somas of neurons whose axons project into each axonal compartment. The CTxB-488 compartment was then treated with control medium for 1 hour, while the CTxB-647 compartment was treated with 1mM sodium arsenite for 1 hour. These cells were then extracted from the somal compartment using 0.25% trypsin-EDTA to form a single cell suspension, which was sorted by fluorescence-activated cell sorting using a BD FACSAria™ Fusion cell sorter. Gating was optimised using the non-CTxB sample for forward and side

scatter (**A**) as well as two fluorescence filters: B 530/30 (“488 gate”; x-axis of **B)** and R 660/20 (“647 gate”; y-axis of **B**). Using this method, two populations of cells were observed for the same sample. CTxB-488-positive cells are detected within the 488 gate and CTxB-647 detected in the 647 gate (**D**). Only 1 cell appeared to be 488- and 647-positive (indicated by a black arrow in **D**).

6.2.3 Extraction of RNA from neuronal somas isolated using fluorescence-activated cell sorting.

The above two sections demonstrate the possibility of sorting CTxB-positive cell bodies by FACS into an Eppendorf tube containing lysis Buffer RLT. I wanted to test whether it was possible to extract RNA from a low number of cells isolated using this method. During the experiment in ***section 6.2.2***, a low number of cells (700) CTxB-negative cells were sorted into 200 µl Buffer RLT and placed on ice for transportation. RNA was extracted from this lysate using the RNeasy Micro Kit, eluted in 14 µl RNase-free water and quantified using the Agilent 4200 TapeStation System as described in ***Chapter 2.10***. For this experiment there were two replicates, which were extracted in parallel with a positive control (non-FAC sorted somal RNA) and a negative control (dH_2O).

Tapestation data demonstrated a high level of RNA in the positive control (50100 pg/µl), and very low levels for the negative control (243 pg/µl) and FAC-sorted somas (427 and 494 pg/µl). ***Figure 6.4*** shows the output for the Tapestation, along with RIN scores (RNA integrity number; a value assigned to assess the integrity of an RNA sample determined by comparing the levels of 28S and 18S rRNA), although RNA concentration was deemed to be outside the range required to calculate RIN scores. The amount of RNA in the sorted cells was almost double that detected in the negative control, demonstrating our ability to extract RNA from FAC-sorted somas which have been obtained via our sorting procedure.

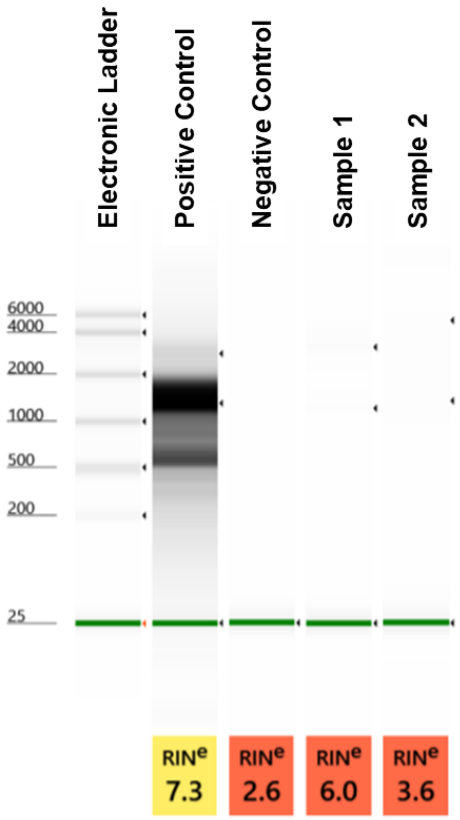

Figure 6.4 The output for the analysis of FACS-sorted cell body RNA using the Agilent 4200 TapeStation System

Samples (left to right): positive somal RNA control, negative dH2O control, sample 1, sample 2 (both samples are 700 cells isolated from a microfluidic chamber using FACS. RIN (RNA integrity number) scores are indicated under each sample.

6.3 Discussion

The results of this chapter demonstrate the ability of a new technique to isolate, by CTxB-FACS, the somas of retrogradely-labelled neurons that have been cultured in MFCs. Before moving on to further discussion, it is necessary to note that this procedure is still in the early days of development, with a key point remaining to be addressed: are the fluorescent cells that I am collecting CTxB-positive somas? Given the use of the CTxB-negative control to determine fluorescence gating, it is very unlikely that these cells are CTxB-negative. However, there remains the possibility that incomplete fluidic isolation within the MFCs or technical artefacts occurring during the trypsinisation step may have resulted in CTxB-membrane-labelling of neurons or non-neuronal cells (NNCs).

An indication that the isolated cells are neurons is that the fluorescence-positive cell populations have a higher forward scatter for all conditions (***Figure 6.2D, G, J***) compared to the bulk cell population; we would expect neurons to be bigger than NNCs. In addition, in ***Figure 6.3*** the CTxB-488 and -647 populations have a similar forward and side scatter, indicating an enrichment for the same cell-type. One way to further assess the identity of these cells is by the collecting them in neuronal culture medium and re-plating them to determine by immunostaining (e.g. by a neuron-specific antibody such as βIII-tubulin) and confocal whether all sorted cells are neurons. An alternative method would be to perform transcriptomics or proteomics experiments on the sorted cells and look for the enrichment of neuronal transcripts or proteins.

Assuming that these cells are neurons, it appears that the optimised technique has been successful in sorting fluorescent cell bodies from the bulk cell population. Cells were obtained in the low hundreds, out of a few hundred-thousand cells investigated: 0-0.1% of the total population. In order to have an idea of the yield of our technique, it may be interesting to count the number of CTxB-positive cells per MFC prior to sorting via confocal microscopy. We would expect efficiency to be low however, as this is a multi-step procedure with numerous opportunities for cell loss. In particular, the NNCs (fibroblasts/glia) in the somal compartment can become overgrown by DIV7, resulting in the trapping of a large number of cells within cell clumps which do not break up following trituration and therefore do not pass through the 40 µm cell strainer. One solution that could improve this is the use of mitotic inhibitors, such as arabinosylcytosine C (AraC) and 5-Fluoro-2'-deoxyuridine (FdU), during cell culture to prevent NNC proliferation (Hui et al., 2016). However, these

agents have been demonstrated to have a detrimental effect on neurons in primary cultures, so may not be suitable (Martin et al., 1990).

An additional factor that may result in the loss of neurons which are CTxB-positive is the arbitrary construction of gates based on the negative control. Unlike the sorting of cells expressing a fluorescent marker at high levels (which can show distinct FAC-sorted populations), the levels of fluorescence observed in this chapter depend on both the time allowed for and the capacity of each neuron to retrogradely transport particles of CTxB towards the soma. The short time scale (3 hours) and heterogeneous capacity of each neuron in the culture to perform retrograde transport results in a highly variable ability of each soma to accumulate fluorescence, which is presents experimentally as a smear on the FACS plots (***Figure 6.2-6.3***). This can result in the issue observed for the “488” gate in both ***Figure 6.2E*** and ***Figure 6.3D***, where a decision must be made as to where to draw the cut-off.

Another concern with the experimental set-up used is the labelling method. It is possible the retrograde transport and subsequent accumulation of CTxB may alter a number of cellular pathways: CTxB is transported along the axon, accumulates in the soma and is transported into dendrites, so may interact with numerous pathways (Lanciego and Wouterlood, 2011). In particular, applying a high concentration of CTxB, which is transported retrogradely via dynein, may compete with other axon-to-soma pathways that are being investigated. It is necessary to compare results to a control which has also had its axons treated with CTxB. To account for this, I used tripartite MFCs, in which the control and treatment cell bodies can be exposed to the same environment and experimental procedures, with only the CTxB fluorescence and axonal treatments differing. Alternative retrograde labelling methods to CTxB include lipophilic dyes, such as DiI (Goshima et al., 2012); DiI labelling was attempted in preliminary experiments, but somal CTxB intensity was much higher following 3 hours axonal incubation.

One major issue highlighted during the optimisation of this technique was my inability to produce the same result with DRGNs using the same methodology. This may be a product of a decreased ability of DRGNs to retrogradely transport or accumulate CTxB compared to CNs. Alternatively, as DRGNs have a much larger cytoplasmic volume than CNs, this may lead to a difficulty in concentrating the fluorophore and hence a lower fluorescent intensity within the soma, which may be difficult to detect via FACS. This may be resolved by incubating DRGN axons for a

longer time to increase the cell body CTxB concentration. It will further be interesting to see if this technique works for other neurons types (e.g. motor neurons).

The number of cells obtained by this technique is very low (a few hundred from 4 MFCs) and the amount of RNA obtained from these cells is comparatively low. Methods to increase cell-yield have already been discussed, but it may also be possible to increase the RNA yield. The Qiagen Micro RNeasy Kit suggest that for less than 100,000 cells, the volume of lysis Buffer RLT should be reduced from 350 to 75 µl. However, this volume had to be traded-off with the volume required to collect the output of the FACS machine: lower volumes increase the chance of a cell being deposited onto the side of the Eppendorf tube, rather than directly into the lysis buffer. This may be optimised to find a condition which improves RNA yield. Despite a low yield, RNA sequencing experiments are regularly performed on single cells (Hwang et al., 2018) and even axons (Nijssen et al., 2018), so the low number of cells and concentration of RNA obtained should be also be suitable for transcriptomics studies. While transcriptomics studies can benefit from the PCR amplification of smaller quantities, the material obtained via this technique may be too low for proteomics (mass spectrometry; western blotting; immunoprecipitation). However, in this chapter I only inputted cells obtained from 4 MFCs. Though it may be time-consuming and expensive to increase the number of MFCs used, in theory your yield will be largely determined by the number of MFCs you are willing to make.

Assuming that the sorted population of cells are what I assume them to be, this novel technique will prove useful for the study of multiple biological questions. Initially this project stemmed from the results presented in ***Chapter 4***, which resulted in the use of ARS as the axonal stimulus in ***section 6.2.2***. The technique was effective despite ARS being a very intense stressor, which causes extensive axon damage (***Figure 4.8A***), suggesting the technique will be suitable for most other applications. For example, it is known that axonal NGF is able to induce transcription in a CRE-luciferase reporter assay (Cox et al., 2008), but with this technique it would be possible to determine which transcripts are specifically altered. Known pathways such as this may also prove useful in the validation of this technique: I would be possible to see if CRE-dependent transcript increase, as previously observed.

Another field-of-study in which it has been demonstrated that axonal stimuli alter the soma is that of mechanical damage, with somal transcriptional changes required for regeneration following peripheral lesion (Mahar and Cavalli, 2018). It has been demonstrated that transcription factors, such as STAT3 can be locally translated following axon damage in primary DRGNs and retrogradely transported to the cell body (Ben-Yaakov et al., 2012). While the technique described in this chapter will be useful for the study of longer term changes in the cell body, it is critical to remember that upon trypsinisation of the somal compartments, all CTxB-positive neurons are axotomized, so may display early transcriptional changes associated with axon damage and regeneration if there is a long delay prior to FACS.

In terms of Chapter 4, while we know that axonal ARS induces somal SGs, it will be interesting to see if this causes alterations in the somal transcriptome or proteome, and whether disease-causing mutations alter the responses of cell bodies to axonal damage.

6.3.1 Future directions

Are the cells isolated by FACS neuron somas?

As mentioned above, it will be critical to determine whether the cells sorted by this technique are CTxB-positive neuron somas. This can be done by either re-plating sorted neurons, or by analysing transcriptomics or proteomics for the enrichment of neuron-specific markers. To determine whether each of the cells collected are neurons, it is possible to sort single cells via FACS into individual wells for single-cell sequencing (Muraro et al., 2016).

Validation of the technique with known transcripts

In order to validate the technique, it should be used to assess established axon-to-soma signalling pathways, where the results can be compared to previous data: for example, axonal NGF and somal CRE-dependent transcription (Cox et al., 2008).

Performing a full run-through

I have not yet performed a full run-through of the technique. This will be performed using the methods in ***section 6.2.2*** and ***section 6.2.3***, comparing the transcriptomes of neurons whose axons have been exposed to either control or 1mM ARS for 1 hour.

6.4 Conclusions

The results of this chapter demonstrate the first stages in the optimisation of a technique by which neuronal cell bodies, whose axons have been exposed to certain stimuli, can be isolated by FACS for subsequent omics studies. There remain a number of questions to be asked, and a full experimental run-through of the procedure, with RNA sequencing, remains to be performed. In future this technique will prove useful for the study of retrograde signalling in multiple fields, including growth factor stimulation, axon damage and axon regeneration. Going forward, we wish to use this technique in conjunction with those used in ***Chapter 4***, to observe the transcriptional responses of cell bodies to axonal stressors, such as arsenite.

7 Conclusions

The work presented in this thesis contributes to the ever-expanding field of research linking cytoplasmic SGs and ALS-FTD. Throughout this body of work a number of methodological concepts have been developed that will aid future investigations of phase-separated granules and their relation to disease:

The use of disease-relevant cell-types

The majority of SG research has been performed using cancer cell lines. While these cell lines are easy-to-use and allow data to be collected rapidly, the data obtained from them should be applied to other cell-types with caution. Multiple studies have shown that different cell-types respond differently to even the same stressor, whether that be the SG protein composition (Markmiller et al., 2018, Hock et al., 2018) or the kinetics of the SG response (Khalfallah et al., 2018). An additional caution with the use of cancer cell lines is that tumorigenic mutations (e.g. in *KRAS*) have been demonstrated to alter the SG response (increased SG coverage per cell) (Grabocka and Bar-Sagi, 2016).

The differences in SG proteome between different cell-types not surprising, given that all cell-types differ in both their proteome and transcriptome. This complexity is heightened in neurons, which use molecular transport to define local proteomes and transcriptomes: including dendritic, axonal and synaptic regions (Lassek et al., 2015, Poulopoulos et al., 2019). In accordance with this, it is possible that different regions of the same cell could respond to the same stressor differently. It has already been demonstrated for example, that phase-separated TDP-43 RNP granules in the axon have different biophysical properties (e.g. viscosity) depending on their proximity to the soma (Gopal et al., 2017).

With these concepts in mind, I aimed to study phase separation in primary mouse tissue, with the knowledge from previous studies that differences in SG assembly/disassembly kinetics are observable between different primary cell-types: motor neurons (MNs), fibroblasts (MEFs) and astrocytes (Khalfallah et al., 2018). The majority of my studies were however performed using primary cortical neurons (CNs) rather than MNs; both of which degenerate in ALS-FTD. While it would have been preferable to study both cell-types, CNs were used because they could be cultured reliably with very few embryos required for a high neuron yield. In addition, MNs were in high demand within the laboratory in which these experiments were performed so in the spirit of the 3Rs (Replacement, Reduction and Refinement)

(Fenwick et al., 2009), I reduced the number of mice being used for culture by choosing CNs. The yield and purity of CN cultures could be improved by obtaining cultures from P0 mice, though comparisons to MNs would not be possible at this age. DRGNs were chosen for two reasons: they comparatively do not degenerate in ALS-FTD and they project extensive axons rapidly, making them ideal for experiments using microfluidic chambers. In future it will be important to perform similar experiments in MNs, prior to drawing conclusions about ALS.

The use of dose-responses and time courses

Throughout SG research it is rare to observe published figures determining the concentrations which induce SGs and those which induce death. The differences in susceptibility of CNs compared to MEFs/DRGNs in the paradigms investigated highlight the necessity of performing dose response and time course experiments. Alterations to the cell-type, length of treatment, culture medium and other factors can result in a drastically different susceptibility of the cells in your chosen set-up to a specific stressor. In light of this, whenever a new SG inducer was used, an acute-DR was performed to test for both SG formation and cell death.

The use of disease-relevant models

Many studies investigating ALS-FTD and its link to SG homeostasis have the issue that the mutant protein being observed is overexpressed at non-physiological levels; usually either by uncontrolled expression using transfection or via transgene expression. This is an issue, as the expression levels of RBPs are tightly regulated (Muller-McNicoll et al., 2019) and overexpression can result in artificial situations, such as the formation of SG-like granules in the absence of a stressor (Gilks et al., 2004, Ju et al., 2011).

Models with single, dominant point-mutations expressed in heterozygosity are likely the best way forward: for example patient fibroblasts, patient iPSCs and knock-in mouse models. I employed the latter for the ALS experiments, using the FUSDelta14 mouse model, demonstrating a significant mislocalisation of FUS to both the cytoplasm and stress granules in the absence of overexpression. These models have a higher construct validity and therefore likely show a closer picture of what early changes are occurring in the cells of heterozygous ALS patients.

In recent years, the use of knock-in models to study ALS has increased (De Giorgio et al., 2019). One recent paper, generated a knock-in mouse model with a FUS^{R521C} mutation, which displayed progressive motor deficits (present at 7, but not at 4

months) and MN loss in both HET and HOM animals (Zhang et al., 2020). After confirming that FUS localises to SGs in HET and HOM primary MNs, they performed *in vivo* experiments, demonstrating that chronic stress (by intragastric injection of ARS) accelerated the progression of the observed motor deficits. Furthermore, they transduced a lentiviral TIA1-GFP reporter construct into the motor cortex of HOM mice and observed TIA1 granule formation longitudinally *in vivo* via two-photon microscopy, demonstrating granule formation (within 2 hours) and granules persistence in neurons up to 3 weeks following intragastric ARS injection; these granules did not form in WT.

The above study demonstrates the possibility of investigating SG formation and dynamics *in vivo*, over a time course. In future my project could use these techniques to investigate the validity of my axonal stress findings for *in vivo* systems. One potential experiment would be to inject arsenite peripherally into the muscle or nerve of a live mouse and subsequently image the dorsal root ganglia (Chen et al., 2019) to observe SGs. It would be preferable to use a mouse model expressing an endogenously-tagged SG marker, rather than using lentiviral transduction, as altering RBP levels can induce artificial aggregation phenotypes (as discussed above).

The use of quantification to observe minor changes

Throughout the SG literature, there is a lack of quantified data from immunofluorescence studies. Of note, when aiming to determine whether a protein localises to SGs, few papers mention using the quantification of fluorescent intensities to determine this. Though immunofluorescence colocalisation does not equate to protein-protein interaction, it provides a quick, straight-forward initial experiement prior to more expensive methods, such as proximity labelling (Markmiller et al., 2018). Protein interactions determined using *in vitro* methods which isolate SG cores following cell lysis should be later confirmed using *in vivo* methods, as cell lysis may disrupt low-affinity interactions in the SG ‘shell’ leading to a potential loss or gain of protein interactions (Markmiller et al., 2018). The observation in ***Chapter 5***, that FUS-WT localises to SGs, provides *in vivo* data to support *in vitro* methods (Jain et al., 2016). Despite a level of FUS which was not detectable by eye, relative intensity values within defined regions-of-interest demonstrated that in fact FUS-WT does co-localise with SG markers.

With these concepts in mind I was able to provide a range of novel information, including novel stressors and axon-to-soma stress granule signalling, to the field of stress granules and ALS-FTD:

Chapter 3 presents of large amount of optimisation which was later applied to the work in the subsequent three chapters. Beyond this, I demonstrated the formation of SGs in sensory neurons, not currently published in the literature, which highlighted an unusual localisation of the granules to the periphery of the cell. Additionally, I identified two novel SG inducers: BAPTA-AM and KB-R7943. This suggests that both acute Ca^{2+} chelation and the inhibition of mitochondrial complex I induce SG assembly; further experiments are required to ensure that SG formation does not result from any off-target effects. In addition, a high amount of cell-death was observed for the concentrations of KB-R7943 which induced SG formation, so these granules will need to be further characterised.

Chapter 4 presents the most-striking results of this thesis: specifically that axonal arsenite stress can induce SGs in the soma of the cell. These FMRP-positive granules require polysome disassembly and may rely on local axonal translation and retrograde transport via the microtubule-motor dynein. This provides the first reports that exogenous stress in the periphery could result in phase separation in a completely separate region of the body, which has major implications for the spread of aggregate pathology. The physiological role of this pan-neuronal pathway remains unknown, but likely forms part of a mechanism by which the soma can protect itself during axonal injury, prioritising stress-related cytoprotective pathways, and inhibiting premature apoptosis (Arimoto et al., 2008).

Throughout aging, both oxidative and ER stresses increase (Martinez et al., 2017, Romano et al., 2010), meaning that the large surface area of peripheral axons, and to some extent that of somas, will be subjected to increased stress; additionally, the large surface area of axons leaves them further exposed to physical damage. Increasing stress over a lifetime, exacerbated but not necessarily caused by ALS mutations, could result in repeated cycling of (or extended) stress-induced phase separation, over time resulting in the accumulations that are associated with disease.

A large body of evidence has linked ALS to SG formation and function, with a large number of ALS-linked proteins, including TDP-43, FUS and C9ORF72, demonstrated to localise to SGs (***Table 1.5***). Further, mutations in these proteins

have been shown to perturb SG dynamics (***Table 1.6***). It remains possible, that the formation of canonical SGs is not required for inclusion formation, but a growing body of evidence has linked cellular stress to the formation of inclusions (McGurk et al., 2018; Gasset-Rosa et al., 2019; Zhang et al., 2020). The ability to perform longitudinal stress studies *in vivo*, will likely give us further insight into the formation of inclusions over time, and hence allow us to draw better comparisons with human pathology.

The targetting of SG pathways for drug discovery still remains in its infancy, and currenty no drugs directly targetting phase separation have approval for use in humans. While perturbing granule dynamics to prevent the formation of inclusions may be an attractive concept, SGs and other phase separated organelles play a lot of key roles physiological roles, so further understanding of SG pathways is required in order to avoid off-target effects. While the current thesis does not provide any direct link to drug development, it does increase our understanding of the processes influencing SG formation in specifically in neurons. A number of studies have already demonstrated *in vivo* that strategies which interrupt SG pathways can alleviate degenerative phenotypes in ALS animal models; these include antisense oligonucleotides (ASOs) against the SG component ataxin-2 (Becker et al., 2017), and small molecule inhibition of eIF2α phosphorylation (Kim et al., 2014). In addtion, high-content screening of SG-modulating compounds using iPSC models has demonstrated both compounds that inhibit SG formation, as well as those which reduce the localisation of ALS-associated RBPs (including TDP-43) to SGs, though these are yet to be tested in animal models (Fang et al., 2019).

Chapter 5 further confirms the observation that ALS-mutant FUS protein mislocalises to both the cytoplasm in basal conditions, but also to cytoplasmic SGs following ARS stress. Further, this mislocalisation is replicated in DRGNs, which are less susceptible to ALS pathogenesis than MNs; this data indicates that neither the mislocalisation of FUS to the cytoplasm, nor to SGs are the reason for this susceptibility difference.

Chapter 6 shows the development of a tool to isolate the somas of neurons whose axons have been exposed to exogenous soluble stimuli. This set-up consists of neuronal culture in MFCs, retrograde-labelling with fluorescently-tagged toxin subunits and subsequent fluorescence-activated cell sorting (FACS). The results in

this chapter are promising and suggest that this technique may be suitable for RNA sequencing experiments, however more optimisation is required.

7.1 Concluding remarks

This research presented in this thesis increases our understanding of how neuronal cells respond to exogenous stressors, and further, how ALS-mutations can alter these responses to cause disease. In particular, it demonstrated the first reports of local axonal stress being converted into aggregation in the soma. This finding has major implications for the spread of RNP aggregates along axonal pathways and hence, throughout the body. A better understanding of stress-related pathways specifically in neurons is necessary for the development of novel therapeutics targeting SGs for the treatment of ALS and similar diseases relating to alterations in intracellular phase separation.

References

Acosta, J. R., Goldsbury, C., Winnick, C., Badrock, A. P., Fraser, S. T., Laird, A. S., Hall, T. E., Don, E. K., Fifita, J. A., Blair, I. P., Nicholson, G. A. and Cole, N. J. (2014) 'Mutant human FUS Is ubiquitously mislocalized and generates persistent stress granules in primary cultured transgenic zebrafish cells', *PLoS One,* 9(6), pp. e90572.

Adjibade, P., St-Sauveur, V. G., Quevillon Huberdeau, M., Fournier, M. J., Savard, A., Coudert, L., Khandjian, E. W. and Mazroui, R. (2015) 'Sorafenib, a multikinase inhibitor, induces formation of stress granules in hepatocarcinoma cells', *Oncotarget,* 6(41), pp. 43927-43.

Ajroud-Driss, S. and Siddique, T. (2015) 'Sporadic and hereditary amyotrophic lateral sclerosis (ALS)', *Biochimica et Biophysica Acta (BBA) - Molecular Basis of Disease,* 1852(4), pp. 679-684.

Alami, N. H., Smith, R. B., Carrasco, M. A., Williams, L. A., Winborn, C. S., Han, S. S. W., Kiskinis, E., Winborn, B., Freibaum, B. D., Kanagaraj, A., Clare, A. J., Badders, N. M., Bilican, B., Chaum, E., Chandran, S., Shaw, C. E., Eggan, K. C., Maniatis, T. and Taylor, J. P. (2014) 'Axonal transport of TDP-43 mRNA granules is impaired by ALS-causing mutations', *Neuron,* 81(3), pp. 536-543.

Alrafiah, A. R. (2018) 'From Mouse Models to Human Disease: An Approach for Amyotrophic Lateral Sclerosis', *In vivo (Athens, Greece),* 32(5), pp. 983-998.

An, H., Tan, J. T. and Shelkovnikova, T. A. (2019) 'Stress granules regulate stress-induced paraspeckle assembly', *J Cell Biol,* 218(12), pp. 4127-4140.

Andersson, M. K., Stahlberg, A., Arvidsson, Y., Olofsson, A., Semb, H., Stenman, G., Nilsson, O. and Aman, P. (2008) 'The multifunctional FUS, EWS and TAF15 proto-oncoproteins show cell type-specific expression patterns and involvement in cell spreading and stress response', *BMC Cell Biol,* 9, pp. 37.

Ansari, M. Y. and Haqqi, T. M. (2016) 'Interleukin-1beta induced Stress Granules Sequester COX-2 mRNA and Regulates its Stability and Translation in Human OA Chondrocytes', *Sci Rep,* 6, pp. 27611.

Antar, L. N., Dictenberg, J. B., Plociniak, M., Afroz, R. and Bassell, G. J. (2005) 'Localization of FMRP-associated mRNA granules and requirement of microtubules for activity-dependent trafficking in hippocampal neurons', *Genes Brain Behav,* 4(6), pp. 350-9.

Antonacci, G., de Turris, V., Rosa, A. and Ruocco, G. (2018) 'Background-deflection Brillouin microscopy reveals altered biomechanics of intracellular stress granules by ALS protein FUS', *Commun Biol,* 1, pp. 139.

Arai, T., Hasegawa, M., Akiyama, H., Ikeda, K., Nonaka, T., Mori, H., Mann, D., Tsuchiya, K., Yoshida, M., Hashizume, Y. and Oda, T. (2006) 'TDP-43 is a component of ubiquitin-positive tau-negative inclusions in frontotemporal lobar degeneration and amyotrophic lateral sclerosis', *Biochem Biophys Res Commun,* 351(3), pp. 602-11.

Arimoto, K., Fukuda, H., Imajoh-Ohmi, S., Saito, H. and Takekawa, M. (2008) 'Formation of stress granules inhibits apoptosis by suppressing stress-responsive MAPK pathways', *Nat Cell Biol,* 10(11), pp. 1324-32.

Arimoto-Matsuzaki, K., Saito, H. and Takekawa, M. (2016) 'TIA1 oxidation inhibits stress granule assembly and sensitizes cells to stress-induced apoptosis', *Nat Commun,* 7, pp. 10252.

Ash, P. E. A., Vanderweyde, T. E., Youmans, K. L., Apicco, D. J. and Wolozin, B. (2014) 'Pathological stress granules in Alzheimer's disease', *Brain research,* 1584, pp. 52-58.

Aulas, A., Fay, M. M., Lyons, S. M., Achorn, C. A., Kedersha, N., Anderson, P. and Ivanov, P. (2017) 'Stress-specific differences in assembly and composition of stress granules and related foci', *Journal of cell science,* 130(5), pp. 927-937.

Aulas, A., Lyons, S. M., Fay, M. M., Anderson, P. and Ivanov, P. (2018) 'Nitric oxide triggers the assembly of "type II" stress granules linked to decreased cell viability', *Cell Death Dis,* 9(11), pp. 1129.

Aulas, A., Stabile, S. and Vande Velde, C. (2012) 'Endogenous TDP-43, but not FUS, contributes to stress granule assembly via G3BP', *Mol Neurodegener,* 7, pp. 54.

Ayuso, M. I., Martinez-Alonso, E., Regidor, I. and Alcazar, A. (2016) 'Stress Granule Induction after Brain Ischemia Is Independent of Eukaryotic Translation Initiation Factor (eIF) 2alpha Phosphorylation and Is Correlated with a Decrease in eIF4B and eIF4E Proteins', *J Biol Chem,* 291(53), pp. 27252-27264.

Baechtold, H., Kuroda, M., Sok, J., Ron, D., Lopez, B. S. and Akhmedov, A. T. (1999) 'Human 75-kDa DNA-pairing protein is identical to the pro-oncoprotein TLS/FUS and is able to promote D-loop formation', *J Biol Chem,* 274(48), pp. 34337-42.

Bai, Y., Dong, Z., Shang, Q., Zhao, H., Wang, L., Guo, C., Gao, F., Zhang, L. and Wang, Q. (2016) 'Pdcd4 Is Involved in the Formation of Stress Granule in Response to Oxidized Low-Density Lipoprotein or High-Fat Diet', *PLoS One,* 11(7), pp. e0159568.

Balendra, R. and Isaacs, A. M. (2018) 'C9orf72-mediated ALS and FTD: multiple pathways to disease', *Nature reviews. Neurology,* 14(9), pp. 544-558.

Baleriola, J., Walker, C. A., Jean, Y. Y., Crary, J. F., Troy, C. M., Nagy, P. L. and Hengst, U. (2014) 'Axonally Synthesized ATF4 Transmits a Neurodegenerative Signal across Brain Regions', *Cell,* 158(5), pp. 1159-1172.

Bampton, A., Gittings, L. M., Fratta, P., Lashley, T. and Gatt, A. (2020) 'The role of hnRNPs in frontotemporal dementia and amyotrophic lateral sclerosis', *Acta Neuropathol*.

Baron, D. M., Kaushansky, L. J., Ward, C. L., Sama, R. R., Chian, R. J., Boggio, K. J., Quaresma, A. J., Nickerson, J. A. and Bosco, D. A. (2013) 'Amyotrophic lateral sclerosis-linked FUS/TLS alters stress granule assembly and dynamics', *Mol Neurodegener,* 8, pp. 30.

Baumer, D., Hilton, D., Paine, S. M., Turner, M. R., Lowe, J., Talbot, K. and Ansorge, O. (2010) 'Juvenile ALS with basophilic inclusions is a FUS proteinopathy with FUS mutations', *Neurology,* 75(7), pp. 611-8.

Becker, L. A., Huang, B., Bieri, G., Ma, R., Knowles, D. A., Jafar-Nejad, P., Messing, J., Kim, H. J., Soriano, A., Auburger, G., Pulst, S. M., Taylor, J. P., Rigo, F. and Gitler, A. D. (2017) 'Therapeutic reduction of ataxin-2 extends lifespan and reduces pathology in TDP-43 mice', *Nature,* 544(7650), pp. 367-371.

Belzil, V. V., Langlais, J. S., Daoud, H., Dion, P. A., Brais, B. and Rouleau, G. A. (2012) 'Novel FUS deletion in a patient with juvenile amyotrophic lateral sclerosis', *Arch Neurol,* 69(5), pp. 653-6.

Ben-Yaakov, K., Dagan, S. Y., Segal-Ruder, Y., Shalem, O., Vuppalanchi, D., Willis, D. E., Yudin, D., Rishal, I., Rother, F., Bader, M., Blesch, A., Pilpel, Y., Twiss, J. L. and Fainzilber, M. (2012) 'Axonal transcription factors signal retrogradely in lesioned peripheral nerve', *The EMBO journal,* 31(6), pp. 1350-1363.

Bentmann, E., Neumann, M., Tahirovic, S., Rodde, R., Dormann, D. and Haass, C. (2012) 'Requirements for stress granule recruitment of fused in sarcoma (FUS) and TAR DNA-binding protein of 43 kDa (TDP-43)', *J Biol Chem,* 287(27), pp. 23079-94.

Berlanga, J. J., Ventoso, I., Harding, H. P., Deng, J., Ron, D., Sonenberg, N., Carrasco, L. and de Haro, C. (2006) 'Antiviral effect of the mammalian translation initiation factor 2alpha kinase GCN2 against RNA viruses', *Embo j,* 25(8), pp. 1730-40.

Bertolin, C., D'Ascenzo, C., Querin, G., Gaiani, A., Boaretto, F., Salvoro, C., Vazza, G., Angelini, C., Cagnin, A., Pegoraro, E., Soraru, G. and Mostacciuolo, M. L. (2014) 'Improving the knowledge of amyotrophic lateral sclerosis genetics: novel SOD1 and FUS variants', *Neurobiology of Aging,* 35(5), pp. 4.

Bilsland, L. G., Sahai, E., Kelly, G., Golding, M., Greensmith, L. and Schiavo, G. (2010) 'Deficits in axonal transport precede ALS symptoms in vivo', *Proc Natl Acad Sci U S A,* 107(47), pp. 20523-8.

Birsa, N., Bentham, M. P. and Fratta, P. (2019) 'Cytoplasmic functions of TDP-43 and FUS and their role in ALS', *Semin Cell Dev Biol*.

Boeynaems, S., Bogaert, E., Kovacs, D., Konijnenberg, A., Timmerman, E., Volkov, A., Guharoy, M., De Decker, M., Jaspers, T., Ryan, V. H., Janke, A. M., Baatsen, P., Vercruysse, T., Kolaitis, R. M., Daelemans, D., Taylor, J. P., Kedersha, N., Anderson, P., Impens, F., Sobott, F., Schymkowitz, J., Rousseau, F., Fawzi, N. L., Robberecht, W., Van Damme, P., Tompa, P. and Van Den Bosch, L. (2017) 'Phase Separation of C9orf72 Dipeptide Repeats Perturbs Stress Granule Dynamics', *Mol Cell,* 65(6), pp. 1044-1055.e5.

Bolt, A. M., Byrd, R. M. and Klimecki, W. T. (2010) 'Autophagy is the predominant process induced by arsenite in human lymphoblastoid cell lines', *Toxicol Appl Pharmacol,* 244(3), pp. 366-73.

Borroni, B., Bonvicini, C., Alberici, A., Buratti, E., Agosti, C., Archetti, S., Papetti, A., Stuani, C., Di Luca, M., Gennarelli, M. and Padovani, A. (2009) 'Mutation within TARDBP leads to frontotemporal dementia without motor neuron disease', *Hum Mutat,* 30(11), pp. E974-83.

Bosco, D. A., Lemay, N., Ko, H. K., Zhou, H., Burke, C., Kwiatkowski, T. J., Jr., Sapp, P., McKenna-Yasek, D., Brown, R. H., Jr. and Hayward, L. J. (2010) 'Mutant FUS proteins that cause amyotrophic lateral sclerosis incorporate into stress granules', *Hum Mol Genet,* 19(21), pp. 4160-75.

Bouchard, P., Penningroth, S. M., Cheung, A., Gagnon, C. and Bardin, C. W. (1981) 'erythro-9-[3-(2-Hydroxynonyl)]adenine is an inhibitor of sperm motility that blocks dynein ATPase and protein carboxylmethylase activities', *Proc Natl Acad Sci U S A,* 78(2), pp. 1033-6.

Boyd, J. D., Lee, P., Feiler, M. S., Zauur, N., Liu, M., Concannon, J., Ebata, A., Wolozin, B. and Glicksman, M. A. (2014) 'A high-content screen identifies novel compounds that inhibit stress-induced TDP-43 cellular aggregation and associated cytotoxicity', *J Biomol Screen,* 19(1), pp. 44-56.

Brenneis, C., Kistner, K., Puopolo, M., Segal, D., Roberson, D., Sisignano, M., Labocha, S., Ferreiros, N., Strominger, A., Cobos, E. J., Ghasemlou, N., Geisslinger, G., Reeh, P. W., Bean, B. P. and Woolf, C. J. (2013) 'Phenotyping the function of TRPV1-expressing sensory neurons by targeted axonal silencing', *J Neurosci,* 33(1), pp. 315-26.

Broustal, O., Camuzat, A., Guillot-Noel, L., Guy, N., Millecamps, S., Deffond, D., Lacomblez, L., Golfier, V., Hannequin, D., Salachas, F., Camu, W., Didic, M., Dubois, B., Meininger, V., Le Ber, I. and Brice, A. (2010) 'FUS mutations in frontotemporal lobar degeneration with amyotrophic lateral sclerosis', *J Alzheimers Dis,* 22(3), pp. 765-9.

Brown, A. (2003) 'Axonal transport of membranous and nonmembranous cargoes: a unified perspective', *J Cell Biol,* 160(6), pp. 817-21.

Brustovetsky, T., Brittain, M. K., Sheets, P. L., Cummins, T. R., Pinelis, V. and Brustovetsky, N. (2011) 'KB-R7943, an inhibitor of the reverse Na+ /Ca2+ exchanger, blocks N-methyl-D-aspartate receptor and inhibits mitochondrial complex I', *Br J Pharmacol,* 162(1), pp. 255-70.

Buchan, J. R., Kolaitis, R. M., Taylor, J. P. and Parker, R. (2013) 'Eukaryotic stress granules are cleared by autophagy and Cdc48/VCP function', *Cell,* 153(7), pp. 1461-74.

Campenot, R. B. (1977) 'Local control of neurite development by nerve growth factor', *Proc Natl Acad Sci U S A,* 74(10), pp. 4516-9.

Cande, W. Z. (1982) 'Inhibition of spindle elongation in permeabilized mitotic cells by erythro-9-[3-(2-hydroxynonyl)] adenine', *Nature,* 295(5851), pp. 700-1.

Chen, C., Zhang, J., Sun, L., Zhang, Y., Gan, W. B., Tang, P. and Yang, G. (2019) 'Long-term imaging of dorsal root ganglia in awake behaving mice', *Nat Commun,* 10(1), pp. 3087.

Chen, L., Stone, M. C., Tao, J. and Rolls, M. M. (2012) 'Axon injury and stress trigger a microtubule-based neuroprotective pathway', *Proc Natl Acad Sci U S A,* 109(29), pp. 11842-7.

Chitiprolu, M., Jagow, C., Tremblay, V., Bondy-Chorney, E., Paris, G., Savard, A., Palidwor, G., Barry, F. A., Zinman, L., Keith, J., Rogaeva, E., Robertson, J., Lavallee-Adam, M., Woulfe, J., Couture, J. F., Cote, J. and Gibbings, D. (2018) 'A complex of C9ORF72 and p62 uses arginine methylation to eliminate stress granules by autophagy', *Nat Commun,* 9(1), pp. 2794.

Cho, Y., Shin, J. E., Ewan, E. E., Oh, Y. M., Pita-Thomas, W. and Cavalli, V. (2015) 'Activating Injury-Responsive Genes with Hypoxia Enhances Axon Regeneration through Neuronal HIF-1alpha', *Neuron,* 88(4), pp. 720-34.

Christen, K. E., Davis, R. A. and Kennedy, D. (2019) 'Psammaplysin F increases the efficacy of bortezomib and sorafenib through regulation of stress granule formation', *Int J Biochem Cell Biol,* 112, pp. 24-38.

Coady, T. H. and Manley, J. L. (2015) 'ALS mutations in TLS/FUS disrupt target gene expression', *Genes Dev,* 29(16), pp. 1696-706.

Collier, N. C., Heuser, J., Levy, M. A. and Schlesinger, M. J. (1988) 'Ultrastructural and biochemical analysis of the stress granule in chicken embryo fibroblasts', *J Cell Biol,* 106(4), pp. 1131-9.

Collier, N. C. and Schlesinger, M. J. (1986) 'The dynamic state of heat shock proteins in chicken embryo fibroblasts', *J Cell Biol,* 103(4), pp. 1495-507.

Colombrita, C., Zennaro, E., Fallini, C., Weber, M., Sommacal, A., Buratti, E., Silani, V. and Ratti, A. (2009) 'TDP-43 is recruited to stress granules in conditions of oxidative insult', *J Neurochem,* 111(4), pp. 1051-61.

Couratier, P., Corcia, P., Lautrette, G., Nicol, M. and Marin, B. (2017) 'ALS and frontotemporal dementia belong to a common disease spectrum', *Revue Neurologique,* 173(5), pp. 273-279.

Cox, L. J., Hengst, U., Gurskaya, N. G., Lukyanov, K. A. and Jaffrey, S. R. (2008) 'Intra-axonal translation and retrograde trafficking of CREB promotes neuronal survival', *Nat Cell Biol,* 10(2), pp. 149-59.

Dadon-Nachum, M., Melamed, E. and Offen, D. (2011) 'The "dying-back" phenomenon of motor neurons in ALS', *J Mol Neurosci,* 43(3), pp. 470-7.

De Giorgio, F., Maduro, C., Fisher, E. M. C. and Acevedo-Arozena, A. (2019) 'Transgenic and physiological mouse models give insights into different aspects of amyotrophic lateral sclerosis', *Dis Model Mech,* 12(1).

De Leeuw, F., Zhang, T., Wauquier, C., Huez, G., Kruys, V. and Gueydan, C. (2007) 'The cold-inducible RNA-binding protein migrates from the nucleus to cytoplasmic stress granules by a methylation-dependent mechanism and acts as a translational repressor', *Exp Cell Res,* 313(20), pp. 4130-44.

De Santis, R., Alfano, V., de Turris, V., Colantoni, A., Santini, L., Garone, M. G., Antonacci, G., Peruzzi, G., Sudria-Lopez, E., Wyler, E., Anink, J. J., Aronica, E., Landthaler, M., Pasterkamp, R. J., Bozzoni, I. and Rosa, A. (2019) 'Mutant FUS and ELAVL4 (HuD) Aberrant Crosstalk in Amyotrophic Lateral Sclerosis', *Cell Rep,* 27(13), pp. 3818-3831.e5.

DeJesus-Hernandez, M., Kocerha, J., Finch, N., Crook, R., Baker, M., Desaro, P., Johnston, A., Rutherford, N., Wojtas, A., Kennelly, K., Wszolek, Z. K., Graff-Radford, N., Boylan, K. and Rademakers, R. (2010) 'De Novo Truncating FUS

Gene Mutation as a Cause of Sporadic Amyotrophic Lateral Sclerosis', *Human Mutation,* 31(5), pp. E1377-E1389.

Deng, J., Wang, P., Chen, X., Cheng, H., Liu, J., Fushimi, K., Zhu, L. and Wu, J. Y. (2018) 'FUS interacts with ATP synthase beta subunit and induces mitochondrial unfolded protein response in cellular and animal models', *Proc Natl Acad Sci U S A,* 115(41), pp. E9678-e9686.

Deng, J., Yang, M., Chen, Y., Chen, X., Liu, J., Sun, S., Cheng, H., Li, Y., Bigio, E. H., Mesulam, M., Xu, Q., Du, S., Fushimi, K., Zhu, L. and Wu, J. Y. (2015) 'FUS Interacts with HSP60 to Promote Mitochondrial Damage', *PLoS Genet,* 11(9), pp. e1005357.

Deshpande, D., Higelin, J., Schoen, M., Vomhof, T., Boeckers, T. M., Demestre, M. and Michaelis, J. (2019) 'Synaptic FUS Localization During Motoneuron Development and Its Accumulation in Human ALS Synapses', *Front Cell Neurosci,* 13, pp. 256.

Devoy, A., Kalmar, B., Stewart, M., Park, H., Burke, B., Noy, S. J., Redhead, Y., Humphrey, J., Lo, K., Jaeger, J., Mejia Maza, A., Sivakumar, P., Bertolin, C., Soraru, G., Plagnol, V., Greensmith, L., Acevedo Arozena, A., Isaacs, A. M., Davies, B., Fratta, P. and Fisher, E. M. C. (2017) 'Humanized mutant FUS drives progressive motor neuron degeneration without aggregation in 'FUSDelta14' knockin mice', *Brain,* 140(11), pp. 2797-2805.

Dewey, C. M., Cenik, B., Sephton, C. F., Dries, D. R., Mayer, P., 3rd, Good, S. K., Johnson, B. A., Herz, J. and Yu, G. (2011) 'TDP-43 is directed to stress granules by sorbitol, a novel physiological osmotic and oxidative stressor', *Mol Cell Biol,* 31(5), pp. 1098-108.

Didiot, M. C., Subramanian, M., Flatter, E., Mandel, J. L. and Moine, H. (2009) 'Cells lacking the fragile X mental retardation protein (FMRP) have normal RISC activity but exhibit altered stress granule assembly', *Mol Biol Cell,* 20(1), pp. 428-37.

Dolzhanskaya, N., Merz, G., Aletta, J. M. and Denman, R. B. (2006) 'Methylation regulates the intracellular protein-protein and protein-RNA interactions of FMRP', *J Cell Sci,* 119(Pt 9), pp. 1933-46.

Dong, G., Liang, F., Sun, B., Wang, C., Liu, Y., Guan, X., Yang, B., Xiu, C., Yang, N., Liu, F., Lu, T. and Han, W. (2019) 'Presence and function of stress granules in atrial fibrillation', *PLoS One,* 14(4), pp. e0213769.

Dormann, D., Rodde, R., Edbauer, D., Bentmann, E., Fischer, I., Hruscha, A., Than, M. E., Mackenzie, I. R., Capell, A., Schmid, B., Neumann, M. and Haass, C. (2010) 'ALS-associated fused in sarcoma (FUS) mutations disrupt Transportin-mediated nuclear import', *Embo j,* 29(16), pp. 2841-57.

Eisinger-Mathason, T. S., Andrade, J., Groehler, A. L., Clark, D. E., Muratore-Schroeder, T. L., Pasic, L., Smith, J. A., Shabanowitz, J., Hunt, D. F., Macara, I. G. and Lannigan, D. A. (2008) 'Codependent functions of RSK2 and the apoptosis-promoting factor TIA-1 in stress granule assembly and cell survival', *Mol Cell,* 31(5), pp. 722-36.

Elden, A. C., Kim, H. J., Hart, M. P., Chen-Plotkin, A. S., Johnson, B. S., Fang, X., Armakola, M., Geser, F., Greene, R., Lu, M. M., Padmanabhan, A., Clay-Falcone, D., McCluskey, L., Elman, L., Juhr, D., Gruber, P. J., Rub, U., Auburger, G., Trojanowski, J. Q., Lee, V. M., Van Deerlin, V. M., Bonini, N. M. and Gitler, A. D. (2010) 'Ataxin-2 intermediate-length polyglutamine expansions are associated with increased risk for ALS', *Nature,* 466(7310), pp. 1069-75.

Emara, M. M., Fujimura, K., Sciaranghella, D., Ivanova, V., Ivanov, P. and Anderson, P. (2012) 'Hydrogen peroxide induces stress granule formation independent of eIF2alpha phosphorylation', *Biochem Biophys Res Commun,* 423(4), pp. 763-9.

Emara, M. M., Ivanov, P., Hickman, T., Dawra, N., Tisdale, S., Kedersha, N., Hu, G. F. and Anderson, P. (2010) 'Angiogenin-induced tRNA-derived stress-induced RNAs promote stress-induced stress granule assembly', *J Biol Chem,* 285(14), pp. 10959-68.

Fang, M. Y., Markmiller, S., Vu, A. Q., Javaherian, A., Dowdle, W. E., Jolivet, P., Bushway, P. J., Castello, N. A., Baral, A., Chan, M. Y., Linsley, J. W., Linsley, D., Mercola, M., Finkbeiner, S., Lecuyer, E., Lewcock, J. W. and Yeo, G. W. (2019) 'Small-Molecule Modulation of TDP-43 Recruitment to Stress Granules Prevents Persistent TDP-43 Accumulation in ALS/FTD', *Neuron,* 103(5), pp. 802-819.e11.

Farg, M. A., Soo, K. Y., Warraich, S. T., Sundaramoorthy, V., Blair, I. P. and Atkin, J. D. (2013) 'Ataxin-2 interacts with FUS and intermediate-length polyglutamine expansions enhance FUS-related pathology in amyotrophic lateral sclerosis', *Hum Mol Genet,* 22(4), pp. 717-28.

Farg, M. A., Sundaramoorthy, V., Sultana, J. M., Yang, S., Atkinson, R. A., Levina, V., Halloran, M. A., Gleeson, P. A., Blair, I. P., Soo, K. Y., King, A. E. and Atkin, J. D. (2014) 'C9ORF72, implicated in amytrophic lateral sclerosis and frontotemporal dementia, regulates endosomal trafficking', *Hum Mol Genet,* 23(13), pp. 3579-95.

Fargier, G., Favard, C., Parmeggiani, A., Sahuquet, A., Merezegue, F., Morel, A., Denis, M., Molinari, N., Mangeat, P. H., Coopman, P. J. and Montcourrier, P. (2013) 'Centrosomal targeting of Syk kinase is controlled by its catalytic activity and depends on microtubules and the dynein motor', *Faseb j,* 27(1), pp. 109-22.

Fathinajafabadi, A., Perez-Jimenez, E., Riera, M., Knecht, E. and Gonzalez-Duarte, R. (2014) 'CERKL, a retinal disease gene, encodes an mRNA-binding protein that localizes in compact and untranslated mRNPs associated with microtubules', *PLoS One,* 9(2), pp. e87898.

Fay, M. M., Anderson, P. J. and Ivanov, P. (2017) 'ALS/FTD-Associated C9ORF72 Repeat RNA Promotes Phase Transitions In Vitro and in Cells', *Cell Rep,* 21(12), pp. 3573-3584.

Fenwick, N., Griffin, G. and Gauthier, C. (2009) 'The welfare of animals used in science: how the "Three Rs" ethic guides improvements', *The Canadian veterinary journal = La revue veterinaire canadienne,* 50(5), pp. 523-530.

Figley, M. D., Bieri, G., Kolaitis, R. M., Taylor, J. P. and Gitler, A. D. (2014) 'Profilin 1 associates with stress granules and ALS-linked mutations alter stress granule dynamics', *J Neurosci,* 34(24), pp. 8083-97.

Fischer, L. R., Culver, D. G., Tennant, P., Davis, A. A., Wang, M., Castellano-Sanchez, A., Khan, J., Polak, M. A. and Glass, J. D. (2004) 'Amyotrophic lateral sclerosis is a distal axonopathy: evidence in mice and man', *Exp Neurol,* 185(2), pp. 232-40.

Fournier, M. J., Gareau, C. and Mazroui, R. (2010) 'The chemotherapeutic agent bortezomib induces the formation of stress granules', *Cancer Cell Int,* 10, pp. 12.

Frey, D., Schneider, C., Xu, L., Borg, J., Spooren, W. and Caroni, P. (2000) 'Early and selective loss of neuromuscular synapse subtypes with low sprouting competence in motoneuron diseases', *J Neurosci,* 20(7), pp. 2534-42.

Fujii, R., Okabe, S., Urushido, T., Inoue, K., Yoshimura, A., Tachibana, T., Nishikawa, T., Hicks, G. G. and Takumi, T. (2005) 'The RNA binding protein TLS is translocated to dendritic spines by mGluR5 activation and regulates spine morphology', *Curr Biol,* 15(6), pp. 587-93.

Fujimura, K., Sasaki, A. T. and Anderson, P. (2012) 'Selenite targets eIF4E-binding protein-1 to inhibit translation initiation and induce the assembly of non-canonical stress granules', *Nucleic Acids Res,* 40(16), pp. 8099-110.

Gal, J., Kuang, L., Barnett, K. R., Zhu, B. Z., Shissler, S. C., Korotkov, K. V., Hayward, L. J., Kasarskis, E. J. and Zhu, H. (2016) 'ALS mutant SOD1 interacts with G3BP1 and affects stress granule dynamics', *Acta neuropathologica,* 132(4), pp. 563-576.

Ganassi, M., Mateju, D., Bigi, I., Mediani, L., Poser, I., Lee, H. O., Seguin, S. J., Morelli, F. F., Vinet, J., Leo, G., Pansarasa, O., Cereda, C., Poletti, A., Alberti, S. and Carra, S. (2016) 'A Surveillance Function of the HSPB8-BAG3-HSP70 Chaperone Complex Ensures Stress Granule Integrity and Dynamism', *Mol Cell,* 63(5), pp. 796-810.

Gao, X., Jiang, L., Gong, Y., Chen, X., Ying, M., Zhu, H., He, Q., Yang, B. and Cao, J. (2019) 'Stress granule: A promising target for cancer treatment', *Br J Pharmacol*.

Garrett, C. A., Barri, M., Kuta, A., Soura, V., Deng, W., Fisher, E. M., Schiavo, G. and Hafezparast, M. (2014) 'DYNC1H1 mutation alters transport kinetics and ERK1/2-cFos signalling in a mouse model of distal spinal muscular atrophy', *Brain,* 137(Pt 7), pp. 1883-93.

Gasset-Rosa, F., Lu, S., Yu, H., Chen, C., Melamed, Z., Guo, L., Shorter, J., Da Cruz, S. and Cleveland, D. W. (2019) 'Cytoplasmic TDP-43 De-mixing Independent of Stress Granules Drives Inhibition of Nuclear Import, Loss of Nuclear TDP-43, and Cell Death', *Neuron,* 102(2), pp. 339-357.e7.

Gerbino, V., Carri, M. T., Cozzolino, M. and Achsel, T. (2013) 'Mislocalised FUS mutants stall spliceosomal snRNPs in the cytoplasm', *Neurobiol Dis,* 55, pp. 120-8.

Gilks, N., Kedersha, N., Ayodele, M., Shen, L., Stoecklin, G., Dember, L. M. and Anderson, P. (2004) 'Stress granule assembly is mediated by prion-like aggregation of TIA-1', *Mol Biol Cell,* 15(12), pp. 5383-98.

Gitcho, M. A., Baloh, R. H., Chakraverty, S., Mayo, K., Norton, J. B., Levitch, D., Hatanpaa, K. J., White, C. L., 3rd, Bigio, E. H., Caselli, R., Baker, M., Al-Lozi, M. T., Morris, J. C., Pestronk, A., Rademakers, R., Goate, A. M. and Cairns, N. J. (2008) 'TDP-43 A315T mutation in familial motor neuron disease', *Ann Neurol,* 63(4), pp. 535-8.

Goggin, K., Beaudoin, S., Grenier, C., Brown, A. A. and Roucou, X. (2008) 'Prion protein aggresomes are poly(A)+ ribonucleoprotein complexes that induce a PKR-mediated deficient cell stress response', *Biochim Biophys Acta,* 1783(3), pp. 479-91.

Gopal, P. P., Nirschl, J. J., Klinman, E. and Holzbaur, E. L. (2017) 'Amyotrophic lateral sclerosis-linked mutations increase the viscosity of liquid-like TDP-43 RNP granules in neurons', *Proc Natl Acad Sci U S A,* 114(12), pp. E2466-e2475.

Goshima, Y., Hida, T. and Gotoh, T. (2012) 'Computational analysis of axonal transport: a novel assessment of neurotoxicity, neuronal development and functions', *International journal of molecular sciences,* 13(3), pp. 3414-3430.

Goulet, I., Boisvenue, S., Mokas, S., Mazroui, R. and Côté, J. (2008) 'TDRD3, a novel Tudor domain-containing protein, localizes to cytoplasmic stress granules', *Human molecular genetics,* 17(19), pp. 3055-3074.

Grabarek, Z. (2011) 'Insights into modulation of calcium signaling by magnesium in calmodulin, troponin C and related EF-hand proteins', *Biochimica et biophysica acta,* 1813(5), pp. 913-921.

Grabocka, E. and Bar-Sagi, D. (2016) 'Mutant KRAS Enhances Tumor Cell Fitness by Upregulating Stress Granules', *Cell,* 167(7), pp. 1803-1813.e12.

Guil, S., Long, J. C. and Cáceres, J. F. (2006) 'hnRNP A1 relocalization to the stress granules reflects a role in the stress response', *Molecular and cellular biology,* 26(15), pp. 5744-5758.

Guo, L., Kim, H. J., Wang, H., Monaghan, J., Freyermuth, F., Sung, J. C., O'Donovan, K., Fare, C. M., Diaz, Z., Singh, N., Zhang, Z. C., Coughlin, M., Sweeny, E. A., DeSantis, M. E., Jackrel, M. E., Rodell, C. B., Burdick, J. A., King, O. D., Gitler, A. D., Lagier-Tourenne, C., Pandey, U. B., Chook, Y. M., Taylor, J. P. and Shorter, J. (2018) 'Nuclear-Import Receptors Reverse Aberrant Phase Transitions of RNA-Binding Proteins with Prion-like Domains', *Cell,* 173(3), pp. 677-692.e20.

Guo, W., Naujock, M., Fumagalli, L., Vandoorne, T., Baatsen, P., Boon, R., Ordovás, L., Patel, A., Welters, M., Vanwelden, T., Geens, N., Tricot, T., Benoy, V., Steyaert, J., Lefebvre-Omar, C., Boesmans, W., Jarpe, M., Sterneckert, J., Wegner, F., Petri, S., Bohl, D., Vanden Berghe, P., Robberecht, W., Van Damme, P., Verfaillie, C. and Van Den Bosch, L. (2017) 'HDAC6 inhibition reverses axonal transport defects in motor neurons derived from FUS-ALS patients', *Nature communications,* 8(1), pp. 861-861.

Gurney, M. E., Pu, H., Chiu, A. Y., Dal Canto, M. C., Polchow, C. Y., Alexander, D. D., Caliendo, J., Hentati, A., Kwon, Y. W., Deng, H. X. and et al. (1994) 'Motor neuron degeneration in mice that express a human Cu,Zn superoxide dismutase mutation', *Science,* 264(5166), pp. 1772-5.

Guzikowski, A. R., Chen, Y. S. and Zid, B. M. (2019) 'Stress-induced mRNP granules: Form and function of processing bodies and stress granules', *Wiley Interdiscip Rev RNA,* 10(3), pp. e1524.

Hackman, P., Sarparanta, J., Lehtinen, S., Vihola, A., Evila, A., Jonson, P. H., Luque, H., Kere, J., Screen, M., Chinnery, P. F., Ahlberg, G., Edstrom, L. and Udd, B. (2013) 'Welander distal myopathy is caused by a mutation in the RNA-binding protein TIA1', *Ann Neurol,* 73(4), pp. 500-9.

Hanz, S., Perlson, E., Willis, D., Zheng, J. Q., Massarwa, R., Huerta, J. J., Koltzenburg, M., Kohler, M., van-Minnen, J., Twiss, J. L. and Fainzilber, M. (2003) 'Axoplasmic importins enable retrograde injury signaling in lesioned nerve', *Neuron,* 40(6), pp. 1095-1104.

Heads, T., Pollock, M., Robertson, A., Sutherland, W. H. and Allpress, S. (1991) 'Sensory nerve pathology in amyotrophic lateral sclerosis', *Acta Neuropathol,* 82(4), pp. 316-20.

Heinicke, L. A., Wong, C. J., Lary, J., Nallagatla, S. R., Diegelman-Parente, A., Zheng, X., Cole, J. L. and Bevilacqua, P. C. (2009) 'RNA dimerization promotes PKR dimerization and activation', *Journal of molecular biology,* 390(2), pp. 319-338.

Hennig, S., Kong, G., Mannen, T., Sadowska, A., Kobelke, S., Blythe, A., Knott, G. J., Iyer, K. S., Ho, D., Newcombe, E. A., Hosoki, K., Goshima, N., Kawaguchi, T., Hatters, D., Trinkle-Mulcahy, L., Hirose, T., Bond, C. S. and Fox, A. H. (2015) 'Prion-like domains in RNA binding proteins are essential for building subnuclear paraspeckles', *J Cell Biol,* 210(4), pp. 529-39.

Herman, A. B., Silva Afonso, M., Kelemen, S. E., Ray, M., Vrakas, C. N., Burke, A. C., Scalia, R. G., Moore, K. and Autieri, M. V. (2019) 'Regulation of Stress Granule Formation by Inflammation, Vascular Injury, and Atherosclerosis', *Arterioscler Thromb Vasc Biol,* 39(10), pp. 2014-2027.

Hicks, G. G., Singh, N., Nashabi, A., Mai, S., Bozek, G., Klewes, L., Arapovic, D., White, E. K., Koury, M. J., Oltz, E. M., Van Kaer, L. and Ruley, H. E. (2000) 'Fus deficiency in mice results in defective B-lymphocyte development and activation, high levels of chromosomal instability and perinatal death', *Nat Genet,* 24(2), pp. 175-9.

Higelin, J., Demestre, M., Putz, S., Delling, J. P., Jacob, C., Lutz, A. K., Bausinger, J., Huber, A. K., Klingenstein, M., Barbi, G., Speit, G., Huebers, A., Weishaupt, J. H., Hermann, A., Liebau, S., Ludolph, A. C. and Boeckers, T. M. (2016) 'FUS Mislocalization and Vulnerability to DNA Damage in ALS Patients Derived hiPSCs and Aging Motoneurons', *Front Cell Neurosci,* 10, pp. 290.

Hock, E. M., Maniecka, Z., Hruska-Plochan, M., Reber, S., Laferriere, F., Sahadevan, M. K. S., Ederle, H., Gittings, L., Pelkmans, L., Dupuis, L., Lashley, T., Ruepp, M. D., Dormann, D. and Polymenidou, M. (2018) 'Hypertonic Stress Causes Cytoplasmic Translocation of Neuronal, but Not Astrocytic, FUS due to Impaired Transportin Function', *Cell Rep,* 24(4), pp. 987-1000.e7.

Hofmann, S., Cherkasova, V., Bankhead, P., Bukau, B. and Stoecklin, G. (2012) 'Translation suppression promotes stress granule formation and cell survival in response to cold shock', *Mol Biol Cell,* 23(19), pp. 3786-800.

Hofweber, M., Hutten, S., Bourgeois, B., Spreitzer, E., Niedner-Boblenz, A., Schifferer, M., Ruepp, M. D., Simons, M., Niessing, D., Madl, T. and Dormann, D. (2018) 'Phase Separation of FUS Is Suppressed by Its Nuclear Import Receptor and Arginine Methylation', *Cell,* 173(3), pp. 706-719.e13.

Hoing, S., Yeh, T. Y., Baumann, M., Martinez, N. E., Habenberger, P., Kremer, L., Drexler, H. C. A., Kuchler, P., Reinhardt, P., Choidas, A., Zischinsky, M. L., Zischinsky, G., Nandini, S., Ledray, A. P., Ketcham, S. A., Reinhardt, L., Abo-Rady, M., Glatza, M., King, S. J., Nussbaumer, P., Ziegler, S., Klebl, B., Schroer, T. A., Scholer, H. R., Waldmann, H. and Sterneckert, J. (2018) 'Dynarrestin, a Novel Inhibitor of Cytoplasmic Dynein', *Cell Chem Biol,* 25(4), pp. 357-369.e6.

Hopkins, K. C., Tartell, M. A., Herrmann, C., Hackett, B. A., Taschuk, F., Panda, D., Menghani, S. V., Sabin, L. R. and Cherry, S. (2015) 'Virus-induced translational arrest through 4EBP1/2-dependent decay of 5'-TOP mRNAs restricts viral infection', *Proceedings of the National Academy of Sciences of the United States of America,* 112(22), pp. E2920-E2929.

Hou, S., Kumar, A., Xu, Z., Airo, A. M., Stryapunina, I., Wong, C. P., Branton, W., Tchesnokov, E., Götte, M., Power, C. and Hobman, T. C. (2017) 'Zika Virus Hijacks Stress Granule Proteins and Modulates the Host Stress Response', *Journal of virology,* 91(16), pp. e00474-17.

Huang, E. J., Zhang, J., Geser, F., Trojanowski, J. Q., Strober, J. B., Dickson, D. W., Brown, R. H., Jr., Shapiro, B. E. and Lomen-Hoerth, C. (2010) 'Extensive FUS-immunoreactive pathology in juvenile amyotrophic lateral sclerosis with basophilic inclusions', *Brain Pathol,* 20(6), pp. 1069-76.

Hui, C. W., Zhang, Y. and Herrup, K. (2016) 'Non-Neuronal Cells Are Required to Mediate the Effects of Neuroinflammation: Results from a Neuron-Enriched Culture System', *PLoS One,* 11(1), pp. e0147134.

Hwang, B., Lee, J. H. and Bang, D. (2018) 'Single-cell RNA sequencing technologies and bioinformatics pipelines', *Exp Mol Med,* 50(8), pp. 96.

Imbert, G., Saudou, F., Yvert, G., Devys, D., Trottier, Y., Garnier, J. M., Weber, C., Mandel, J. L., Cancel, G., Abbas, N., Durr, A., Didierjean, O., Stevanin, G., Agid, Y. and Brice, A. (1996) 'Cloning of the gene for spinocerebellar ataxia 2 reveals a locus with high sensitivity to expanded CAG/glutamine repeats', *Nat Genet,* 14(3), pp. 285-91.

Ito, D., Hatano, M. and Suzuki, N. (2017) 'RNA binding proteins and the pathological cascade in ALS/FTD neurodegeneration', *Sci Transl Med,* 9(415).

Ivanov, P., Emara, M. M., Villen, J., Gygi, S. P. and Anderson, P. (2011) 'Angiogenin-induced tRNA fragments inhibit translation initiation', *Mol Cell,* 43(4), pp. 613-23.

Ivanov, P., O'Day, E., Emara, M. M., Wagner, G., Lieberman, J. and Anderson, P. (2014) 'G-quadruplex structures contribute to the neuroprotective effects of angiogenin-induced tRNA fragments', *Proceedings of the National Academy of Sciences of the United States of America,* 111(51), pp. 18201-18206.

Jackson, T. R., Patterson, S. I., Thastrup, O. and Hanley, M. R. (1988) 'A novel tumour promoter, thapsigargin, transiently increases cytoplasmic free Ca2+ without generation of inositol phosphates in NG115-401L neuronal cells', *The Biochemical journal,* 253(1), pp. 81-86.

Jain, S., Wheeler, J. R., Walters, R. W., Agrawal, A., Barsic, A. and Parker, R. (2016) 'ATPase-Modulated Stress Granules Contain a Diverse Proteome and Substructure', *Cell,* 164(3), pp. 487-98.

Ji, S.-J. and Jaffrey, S. R. (2014) 'Axonal transcription factors: novel regulators of growth cone-to-nucleus signaling', *Developmental neurobiology,* 74(3), pp. 245-258.

Johnson, B. S., McCaffery, J. M., Lindquist, S. and Gitler, A. D. (2008) 'A yeast TDP-43 proteinopathy model: Exploring the molecular determinants of TDP-43 aggregation and cellular toxicity', *Proceedings of the National Academy of Sciences of the United States of America,* 105(17), pp. 6439-6444.

Johnson, J. O., Pioro, E. P., Boehringer, A., Chia, R., Feit, H., Renton, A. E., Pliner, H. A., Abramzon, Y., Marangi, G., Winborn, B. J., Gibbs, J. R., Nalls, M. A., Morgan, S., Shoai, M., Hardy, J., Pittman, A., Orrell, R. W., Malaspina, A., Sidle, K. C., Fratta, P., Harms, M. B., Baloh, R. H., Pestronk, A., Weihl, C. C., Rogaeva,

E., Zinman, L., Drory, V. E., Borghero, G., Mora, G., Calvo, A., Rothstein, J. D., Drepper, C., Sendtner, M., Singleton, A. B., Taylor, J. P., Cookson, M. R., Restagno, G., Sabatelli, M., Bowser, R., Chio, A. and Traynor, B. J. (2014) 'Mutations in the Matrin 3 gene cause familial amyotrophic lateral sclerosis', *Nat Neurosci,* 17(5), pp. 664-6.

Johnson, M. E., Grassetti, A. V., Taroni, J. N., Lyons, S. M., Schweppe, D., Gordon, J. K., Spiera, R. F., Lafyatis, R., Anderson, P. J., Gerber, S. A. and Whitfield, M. L. (2016) 'Stress granules and RNA processing bodies are novel autoantibody targets in systemic sclerosis', *Arthritis Res Ther,* 18, pp. 27.

Ju, S., Tardiff, D. F., Han, H., Divya, K., Zhong, Q., Maquat, L. E., Bosco, D. A., Hayward, L. J., Brown, R. H., Jr., Lindquist, S., Ringe, D. and Petsko, G. A. (2011) 'A yeast model of FUS/TLS-dependent cytotoxicity', *PLoS Biol,* 9(4), pp. e1001052.

Jun, B. K., Chandra, A., Kuljis, D., Schmidt, B. P. and Eichler, F. S. (2015) 'Substrate Availability of Mutant SPT Alters Neuronal Branching and Growth Cone Dynamics in Dorsal Root Ganglia', *The Journal of neuroscience : the official journal of the Society for Neuroscience,* 35(40), pp. 13713-13719.

Kaehler, C., Isensee, J., Hucho, T., Lehrach, H. and Krobitsch, S. (2014) '5-Fluorouracil affects assembly of stress granules based on RNA incorporation', *Nucleic Acids Res,* 42(10), pp. 6436-47.

Kamelgarn, M., Chen, J., Kuang, L., Jin, H., Kasarskis, E. J. and Zhu, H. (2018) 'ALS mutations of FUS suppress protein translation and disrupt the regulation of nonsense-mediated decay', *Proc Natl Acad Sci U S A,* 115(51), pp. E11904-e11913.

Kanai, Y., Dohmae, N. and Hirokawa, N. (2004) 'Kinesin transports RNA: Isolation and characterization of an RNA-transporting granule', *Neuron,* 43(4), pp. 513-525.

Kapeli, K., Pratt, G. A., Vu, A. Q., Hutt, K. R., Martinez, F. J., Sundararaman, B., Batra, R., Freese, P., Lambert, N. J., Huelga, S. C., Chun, S. J., Liang, T. Y., Chang, J., Donohue, J. P., Shiue, L., Zhang, J., Zhu, H., Cambi, F., Kasarskis, E., Hoon, S., Ares, M., Jr., Burge, C. B., Ravits, J., Rigo, F. and Yeo, G. W.

(2016) 'Distinct and shared functions of ALS-associated proteins TDP-43, FUS and TAF15 revealed by multisystem analyses', *Nat Commun,* 7, pp. 12143.

Kedersha, N., Chen, S., Gilks, N., Li, W., Miller, I. J., Stahl, J. and Anderson, P. (2002) 'Evidence that ternary complex (eIF2-GTP-tRNA(i)(Met))-deficient preinitiation complexes are core constituents of mammalian stress granules', *Mol Biol Cell,* 13(1), pp. 195-210.

Kedersha, N., Cho, M. R., Li, W., Yacono, P. W., Chen, S., Gilks, N., Golan, D. E. and Anderson, P. (2000) 'Dynamic shuttling of TIA-1 accompanies the recruitment of mRNA to mammalian stress granules', *The Journal of cell biology,* 151(6), pp. 1257-1268.

Kedersha, N., Panas, M. D., Achorn, C. A., Lyons, S., Tisdale, S., Hickman, T., Thomas, M., Lieberman, J., McInerney, G. M., Ivanov, P. and Anderson, P. (2016) 'G3BP-Caprin1-USP10 complexes mediate stress granule condensation and associate with 40S subunits', *The Journal of cell biology,* 212(7), pp. 845-860.

Kedersha, N., Tisdale, S., Hickman, T. and Anderson, P. (2008) 'Real-time and quantitative imaging of mammalian stress granules and processing bodies', *Methods Enzymol,* 448, pp. 521-52.

Kedersha, N. L., Gupta, M., Li, W., Miller, I. and Anderson, P. (1999) 'RNA-binding proteins TIA-1 and TIAR link the phosphorylation of eIF-2 alpha to the assembly of mammalian stress granules', *J Cell Biol,* 147(7), pp. 1431-42.

Kennel, P. F., Finiels, F., Revah, F. and Mallet, J. (1996) 'Neuromuscular function impairment is not caused by motor neurone loss in FALS mice: an electromyographic study', *Neuroreport,* 7(8), pp. 1427-31.

Khalfallah, Y., Kuta, R., Grasmuck, C., Prat, A., Durham, H. D. and Vande Velde, C. (2018) 'TDP-43 regulation of stress granule dynamics in neurodegenerative disease-relevant cell types', *Sci Rep,* 8(1), pp. 7551.

Khong, A., Matheny, T., Jain, S., Mitchell, S. F., Wheeler, J. R. and Parker, R. (2017) 'The Stress Granule Transcriptome Reveals Principles of mRNA Accumulation in Stress Granules', *Mol Cell,* 68(4), pp. 808-820.e5.

Kim, H.-J., Raphael, A. R., LaDow, E. S., McGurk, L., Weber, R. A., Trojanowski, J. Q., Lee, V. M. Y., Finkbeiner, S., Gitler, A. D. and Bonini, N. M. (2014) 'Therapeutic modulation of eIF2α phosphorylation rescues TDP-43 toxicity in amyotrophic lateral sclerosis disease models', *Nature genetics,* 46(2), pp. 152-160.

Kim, H. J., Kim, N. C., Wang, Y. D., Scarborough, E. A., Moore, J., Diaz, Z., MacLea, K. S., Freibaum, B., Li, S., Molliex, A., Kanagaraj, A. P., Carter, R., Boylan, K. B., Wojtas, A. M., Rademakers, R., Pinkus, J. L., Greenberg, S. A., Trojanowski, J. Q., Traynor, B. J., Smith, B. N., Topp, S., Gkazi, A. S., Miller, J., Shaw, C. E., Kottlors, M., Kirschner, J., Pestronk, A., Li, Y. R., Ford, A. F., Gitler, A. D., Benatar, M., King, O. D., Kimonis, V. E., Ross, E. D., Weihl, C. C., Shorter, J. and Taylor, J. P. (2013) 'Mutations in prion-like domains in hnRNPA2B1 and hnRNPA1 cause multisystem proteinopathy and ALS', *Nature,* 495(7442), pp. 467-73.

Kim, W. J., Back, S. H., Kim, V., Ryu, I. and Jang, S. K. (2005) 'Sequestration of TRAF2 into stress granules interrupts tumor necrosis factor signaling under stress conditions', *Molecular and cellular biology,* 25(6), pp. 2450-2462.

Kimball, S. R., Horetsky, R. L., Ron, D., Jefferson, L. S. and Harding, H. P. (2003) 'Mammalian stress granules represent sites of accumulation of stalled translation initiation complexes', *Am J Physiol Cell Physiol,* 284(2), pp. C273-84.

Kitagawa, Y., Suzuki, K., Yoneda, A. and Watanabe, T. (2004) 'Effects of oxygen concentration and antioxidants on the in vitro developmental ability, production of reactive oxygen species (ROS), and DNA fragmentation in porcine embryos', *Theriogenology,* 62(7), pp. 1186-97.

Koppers, M., van Blitterswijk, M. M., Vlam, L., Rowicka, P. A., van Vught, P. W., Groen, E. J., Spliet, W. G., Engelen-Lee, J., Schelhaas, H. J., de Visser, M., van der Kooi, A. J., van der Pol, W. L., Pasterkamp, R. J., Veldink, J. H. and van den Berg, L. H. (2012) 'VCP mutations in familial and sporadic amyotrophic lateral sclerosis', *Neurobiol Aging,* 33(4), pp. 837.e7-13.

Kramer, S., Queiroz, R., Ellis, L., Webb, H., Hoheisel, J. D., Clayton, C. and Carrington, M. (2008) 'Heat shock causes a decrease in polysomes and the appearance of stress granules in trypanosomes independently of eIF2(alpha) phosphorylation at Thr169', *J Cell Sci,* 121(Pt 18), pp. 3002-14.

Kwiatkowski, T. J., Jr., Bosco, D. A., Leclerc, A. L., Tamrazian, E., Vanderburg, C. R., Russ, C., Davis, A., Gilchrist, J., Kasarskis, E. J., Munsat, T., Valdmanis, P., Rouleau, G. A., Hosler, B. A., Cortelli, P., de Jong, P. J., Yoshinaga, Y., Haines, J. L., Pericak-Vance, M. A., Yan, J., Ticozzi, N., Siddique, T., McKenna-Yasek, D., Sapp, P. C., Horvitz, H. R., Landers, J. E. and Brown, R. H., Jr. (2009) 'Mutations in the FUS/TLS gene on chromosome 16 cause familial amyotrophic lateral sclerosis', *Science,* 323(5918), pp. 1205-8.

Kwon, S., Zhang, Y. and Matthias, P. (2007) 'The deacetylase HDAC6 is a novel critical component of stress granules involved in the stress response', *Genes Dev,* 21(24), pp. 3381-94.

Lanciego, J. L. and Wouterlood, F. G. (2011) 'A half century of experimental neuroanatomical tracing', *J Chem Neuroanat,* 42(3), pp. 157-83.

Lassek, M., Weingarten, J. and Volknandt, W. (2015) 'The synaptic proteome', *Cell Tissue Res,* 359(1), pp. 255-65.

Le Sage, V., Cinti, A., McCarthy, S., Amorim, R., Rao, S., Daino, G. L., Tramontano, E., Branch, D. R. and Mouland, A. J. (2017) 'Ebola virus VP35 blocks stress granule assembly', *Virology,* 502, pp. 73-83.

Lee, K. H., Zhang, P., Kim, H. J., Mitrea, D. M., Sarkar, M., Freibaum, B. D., Cika, J., Coughlin, M., Messing, J., Molliex, A., Maxwell, B. A., Kim, N. C., Temirov, J., Moore, J., Kolaitis, R. M., Shaw, T. I., Bai, B., Peng, J., Kriwacki, R. W. and Taylor, J. P. (2016) 'C9orf72 Dipeptide Repeats Impair the Assembly, Dynamics, and Function of Membrane-Less Organelles', *Cell,* 167(3), pp. 774-788.e17.

Lenzi, J., De Santis, R., de Turris, V., Morlando, M., Laneve, P., Calvo, A., Caliendo, V., Chio, A., Rosa, A. and Bozzoni, I. (2015) 'ALS mutant FUS proteins are recruited into stress granules in induced pluripotent stem cell-derived motoneurons', *Dis Model Mech,* 8(7), pp. 755-66.

Li, W. and Chou, I. N. (1992) 'Effects of sodium arsenite on the cytoskeleton and cellular glutathione levels in cultured cells', *Toxicol Appl Pharmacol,* 114(1), pp. 132-9.

Lin, J., Okada, K., Raytchev, M., Smith, M. C. and Nicastro, D. (2014) 'Structural mechanism of the dynein power stroke', *Nature cell biology,* 16(5), pp. 479-485.

Lin, Y., Protter, D. S., Rosen, M. K. and Parker, R. (2015) 'Formation and Maturation of Phase-Separated Liquid Droplets by RNA-Binding Proteins', *Mol Cell,* 60(2), pp. 208-19.

Ling, S.-C., Dastidar, S. G., Tokunaga, S., Ho, W. Y., Lim, K., Ilieva, H., Parone, P. A., Tyan, S.-H., Tse, T. M., Chang, J.-C., Platoshyn, O., Bui, N. B., Bui, A., Vetto, A., Sun, S., McAlonis-Downes, M., Han, J. S., Swing, D., Kapeli, K., Yeo, G. W., Tessarollo, L., Marsala, M., Shaw, C. E., Tucker-Kellogg, G., La Spada, A. R., Lagier-Tourenne, C., Da Cruz, S. and Cleveland, D. W. (2019) 'Overriding FUS autoregulation in mice triggers gain-of-toxic dysfunctions in RNA metabolism and autophagy-lysosome axis', *eLife,* 8, pp. e40811.

Ling, S. C., Polymenidou, M. and Cleveland, D. W. (2013) 'Converging mechanisms in ALS and FTD: disrupted RNA and protein homeostasis', *Neuron,* 79(3), pp. 416-38.

Liu-Yesucevitz, L., Bilgutay, A., Zhang, Y. J., Vanderweyde, T., Citro, A., Mehta, T., Zaarur, N., McKee, A., Bowser, R., Sherman, M., Petrucelli, L. and Wolozin, B. (2010) 'Tar DNA binding protein-43 (TDP-43) associates with stress granules: analysis of cultured cells and pathological brain tissue', *PLoS One,* 5(10), pp. e13250.

Lo Bello, M., Di Fini, F., Notaro, A., Spataro, R., Conforti, F. L. and La Bella, V. (2017) 'ALS-Related Mutant FUS Protein Is Mislocalized to Cytoplasm and Is Recruited into Stress Granules of Fibroblasts from Asymptomatic FUS P525L Mutation Carriers', *Neurodegener Dis,* 17(6), pp. 292-303.

Lopez-Erauskin, J., Tadokoro, T., Baughn, M. W., Myers, B., McAlonis-Downes, M., Chillon-Marinas, C., Asiaban, J. N., Artates, J., Bui, A. T., Vetto, A. P., Lee, S. K., Le, A. V., Sun, Y., Jambeau, M., Boubaker, J., Swing, D., Qiu, J., Hicks, G. G., Ouyang, Z., Fu, X. D., Tessarollo, L., Ling, S. C., Parone, P. A., Shaw, C. E., Marsala, M., Lagier-Tourenne, C., Cleveland, D. W. and Da Cruz, S. (2018) 'ALS/FTD-Linked Mutation in FUS Suppresses Intra-axonal Protein Synthesis and Drives Disease Without Nuclear Loss-of-Function of FUS', *Neuron,* 100(4), pp. 816-830.e7.

Luo, Y., Blechingberg, J., Fernandes, A. M., Li, S., Fryland, T., Borglum, A. D., Bolund, L. and Nielsen, A. L. (2015) 'EWS and FUS bind a subset of transcribed

genes encoding proteins enriched in RNA regulatory functions', *BMC Genomics,* 16, pp. 929.

Mackenzie, I. R., Bigio, E. H., Ince, P. G., Geser, F., Neumann, M., Cairns, N. J., Kwong, L. K., Forman, M. S., Ravits, J., Stewart, H., Eisen, A., McClusky, L., Kretzschmar, H. A., Monoranu, C. M., Highley, J. R., Kirby, J., Siddique, T., Shaw, P. J., Lee, V. M. and Trojanowski, J. Q. (2007) 'Pathological TDP-43 distinguishes sporadic amyotrophic lateral sclerosis from amyotrophic lateral sclerosis with SOD1 mutations', *Ann Neurol,* 61(5), pp. 427-34.

Mackenzie, I. R. and Neumann, M. (2016) 'Molecular neuropathology of frontotemporal dementia: insights into disease mechanisms from postmortem studies', *J Neurochem,* 138 Suppl 1, pp. 54-70.

Mackenzie, I. R., Nicholson, A. M., Sarkar, M., Messing, J., Purice, M. D., Pottier, C., Annu, K., Baker, M., Perkerson, R. B., Kurti, A., Matchett, B. J., Mittag, T., Temirov, J., Hsiung, G. R., Krieger, C., Murray, M. E., Kato, M., Fryer, J. D., Petrucelli, L., Zinman, L., Weintraub, S., Mesulam, M., Keith, J., Zivkovic, S. A., Hirsch-Reinshagen, V., Roos, R. P., Zuchner, S., Graff-Radford, N. R., Petersen, R. C., Caselli, R. J., Wszolek, Z. K., Finger, E., Lippa, C., Lacomis, D., Stewart, H., Dickson, D. W., Kim, H. J., Rogaeva, E., Bigio, E., Boylan, K. B., Taylor, J. P. and Rademakers, R. (2017) 'TIA1 Mutations in Amyotrophic Lateral Sclerosis and Frontotemporal Dementia Promote Phase Separation and Alter Stress Granule Dynamics', *Neuron,* 95(4), pp. 808-816.e9.

Mahar, M. and Cavalli, V. (2018) 'Intrinsic mechanisms of neuronal axon regeneration', *Nature reviews. Neuroscience,* 19(6), pp. 323-337.

Maharana, S., Wang, J., Papadopoulos, D. K., Richter, D., Pozniakovsky, A., Poser, I., Bickle, M., Rizk, S., Guillen-Boixet, J., Franzmann, T. M., Jahnel, M., Marrone, L., Chang, Y. T., Sterneckert, J., Tomancak, P., Hyman, A. A. and Alberti, S. (2018) 'RNA buffers the phase separation behavior of prion-like RNA binding proteins', *Science,* 360(6391), pp. 918-921.

Maharjan, N., Kunzli, C., Buthey, K. and Saxena, S. (2017) 'C9ORF72 Regulates Stress Granule Formation and Its Deficiency Impairs Stress Granule Assembly, Hypersensitizing Cells to Stress', *Mol Neurobiol,* 54(4), pp. 3062-3077.

Majounie, E., Renton, A. E., Mok, K., Dopper, E. G., Waite, A., Rollinson, S., Chio, A., Restagno, G., Nicolaou, N., Simon-Sanchez, J., van Swieten, J. C., Abramzon, Y., Johnson, J. O., Sendtner, M., Pamphlett, R., Orrell, R. W., Mead, S., Sidle, K. C., Houlden, H., Rohrer, J. D., Morrison, K. E., Pall, H., Talbot, K., Ansorge, O., Hernandez, D. G., Arepalli, S., Sabatelli, M., Mora, G., Corbo, M., Giannini, F., Calvo, A., Englund, E., Borghero, G., Floris, G. L., Remes, A. M., Laaksovirta, H., McCluskey, L., Trojanowski, J. Q., Van Deerlin, V. M., Schellenberg, G. D., Nalls, M. A., Drory, V. E., Lu, C. S., Yeh, T. H., Ishiura, H., Takahashi, Y., Tsuji, S., Le Ber, I., Brice, A., Drepper, C., Williams, N., Kirby, J., Shaw, P., Hardy, J., Tienari, P. J., Heutink, P., Morris, H. R., Pickering-Brown, S. and Traynor, B. J. (2012) 'Frequency of the C9orf72 hexanucleotide repeat expansion in patients with amyotrophic lateral sclerosis and frontotemporal dementia: a cross-sectional study', *Lancet Neurol,* 11(4), pp. 323-30.

Mann, J. R., Gleixner, A. M., Mauna, J. C., Gomes, E., DeChellis-Marks, M. R., Needham, P. G., Copley, K. E., Hurtle, B., Portz, B., Pyles, N. J., Guo, L., Calder, C. B., Wills, Z. P., Pandey, U. B., Kofler, J. K., Brodsky, J. L., Thathiah, A., Shorter, J. and Donnelly, C. J. (2019) 'RNA Binding Antagonizes Neurotoxic Phase Transitions of TDP-43', *Neuron,* 102(2), pp. 321-338.e8.

Markmiller, S., Soltanieh, S., Server, K. L., Mak, R., Jin, W., Fang, M. Y., Luo, E. C., Krach, F., Yang, D., Sen, A., Fulzele, A., Wozniak, J. M., Gonzalez, D. J., Kankel, M. W., Gao, F. B., Bennett, E. J., Lecuyer, E. and Yeo, G. W. (2018) 'Context-Dependent and Disease-Specific Diversity in Protein Interactions within Stress Granules', *Cell,* 172(3), pp. 590-604.e13.

Martin, D. P., Wallace, T. L. and Johnson, E. M., Jr. (1990) 'Cytosine arabinoside kills postmitotic neurons in a fashion resembling trophic factor deprivation: evidence that a deoxycytidine-dependent process may be required for nerve growth factor signal transduction', *J Neurosci,* 10(1), pp. 184-93.

Martinez, F. J., Pratt, G. A., Van Nostrand, E. L., Batra, R., Huelga, S. C., Kapeli, K., Freese, P., Chun, S. J., Ling, K., Gelboin-Burkhart, C., Fijany, L., Wang, H. C., Nussbacher, J. K., Broski, S. M., Kim, H. J., Lardelli, R., Sundararaman, B., Donohue, J. P., Javaherian, A., Lykke-Andersen, J., Finkbeiner, S., Bennett, C. F., Ares, M., Jr., Burge, C. B., Taylor, J. P., Rigo, F. and Yeo, G. W. (2016) 'Protein-RNA Networks Regulated by Normal and ALS-Associated Mutant HNRNPA2B1 in the Nervous System', *Neuron,* 92(4), pp. 780-795.

Martinez, G., Duran-Aniotz, C., Cabral-Miranda, F., Vivar, J. P. and Hetz, C. (2017) 'Endoplasmic reticulum proteostasis impairment in aging', *Aging Cell,* 16(4), pp. 615-623.

Mateju, D., Franzmann, T. M., Patel, A., Kopach, A., Boczek, E. E., Maharana, S., Lee, H. O., Carra, S., Hyman, A. A. and Alberti, S. (2017) 'An aberrant phase transition of stress granules triggered by misfolded protein and prevented by chaperone function', *Embo j,* 36(12), pp. 1669-1687.

Mazroui, R., Di Marco, S., Kaufman, R. J. and Gallouzi, I.-E. (2007) 'Inhibition of the ubiquitin-proteasome system induces stress granule formation', *Molecular biology of the cell,* 18(7), pp. 2603-2618.

McDonald, K. K., Aulas, A., Destroismaisons, L., Pickles, S., Beleac, E., Camu, W., Rouleau, G. A. and Vande Velde, C. (2011) 'TAR DNA-binding protein 43 (TDP-43) regulates stress granule dynamics via differential regulation of G3BP and TIA-1', *Hum Mol Genet,* 20(7), pp. 1400-10.

McEwen, E., Kedersha, N., Song, B., Scheuner, D., Gilks, N., Han, A., Chen, J. J., Anderson, P. and Kaufman, R. J. (2005) 'Heme-regulated inhibitor kinase-mediated phosphorylation of eukaryotic translation initiation factor 2 inhibits translation, induces stress granule formation, and mediates survival upon arsenite exposure', *J Biol Chem,* 280(17), pp. 16925-33.

McGurk, L., Gomes, E., Guo, L., Mojsilovic-Petrovic, J., Tran, V., Kalb, R. G., Shorter, J. and Bonini, N. M. (2018) 'Poly(ADP-Ribose) Prevents Pathological Phase Separation of TDP-43 by Promoting Liquid Demixing and Stress Granule Localization', *Mol Cell,* 71(5), pp. 703-717.e9.

McGurk, L., Lee, V. M., Trojanowksi, J. Q., Van Deerlin, V. M., Lee, E. B. and Bonini, N. M. (2014) 'Poly-A binding protein-1 localization to a subset of TDP-43 inclusions in amyotrophic lateral sclerosis occurs more frequently in patients harboring an expansion in C9orf72', *J Neuropathol Exp Neurol,* 73(9), pp. 837-45.

Mensch, A., Meinhardt, B., Bley, N., Huttelmaier, S., Schneider, I., Stoltenburg-Didinger, G., Kraya, T., Muller, T. and Zierz, S. (2018) 'The p.S85C-mutation in MATR3 impairs stress granule formation in Matrin-3 myopathy', *Exp Neurol,* 306, pp. 222-231.

Meyer, H. and Weihl, C. C. (2014) 'The VCP/p97 system at a glance: connecting cellular function to disease pathogenesis', *Journal of cell science,* 127(Pt 18), pp. 3877-3883.

Meyerowitz, J., Parker, S. J., Vella, L. J., Ng, D., Price, K. A., Liddell, J. R., Caragounis, A., Li, Q. X., Masters, C. L., Nonaka, T., Hasegawa, M., Bogoyevitch, M. A., Kanninen, K. M., Crouch, P. J. and White, A. R. (2011) 'C-Jun N-terminal kinase controls TDP-43 accumulation in stress granules induced by oxidative stress', *Mol Neurodegener,* 6, pp. 57.

Mitchell, J. C., McGoldrick, P., Vance, C., Hortobagyi, T., Sreedharan, J., Rogelj, B., Tudor, E. L., Smith, B. N., Klasen, C., Miller, C. C. J., Cooper, J. D., Greensmith, L. and Shaw, C. E. (2013) 'Overexpression of human wild-type FUS causes progressive motor neuron degeneration in an age- and dose-dependent fashion', *Acta neuropathologica,* 125(2), pp. 273-288.

Moisse, K., Volkening, K., Leystra-Lantz, C., Welch, I., Hill, T. and Strong, M. J. (2009) 'Divergent patterns of cytosolic TDP-43 and neuronal progranulin expression following axotomy: implications for TDP-43 in the physiological response to neuronal injury', *Brain Res,* 1249, pp. 202-11.

Molliex, A., Temirov, J., Lee, J., Coughlin, M., Kanagaraj, A. P., Kim, H. J., Mittag, T. and Taylor, J. P. (2015) 'Phase separation by low complexity domains promotes stress granule assembly and drives pathological fibrillization', *Cell,* 163(1), pp. 123-33.

Morlando, M., Dini Modigliani, S., Torrelli, G., Rosa, A., Di Carlo, V., Caffarelli, E. and Bozzoni, I. (2012) 'FUS stimulates microRNA biogenesis by facilitating co-transcriptional Drosha recruitment', *Embo j,* 31(24), pp. 4502-10.

Moujalled, D., James, J. L., Parker, S. J., Lidgerwood, G. E., Duncan, C., Meyerowitz, J., Nonaka, T., Hasegawa, M., Kanninen, K. M., Grubman, A., Liddell, J. R., Crouch, P. J. and White, A. R. (2013) 'Kinase Inhibitor Screening Identifies Cyclin-Dependent Kinases and Glycogen Synthase Kinase 3 as Potential Modulators of TDP-43 Cytosolic Accumulation during Cell Stress', *PLoS One,* 8(6), pp. e67433.

Muller-McNicoll, M., Rossbach, O., Hui, J. and Medenbach, J. (2019) 'Auto-regulatory feedback by RNA-binding proteins', *J Mol Cell Biol,* 11(10), pp. 930-939.

Murakami, T., Qamar, S., Lin, J. Q., Schierle, G. S., Rees, E., Miyashita, A., Costa, A. R., Dodd, R. B., Chan, F. T., Michel, C. H., Kronenberg-Versteeg, D., Li, Y., Yang, S. P., Wakutani, Y., Meadows, W., Ferry, R. R., Dong, L., Tartaglia, G. G., Favrin, G., Lin, W. L., Dickson, D. W., Zhen, M., Ron, D., Schmitt-Ulms, G., Fraser, P. E., Shneider, N. A., Holt, C., Vendruscolo, M., Kaminski, C. F. and St George-Hyslop, P. (2015) 'ALS/FTD Mutation-Induced Phase Transition of FUS Liquid Droplets and Reversible Hydrogels into Irreversible Hydrogels Impairs RNP Granule Function', *Neuron,* 88(4), pp. 678-90.

Muraro, M. J., Dharmadhikari, G., Grun, D., Groen, N., Dielen, T., Jansen, E., van Gurp, L., Engelse, M. A., Carlotti, F., de Koning, E. J. and van Oudenaarden, A. (2016) 'A Single-Cell Transcriptome Atlas of the Human Pancreas', *Cell Syst,* 3(4), pp. 385-394.e3.

Murphy, J., Henry, R. and Lomen-Hoerth, C. (2007) 'Establishing subtypes of the continuum of frontal lobe impairment in amyotrophic lateral sclerosis', *Arch Neurol,* 64(3), pp. 330-4.

Naganuma, T., Nakagawa, S., Tanigawa, A., Sasaki, Y. F., Goshima, N. and Hirose, T. (2012) 'Alternative 3'-end processing of long noncoding RNA initiates construction of nuclear paraspeckles', *The EMBO journal,* 31(20), pp. 4020-4034.

Nakaya, T. and Maragkakis, M. (2018) 'Amyotrophic Lateral Sclerosis associated FUS mutation shortens mitochondria and induces neurotoxicity', *Sci Rep,* 8(1), pp. 15575.

Naruse, H., Ishiura, H., Mitsui, J., Date, H., Takahashi, Y., Matsukawa, T., Tanaka, M., Ishii, A., Tamaoka, A., Hokkoku, K., Sonoo, M., Segawa, M., Ugawa, Y., Doi, K., Yoshimura, J., Morishita, S., Goto, J. and Tsuji, S. (2018) 'Molecular epidemiological study of familial amyotrophic lateral sclerosis in Japanese population by whole-exome sequencing and identification of novel HNRNPA1 mutation', *Neurobiol Aging,* 61, pp. 255.e9-255.e16.

Nascimento, A. I., Mar, F. M. and Sousa, M. M. (2018) 'The intriguing nature of dorsal root ganglion neurons: Linking structure with polarity and function', *Prog Neurobiol,* 168, pp. 86-103.

Neumann, M., Bentmann, E., Dormann, D., Jawaid, A., DeJesus-Hernandez, M., Ansorge, O., Roeber, S., Kretzschmar, H. A., Munoz, D. G., Kusaka, H., Yokota, O., Ang, L. C., Bilbao, J., Rademakers, R., Haass, C. and Mackenzie, I. R. (2011) 'FET proteins TAF15 and EWS are selective markers that distinguish FTLD with FUS pathology from amyotrophic lateral sclerosis with FUS mutations', *Brain,* 134(Pt 9), pp. 2595-609.

Neumann, M., Sampathu, D. M., Kwong, L. K., Truax, A. C., Micsenyi, M. C., Chou, T. T., Bruce, J., Schuck, T., Grossman, M., Clark, C. M., McCluskey, L. F., Miller, B. L., Masliah, E., Mackenzie, I. R., Feldman, H., Feiden, W., Kretzschmar, H. A., Trojanowski, J. Q. and Lee, V. M. (2006) 'Ubiquitinated TDP-43 in frontotemporal lobar degeneration and amyotrophic lateral sclerosis', *Science,* 314(5796), pp. 130-3.

Ng, C. S., Jogi, M., Yoo, J. S., Onomoto, K., Koike, S., Iwasaki, T., Yoneyama, M., Kato, H. and Fujita, T. (2013) 'Encephalomyocarditis virus disrupts stress granules, the critical platform for triggering antiviral innate immune responses', *J Virol,* 87(17), pp. 9511-22.

Nguyen, H. P., Van Broeckhoven, C. and van der Zee, J. (2018) 'ALS Genes in the Genomic Era and their Implications for FTD', *Trends in Genetics*.

Niesen, C., Charlton, M. P. and Carlen, P. L. (1991) 'Postsynaptic and presynaptic effects of the calcium chelator BAPTA on synaptic transmission in rat hippocampal dentate granule neurons', *Brain Res,* 555(2), pp. 319-25.

Nihei, Y., Ito, D. and Suzuki, N. (2012) 'Roles of ataxin-2 in pathological cascades mediated by TAR DNA-binding protein 43 (TDP-43) and Fused in Sarcoma (FUS)', *The Journal of biological chemistry,* 287(49), pp. 41310-41323.

Nijssen, J., Aguila, J., Hoogstraaten, R., Kee, N. and Hedlund, E. (2018) 'Axon-Seq Decodes the Motor Axon Transcriptome and Its Modulation in Response to ALS', *Stem Cell Reports,* 11(6), pp. 1565-1578.

Nishimoto, Y., Nakagawa, S., Hirose, T., Okano, H. J., Takao, M., Shibata, S., Suyama, S., Kuwako, K., Imai, T., Murayama, S., Suzuki, N. and Okano, H.

(2013) 'The long non-coding RNA nuclear-enriched abundant transcript 1_2 induces paraspeckle formation in the motor neuron during the early phase of amyotrophic lateral sclerosis', *Mol Brain,* 6, pp. 31.

Nonhoff, U., Ralser, M., Welzel, F., Piccini, I., Balzereit, D., Yaspo, M. L., Lehrach, H. and Krobitsch, S. (2007) 'Ataxin-2 interacts with the DEAD/H-box RNA helicase DDX6 and interferes with P-bodies and stress granules', *Mol Biol Cell,* 18(4), pp. 1385-96.

Ohn, T., Kedersha, N., Hickman, T., Tisdale, S. and Anderson, P. (2008) 'A functional RNAi screen links O-GlcNAc modification of ribosomal proteins to stress granule and processing body assembly', *Nature cell biology,* 10(10), pp. 1224-1231.

Ohshima, D., Arimoto-Matsuzaki, K., Tomida, T., Takekawa, M. and Ichikawa, K. (2015) 'Spatio-temporal Dynamics and Mechanisms of Stress Granule Assembly', *PLoS Comput Biol,* 11(6), pp. e1004326.

Orru, S., Coni, P., Floris, A., Littera, R., Carcassi, C., Sogos, V. and Brancia, C. (2016) 'Reduced stress granule formation and cell death in fibroblasts with the A382T mutation of TARDBP gene: evidence for loss of TDP-43 nuclear function', *Hum Mol Genet,* 25(20), pp. 4473-4483.

Palangi, F., Samuel, S. M., Thompson, I. R., Triggle, C. R. and Emara, M. M. (2017) 'Effects of oxidative and thermal stresses on stress granule formation in human induced pluripotent stem cells', *PLoS One,* 12(7), pp. e0182059.

Park, J. W., Vahidi, B., Taylor, A. M., Rhee, S. W. and Jeon, N. L. (2006) 'Microfluidic culture platform for neuroscience research', *Nat Protoc,* 1(4), pp. 2128-36.

Parker, S. J., Meyerowitz, J., James, J. L., Liddell, J. R., Crouch, P. J., Kanninen, K. M. and White, A. R. (2012) 'Endogenous TDP-43 localized to stress granules can subsequently form protein aggregates', *Neurochem Int,* 60(4), pp. 415-24.

Paschen, W., Hotop, S. and Aufenberg, C. (2003) 'Loading neurons with BAPTA-AM activates xbp1 processing indicative of induction of endoplasmic reticulum stress', *Cell Calcium,* 33(2), pp. 83-9.

Patel, A., Lee, H. O., Jawerth, L., Maharana, S., Jahnel, M., Hein, M. Y., Stoynov, S., Mahamid, J., Saha, S., Franzmann, T. M., Pozniakovski, A., Poser, I., Maghelli, N., Royer, L. A., Weigert, M., Myers, E. W., Grill, S., Drechsel, D., Hyman, A. A. and Alberti, S. (2015) 'A Liquid-to-Solid Phase Transition of the ALS Protein FUS Accelerated by Disease Mutation', *Cell,* 162(5), pp. 1066-77.

Perry, R. B., Doron-Mandel, E., Iavnilovitch, E., Rishal, I., Dagan, S. Y., Tsoory, M., Coppola, G., McDonald, M. K., Gomes, C., Geschwind, D. H., Twiss, J. L., Yaron, A. and Fainzilber, M. (2012) 'Subcellular Knockout of Importin beta 1 Perturbs Axonal Retrograde Signaling', *Neuron,* 75(2), pp. 294-305.

Pizzo, E., Sarcinelli, C., Sheng, J., Fusco, S., Formiggini, F., Netti, P., Yu, W., D'Alessio, G. and Hu, G. F. (2013) 'Ribonuclease/angiogenin inhibitor 1 regulates stress-induced subcellular localization of angiogenin to control growth and survival', *J Cell Sci,* 126(Pt 18), pp. 4308-19.

Podzuweit, T., Nennstiel, P. and Muller, A. (1995) 'Isozyme selective inhibition of cGMP-stimulated cyclic nucleotide phosphodiesterases by erythro-9-(2-hydroxy-3-nonyl) adenine', *Cell Signal,* 7(7), pp. 733-8.

Porter, A. G. and Janicke, R. U. (1999) 'Emerging roles of caspase-3 in apoptosis', *Cell Death Differ,* 6(2), pp. 99-104.

Porter, D. J. and Abushanab, E. (1992) 'Kinetics of inhibition of calf intestinal adenosine deaminase by (+)- and (-)-erythro-9-(2-hydroxy-3-nonyl)adenine', *Biochemistry,* 31(35), pp. 8216-20.

Poulopoulos, A., Murphy, A. J., Ozkan, A., Davis, P., Hatch, J., Kirchner, R. and Macklis, J. D. (2019) 'Subcellular transcriptomes and proteomes of developing axon projections in the cerebral cortex', *Nature,* 565(7739), pp. 356-360.

Pradat, P.-F. and El Mendili, M.-M. (2014) 'Neuroimaging to investigate multisystem involvement and provide biomarkers in amyotrophic lateral sclerosis', *BioMed research international,* 2014, pp. 467560-467560.

Pugdahl, K., Fuglsang-Frederiksen, A., de Carvalho, M., Johnsen, B., Fawcett, P. R., Labarre-Vila, A., Liguori, R., Nix, W. A. and Schofield, I. S. (2007) 'Generalised sensory system abnormalities in amyotrophic lateral sclerosis: a European multicentre study', *J Neurol Neurosurg Psychiatry,* 78(7), pp. 746-9.

Qiu, H., Lee, S., Shang, Y., Wang, W. Y., Au, K. F., Kamiya, S., Barmada, S. J., Finkbeiner, S., Lui, H., Carlton, C. E., Tang, A. A., Oldham, M. C., Wang, H., Shorter, J., Filiano, A. J., Roberson, E. D., Tourtellotte, W. G., Chen, B., Tsai, L. H. and Huang, E. J. (2014) 'ALS-associated mutation FUS-R521C causes DNA damage and RNA splicing defects', *J Clin Invest,* 124(3), pp. 981-99.

Rabbitts, T. H., Forster, A., Larson, R. and Nathan, P. (1993) 'Fusion of the dominant negative transcription regulator CHOP with a novel gene FUS by translocation t(12;16) in malignant liposarcoma', *Nat Genet,* 4(2), pp. 175-80.

Ralser, M., Albrecht, M., Nonhoff, U., Lengauer, T., Lehrach, H. and Krobitsch, S. (2005) 'An integrative approach to gain insights into the cellular function of human ataxin-2', *J Mol Biol,* 346(1), pp. 203-14.

Ramesh, N. and Pandey, U. B. (2017) 'Autophagy Dysregulation in ALS: When Protein Aggregates Get Out of Hand', *Front Mol Neurosci,* 10, pp. 263.

Ratnavalli, E., Brayne, C., Dawson, K. and Hodges, J. R. (2002) 'The prevalence of frontotemporal dementia', *Neurology,* 58(11), pp. 1615-21.

Ravel-Chapuis, A., Klein Gunnewiek, A., Belanger, G., Crawford Parks, T. E., Cote, J. and Jasmin, B. J. (2016) 'Staufen1 impairs stress granule formation in skeletal muscle cells from myotonic dystrophy type 1 patients', *Mol Biol Cell,* 27(11), pp. 1728-39.

Reineke, L. C., Cheema, S. A., Dubrulle, J. and Neilson, J. R. (2018) 'Chronic starvation induces noncanonical pro-death stress granules', *J Cell Sci,* 131(19).

Renton, A. E., Chio, A. and Traynor, B. J. (2014) 'State of play in amyotrophic lateral sclerosis genetics', *Nat Neurosci,* 17(1), pp. 17-23.

Repici, M., Hassanjani, M., Maddison, D. C., Garcao, P., Cimini, S., Patel, B., Szego, E. M., Straatman, K. R., Lilley, K. S., Borsello, T., Outeiro, T. F., Panman, L. and Giorgini, F. (2019) 'The Parkinson's Disease-Linked Protein DJ-1 Associates with Cytoplasmic mRNP Granules During Stress and Neurodegeneration', *Mol Neurobiol,* 56(1), pp. 61-77.

Richardson, P. M., Miao, T., Wu, D., Zhang, Y., Yeh, J. and Bo, X. (2009) 'Responses of the nerve cell body to axotomy', *Neurosurgery,* 65(4 Suppl), pp. A74-9.

Rodriguez-Ortiz, C. J., Flores, J. C., Valenzuela, J. A., Rodriguez, G. J., Zumkehr, J., Tran, D. N., Kimonis, V. E. and Kitazawa, M. (2016) 'The Myoblast C2C12 Transfected with Mutant Valosin-Containing Protein Exhibits Delayed Stress Granule Resolution on Oxidative Stress', *Am J Pathol,* 186(6), pp. 1623-34.

Rogelj, B., Easton, L. E., Bogu, G. K., Stanton, L. W., Rot, G., Curk, T., Zupan, B., Sugimoto, Y., Modic, M., Haberman, N., Tollervey, J., Fujii, R., Takumi, T., Shaw, C. E. and Ule, J. (2012) 'Widespread binding of FUS along nascent RNA regulates alternative splicing in the brain', *Sci Rep,* 2, pp. 603.

Rohrer, J. D., Guerreiro, R., Vandrovcova, J., Uphill, J., Reiman, D., Beck, J., Isaacs, A. M., Authier, A., Ferrari, R., Fox, N. C., Mackenzie, I. R. A., Warren, J. D., de Silva, R., Holton, J., Revesz, T., Hardy, J., Mead, S. and Rossor, M. N. (2009) 'The heritability and genetics of frontotemporal lobar degeneration', *Neurology,* 73(18), pp. 1451-1456.

Rojas, M., Arias, C. F. and López, S. (2010) 'Protein kinase R is responsible for the phosphorylation of eIF2alpha in rotavirus infection', *Journal of virology,* 84(20), pp. 10457-10466.

Romano, A. D., Serviddio, G., de Matthaeis, A., Bellanti, F. and Vendemiale, G. (2010) 'Oxidative stress and aging', *J Nephrol,* 23 Suppl 15, pp. S29-36.

Roossien, D. H., Miller, K. E. and Gallo, G. (2015) 'Ciliobrevins as tools for studying dynein motor function', *Frontiers in cellular neuroscience,* 9, pp. 252-252.

Rosen, D. R., Siddique, T., Patterson, D., Figlewicz, D. A., Sapp, P., Hentati, A., Donaldson, D., Goto, J., O'Regan, J. P., Deng, H. X. and et al. (1993) 'Mutations in Cu/Zn superoxide dismutase gene are associated with familial amyotrophic lateral sclerosis', *Nature,* 362(6415), pp. 59-62.

Ruggieri, A., Dazert, E., Metz, P., Hofmann, S., Bergeest, J.-P., Mazur, J., Bankhead, P., Hiet, M.-S., Kallis, S., Alvisi, G., Samuel, C. E., Lohmann, V., Kaderali, L., Rohr, K., Frese, M., Stoecklin, G. and Bartenschlager, R. (2012) 'Dynamic oscillation of translation and stress granule formation mark the cellular response to virus infection', *Cell host & microbe,* 12(1), pp. 71-85.

Ruiz-Ramos, R., Lopez-Carrillo, L., Rios-Perez, A. D., De Vizcaya-Ruiz, A. and Cebrian, M. E. (2009) 'Sodium arsenite induces ROS generation, DNA oxidative

damage, HO-1 and c-Myc proteins, NF-kappaB activation and cell proliferation in human breast cancer MCF-7 cells', *Mutat Res,* 674(1-2), pp. 109-15.

Rulten, S. L., Rotheray, A., Green, R. L., Grundy, G. J., Moore, D. A., Gomez-Herreros, F., Hafezparast, M. and Caldecott, K. W. (2014) 'PARP-1 dependent recruitment of the amyotrophic lateral sclerosis-associated protein FUS/TLS to sites of oxidative DNA damage', *Nucleic Acids Res,* 42(1), pp. 307-14.

Ryu, H. H., Jun, M. H., Min, K. J., Jang, D. J., Lee, Y. S., Kim, H. K. and Lee, J. A. (2014) 'Autophagy regulates amyotrophic lateral sclerosis-linked fused in sarcoma-positive stress granules in neurons', *Neurobiol Aging,* 35(12), pp. 2822-2831.

Sahoo, P. K., Smith, D. S., Perrone-Bizzozero, N. and Twiss, J. L. (2018) 'Axonal mRNA transport and translation at a glance', *J Cell Sci,* 131(8).

Salapa, H. E., Johnson, C., Hutchinson, C., Popescu, B. F. and Levin, M. C. (2018) 'Dysfunctional RNA binding proteins and stress granules in multiple sclerosis', *J Neuroimmunol,* 324, pp. 149-156.

Sama, R. R., Ward, C. L., Kaushansky, L. J., Lemay, N., Ishigaki, S., Urano, F. and Bosco, D. A. (2013) 'FUS/TLS assembles into stress granules and is a prosurvival factor during hyperosmolar stress', *J Cell Physiol,* 228(11), pp. 2222-31.

Sayir, F., Kavak, S., Meral, I., Demir, H., Cengiz, N. and Cobanoglu, U. (2013) 'Effects of crush and axotomy on oxidative stress and some trace element levels in phrenic nerve of rats', *Brain Res Bull,* 92, pp. 84-8.

Scekic-Zahirovic, J., Sendscheid, O., El Oussini, H., Jambeau, M., Sun, Y., Mersmann, S., Wagner, M., Dieterle, S., Sinniger, J., Dirrig-Grosch, S., Drenner, K., Birling, M. C., Qiu, J. S., Zhou, Y., Li, H. R., Fu, X. D., Rouaux, C., Shelkovnikova, T., Witting, A., Ludolph, A. C., Kiefer, F., Storkebaum, E., Lagier-Tourenne, C. and Dupuis, L. (2016) 'Toxic gain of function from mutant FUS protein is crucial to trigger cell autonomous motor neuron loss', *Embo Journal,* 35(10), pp. 1077-1097.

Schwartz, J. C., Ebmeier, C. C., Podell, E. R., Heimiller, J., Taatjes, D. J. and Cech, T. R. (2012) 'FUS binds the CTD of RNA polymerase II and regulates its phosphorylation at Ser2', *Genes Dev,* 26(24), pp. 2690-5.

Scotter, E. L., Chen, H. J. and Shaw, C. E. (2015) 'TDP-43 Proteinopathy and ALS: Insights into Disease Mechanisms and Therapeutic Targets', *Neurotherapeutics,* 12(2), pp. 352-63.

Seguin, S. J., Morelli, F. F., Vinet, J., Amore, D., De Biasi, S., Poletti, A., Rubinsztein, D. C. and Carra, S. (2014) 'Inhibition of autophagy, lysosome and VCP function impairs stress granule assembly', *Cell Death Differ,* 21(12), pp. 1838-51.

Shang, Y. and Huang, E. J. (2016) 'Mechanisms of FUS mutations in familial amyotrophic lateral sclerosis', *Brain Res,* 1647, pp. 65-78.

Sharma, A., Lyashchenko, A. K., Lu, L., Nasrabady, S. E., Elmaleh, M., Mendelsohn, M., Nemes, A., Tapia, J. C., Mentis, G. Z. and Shneider, N. A. (2016) 'ALS-associated mutant FUS induces selective motor neuron degeneration through toxic gain of function', *Nature communications,* 7, pp. 10465-10465.

Shelkovnikova, T. A., Dimasi, P., Kukharsky, M. S., An, H., Quintiero, A., Schirmer, C., Buee, L., Galas, M. C. and Buchman, V. L. (2017) 'Chronically stressed or stress-preconditioned neurons fail to maintain stress granule assembly', *Cell Death Dis,* 8(5), pp. e2788.

Shelkovnikova, T. A., Robinson, H. K., Southcombe, J. A., Ninkina, N. and Buchman, V. L. (2014) 'Multistep process of FUS aggregation in the cell cytoplasm involves RNA-dependent and RNA-independent mechanisms', *Human Molecular Genetics,* 23(19), pp. 5211-5226.

Singh, A. P., Goel, R. K. and Kaur, T. (2011) 'Mechanisms pertaining to arsenic toxicity', *Toxicol Int,* 18(2), pp. 87-93.

Skaper, S. D. (2017) 'Impact of Inflammation on the Blood-Neural Barrier and Blood-Nerve Interface: From Review to Therapeutic Preview', *Int Rev Neurobiol,* 137, pp. 29-45.

Soo, K. Y., Sultana, J., King, A. E., Atkinson, R., Warraich, S. T., Sundaramoorthy, V., Blair, I., Farg, M. A. and Atkin, J. D. (2015) 'ALS-associated mutant FUS inhibits macroautophagy which is restored by overexpression of Rab1', *Cell Death Discov,* 1, pp. 15030.

Sousa-Valente, J., Andreou, A. P., Urban, L. and Nagy, I. (2014) 'Transient receptor potential ion channels in primary sensory neurons as targets for novel analgesics', *Br J Pharmacol,* 171(10), pp. 2508-27.

Sreedharan, J., Blair, I. P., Tripathi, V. B., Hu, X., Vance, C., Rogelj, B., Ackerley, S., Durnall, J. C., Williams, K. L., Buratti, E., Baralle, F., de Belleroche, J., Mitchell, J. D., Leigh, P. N., Al-Chalabi, A., Miller, C. C., Nicholson, G. and Shaw, C. E. (2008) 'TDP-43 mutations in familial and sporadic amyotrophic lateral sclerosis', *Science,* 319(5870), pp. 1668-72.

Stifani, N. (2014) 'Motor neurons and the generation of spinal motor neuron diversity', *Frontiers in cellular neuroscience,* 8, pp. 293-293.

Stoecklin, G., Stubbs, T., Kedersha, N., Wax, S., Rigby, W. F., Blackwell, T. K. and Anderson, P. (2004) 'MK2-induced tristetraprolin:14-3-3 complexes prevent stress granule association and ARE-mRNA decay', *Embo j,* 23(6), pp. 1313-24.

Svetoni, F., Frisone, P. and Paronetto, M. P. (2016) 'Role of FET proteins in neurodegenerative disorders', *RNA biology,* 13(11), pp. 1089-1102.

Swetha, R. G., Ramaiah, S. and Anbarasu, A. (2017) 'R521C and R521H mutations in FUS result in weak binding with Karyopherinbeta2 leading to Amyotrophic lateral sclerosis: a molecular docking and dynamics study', *J Biomol Struct Dyn,* 35(10), pp. 2169-2185.

Szaflarski, W., Fay, M. M., Kedersha, N., Zabel, M., Anderson, P. and Ivanov, P. (2016) 'Vinca alkaloid drugs promote stress-induced translational repression and stress granule formation', *Oncotarget,* 7(21), pp. 30307-22.

Takada, L. T. (2015) 'The Genetics of Monogenic Frontotemporal Dementia', *Dementia & neuropsychologia,* 9(3), pp. 219-229.

Takahashi, M., Higuchi, M., Matsuki, H., Yoshita, M., Ohsawa, T., Oie, M. and Fujii, M. (2013) 'Stress granules inhibit apoptosis by reducing reactive oxygen species production', *Mol Cell Biol,* 33(4), pp. 815-29.

Takeuchi, K., Kogure, M. and Hashimoto, T. (1987) 'Comparison of agonistic and antagonistic actions of guanabenz and guanfacin on alpha 1 and alpha 2-adrenoceptors in isolated smooth muscles', *Jpn J Pharmacol,* 43(3), pp. 267-75.

Tao, Q. Q., Wei, Q. and Wu, Z. Y. (2018) 'Sensory nerves disturbance in amyotrophic lateral sclerosis', *Life Sci*.

Taylor, A. M., Blurton-Jones, M., Rhee, S. W., Cribbs, D. H., Cotman, C. W. and Jeon, N. L. (2005) 'A microfluidic culture platform for CNS axonal injury, regeneration and transport', *Nat Methods,* 2(8), pp. 599-605.

Terenzio, M., Koley, S., Samra, N., Rishal, I., Zhao, Q., Sahoo, P. K., Urisman, A., Marvaldi, L., Oses-Prieto, J. A., Forester, C., Gomes, C., Kalinski, A. L., Di Pizio, A., Doron-Mandel, E., Perry, R. B., Koppel, I., Twiss, J. L., Burlingame, A. L. and Fainzilber, M. (2018) 'Locally translated mTOR controls axonal local translation in nerve injury', *Science,* 359(6382), pp. 1416-1421.

Thedieck, K., Holzwarth, B., Prentzell, M. T., Boehlke, C., Klasener, K., Ruf, S., Sonntag, A. G., Maerz, L., Grellscheid, S. N., Kremmer, E., Nitschke, R., Kuehn, E. W., Jonker, J. W., Groen, A. K., Reth, M., Hall, M. N. and Baumeister, R. (2013) 'Inhibition of mTORC1 by astrin and stress granules prevents apoptosis in cancer cells', *Cell,* 154(4), pp. 859-74.

Thomas, M. G., Martinez Tosar, L. J., Desbats, M. A., Leishman, C. C. and Boccaccio, G. L. (2009) 'Mammalian Staufen 1 is recruited to stress granules and impairs their assembly', *J Cell Sci,* 122(Pt 4), pp. 563-73.

Thomas-Jinu, S., Gordon, P. M., Fielding, T., Taylor, R., Smith, B. N., Snowden, V., Blanc, E., Vance, C., Topp, S., Wong, C. H., Bielen, H., Williams, K. L., McCann, E. P., Nicholson, G. A., Pan-Vazquez, A., Fox, A. H., Bond, C. S., Talbot, W. S., Blair, I. P., Shaw, C. E. and Houart, C. (2017) 'Non-nuclear Pool of Splicing Factor SFPQ Regulates Axonal Transcripts Required for Normal Motor Development', *Neuron,* 94(2), pp. 322-336.e5.

Tourrière, H., Chebli, K., Zekri, L., Courselaud, B., Blanchard, J. M., Bertrand, E. and Tazi, J. (2003) 'The RasGAP-associated endoribonuclease G3BP assembles stress granules', *The Journal of cell biology,* 160(6), pp. 823-831.

Towers, E. R., Kelly, J. J., Sud, R., Gale, J. E. and Dawson, S. J. (2011) 'Caprin-1 is a target of the deafness gene Pou4f3 and is recruited to stress granules in cochlear hair cells in response to ototoxic damage', *J Cell Sci,* 124(Pt 7), pp. 1145-55.

Trojanowski, J. Q. (1983) 'Native and derivatized lectins for in vivo studies of neuronal connectivity and neuronal cell biology', *J Neurosci Methods,* 9(3), pp. 185-204.

Tsai, N. P., Tsui, Y. C. and Wei, L. N. (2009) 'Dynein motor contributes to stress granule dynamics in primary neurons', *Neuroscience,* 159(2), pp. 647-56.

Tsaytler, P., Harding, H. P., Ron, D. and Bertolotti, A. (2011) 'Selective inhibition of a regulatory subunit of protein phosphatase 1 restores proteostasis', *Science,* 332(6025), pp. 91-4.

Tymianski, M., Spigelman, I., Zhang, L., Carlen, P. L., Tator, C. H., Charlton, M. P. and Wallace, M. C. (1994) 'Mechanism of action and persistence of neuroprotection by cell-permeant Ca2+ chelators', *J Cereb Blood Flow Metab,* 14(6), pp. 911-23.

Udagawa, T., Fujioka, Y., Tanaka, M., Honda, D., Yokoi, S., Riku, Y., Ibi, D., Nagai, T., Yamada, K., Watanabe, H., Katsuno, M., Inada, T., Ohno, K., Sokabe, M., Okado, H., Ishigaki, S. and Sobue, G. (2015) 'FUS regulates AMPA receptor function and FTLD/ALS-associated behaviour via GluA1 mRNA stabilization', *Nat Commun,* 6, pp. 7098.

Valentin-Vega, Y. A., Wang, Y. D., Parker, M., Patmore, D. M., Kanagaraj, A., Moore, J., Rusch, M., Finkelstein, D., Ellison, D. W., Gilbertson, R. J., Zhang, J., Kim, H. J. and Taylor, J. P. (2016) 'Cancer-associated DDX3X mutations drive stress granule assembly and impair global translation', *Sci Rep,* 6, pp. 25996.

van der Spek, R. A., van Rheenen, W., Pulit, S. L., Kenna, K. P., Ticozzi, N., Kooyman, M., McLaughlin, R. L., Moisse, M., van Eijk, K. R., van Vugt, J. J. F. A., Iacoangeli, A., Andersen, P., Nazli Basak, A., Blair, I., de Carvalho, M., Chio, A., Corcia, P., Couratier, P., Drory, V. E., Glass, J. D., Hardiman, O., Mora, J. S., Morrison, K. E., Mitne-Neto, M., Robberecht, W., Shaw, P. J., Panadés, M. P., van Damme, P., Silani, V., Gotkine, M., Weber, M., van Es, M. A., Landers, J. E., Al-Chalabi, A., van den Berg, L. H., Veldink, J. H. and Project Mine Als Sequencing, C. (2018) 'Reconsidering the causality of TIA1 mutations in ALS', *Amyotrophic lateral sclerosis & frontotemporal degeneration,* 19(1-2), pp. 1-3.

van der Staay, F. J., Arndt, S. S. and Nordquist, R. E. (2009) 'Evaluation of animal models of neurobehavioral disorders', *Behav Brain Funct,* 5, pp. 11.

Van Treeck, B. and Parker, R. (2018) 'Emerging Roles for Intermolecular RNA-RNA Interactions in RNP Assemblies', *Cell,* 174(4), pp. 791-802.

Vance, C., Rogelj, B., Hortobagyi, T., De Vos, K. J., Nishimura, A. L., Sreedharan, J., Hu, X., Smith, B., Ruddy, D., Wright, P., Ganesalingam, J., Williams, K. L., Tripathi, V., Al-Saraj, S., Al-Chalabi, A., Leigh, P. N., Blair, I. P., Nicholson, G., de Belleroche, J., Gallo, J. M., Miller, C. C. and Shaw, C. E. (2009) 'Mutations in FUS, an RNA processing protein, cause familial amyotrophic lateral sclerosis type 6', *Science,* 323(5918), pp. 1208-1211.

Vance, C., Scotter, E. L., Nishimura, A. L., Troakes, C., Mitchell, J. C., Kathe, C., Urwin, H., Manser, C., Miller, C. C., Hortobagyi, T., Dragunow, M., Rogelj, B. and Shaw, C. E. (2013) 'ALS mutant FUS disrupts nuclear localization and sequesters wild-type FUS within cytoplasmic stress granules', *Hum Mol Genet,* 22(13), pp. 2676-88.

Vanderweyde, T., Yu, H., Varnum, M., Liu-Yesucevitz, L., Citro, A., Ikezu, T., Duff, K. and Wolozin, B. (2012) 'Contrasting pathology of the stress granule proteins TIA-1 and G3BP in tauopathies', *J Neurosci,* 32(24), pp. 8270-83.

Vaughan, S. K., Sutherland, N. M., Zhang, S., Hatzipetros, T., Vieira, F. and Valdez, G. (2018) 'The ALS-inducing factors, TDP43(A315T) and SOD1(G93A), directly affect and sensitize sensory neurons to stress', *Sci Rep,* 8(1), pp. 16582.

Vernon, R. M., Chong, P. A., Tsang, B., Kim, T. H., Bah, A., Farber, P., Lin, H. and Forman-Kay, J. D. (2018) 'Pi-Pi contacts are an overlooked protein feature relevant to phase separation', *eLife,* 7, pp. e31486.

Visser, L. J., Medina, G. N., Rabouw, H. H., de Groot, R. J., Langereis, M. A., de Los Santos, T. and van Kuppeveld, F. J. M. (2019) 'Foot-and-Mouth Disease Virus Leader Protease Cleaves G3BP1 and G3BP2 and Inhibits Stress Granule Formation', *J Virol,* 93(2).

Vonaesch, P., Sansonetti, P. J. and Schnupf, P. (2017) 'Immunofluorescence Analysis of Stress Granule Formation After Bacterial Challenge of Mammalian Cells', *J Vis Exp,* (125).

Waite, A. J., Baumer, D., East, S., Neal, J., Morris, H. R., Ansorge, O. and Blake, D. J. (2014) 'Reduced C9orf72 protein levels in frontal cortex of amyotrophic lateral sclerosis and frontotemporal degeneration brain with the C9ORF72

hexanucleotide repeat expansion', *Neurobiol Aging,* 35(7), pp. 1779.e5-1779.e13.

Wang, B., Maxwell, B. A., Joo, J. H., Gwon, Y., Messing, J., Mishra, A., Shaw, T. I., Ward, A. L., Quan, H., Sakurada, S. M., Pruett-Miller, S. M., Bertorini, T., Vogel, P., Kim, H. J., Peng, J., Taylor, J. P. and Kundu, M. (2019a) 'ULK1 and ULK2 Regulate Stress Granule Disassembly Through Phosphorylation and Activation of VCP/p97', *Mol Cell,* 74(4), pp. 742-757.e8.

Wang, H., Guo, W., Mitra, J., Hegde, P. M., Vandoorne, T., Eckelmann, B. J., Mitra, S., Tomkinson, A. E., Van Den Bosch, L. and Hegde, M. L. (2018) 'Mutant FUS causes DNA ligation defects to inhibit oxidative damage repair in Amyotrophic Lateral Sclerosis', *Nat Commun,* 9(1), pp. 3683.

Wang, S., An, T., Wang, J., Zhao, J., Wang, Z., Zhuo, M., Bai, H., Yang, L., Zhang, Y., Wang, X., Duan, J., Wang, Y., Guo, Q. and Wu, M. (2010) 'Potential clinical significance of a plasma-based KRAS mutation analysis in patients with advanced non-small cell lung cancer', *Clin Cancer Res,* 16(4), pp. 1324-30.

Wang, S., Kwon, S. H., Su, Y. and Dong, Z. (2019b) 'Stress granules are formed in renal proximal tubular cells during metabolic stress and ischemic injury for cell survival', *Am J Physiol Renal Physiol,* 317(1), pp. F116-f123.

Wang, T., Martin, S., Nguyen, T. H., Harper, C. B., Gormal, R. S., Martinez-Marmol, R., Karunanithi, S., Coulson, E. J., Glass, N. R., Cooper-White, J. J., van Swinderen, B. and Meunier, F. A. (2016a) 'Flux of signalling endosomes undergoing axonal retrograde transport is encoded by presynaptic activity and TrkB', *Nat Commun,* 7, pp. 12976.

Wang, T., Xu, W., Qin, M., Yang, Y., Bao, P., Shen, F., Zhang, Z. and Xu, J. (2016b) 'Pathogenic Mutations in the Valosin-containing Protein/p97(VCP) N-domain Inhibit the SUMOylation of VCP and Lead to Impaired Stress Response', *J Biol Chem,* 291(27), pp. 14373-84.

Wang, W. Y., Pan, L., Su, S. C., Quinn, E. J., Sasaki, M., Jimenez, J. C., Mackenzie, I. R., Huang, E. J. and Tsai, L. H. (2013) 'Interaction of FUS and HDAC1 regulates DNA damage response and repair in neurons', *Nat Neurosci,* 16(10), pp. 1383-91.

Westlund, K. N., Kochukov, M. Y., Lu, Y. and McNearney, T. A. (2010) 'Impact of central and peripheral TRPV1 and ROS levels on proinflammatory mediators and nociceptive behavior', *Mol Pain,* 6, pp. 46.

Wheeler, J. R., Matheny, T., Jain, S., Abrisch, R. and Parker, R. (2016) 'Distinct stages in stress granule assembly and disassembly', *Elife,* 5.

White, J. P., Cardenas, A. M., Marissen, W. E. and Lloyd, R. E. (2007) 'Inhibition of cytoplasmic mRNA stress granule formation by a viral proteinase', *Cell Host Microbe,* 2(5), pp. 295-305.

Wiesner, D., Tar, L., Linkus, B., Chandrasekar, A., Olde Heuvel, F., Dupuis, L., Tsao, W., Wong, P. C., Ludolph, A. and Roselli, F. (2018) 'Reversible induction of TDP-43 granules in cortical neurons after traumatic injury', *Exp Neurol,* 299(Pt A), pp. 15-25.

Willis, K. L., Langland, J. O. and Shisler, J. L. (2011) 'Viral double-stranded RNAs from vaccinia virus early or intermediate gene transcripts possess PKR activating function, resulting in NF-kappaB activation, when the K1 protein is absent or mutated', *The Journal of biological chemistry,* 286(10), pp. 7765-7778.

Wolozin, B. and Ivanov, P. (2019) 'Stress granules and neurodegeneration', *Nat Rev Neurosci,* 20(11), pp. 649-666.

Wong, H. H., Lin, J. Q., Strohl, F., Roque, C. G., Cioni, J. M., Cagnetta, R., Turner-Bridger, B., Laine, R. F., Harris, W. A., Kaminski, C. F. and Holt, C. E. (2017) 'RNA Docking and Local Translation Regulate Site-Specific Axon Remodeling In Vivo', *Neuron,* 95(4), pp. 852-868.e8.

Wu, C. H., Fallini, C., Ticozzi, N., Keagle, P. J., Sapp, P. C., Piotrowska, K., Lowe, P., Koppers, M., McKenna-Yasek, D., Baron, D. M., Kost, J. E., Gonzalez-Perez, P., Fox, A. D., Adams, J., Taroni, F., Tiloca, C., Leclerc, A. L., Chafe, S. C., Mangroo, D., Moore, M. J., Zitzewitz, J. A., Xu, Z. S., van den Berg, L. H., Glass, J. D., Siciliano, G., Cirulli, E. T., Goldstein, D. B., Salachas, F., Meininger, V., Rossoll, W., Ratti, A., Gellera, C., Bosco, D. A., Bassell, G. J., Silani, V., Drory, V. E., Brown, R. H., Jr. and Landers, J. E. (2012) 'Mutations in the profilin 1 gene cause familial amyotrophic lateral sclerosis', *Nature,* 488(7412), pp. 499-503.

Wu, D., Yu, W., Kishikawa, H., Folkerth, R. D., Iafrate, A. J., Shen, Y., Xin, W., Sims, K. and Hu, G. F. (2007) 'Angiogenin loss-of-function mutations in amyotrophic lateral sclerosis', *Ann Neurol,* 62(6), pp. 609-17.

Yamaguchi, A. and Takanashi, K. (2016) 'FUS interacts with nuclear matrix-associated protein SAFB1 as well as Matrin3 to regulate splicing and ligand-mediated transcription', *Scientific Reports,* 6, pp. 14.

Yamazaki, T., Chen, S., Yu, Y., Yan, B., Haertlein, T. C., Carrasco, M. A., Tapia, J. C., Zhai, B., Das, R., Lalancette-Hebert, M., Sharma, A., Chandran, S., Sullivan, G., Nishimura, A. L., Shaw, C. E., Gygi, S. P., Shneider, N. A., Maniatis, T. and Reed, R. (2012) 'FUS-SMN protein interactions link the motor neuron diseases ALS and SMA', *Cell reports,* 2(4), pp. 799-806.

Yancy, S. L., Shelden, E. A., Gilmont, R. R. and Welsh, M. J. (2005) 'Sodium arsenite exposure alters cell migration, focal adhesion localization and decreases tyrosine phosphorylation of focal adhesion kinase in H9C2 myoblasts', *Toxicol Sci,* 84(2), pp. 278-86.

Yang, L., Gal, J., Chen, J. and Zhu, H. (2014) 'Self-assembled FUS binds active chromatin and regulates gene transcription', *Proc Natl Acad Sci U S A,* 111(50), pp. 17809-14.

Yasuda, K., Clatterbuck-Soper, S. F., Jackrel, M. E., Shorter, J. and Mili, S. (2017) 'FUS inclusions disrupt RNA localization by sequestering kinesin-1 and inhibiting microtubule detyrosination', *The Journal of cell biology,* 216(4), pp. 1015-1034.

Yasuda, K., Zhang, H., Loiselle, D., Haystead, T., Macara, I. G. and Mili, S. (2013) 'The RNA-binding protein Fus directs translation of localized mRNAs in APC-RNP granules', *J Cell Biol,* 203(5), pp. 737-46.

Yoshida, T., Inoue, R., Morii, T., Takahashi, N., Yamamoto, S., Hara, Y., Tominaga, M., Shimizu, S., Sato, Y. and Mori, Y. (2006) 'Nitric oxide activates TRP channels by cysteine S-nitrosylation', *Nat Chem Biol,* 2(11), pp. 596-607.

Yoshimura, A., Fujii, R., Watanabe, Y., Okabe, S., Fukui, K. and Takumi, T. (2006) 'Myosin-Va facilitates the accumulation of mRNA/protein complex in dendritic spines', *Curr Biol,* 16(23), pp. 2345-51.

Yoshizawa, T., Ali, R., Jiou, J., Fung, H. Y. J., Burke, K. A., Kim, S. J., Lin, Y., Peeples, W. B., Saltzberg, D., Soniat, M., Baumhardt, J. M., Oldenbourg, R., Sali, A., Fawzi, N. L., Rosen, M. K. and Chook, Y. M. (2018) 'Nuclear Import Receptor Inhibits Phase Separation of FUS through Binding to Multiple Sites', *Cell,* 173(3), pp. 693-705.e22.

Yuan, X., Klein, D., Kerscher, S., West, B. L., Weis, J., Katona, I. and Martini, R. (2018) 'Macrophage Depletion Ameliorates Peripheral Neuropathy in Aging Mice', *J Neurosci,* 38(19), pp. 4610-4620.

Zhang, P., Fan, B., Yang, P., Temirov, J., Messing, J., Kim, H. J. and Taylor, J. P. (2019a) 'Chronic optogenetic induction of stress granules is cytotoxic and reveals the evolution of ALS-FTD pathology', *eLife,* 8, pp. e39578.

Zhang, Q., Sharma, N. R., Zheng, Z. M. and Chen, M. (2019b) 'Viral Regulation of RNA Granules in Infected Cells', *Virol Sin,* 34(2), pp. 175-191.

Zhang, T., Wu, Y.-C., Mullane, P., Ji, Y. J., Liu, H., He, L., Arora, A., Hwang, H.-Y., Alessi, A. F., Niaki, A. G., Periz, G., Guo, L., Wang, H., Elkayam, E., Joshua-Tor, L., Myong, S., Kim, J. K., Shorter, J., Ong, S.-E., Leung, A. K. L. and Wang, J. (2018) 'FUS Regulates Activity of MicroRNA-Mediated Gene Silencing', *Molecular cell,* 69(5), pp. 787-801.e8.

Zhang, X., Wang, F., Hu, Y., Chen, R., Meng, D., Guo, L., Lv, H., Guan, J. and Jia, Y. (2020) 'In vivo stress granule misprocessing evidenced in a FUS knock-in ALS mouse model', *Brain,* 143(5), pp. 1350-1367.

Zhang, Z. C. and Chook, Y. M. (2012) 'Structural and energetic basis of ALS-causing mutations in the atypical proline-tyrosine nuclear localization signal of the Fused in Sarcoma protein (FUS)', *Proc Natl Acad Sci U S A,* 109(30), pp. 12017-21.

Zhao, Y., Toselli, P. and Li, W. (2012) 'Microtubules as a critical target for arsenic toxicity in lung cells in vitro and in vivo', *Int J Environ Res Public Health,* 9(2), pp. 474-95.

Zhou, Y., Liu, S., Liu, G., Ozturk, A. and Hicks, G. G. (2013) 'ALS-associated FUS mutations result in compromised FUS alternative splicing and autoregulation', *PLoS Genet,* 9(10), pp. e1003895.

Zou, T., Yang, X., Pan, D., Huang, J., Sahin, M. and Zhou, J. (2011) 'SMN deficiency reduces cellular ability to form stress granules, sensitizing cells to stress', *Cell Mol Neurobiol,* 31(4), pp. 541-50.